RELAMINARIZATION IN A SHORT ACCELERATION ZONE ON A CONVEX SURFACE

A Thesis
Submitted for the degree of

Doctor of Philosophy

in the Faculty of Engineering

By

R Mukund

Department of Aerospace Engineering
Indian Institute of Science
Bangalore 560 012, India
August 2002

(Published as NAL PD EA 0511,
National Aerospace Laboratories, Bangalore, India, 2005)

CONTENTS

ACKNOWLEDGMENTS

I take this opportunity to express my sincere gratitude to my research supervisors Dr. Viswanath P. R., Head, Experimental Aerodynamics Division (EAD), National Aerospace Laboratories (NAL), Prof. Prabhu A., Department of Aerospace Engineering, Prof. Narasimha R., Center for Atmospheric & Oceanic Sciences and Dr. Ramesh O.N., Department of Aerospace Engineering for their contribution towards the research work and for guiding me through the project.

I thank the Director, NAL for encouraging me and for extending the laboratory facilities required for the work. Part of the experimental work was sponsored by Boeing Commercial Aircraft Co, Seattle, USA and I thank Dr. Crouch J. of Boeing for his interest and suggestions made during the course of the project work. I gratefully acknowledge the disscussions I had with Prof.Sreenivasan K.R., Yale University, USA and thank him for his suggestions. I thank Dr. Seshadri, S. N., Head, NTAF, NAL for several facilities provided, Dr. Desai, S. S., Dr. Narayana, C. L. and Dr. Ramesh V., from CTFD, NAL for providing me the computational tools required.

I am grateful to all my colleagues at NAL for their contribution in model design, its fabrication and experiments and specially to (Dr./Mr.) Bharathan T, Deshpande V, Gopal S N, Joseph K A, Mahesh Kadam, Ramachandra G, Ramesh G, Varadharaj T and Verma R S. I thank my colleagues for the moral support provided - (Dr./Mr.) Amarnarayan D, Channa Raju, Lakshman Babu B, Madhavan K T, Mahalingam R, Raja Annamalai, Rajan Kumar, Sajeer Ahmed, Srinatha Sastry C V, Subhaschandar N, Suryanarayana G K, Venkatakrishnan L and Vipan Kumar.

Finally I appreciate the cooperation rendered by my parents Mrs. Padma R and Mr. Raghavendra Rao L, my wife Shashi and son Vishwas. I dedicate this thesis to my wife and my son.

NOMENCLATURE

Symbol	Definition, units
C_f	Coefficient of friction
C_p	Surface pressure coefficient based on freestream conditions
E	Voltage output from anemometer, V
H	Boundary layer shape factor = δ^*/θ
$I(K)$	Acceleration integral = $\frac{1}{\delta_o}\int_0^{x_a} K dx$
K	Launder's acceleration parameter = $\frac{\nu}{U^2}\frac{dU}{dx}$
K^*	Brandt's acceleration parameter = $\frac{\nu}{U_o^2}\frac{dU}{dx}$
k^{-1}	Wall radius of curvature, m
QLE	Quasi-Laminar Equations
R	Reynolds number
R_θ	Reynolds number based on θ
U	Potential velocity at the wall = $U_\infty\sqrt{1-C_p}$, m/s
U_e	Velocity at the edge of the boundary layer, m/s
U_o	Velocity at the beginning of acceleration, m/s
U_∞	Tunnel freestream velocity, m/s
u	Mean velocity component along x, m/s
u'	RMS of streamwise turbulence, m/s
u^*	Friction velocity = $\sqrt{\tau_o/\rho}$, m/s
u^+	= u/u^*
v	Mean velocity component along y, m/s
x	Streamwise direction parallel to wall, m

x_a Streamwise distance in the acceleration region, m

y Direction normal to the wall and x direction, m

$y+$ $= yu^* / \nu$

Δ_p Patel's pressure gradient parameter= $\frac{\nu}{u^{*3}} \frac{dp}{dx} = K\left(\frac{C_f}{2}\right)^{-3/2}$

Δ_τ Patel's pressure gradient parameter= $\frac{\nu}{u^{*3}} \frac{d\tau}{dx}$

Λ Narasimha and Sreenivasan's pressure gradient parameter = $-\frac{\delta}{\tau_o} \frac{dp}{dx}$

δ Boundary layer thickness, mm

δ^* Boundary layer displacement thickness, mm

ν Kinematic viscosity, m^2/s

θ Boundary layer momentum defect thickness, mm

ρ Density of air, kg/m^3

τ Reynolds shear stress, kg/m^2

τ_o Wall shear stress, kg/m^2

Subscripts

cr Critical value at and above which quasi-laminar theory works well

e edge of boundary layer

i start of acceleration

max maximum value

min minimum value

o characteristic no. / reference condition

s Streamline separating inner and outer layer in quasi-laminar equations

∞ Freestream conditions

Crown

– Outer variables in quasi-laminar equations

^ Inner variables in quasi-laminar equations

ABSTRACT

This thesis is essentially an experimental study investigating two-dimensional relaminarizing turbulent boundary layer flows under the combined influence of acceleration and convex surface curvature at low speeds.

Relaminarization of turbulent flow is a process by which the mean flow reverts to an effectively laminar state. The phenomenon of relaminarization in severely accelerated turbulent boundary layers on a flat plate has been studied in the past by several investigations and reviews can be found in Narasimha & Sreenivasan [1979] and Sreenivasan [1982]. Narasimha & Sreenivasan [1973] have proposed that relaminarization is an asymptotic process involving a large ratio of the streamwise pressure gradient to a characteristic Reynolds stress, and developed a two-layer integral model (called the quasi-laminar equations, QLE) for predicting the boundary layer mean flow parameters in the latter part of the relaminarization process.

While early work on relaminarization was largely motivated by scientific curiosity, interest in the problem has recently revived because of aircraft design applications involving relaminarization at swept leading-edges at high-lift, both in flight and in wind tunnels. The boundary layer near the leading edge of a swept wing, following attachment line transition, encounters not only strong streamwise acceleration but also convex surface curvature. It is well known that convex curvature can have a considerable stabilizing effect on a turbulent boundary layer (Bradshaw [1969]), so it is possible that relaminarization at a swept wing leading edge is influenced by streamwise convex curvature in addition to strong acceleration; such combined effects on relaminarization have not been studied before.

A complete understanding of relaminarization phenomena relevant to swept wings would further involve study of the effects of additional parameters like three-dimensionality and transition to turbulence by different mechanisms preceding relaminarization. Flow measurements on a swept wing, particularly in the leading edge zone, are difficult due to the relative thinness of the boundary layers in the zone. Two-dimensional building block experiments, systematically investigating the different effects on relaminarization, can therefore prove to be useful for understanding many features of 3D relaminarization such as those at a swept wing leading edge.

Against this background, an experimental investigation of 2D low-speed relaminarizing turbulent boundary layer flows, under the combined influence of acceleration and convex surface curvature, is reported here. The present experiments differ from earlier work on 2D relaminarizing flows in the following major respects; (i) inclusion of streamwise convex curvature, (ii) significantly reduced extent of acceleration, being between 10 - 14δ_o (where δ_o is the boundary layer thickness prior to acceleration) for the different flows investigated here, as against 25-30δ_o in flows investigated earlier and (iii) a region of adverse pressure gradient at the end of acceleration (like what is encountered on a swept wing at high-lift) affecting the retransition process. The experimental geometry and test parameters have been chosen to provide conditions very similar to those that occur on swept wings at realistic Reynolds numbers.

Three relaminarizing boundary layer flows on the convex wall (designated CP1, DP1 and CP2), having different pressure gradient histories and different acceleration levels, have been experimentally investigated here. To provide an assessment of convex curvature effects on relaminarization, two strategies were adopted. First, additional measurements on a relaminarizing flow on a flat surface (designated FP1), with experimental conditions and pressure gradient history maintained very similar to the flow CP1, were made. Comparison of the results of CP1 and FP1 enable identification of the effects on relaminarization arising from convex surface curvature. Second, the usefulness and applicability of QLE for predicting the three relaminarizing flows on a convex wall have been examined (without any additional treatment to take care of the surface curvature).

The measurements made for CP1, DP1 and FP1 consisted of surface pressure distributions along the model centerline, streamwise mean velocity and turbulent intensity profiles in the boundary layer using hot-wire probes, and mean and fluctuating components of wall shear stress at several streamwise stations using surface mounted hot-films. In the case of CP2, the measurements made consisted of surface pressure distributions along the model centerline and mean and fluctuating components of wall shear stress at several streamwise stations.

The experimental results provide strong evidence of relaminarization in all the four flows (including on the flat plate). The degree of relaminarization, as judged by the maximum attained value of the boundary layer shape factor, was appreciably higher for the flows CP1 and DP1 compared to FP1, indicating the stabilizing influence of convex

surface curvature in promoting relaminarization. In flow CP2, which had much higher acceleration levels extending over a very short distance, the skin friction coefficient decreased to very low values, indicating relaminarization. Also, during relaminarization, the fall in skin friction coefficient was more rapid for CP1 relative to FP1; there was a significant reduction of the relative turbulence intensities in the inner layer in flow CP1 as compared to FP1. All these observations show characteristics that must be attributed to effects of convex curvature. Retransition of the relaminarized boundary layers was quickly triggered in the adverse pressure gradient region in each case.

The predictions of skin friction using QLE (without modeling for curvature effects) for flows CP1 and CP2 on the convex surface were surprisingly good, suggesting that curvature effects are weak once the flow is relaminarized. This observation is consistent with the fact that the boundary layer thins down considerably during acceleration, thereby reducing the non-dimensional curvature parameter and consequently weakening the curvature effect. Further it is well known that the effect of curvature on a laminar (or a relaminarized) boundary layer is only of second order. In contrast, the predictions using QLE were less satisfactory for the flat surface flow FP1, which is at first sight surprising. Further analysis has suggested that this is linked to the fact that the zone of acceleration is very short ($\approx 12\delta_o$). The ability of QLE to satisfactorily predict CP1 and CP2 with curvature effects, but not FP1 on a flat plate, strongly suggests that the boundary layers on the convex wall have relaminarized more completely than on the flat surface. This finding further supports the experimental observations of a higher degree of relaminarization on the convex surface. For the other convex surface flow DP1, the calculations reflected the same trend as the experiments, but some disagreement was seen – the deficiency has been traced to the fact that the approximations made for QLE were barely satisfactory for DP1.

In summary, the new experimental results obtained here for examining the effects of convex surface curvature on relaminarization, and the detailed comparisons of the data with predictions based on QLE, indicate that streamwise convex curvature can have surprisingly strong effects in promoting or aiding the relaminarization process of an accelerated turbulent boundary layer. This fact clearly would have to be taken into account in assessing the effects of possible relaminarization on swept wings in the aerodynamic design of flight vehicles.

LIST OF FIGURES

LIST OF TABLES

CHAPTER 1
INTRODUCTION

Relaminarization of turbulent flow is a process by which the mean flow reverts to an effectively laminar state. Relaminarization has been observed in a variety of flows; for example, boundary layers subjected to severe acceleration (for e.g., Sternberg [1954], Wilson & Pope [1954]), in pipes and channels when subjected to divergence (Laufer [1962], Badri Narayanan [1968]), and under the action of stable density gradients as e.g., in the atmosphere (Narasimha [1977]). Narasimha [1977] classified the different mechanisms by which relaminarization may occur in these diverse situations under three basic archetypes: (*a*) by dissipation of turbulence through the action of a molecular property like viscosity as in enlarging pipes/channels, (*b*) by destruction of turbulence due to a stabilizing body-force like buoyancy as observed in stable density-gradient flows and (*c*) by the domination of pressure forces as seen in severely accelerated turbulent boundary layers. The review article by Narasimha & Sreenivasan [1979] provides a detailed discussion of these different mechanisms influencing relaminarization.

The phenomenon of relaminarization in severely accelerated turbulent boundary layers on a flat plate has been studied in the past by several investigators (Sreenivasan [1974]). A review of the literature on relaminarizing boundary layers with emphasis on issues like experimental difficulties and trustworthiness of the data has been reported by Sreenivasan [1982]. These experimental investigations reveal that this type of relaminarization is a gradual process accompanied by large changes in the structure of the turbulent boundary layer. The events leading to relaminarization include the breakdown of the law-of-the-wall with the velocity profile having a tendency to revert to the laminar profile, a significant decrease in the skin friction coefficient and an increase in shape factor towards laminar boundary layer values. Velocity fluctuations may still remain in the relaminarized state, but their contribution to mean flow dynamics appears to be small; however, they promote retransition of the relaminarized boundary layer after the favorable pressure gradient is relieved.

Several authors have proposed different parameters as criteria for the onset or occurrence of relaminarization. These parameters depend heavily on different symptoms used in identifying or recognizing the onset. A summary of the different criteria proposed and the difficulties faced in dealing with them are contained in the paper by Narasimha & Sreenivasan [1973]. They have suggested that, as opposed to the occurrence of relaminarization, its completion can be defined with some degree of confidence and certainty. They have argued that relaminarization may be assumed to be complete when the effect of the Reynolds shear stress on the mean flow development is small. Further, they proposed that relaminarization is an asymptotic process involving a large ratio of the streamwise pressure gradient to a characteristic Reynolds stress, and developed a two-layer integral model (called the quasi-laminar equations, QLE) for predicting the mean flow parameters in the latter part of the relaminarization process. Based on extensive comparisons of their calculations with experimental data for a variety of relaminarizing boundary layer flows, Narasimha & Sreenivasan [1973] suggested that QLE are applicable for values of the pressure gradient parameter Λ greater than about 50, but emphasized that this number is not to be seen as a 'critical' value.

While early work on relaminarization was motivated by scientific curiosity, interest in the problem recent has revived because of aircraft design applications involving relaminarization at swept leading-edges at high-lift, both in flight and in the wind tunnels (Van Dam et al [1993], Arnal & Juillen [1990]; Thompson [1973] appears to have been the first to suggest the possibility of relaminarization on swept wings). Relaminarization under such conditions can have considerable impact on airplane aerodynamics. Fig.1.1 shows a sketch (Yip et al [1993]) of the possible variation of the maximum lift-coefficient ($C_{L,max}$) with Reynolds number on a swept wing having a modern supercritical airfoil section. The attachment line can become turbulent under certain conditions and results in a loss of lift due to thicker boundary layers at the trailing edge. However, in the presence of strong acceleration around the wing leading edge at high-lift, the turbulent boundary layer may relaminarize leading to a certain recovery in the loss of maximum lift – the interplay between attachment line transition and relaminarization, which are both Reynolds number dependent, can cause significant scale effects.

The turbulent boundary layer near the leading edge of a swept wing, following attachment line transition, encounters not only strong streamwise acceleration but also

convex surface curvature. It is known that convex curvature can have profound stabilizing effects on turbulence (Bradshaw [1969]). Hence, it is likely that relaminarization at a swept wing leading edge is influenced by streamwise convex curvature in addition to strong acceleration; such combined effects on relaminarization have not been examined in the literature.

Further understanding of relaminarization phenomena relevant to swept wings would therefore involve study of the effects of additional parameters like three-dimensionality, streamwise convex curvature and transition to turbulence by different mechanisms preceding relaminarization. Flow measurements on a swept wing, particularly in the leading edge zone, are difficult due to relatively thin boundary layers. Two-dimensional building block experiments, systematically investigating the different effects on relaminarization, may therefore prove to be very useful for understanding many features of 3D relaminarization such as those at a swept wing leading edge.

This thesis is essentially an experimental study, where we have investigated features of 2D relaminarizing boundary layer flows under the combined influence of acceleration and convex surface curvature at low speeds. The present experiments differ from most earlier work on 2D relaminarizing flows in the following major aspects; (*i*) inclusion of streamwise convex curvature, (*ii*) significantly reduced extent of acceleration (relative to the boundary layer thickness) and (*iii*) a region of adverse pressure gradient at the end of acceleration (like on a swept wing at high-lift) affecting the retransition process. The experimental geometry and test parameters have been chosen to provide conditions very similar to those that occur on swept wings at realistic Reynolds numbers.

Three relaminarizing boundary layer flows on the convex surface (designated CP1, DP1 and CP2*), having different pressure gradient histories and different maximum values of the acceleration parameter K, have been documented. In order to bring out the history effects of the pressure gradient on relaminarization, the three flows were tailored to provide nearly the same acceleration integral.

The measurements made for CP1, DP1 and FP1 consisted of surface pressure distribution along the model centerline, streamwise mean velocity and turbulence intensity profiles in the boundary layer using hot-wire probes, and mean and fluctuating components of wall shear stress using surface mounted hot-films at several

* Only surface pressure and wall shear stress measurements were made for CP2

streamwise stations. In the case of CP2, the measurements made consisted of surface pressure distributions along the model centerline and mean and fluctuating components of wall shear stress at several streamwise stations.

To provide an assessment of convex curvature effects on relaminarization, two strategies were adopted. *First,* additional measurements on a relaminarizing flow on a flat surface (designated FP1), with experimental conditions and pressure gradient history maintained very similar to the flow CP1, were made. Comparison of results of CP1 and FP1 would enable identifying certain effects on relaminarization arising from convex surface curvature. *Second*, the usefulness and applicability of QLE for predicting the three relaminarizing flows on a convex surface have been examined, without any modeling for the mean flow or turbulence.

The experimental results showed strong features of relaminarization in all the four flows (including on the flat plate). The degree of relaminarization, as judged by the maximum attained value of the boundary layer shape factor, was appreciably higher for the flows CP1 and DP1 compared to FP1, indicating the stabilizing influence of convex surface curvature in promoting relaminarization. In flow CP2, which had much higher acceleration levels extending over a very short distance, the skin friction coefficient decreased to very low values, indicating relaminarization. The fall in skin friction coefficient during relaminarization was more rapid for CP1 relative to FP1. During relaminarization, significant reduction of the (normalized) turbulence intensities in the inner layer was observed for the flow CP1 compared to FP1. All these observations show characteristics that can be attributed to convex curvature. Retransition of the relaminarized boundary layers was quickly triggered in the adverse pressure gradient region in each case.

The predictions of skin friction using QLE (without modeling for curvature effects) for flows CP1 and CP2 on convex surface were surprisingly good, suggesting that curvature effects are weak once the flow is relaminarized. This observation is consistent with the fact that the boundary layer thins down considerably during acceleration and that the streamwise surface curvature effect for a laminar boundary layer is only of second order. For the other convex surface flow DP1, the calculations reflected the experimental trend, some quantitative disagreement was seen – the deficiency of the predictions has been traced to the fact that Λ_{max} for DP1 is just around the critical regime (≈ 50).

In contrast with flows CP1 and CP2, the predictions using QLE were less satisfactory for the relaminarizing flow on the flat plate (FP1), although Λ_{max} for the flow was appreciably higher than critical and the streamwise extent of the zone of acceleration is about the same as CP1. Further analysis has suggested that the less-satisfactory predictions are linked to the fact that the zone of acceleration is very short ($\approx 12\delta_o$), so that the boundary layer approximation (relatively small streamwise derivatives) may itself be called into question. This is possibly the first time that the applicability of QLE is being assessed for a relaminarizing flow on a flat plate like FP1 with a very short acceleration zone.

The ability of QLE to satisfactorily predict CP1 and CP2 with curvature effects, but not FP1 on a flat plate, strongly suggests that the boundary layers on the convex surface have relaminarized more completely than on the flat surface. This finding further supports the experimental observations of a higher degree of relaminarization on the convex surface.

In summary, the new experimental results obtained here for examining the effects of convex surface curvature on relaminarization, and the detailed comparisons of the data with predictions based on QLE, indicate that streamwise convex curvature can have surprisingly strong effects in promoting or aiding the relaminarization process of an accelerated turbulent boundary layer. This fact clearly would have to be taken into account in assessing the effects of possible relaminarization on swept wings in the aerodynamic design of flight vehicles.

The thesis is divided into six chapters. Chapter 2 consists of a literature survey, basically dealing with relevant literature on relaminarization on low-speed 2D turbulent boundary layers due to acceleration; followed by a summary of previous literature on turbulent boundary layers on convex surfaces. The experiments conducted are described in chapter 3 and the results of these experiments and discussion are found in chapter 4. Chapter 5 describes an attempt to model the experimental results for not only the relaminarization region but also for the initial and the post-retransition turbulent boundary layers. The thesis ends (Chapter 6) with conclusions and suggestions for future work.

CHAPTER 2
REVIEW OF LITERATURE

This thesis addresses relaminarization under the combined influence of acceleration and convex curvature. Appropriately, this review of earlier literature deals first with the experiments and analyses of relaminarization of 2D turbulent boundary layers on flat surfaces due to high acceleration. In the second part, a summary of the literature on turbulent boundary layers on convex surfaces at zero pressure-gradient is presented. Finally, some relaminarization experiments on convex surfaces with pressure gradients are reviewed.

2.1 Relaminarization by severe acceleration

2.1.1 Experimental observations

It was Sternberg [1954] who perhaps found the first evidence of relaminarization due to large favorable pressure gradients in the behavior of a supersonic turbulent boundary layer across a Prandtl-Meyer expansion. While there have been other studies in supersonic flow where symptoms of relaminarization have been observed (see Narasimha & Viswanath [1975]), the most detailed investigations have been conducted at low speeds; a catalogue of these experiments is given in Table 2.1.

While relaminarization in supersonic flow across an expansion corner can be relatively abrupt, the experimental data at low speeds reveal that relaminarization is a gradual process in which an initially turbulent boundary layer is rendered effectively laminar over several boundary layer thicknesses. Typical variations of the boundary layer thickness parameters and skin friction coefficient C_f during relaminarization, taken from the experiments of Blackwelder & Kovasznay [1972], are shown in Fig.2.1. Some more results are found in Appendix E. The results show that during relaminarization, the boundary layer thins down, the shape factor initially decreases in response to strong acceleration and then increases approaching laminar values towards the end of acceleration. Correspondingly, C_f initially increases before decreasing towards laminar values.

Several experiments have revealed that that the law of the wall breaks down during severe acceleration and a typical result is shown in Fig.2.2. Under suitable circumstances, the velocity profile may tend towards a laminar profile (Launder [1964] and Ramjee [1968]), but this need not always occur.

The variation of the three components of the turbulence intensities (u', v' and w'), normalized with respect to the local free-stream velocity $U_e\ (x)$, are shown plotted in Fig.2.3 for the flow of Blackwelder & Kovasznay [1972]. The solid lines are the calculations of Narasimha & Sreenivasan [1973] which will be explained in Sec. 2.1.3. The experimental data reveal that the turbulence intensities, normalized with respect to the edge velocity, in the outer region of the boundary layer decay along the mean streamlines, although most of this decay is caused by the increase in $U(x)$. The absolute values of the turbulence intensities in the outer layer remain approximately constant along a mean streamline. Interestingly, the absolute value of the Reynolds shear stress remains nearly frozen as may be seen in Fig.2.4.

In most earlier experiments, the pressure gradient following $C_{p,min}$ is so small (or even zero) that the relaminarized boundary layer undergoes retransition to turbulence, the process occurring more rapidly than natural transition due to the existence of residual velocity fluctuations inside the relaminarized boundary layer. The effect of retransition (Fig.2.1) is to increase C_f and decrease H towards their respective turbulent boundary layer values.

2.1.2 Recent Experiments

Table 2.1 shows that the early experiments on relaminarization by acceleration in the 1960's and early 1970's, these experiments have been reviewed by Narasimha & Sreenivasan [1973]. After a gap of nearly two decades, the interest on problem has been revived with the experimental work of Brandt [1993], Escudier et al [1998], Ichmiya et al [1998], Warnack & Fernholz [1998], Bourassa et al [2000] and Kobashi [2002], the details of which are also included in Table 2.1. The findings in all these experiments are broadly consistent with what has been discussed in the previous sections. In this section, summary some of these experiments are provided.

Brandt [1993], motivated by the recent interest in swept wing boundary layer flows, conducted eight experiments on a flat plate in favorable pressure gradient having different values of initial R_θ (373-839) and the maximum values of the

acceleration parameter K (defined in Eqn.2.1 in the next section). Based on the values of C_f and H attained in the flows Brandt concluded that the flows A1, A2, A3, A4 and B1 had relaminarized. In flows A3, A4 and B1 turbulent spots were observed during relaminarization, this phenomenon was termed intermittent relaminarization by Brandt as against the term homogenous relaminarization he used for the cases A1 and A2, where the spots were not observed. These were perhaps the first relaminarization experiments where hot-films were extensively used for measuring C_f. An interesting feature of the relaminarizing flows was that C_f continued to decrease beyond the location of $C_{p,min}$, (Fig.2.5) indicating that retransition was not triggered at the location of $C_{p,min}$ (as observed in most experiments e.g., Badri Narayanan & Ramjee [1969]) and the process of relaminarization continued into the mild adverse pressure gradient region further downstream. Another interesting aspect in flow A1 was that a laminar separation bubble was observed at the end of relaminarization, this region is marked with a dotted line in Fig.2.5. Brandt has proposed the criteria K^* for relaminarization which is discussed in the next section.

Escudier et al [1998] conducted a set of systematic experiments on relaminarization by acceleration on a flat plate at $R_{\theta i}$ of 1700 with a motivation to study some aspects of turbulence. Boundary layer measurements included the mean velocity and streamwise turbulence using a single hot-wire, and shear stress was measured using hot-films. The mean flow results indicate that the flow relaminarized. Intermittency was calculated from the time traces using the windowing technique; the results show that when the value of the acceleration parameter K increased beyond a critical value of $3\text{x}10^{-6}$, the intermittency factor started decreasing from unity, rapidly reaching zero almost throughout the boundary layer. Further downstream as K decreased to lesser that the critical value the intermittency started increasing showing the onset of retransition.

Ichmiya et al [1998] conducted a relaminarization experiment on a flat plate by the action of flow acceleration ($R_{\theta i}$ = 799, K_{max} = $6\text{x}10^{-6}$), basically examining the turbulence structure from the ensemble average of the streamwise velocity fluctuations and the bursting phenomenon using the VITA technique.. The results showed that the vorticity increased in a large eddy and decreased in a small one. It was inferred from analyzing the ensemble averages of the velocity fluctuations that relaminarization changes the ejection and sweep, though not particularly attenuating the bursting in the inner layer.

Systematic experiments investigating the development of the turbulent boundary layer on an axisymmetric body subjected to favorable pressure gradients were reported in twin papers Fernholz & Warnack [1998] and Warnack & Fernholz [1998]. Four flows having different values of $R_{\theta i}$ and K_{max} were documented. Measurements included boundary layer mean velocities and two components of turbulence. The results show that two flows having higher and nearly identical pressure distributions (K_{max} = 4.0x10^{-6} & 3.88x10^{-6} respectively) but having different $R_{\theta i}$ (862 & 2564 respectively) relaminarized successfully. In spite of large differences in $R_{\theta i}$, the two flows developed nearly identically showing that the pressure gradients effects were dominant compared to the Reynolds number effect. These experiments have provided excellent results for both mean flow and turbulence and could be considered as test cases for validating relaminarization calculations.

Bourassa et al [2000] have documented two experiments on a flat plate with flow acceleration exploring the role of relaminarization in high-lift systems and to examine the critical value of the acceleration parameter K. They contoured the top wall of the wind tunnel so as to obtain flow with constant K in the bottom wall, the two flows achieving values of constant K of 2.05x10^{-6} and 4.1x10^{-6} respectively. The wall shear stress was measured using the oil-flow interferometry technique. The results show that the higher acceleration flow relaminarized and though the lower acceleration flow did not have complete relaminarization, it showed evidence of the breakdown of the law of the wall and some decrease in C_f. They inferred that K is not a viable parameter for determining the onset of relaminarization.

2.1.3 CRITERIA FOR RELAMINARIZATION

Several investigators have proposed different criteria for relaminarization, which depend in part on the 'symptom' used to recognize relaminarization. An extensive survey of these criteria was carried out by Narasimha & Sreenivasan [1973]. These criteria are presented in Table 2.2 and some important ones are discussed here.

Launder [1964] proposed that the dimensionless acceleration parameter

$$K = \frac{\nu}{U^2}\frac{\mathrm{d}U}{\mathrm{d}x} \qquad \ldots\ldots 2.1$$

is a convenient indicator for relaminarization; the critical value suggested by different investigators has varied from K_{cr} = 3.0x10^{-6} to 3.5x10^{-6} for the onset of relaminarization.

According to Launder & Stinchcombe [1967], the parameter indicating the onset of reversion would be of the type $K.C_f^{-n}$ (n lying between 1/2 and 3/2); they specifically suggested that above a certain critical range of the parameter $K.C_f^{-3/2}$, the boundary layer ceases to be the normal turbulent boundary layer. Schraub & Kline [1965] inferred, from their experiments, that cessation of bursting causes departure of the boundary layer from the standard turbulent characteristics and arrived at the parameter $K.C_f^{-1/2}$ as the criterion governing the cessation of bursting.

Based on relaminarization experiments in pipe flows, Patel [1965] and Patel & Head [1968] suggested two criteria, namely,

$$\Delta_p = \frac{\nu}{u^{*3}}\frac{\mathrm{d}p}{\mathrm{d}x} = K\left(\frac{C_f}{2}\right)^{-3/2} \quad \text{and} \quad \Delta_\tau = \frac{\nu}{u^{*3}}\frac{\mathrm{d}\tau}{\mathrm{d}x} \qquad \ldots\ldots 2.2$$

for the breakdown of the universal log-law and the onset of relaminarization respectively. They also inferred that the point where H minimum occurs closely corresponds to the position where relaminarization is initiated.

Narasimha & Sreenivasan [1973] critically analyzed various parameters governing the occurrence of relaminarization and found that there was no agreement on either a precise criterion for the occurrence of relaminarization, or on how its onset may be recognized. They pointed out that K is no doubt a convenient measure of acceleration, but being a freestream parameter, it does not represent the physics of the flow inside the boundary layer. In fact, the inconsistency of K in predicting relaminarization can be observed from the results of recent experiments of Warnack & Fernholz [1998] and Bourassa et al [2000], where a noticeable deviation from the log-law behavior was observed even for $K << 3\text{x}10^{-6}$.

According to Narasimha & Sreenivasan [1973], parameters like K and others of form $K.C_f^{-n}$ are some kind of (an inverse of) a Reynolds number and invariably depend on the similarity of flow in the wall region. Further, inferring relaminarization from the observed departure from a presumed ‘standard’ turbulent law suffers from an inherent difficulty in that the standard may not so much be an indication of reversion as of our ignorance of turbulence.

Narasimha & Sreenivasan [1973] argued that, in contrast the completion of relaminarization could be assigned a definite meaning, for it certainly occurs for the mean flow field when the net effect of the Reynolds shear stress is negligible. They

postulated that relaminarization occurs under the domination of pressure forces over the nearly frozen Reynolds stress. Thus the controlling factor, suggested by Sreenivasan & Narasimha [1971] for relaminarization in accelerated flows, is the ratio of the pressure gradient to a characteristic Reynolds stress gradient given by

$$\Lambda = -\frac{\delta}{\tau_o}\frac{\mathrm{d}p}{\mathrm{d}x} \qquad \ldots\ldots 2.3$$

where τ_o is the wall shear stress in the boundary layer just before pressure gradient is applied.

Narasimha & Sreenivasan [1973] formulated the quasi-laminar limit for large values of Λ and demonstrated the usefulness of their methodology by comparing their calculations with a large number of the experimental data sets then available.

More recently Brandt [1993] proposed the parameter

$$K^* = \frac{\nu}{U_o^2}\frac{\mathrm{d}U}{\mathrm{d}x} \qquad \ldots\ldots 2.4$$

(where U_o is the freestream velocity ahead of acceleration) and found that $K^* > 8.1 \times 10^{-6}$ for all the relaminarizing flows and generally lower than this value for all non-relaminarizing flows (Fig.2.6). It may be noted that K^* involves the same fundamental hypothesis as implied in the definition of Λ, as it represents the ratio of the pressure gradient to the Reynolds stress gradient at the beginning of acceleration (τ_o being taken proportional to U_o^2). Brandt's proposal seems to provide a useful parameter as it is simple to calculate.

2.1.4 CALCULATION METHODS

Unlike the large body of experimental results on relaminarization, there have been very few attempts to calculate relaminarizing flows. These are the differential methods of Kreskovsky et al [1974] and Viala & Aupoix [1995] and the integral method of Narasimha & Sreenivasan [1973]).

Kreskovsky et al [1974] computed the relaminarizing boundary layers at a wide variety of Mach numbers using their UARL prediction procedure, which involves the solution of the boundary layer equations in conjunction with an integral turbulent kinetic energy equation and a turbulent structure model. According to the authors, transition and relaminarization are a natural occurrence of the turbulence model and are not

being triggered by some semi-empirical criteria. Their computation of incompressible flows showed reasonable agreement with H and R_θ, though C_f was poorly predicted. On application of their code to compressible flow data, they found that the prediction of neither H nor C_f was very reliable.

Viala & Aupoix [1995] developed a computational method for predicting relaminarization of compressible flow turbulent boundary layers. They solved the time-averaged boundary layer equations using a variety of closure models. They derived a compressible flow criterion, similar to Δ_p of Patel & Head [1968], to mark the disappearance of the log-law region and damped the eddy viscosity from that streamwise location. Their computations showed reasonable agreement of C_f, whereas the shape factor was qualitatively similar but increased at a too slowly.

INTEGRAL METHOD - THE QUASI-LAMINAR EQUATIONS

Narasimha & Sreenivasan [1973] developed an integral method called the 'quasi-laminar' equations for predicting mean flow parameters during the latter stages of relaminarization of turbulent boundary layers subjected to high acceleration. According to this asymptotic theory, when the pressure gradient reaches such high magnitudes that the turbulence shear stress is effectively overwhelmed by the dominating pressure force, the turbulence stresses become relatively unimportant in determining the mean flow dynamics. Random fluctuations inherited from previous history might still remain in a large part of the flow, with their absolute magnitudes being comparable to their initial values, but they are no longer relevant to the dynamics of the mean flow in the lowest approximation. The region where these mechanisms were operating was termed 'quasi-laminar'.

Using the quasi-laminar equations, valid for a large value of Λ (Eqn.2.4), Narasimha & Sreenivasan [1973] showed how the mean flow field could be split into an inner laminar sub-boundary layer and an inviscid but rotational outer layer. Fig.2.7 shows a schematic representation of the formulation of the quasi-laminar equations: the details are given in Appendix E. The usefulness of the quasi-laminar equations was demonstrated by comparing the predictions with experimental data on a variety of relaminarizing flows developing on a flat plate, for which the zone of acceleration was sufficiently long (>25δ_o). They suggested that the asymptotic theory is approximately valid for $\Lambda \geq 50$. Comparisons of the quasi-laminar predictions with the experimental

data of Badri Narayanan & Ramjee [1969] and Blackwelder & Kovasznay [1972] are given in Fig.E1 and Fig.E2 respectively in Appendix E.

The predictions made using the quasi-laminar equations show that while integral parameters like δ, H and R_θ agree from the beginning of acceleration, wall parameters like C_f show agreement only in the later stages of relaminarization (Fig.2.8). The intermediate zone (Fig.2.8) that can be predicted neither by turbulent boundary layer calculations nor by the quasi-laminar theory was termed by Sreenivasan [1982] as the island of ignorance. Not much progress has been made in the last two decades towards further understanding of this zone.

VELOCITY FLUCTUATIONS DURING RELAMINARIZATION

The quasi-laminar theory also provides a framework for understanding the behavior of fluctuating quantities; Narasimha & Sreenivasan [1973] developed this model, details of which are given in Sreenivasan [1974]. In the outer layer, Sreenivasan & Narasimha [1978] showed that the distortion of turbulence vortex lines due to turbulent motion is much smaller than that produced by the mean rate of strain (i.e., the acceleration) and the viscous effects are anyway small. With this assumption, they modified the rapid-distortion theory of Batchelor & Proudman [1954] to account for departures from isotropy and applied it to calculate the changes in turbulence intensities in the outer layer of the boundary layer during relaminarization. An example of such a calculation is compared with the experiments of Blackwelder & Kovasznay [1972] in Fig.2.3. In general, Sreenivasan [1974] found that the calculations were quite successful for u' but somewhat less so for v' and w'.

The decay of fluctuations in the inner layer has also been calculated by Narasimha & Sreenivasan [1973]. Assuming that the fluctuating motion is 2D and quasi-steady, they analyzed the problem as similar to the development of steady perturbations on a laminar boundary layer. They utilized for the purpose the appropriate eigen-solutions for the Falkner-Skan family obtained by Chen & Libby [1968]. The comparison of their calculations with the experimental data of Badri Narayanan & Ramjee [1969] showed reasonable agreement.

2.1.5 FLOW FEATURES DURING RELAMINARIZATION

Fig.2.9 shows a broad classification of the flow features leading to relaminarization as suggested by Sreenivasan [1982]. In the initial region (*a*), the

pressure gradient is small and the boundary layer can be calculated using standard turbulent laws. The term laminarescence (region *b*) signifies the earlier stages of relaminarization – loosely, a precursor to relaminarization – where large departures occur from the 'laws' applicable to region (*a*). In the reverse transitional region (*c*), the flow ceases to be fully turbulent and is the least understood even to date. Under sustained acceleration, region (*d*), the boundary layer can be calculated using the quasi-laminar theory. Finally, when the acceleration relaxes (*e*), the boundary layer eventually undergoes retransition to turbulence, thus completing the cycle.

It should be emphasized here that the present understanding on relaminarization is that it is a gradual process accompanied by large changes in the structure of the boundary layer. Hence relaminarization cannot be predicted like a critical phenomenon, occurring when the value of a particular parameter crosses a critical value. Since the quasi-laminar equations are based on asymptotic assumptions, it is reasonable to state that relaminarization is likely to occur when Λ is maintained sufficiently high for a considerable distance.

2.2 Turbulent boundary layer on a longitudinally convex surface at zero pressure-gradient

Boundary layer flows on surfaces with longitudinal (or streamwise) curvature are very common. Experiments reveal (Bradshaw [1973]) that longitudinal convex curvature inhibits turbulence and has a first order stabilizing effect on a turbulent boundary layer, whereas concave curvature increases turbulence levels, and, along with the Görtler vortices present, destabilizes the boundary layer. Reviews by Bradshaw [1973] and Patel & Sotiropoulus [1997] deal with various aspects of turbulent boundary layer flows on longitudinally curved surfaces.

The magnitude of curvature in the boundary layer is generally described by the parameter $k\delta_o$, which is the ratio of the initial boundary layer thickness δ_o and the wall radius of curvature *1/k.* Curvature has a second order effect in the laminar case (Van Dyke [1962] and Narasimha & Ojha [1967]). In a turbulent boundary layer, however, the presence of the normal pressure-gradient imposed by convex curvature suppresses the vertical component of turbulence fluctuations, and causes large changes in the turbulence structure (Bradshaw [1969]). The effect of this can be one order more than what is obvious from the boundary layer equations. Bradshaw [1973] showed from his analogy of streamline curvature and buoyancy that even at very small

values of $k\delta_o$ (=1/300), when static pressure variation across the boundary layer is very small, the length scale of turbulence could be altered by as much as 10%. Experimental evidence of the stabilizing effect in turbulent flow has been observed by a large number of investigators both in channel and boundary layer flows (see Table 2.3). A summary of the major findings, leading to the present understanding of the flow, is presented below.

On a convex surface, the boundary layer velocity profiles plotted in wall coordinates show a distinct logarithmic region, whose extent decreases with downstream distance. An example of such behavior may be seen in Fig.2.10 from Gillis & Johnston [1983]. Prabhu et al [1982] plotted the intercept of the log-law against $k\delta_o$ (see Fig.2.11) and found that while the intercept is constant ($\cong$5.5) for boundary layers on concave surfaces (up to $k\delta_o$ = -0.1), for flat surfaces and up to a convex curvature of $k\delta_o$ = 0.03, it decreases to about 4.0 at $k\delta_o$ = 0.12.

Patel [1969] observed that the wake region, as seen in inner variables, is more pronounced than on a flat plate and is similar to that observed in adverse pressure gradients. Measurements of Prabhu et al [1982], So & Mellor [1973] and Ellis & Joubert [1974] also reflect this feature. Further, Prabhu et al [1982] observed that the intercept in the outer law increases with streamwise distance on a surface of constant curvature.

Prabhu et al [1982] analyzed the data of Prabhu & Sundarasiva Rao [1981] and showed an excellent collapse of velocity profiles centered around the position of the value of the maximum velocity (Fig.2.12). The collapse shows that the outer flow is stress free and vorticity is conserved along streamlines; and hence the outer profile must be an advection of the initial profile.

Certain interesting features with regard to the mean flow parameters have been observed in different convex surface experiments. The growth of the boundary layer thickness becomes slower than on a flat surface for small $k\delta_o$ (Gibson et al [1984]), and becomes negligible for high $k\delta_o$ (Prabhu & Sundarasiva Rao [1981] and So & Mellor [1973]), reducing entrainment very appreciably. The skin friction coefficient decreases with streamwise distance faster than on a flat surface, while the shape factor increases; these variations show a strong dependence on the curvature parameter $k\delta_o$ as illustrated in Fig.2.13 from Patel & Sotiropoulus [1997]. These results also show that

the response to convex curvature is immediate and continues as long as curvature is maintained.

A typical example of the effect of convex surface curvature on the turbulence structure is illustrated in Fig.2.14 from the experiments of So & Mellor [1973]. A dramatic reduction in all the three components of turbulence intensity and the shear stress on the convex surface, compared to their values on the flat plate, may be observed; also note the spectacular drop in the correlation coefficient, and the implied disappearance of shear stress at $y/\delta > 0.4$.

There have been several attempts to compute surface curvature effects on the turbulent boundary layer. Reviews by Patel & Sotiropoulos [1997] and by Kline et al [1982] deal with these computations. These reviews conclude that the turbulence and the Reynolds-stress models require to be tuned for making reasonable predictions.

The present overall status of understanding of the effects of longitudinal curvature on the turbulent boundary layer in zero pressure-gradient can be summed up using the remarks of Patel & Sotiropoulus [1997] that little progress has been made in demystifying, and particularly in quantifying, the effects of curvature in spite of the high level of effort devoted to the subject through laboratory, modeling and computational studies.

2.3 Accelerated turbulent boundary layers on convex surfaces

There has not been much experimental effort studying the combined effects of convex surface curvature and favorable pressure gradients. Launder & Loizou [1992] conducted experiments in developing turbulent flow in a rectangular-sectioned 90° bend having a converging sidewall. The average curvature parameter $k\delta$ was about 0.04. Two flows were documented at Reynolds numbers $R_{\theta o}$ of 600 and 820, for which K_{max} values were about 2.4×10^{-6} and 3.3×10^{-6} respectively. Measurements of the streamwise mean velocity profiles and the turbulence intensities showed substantial thickening of the sublayer and a diminution of near-wall turbulence levels on both convex and concave surfaces, with a greater damping on the convex surface. The relative insensitivity of turbulence decay to wall curvature was attributed by the authors to the secondary flow induced by curvature.

Schwarz & Plesniak [1996] made LDV measurements in turbulent boundary layers subjected to favorable pressure gradients on a convex surface with $k\delta_o$=0.1.

Three flows were documented namely (*a*) zero pressure gradient, (*b*) K_{max} = 0.55×10^{-6} and (*c*) K_{max} = 1.01×10^{-6}, designated ZPG, FPG and SFPG respectively. A comparison of the Reynolds shear stress profiles on the convex surface subjected to different pressure gradients (Fig.2.15) indicates that in ZPG and FPG, the Reynolds stress does not show any change in the inner region ($y^+ \leq 100$) and reduces considerably relative to the flat plate values in the outer region. A further all round reduction is apparent for the stronger favorable pressure gradient flow SFPG. This experiment shows that the influence of even small favorable pressure gradients acting in combination with convex curvature can be substantial.

2.4 Summary

The first part of the review dealing with relaminarization of accelerated turbulent boundary layers on flat plates shows that a large quantity of experimental data exist at low speeds. These investigations, generally at low to moderate R_θ, have revealed certain important features of relaminarizing boundary layers, like the break-down of the law of the wall, freezing of the Reynolds stress in the outer layer and the development of an inner laminar layer. Attempts to calculate relaminarizing flows have been rather few. Notable among these is the quasi-laminar theory of Narasimha and Sreenivasan [1973], which has been successfully used to calculate the boundary layer thickness parameters and skin friction in the latter stages of relaminarization. The intermediate zone (referred to as region (c) in Fig.2.9) continues to be a gray area for which no satisfactory modeling exists.

The second part dealt with the development of a turbulent boundary layer with streamwise convex curvature. There is sufficient evidence to show that both the mean velocity profile and the turbulence parameters are significantly affected by convex curvature; in particular, the outer part of the boundary layer behaves like an inviscid rotational flow even in a zero pressure-gradient flow. The limited data that exist on the combined effects of acceleration and convex curvature show greater stabilizing influence on the turbulent boundary layer as compared to the individual effects.

As indicated in Chapter I, this thesis presents a detailed investigation of the combined effects of convex curvature and streamwise acceleration with a view to gain better understanding of the role of convex curvature in promoting relaminarization at low speeds. The flow conditions have been so chosen as to be representative of the relaminarizing boundary layers near the leading edge region of swept wing.

CHAPTER 3
EXPERIMENTS

The major emphasis in the present work is on the study of relaminarizing boundary layer flows under the combined influence of streamwise acceleration and convex curvature. An attempt has been made to simulate certain important flow parameters similar to those on swept wing leading edges at high-lift, but in two-dimensional flow. In what follows, we shall describe in detail the facility, the design of the experiments, model geometry, test conditions, instrumentation and other related aspects.

3.1 Experimental Facility

The experiments were performed in the NAL 1.5m x 1.5m low-speed suction wind tunnel (Fig.3.1). The tunnel is equipped with a variable speed DC motor which provides a freestream velocity up to 50m/s that can be controlled to better than 1%. The entrance to the tunnel is equipped with honeycombs and a set of three screens followed by a 12:1 contraction section. The uniformity of the tunnel flow mean velocity is better than 0.3%. The streamwise turbulence in the test section is quite low (varying from 0.06% to 0.11% in the velocity range of 10-50 m/s respectively). More details of the tunnel flow characteristics are in Krishnan et al [1998].

3.2 Design criteria for the present experiments

As discussed in Chapter 2, the acceleration parameter K has been found to be useful to broadly indicate the occurrence of relaminarization at low speeds. In 2D flows, a critical value of K_{max} of about 3.5×10^{-6} has often been suggested (Launder [1964], Moretti & Kays [1965], Back & Seban [1967]) to indicate the onset of relaminarization. Such suggestions have been based on observations of a variety of relaminarizing flows (Fig.3.2) in which the streamwise zone or duration of acceleration extended typically over 25-35δ_o (where δ_o is the initial boundary layer thickness), with the shortest extent being about 20δ_o in the flow of Warnack & Fernholz [1998]. On swept wings at high lift, where relaminarization has been observed (for example Arnal & Juillen [1990], Van

Dam et al [1993]), the values of K_{max} estimated along the external inviscid streamlines is as high as 10×10^{-6}. In the absence of any more suitable criterion for relaminarization in a 3D flow, the 2D criterion based on K_{max} appears to have been taken as useful to indicate the possibility relaminarization at a swept leading edge.

The present experiments have been designed to provide different levels of K_{max} on a convex surface. The region of acceleration is maintained relatively short in terms of the initial boundary layer thickness ($<15\delta_o$), (as suggested by Crouch [1996]) so as to reflect conditions similar to those encountered on swept wing flows. At the end of acceleration, a zone of moderate adverse pressure gradient is imposed so that the features of retransition, following relaminarization, are broadly similar to those on a swept wing. After an examination of the estimated values of curvature parameter ($k\delta_o$) on swept wings (Appendix A), which vary in the range of 0.015 to 0.050, a nominal value of about 0.025 has been chosen as being most realistic.

Three flows have been investigated on the convex surface with different pressure gradient histories (i.e., K variations) and one flow on a flat wall. In order to bring out likely effects of pressure gradient histories on relaminarization, the above four flows have been chosen so that a suitably defined integral of the acceleration parameter,

$$I(K) = \frac{1}{\delta_o} \int_0^{x_a} K dx, \qquad \ldots \ 3.1$$

has about the same value in all cases. Here x_a is the distance from start to end of acceleration.

3.3 Description of model geometry

The geometric details of the two models used for the convex surface and the flat wall experiments respectively are described here.

3.3.1 Model for convex surface experiments

The model configuration (Fig. 3.3) used for the convex surface experiments, to be called 'curved-aft model', is a long and thick flat plate with an aft section having convex surface curvature. The flat section 0.8m long and 0.3m thick (Fig.3.3) provides a thick and reasonably well developed turbulent boundary layer growing essentially at constant pressure. The convex rear section is 0.7m long having a radius of curvature of 0.967m; this radius was chosen to provide a nominal value of $k\delta_o$ of about 0.025. The

upper surface of this curved-aft model will be referred to as the “test surface” in further discussion. The required favorable pressure gradients are imposed on the convex surface by locating a pressure-generator airfoil in its close proximity (Fig.3.3). The advantage of the airfoil is the flexibility it offers in generating a variety of pressure gradient histories, achieved by varying its location and incidence.

The curved-aft model is constructed essentially as a hollow wooden box with a smooth top surface made of glass fiber composite. It is placed between 2D side-wall inserts located 0.6m apart (Fig.3.4). The inserts, spanning the top and bottom walls, extend 0.5m upstream of the model nose and 1.0m downstream of its trailing edge, in order to minimize any interference from the tunnel flow present outside the inserts. A 10mm gap on each end of the pressure-generator airfoil was made with a view to reduce the possible interaction of the side-wall boundary layer with the main flow. A horizontal splitter plate was added downstream of the trailing edge of the model to reduce possible upstream influence that may arise due to the merging of the upper and lower flows on the model. A wedge-like fairing was introduced in the trailing-edge region of the curved-aft section to reduce the severity of the associated adverse pressure gradient, and to avoid boundary layer separation that may otherwise be expected in the region. A 10mm band of rough emery paper, having a maximum height of approximately 1mm, was glued to the test surface at x= 0.24m to trip the boundary layer. A photograph of the front view of the model set up including the pressure-generator airfoil section and the end-walls is shown in Fig.3.4.

The coordinate system used is shown in Fig.3.3. The streamwise distance x is measured starting from the leading edge of the cylindrical nose, proceeding in the streamwise direction along the contour of the cylindrical section, the flat surface and finally the convex surface. The distance normal to the surface is designated *y*.

3.3.2 Model for Flat Plate Experiments

The model geometry used for relaminarization studies on a flat plate is shown in Fig.3.5. It consists of a flat plate section 0.04m thick, 2m long, and has a super-elliptic nose of ratio 5:1. It is placed between the two side-wall inserts located 0.6m apart (Fig.3.5), similar to the manner in which the model used for the convex surface experiments was installed. The pressure-generator airfoil spanned 0.58m for the reasons mentioned above.

3.3.3 SELECTION OF AIRFOIL SHAPES

The profiles of the pressure-generator airfoil required for the convex and flat surface experiments were designed using a panel method of calculation utilizing an existing code (Ahmed [1973]). For simplicity, the flow was modeled in two dimensions by having a large span to chord ratio (100:1), the side walls and the vertical walls of the wind tunnel were not considered for modeling. Over 50 calculations were made on different pressure-generator airfoils and finally the three profiles capable of providing the required pressure-gradient histories were selected; the coordinates of the selected configurations are given in Appendix B and some salient design features are presented in Table 3.1.

3.4 Instrumentation

3.4.1 SURFACE PRESSURE MEASUREMENTS

The test surface used for the convex wall experiments was provided with 48 static pressure ports (0.7mm ID), located typically 20mm apart along the centerline (Table 3.2). To assess the two-dimensionality of surface pressures, spanwise static pressure taps were provided at selected streamwise stations (Table 3.3) on the convex surface covering a central span of 25%.

The test surface used for the flat plate relaminarization experiments was provided with 53 static pressure ports (0.7mm ID), located typically 20mm apart along the centerline (Table 3.4). Spanwise static pressure taps were provided at the locations indicated in Table 3.5.

All the static pressure tubes were connected to two units of 48-port Scanivalves, coupled to micro-manometers from Furness Control, UK, of ranges $\pm$200mm and $\pm$20mm of water. These pressure transducers were calibrated against a projection manometer having an accuracy of $\pm$0.2mm

3.4.2 VELOCITY AND TURBULENT INTENSITY PROFILE MEASUREMENTS

The mean velocity and streamwise turbulent intensity profiles in the boundary layer were measured at several streamwise locations on the test surfaces using a single hot-wire connected to a DISA 55M01 constant temperature anemometer (CTA).

A schematic of the special hot-wire probe used is shown in Fig.3.6. The hot-wire element consisted of a 5μm tungsten wire, 2.5mm long, welded at the tip of two steel

prongs 20mm long. The prongs were fixed on to a long and rigid steel tube (Fig.3.6) suitably designed to enable traversing the boundary layer on the test surfaces. The steel tube was connected to a precision height gage, with a least count of 0.02mm. The height gage was mounted outside the side-wall of the tunnel on a horizontal platform and was used to traverse the hot-wire probe vertically.

The hot-wire probe was calibrated in a smaller wind tunnel. The hot-wire calibration can be expressed by a generalized King's formula relating the wire voltage E to the normal velocity U as

$$E^2 - E_0^2 = AU^{1/n} \qquad \ldots 3.2$$

where E_o is the no-flow voltage, and A and n are constants to be determined by calibration. Since n was found to be very close to 0.5 in the present calibrations it was put equal to 0.5 following the recommendation of Bradshaw [1971]. The hot-wire probe was calibrated in the tunnel freestream at an overheat ratio of 1.60. A typical calibration plot is displayed in Fig.3.7.

For convenience and ease of moving the probe, all the velocity measurements in the boundary layer including on the convex surface were made by traversing the probe normal to the tunnel axis. The distances normal to the convex surface were subsequently calculated. The likely errors in the mean velocity due to traversing vertically on the convex surface were assessed and found to be small. Details of the error assessment are presented in Appendix C.

3.4.3 WALL SHEAR STRESS MEASUREMENTS

The mean and the fluctuating wall shear stress were measured using hot-film gauges (No. WTG-50, Micro Measurements, USA) having a cold resistance of 50Ω, connected to the same DISA CTA used for hot-wire measurements.

In the application of hot-films to the present work on relaminarization on a convex surface, two aspects required careful attention. The first involves the difficulty associated with calibrating the gages on a convex surface. The second requirement is that the calibration should be valid for measuring wall shear stress in both laminar and turbulent boundary layer regimes. The procedures adopted to meet the above requirements are described below.

There are several difficulties encountered in the in-situ calibration of the hot-film gages on the convex surface. Primarily, one does not know the exact nature of the law

of the wall on the convex surface, and secondly each gage has to be independently calibrated. It was therefore decided that the turbulent boundary layer on the flat plate (ahead of the convex surface) be utilized for calibration. This necessitated that hot-films be bonded on cylindrical plugs (of low thermal conductivity like Teflon) and moved to different locations on the model for measurement. This method had the added advantage that measurements at different locations could be done with a single film.

Cylindrical plugs 14mmϕ made of Teflon were utilized for mounting the films; other unused holes were closed with dummy plugs. The use of flat top plugs was feasible as the radius of curvature of the convex test surface was large (0.966m) compared to the plug dimensions. As seen in Fig.3.8, the discontinuity ($\cong$0.03mm) is negligible being well within the laminar sub-layer. As we shall see in Sec.4.5, this procedure did provide very reliable measurements of shear stress on the convex surface. The gage locations for the convex and flat surface experiments are listed in Tables 3.6 and 3.7 respectively.

In order that the hot-film gage can be used with a common calibration for both laminar and turbulent boundary layers, it is necessary that the thermal boundary layer formed by the heated gage is well within the viscous sub-layer (Liepmann & Skinner [1954]). Experiments made by Subaschandar [1996] using similar hot films showed that the calibration was the same for both laminar and turbulent boundary layers up to an overheat ratio of 1.20. Based on these observations, an overheat ratio of 1.20 was adopted for all the wall shear stress measurements.

Two hot-film gages were calibrated in the zero pressure-gradient turbulent boundary layer present on the upstream flat surface at x = 0.76m. These gages were utilized for the measurement of wall shear stress in the convex as well as flat surface relaminarization experiments. The results from both gages showed good consistency and repeatability of the wall shear stress.

For the calibration of the hot films, the existence of the standard law of the wall was first established at different velocities on the flat surface (x = 0.76m). It was ensured that the range of freestream velocities used covered the range of shear stress expected in the both the turbulent and relaminarized regions of the flow. Sample plots of the measured velocity profiles are shown in Fig.3.9 and a typical calibration plot of the hot film is given in Fig.3.10. Details of the calibration procedure used and the care taken during the shear stress measurements are discussed in Appendix D.

3.5 Data Acquisition and Processing

All the measured data were logged into a personal computer through a 16-channel ADC card installed in it using C programs written for specific purposes (Krishnan et al [1998]). During measurement of mean parameters, the program sequentially acquired data at 100 samples/second for 10 seconds and calculated the mean. The data from the pressure transducer and the CTA were normalized with the tunnel dynamic pressure and freestream velocity respectively. The instantaneous signals from hot-wire and hot-film anemometers were acquired at a rate of 4kHz and 2kHz respectively for 15 seconds; this was based on a preliminary analysis of the spectral content of the signals, which showed that more than 95% of the energy content was within 2kHz and 1 kHz for the two gages respectively.

3.6 Test flows documented

Three different flows CP1, DP1 and CP2 on the convex surface and one flow FP1 on the flat surface were documented using the appropriate pressure-generator airfoils designed as in Sec.3.3.3. Detailed measurements made for flows CP1, DP1 and FP1 consisted of surface pressure, streamwise velocity and turbulent intensity profiles in the boundary layer and the wall shear stress. In the case of flow CP2, only surface pressure and wall shear stress measurements were made.

3.6.1 Features of the upstream flat plate boundary layer

The boundary layer developing on the flat plate just ahead of acceleration and convex curvature was used as a reference flow in all experiments. The location chosen was at x=0.76m for the convex surface experiments and at x=0.84m for the flat surface experiments. The mean velocity profiles at the respective reference locations plotted both in linear and log-law scales are presented in Fig.3.11 for CP1 & DP1 and in Fig.3.12 for FP1. The results show that the boundary layer is fairly well developed to a standard log-law. Some of the boundary layer parameters are listed in Table 3.8.

Table 3.8 Features of the Initial boundary layer

Flow	Surface	U_∞, m/s	U_o, m/s	δ_o, mm	$k\delta_o$	$R_{\theta o}$
CP1	Convex	9.6	11.3	26.5	0.0275	1710
DP1	Convex	9.6	11.3	26.5	0.0275	1710
CP2	Convex	13.0	not measured		$\cong$ 0.0275	$\cong$ 2000
FP1	Flat	12.5	11.72	24.1	---	1670

3.6.2 SURFACE PRESSURE DISTRIBUTIONS

The streamwise variations of the surface static pressure coefficient, C_p, for the three convex surface flows are shown in Fig.3.13. For the three test cases, the pressure is essentially constant on the flat portion of the model, decreases to different levels and is followed by a zone of adverse pressure gradient. It may be observed that the magnitude of the mean pressure gradient as well as the minimum pressure levels ($C_{p,min}$) reached for each flow are different. The figure also shows that the value of $C_{p,min}$ reached in CP1 is lower compared to DP1, with CP2 being the least.

Based on the measured C_p distributions and the freestream velocity U_∞ (tabulated in Table 3.8), the acceleration parameter K (Eqn2.1) of Launder [1964], the acceleration parameter K^* (Eqn2.3) of Brandt [1993], and the pressure gradient parameter Λ (Eqn2.4) of Narasimha and Sreenivasan [1973] were calculated. For the initial estimates of Λ, the thickness of the boundary layer was obtained from a turbulent boundary layer calculation method (Desai & Kiske [1982]). These parameters are plotted in Fig.3.14 - 3.16 for the three convex flows and the maximum values these parameters attained are tabulated in Table 3.9; also tabulated are the respective critical values suggested for relaminarization on a flat plate. The figures and the table show that all the different acceleration parameters are much above critical values for CP1 and CP2, being very high in flow CP2. In the case of DP1, K and Λ are just about critical, while K^* is less than critical.

Table 3.9 The acceleration and related parameters in the experiments

Flow	**Surface**	***Free-stream velocity*** U_∞, m/s	$C_{p,min}$	x_a/δ_o	K_{max} x10^6	$I(K)$ x10^6	K^*_{max} x10^6	Λ_{max}
Flat plate critical values	Flat	----	----	---	≅3.5	----	≅8.1	≅50
CP1	Convex	9.6	-4.74	10	6.2	30.1	13.4	158
DP1	Convex	9.6	-4.15	14	3.8	29.2	6.4	58
CP2	Convex	13.0	-6.07	7	9.0	29.1	30.0	325
FP1	Flat	12.5	-3.35	12	6.2	34.0	16.4	159

Table 3.9 also shows the distance x_a/δ_o, (which is the normalized streamwise extent of acceleration). The variation of K with x_a/δ_o is shown in Fig.3.17 for all the flows. As required in the present experiments, the duration of acceleration is much lower ($<14\delta_o$) for all the four flows in comparison with some of the flat-plate

relaminarizing flow experiments from the literature (shown in Fig.3.2). The area under each curve in Fig.3.16 (i.e., $I(K)$ of Eqn.3.1) is also about the same (see Table 3.9) for the three convex surface flows.

As mentioned earlier, the flat plate flow FP1 was designed to match the distribution of C_p and K with those for the convex surface flow CP1. Fig.3.18 shows the streamwise variation of C_p, K and Λ for FP1; their respective maximum values (Table 3.9) are much above critical and are comparable with those for CP1. A comparison of C_p for FP1 and CP1 is shown in Fig.3.19. The plots have been shifted on both abscissa and the ordinate to match the location of $C_{p,min}$ and the initial flat surface static pressure respectively. After several iterations, a good degree of C_p match, except around $C_{p,min}$, has been obtained. Unfortunately the matching is unsatisfactory close to $C_{p,min}$ and could not be improved. Nevertheless, the streamwise variation of K (Fig.3.20) shows a good comparison with CP1. As discussed in Sec.3.2, it is more relevant to match the K variation rather than exactly matching C_p.

3.7 Measurement Uncertainties

The uncertainties of the different measurements made were estimated using data from the specifications of the instrument manufacturer, from calibration curves and from repeatability tests. The overall uncertainty for each measurement was evaluated by the method suggested by Kline & McClintock [1953], using the uncertainty components of errors. For various measurements made the overall uncertainties estimated are as follows.

$\Delta C_p \leq \pm 0.02 \times C_p$

$\Delta u \leq \pm 0.025 \times u$

$\Delta u' \leq \pm 0.04 \times u'$

$\Delta C_f \leq \pm 0.08 \times C_f$

3.8 Mean Flow Two-Dimensionality

The two-dimensionality of the flow was assessed by two methods as follows.

3.8.1 Spanwise pressure distribution

Fig.3.20 shows the results of measured C_p distribution over the central mid-span of the model at some specific streamwise locations for CP1, DP1 and FP1 respectively. In general, it may be observed that the spanwise uniformity over the central quarter of the model span is very good (being comparable to the measurement accuracy of C_p addressed in the previous section). While the maximum difference about the centerline

is about 5% over the central halfspan, larger deviations are noticed in the adverse pressure gradient for DP1 and FP1.

3.8.2 2D Momentum Integral Balance

The two-dimensional momentum integral equation provides a tool for checking the two-dimensionality of the mean flow in the boundary layer. For a flat plate boundary layer, the equation can be expressed in the form

$$\theta_x = \theta_{xi} + \int_{x_i}^{x} \left[\frac{c_f}{2} - (H+2)\frac{\theta}{U}\left(\frac{dU}{dx}\right) \right] dx \qquad \ldots 3.4$$

where θ_{xi} denotes the value of θ at the initial x station. Here, all quantities on the right side are taken from measurements and the left side term θ_x is calculated and compared with the measured value.

For assessing the momentum integral balance in the context of the convex surface flows, the above equation has been used as an approximation, with streamwise distances measured along the curved wall. As will be discussed in detail in Sec.4.3, a mild normal gradient was observed in the potential velocity distribution outside the boundary layer, which was apparently caused by the pressure-generator airfoil present in the vicinity of the convex surface. However, for the purpose of establishing the mean flow two-dimensionality, these small velocity gradients have been neglected and the velocity calculated from the surface pressure has been used for normalizing the wall shear stress (measured using hot-films) and also for the determination of the streamwise velocity gradient *dU/dx*. Further, as will be discussed in detail in Sec.4.3, after evaluating the integral parameters δ^* and θ using two different definitions, it was decided to adopt the curved wall definition; and the same definition has been adopted in the present calculations as well.

The comparisons of the calculated values of the momentum thickness with the experiments are presented in Fig.3.21-3.23 for CP1, DP1 and FP1 respectively. The results show that the momentum balance is maintained in all the three flows except in certain zones in flows CP1 and DP1, which can be partly attributed to difficulties in differentiating the experimentally measured edge velocities from different profiles. The satisfactory overall predictions of the momentum equation confirm the two dimensionality of the mean flow in the central span region.

CHAPTER 4

Experimental Results

4.1 Introduction

The results of the measurements made on the convex surface (CP1, DP1 and CP2) and on the flat surface (FP1) are presented in this chapter. The mean flow parameters are presented first, followed by a presentation of turbulence intensity profiles and the fluctuations of velocity and shear stress.

Before presenting the results, it is considered appropriate to introduce some flow features and list certain assumptions made so as to understand the results in the right perspective. In the convex surface experiments, the presence of the airfoil-like body, used for accelerating the flow, introduced a weak positive gradient of the streamwise velocity at the edge of the boundary layer at certain locations in the acceleration region; this is in contrast with a negative velocity gradient that would be normally expected in the presence of convex curvature alone (in the absence of the body). This is possibly caused by the combination of the proximity of the pressure-generator airfoil and the convex surface. As a result, there is some difficulty in using the standard definitions for the estimation of the integral thickness parameters, for which knowledge of the inviscid potential velocity $U_p(y)$ in the immediate neighborhood of the surface is required.

In view of the above feature, certain approximations within the frame work of boundary layer theory have been made for the evaluation of the boundary layer thickness parameters (both total and integral) required for the analysis of the data and for comparison with quasi-laminar calculations. The approximations are needed essentially to take care of the observed velocity-gradient along the normal to the surface at the edge of the boundary layer, and of the small velocity differences that arise at certain streamwise locations, between the measured values at the edge of the boundary layer (U_e) and those calculated from the measured wall pressures (U); this feature is illustrated for CP1 and DP1 in Fig.4.1. Except in the neighborhood of the

location of $C_{p,min}$, the agreement between the values of the two velocities are within the experimental scatter of the hot-wire measurement. While the potential flow velocity field between the curved surface and the pressure-generator airfoil could in principle be computed (e.g. using a panel code), such an attempt would be inadequate as it has to account for viscous effects (present in the experiments) on all surfaces involved to be useful. This would be a major effort in itself and is hence beyond the scope of this work.

We have basically defined two strategies to analyze the present experimental data on curved surfaces. Two definitions for the evaluation of the boundary layer integral thickness parameters, with and without taking into account the observed velocity variation at the edge of the boundary layer, have been explored and discussed in detail in Sec.4.2. The measured wall pressure distributions have been consistently used for the calculation of the curved flows using quasi-laminar equations and for the calculation of the momentum integral equation discussed in Sec.3.8.2.

4.2 Mean velocity profiles

4.2.1 FLOW CP1

The boundary layer streamwise mean-velocity profiles measured using a hot-wire at different x locations are presented in Fig.4.2a - 4.2c for CP1. The inset shows a plot of U/U_o (U_o being the edge velocity in the upstream constant pressure region at x = 0.8m), with symbols for the points in the inset being the same as those used in the profile plots at the respective streamwise locations.

As discussed in the previous section, a weak positive normal velocity-gradient may be observed at certain stations at the edge of the boundary layer along the convex surface. Since the velocity variation seems linear, a tangent is drawn through this data as shown in the figures. The edge of the boundary layer (marked in the figures with a small horizontal line) is defined to be at the point $y=\delta$, where the velocity profile data differs from the tangent drawn by 1%.

The mean-velocity profiles in the favorable pressure gradient region for CP1 (Fig.4.2a) show features typical of accelerated turbulent boundary layers involving a large reduction in the boundary layer thickness accompanied by a fuller velocity distribution close to the wall. In the beginning of the adverse pressure gradient region (Fig.4.2b), the boundary layer thickness remains nearly constant and the profiles

exhibit some degree of retardation near the wall. Further downstream (Fig.4.2c) the profiles show typical effects of an adverse pressure gradient, including an increase in the boundary layer thickness.

4.2.2 FLOW DP1

The mean velocity profiles for DP1, plotted (Fig.4.3a - 4.3b) in a manner similar to CP1, show features qualitatively similar to those observed for CP1. However, it may be observed in Fig.4.3a that the drop in the boundary layer thickness during acceleration appears to be more pronounced compared to CP1, possibly due to increased duration of acceleration in DP1. Also, the boundary layer thickness starts increasing right from the $C_{p,min}$ location unlike CP1. The gradient of the velocity outside the boundary layer in the adverse pressure gradient region (Fig.4.3b) is more prominent in DP1.

4.2.3 FLOW FP1

The mean velocity profiles for the flat surface flow FP1 (Fig.4.4a - 4.4c) show that the streamwise trends of the profiles are similar to CP1 and DP1 and do not show any velocity gradient outside the boundary layer in spite of the presence of the airfoil. As in CP1, the boundary thickness is nearly constant in the initial region of adverse pressure gradient.

4.3 Boundary layer parameters - definitions

The definitions of the integral thickness parameters usually adopted for curved surface boundary layers are (from So & Mellor [1972])

Displacement thickness $$\delta^* = \int_0^{\delta} \left(1 - \frac{u}{U_p}\right) dy \qquad \ldots 4.1$$

Momentum thickness $$\theta = \int_0^{\delta} \frac{u}{U_p}\left(1 - \frac{u}{U_p}\right) dy \qquad \ldots 4.2$$

Shape Factor $$H = \delta^*/\theta \qquad \ldots 4.3$$

Momentum thickness Reynolds number $$R_\theta = \frac{U_e \theta}{\nu} \qquad \ldots 4.4$$

where u =u(y) is the measured velocity and $U_p(y)$ is the potential velocity.

As mentioned in Sec. 4.1, we adopt two definitions for the potential velocity $U_p(y)$ as follows. The two definitions are graphically depicted in Fig.4.5.

1. CURVED SURFACE definition : $U_p(y)$ is assumed to be the linear extrapolation to the wall of the tangent at the edge of the boundary layer at each x station.

2. FLAT SURFACE definition : U_p is assumed to be a constant for the boundary layer profile and equal to the velocity U_e at the edge of the boundary layer.

4.4 Boundary layer parameters – results for CP1

The streamwise variations of different mean flow parameters in the boundary layer for CP1 are presented in Fig. 4.6a,b; the thickness related parameters δ, δ^*, θ and R_θ are in part (a) of the figure while C_f and H are in part (b). The plots of δ^*, θ, R_θ, and H contain estimates using both the curved and flat surface definitions and since these agree very well with each other, only the curved surface definition will be used in future. The plots also indicate the locations of K_{max}, Λ_{max}, $C_{p,min}$ and of the beginning of curvature.

In general, all these plots depict variations typical of highly accelerated turbulent boundary layers leading to relaminarization as may be observed in the results of Blackwelder & Kovasznay [1972] replotted in Fig.2.2.

4.4.1 THICKNESS RELATED PARAMETERS – CP1

Fig.4.6a shows a progressive decrease of the thickness parameters δ, δ^*, θ and R_θ in the favorable pressure gradient region. In the beginning of the adverse pressure gradient δ and θ become nearly constant, while an increasing trend is observed for δ^*. Further downstream, all the three parameters show considerable increase due to the adverse pressure gradient. The variation of R_θ is similar to that of θ in spite of high acceleration and deceleration.

4.4.2 SKIN FRICTION COEFFICIENT– CP1

The streamwise variation of C_f for CP1 is shown in Fig.4.6b. The initial increase of C_f is an effect of the favorable pressure gradient on the turbulent boundary layer. As the flow accelerates further, C_f reaches a peak and thereafter progressively decreases to relatively low values indicating relaminarization. It is noticed that the change in C_f in the region beyond the $C_{p,min}$ location and before the start of the adverse pressure

gradient is small. This indicates that retransition has not occurred at the $C_{p,min}$ location but is postponed. Brandt [1993] had observed a similar feature in his flat plate relaminarization experiments A1, A2, A3 and B1, sample plots of which are shown in Fig.2.5. As the adverse pressure gradient increases downstream, C_f rapidly increases, reaching a second peak, indicating retransition. The decrease that follows is the effect of the adverse pressure gradient on the newly formed turbulent boundary layer.

The four regions discussed, namely, the turbulent boundary layer in favorable pressure gradient, the relaminarization zone, the retransition zone, and the turbulent boundary layer in adverse pressure gradient are marked approximately in Fig.4.6b.

4.4.3 SHAPE FACTOR – CP1

It is noticed in Fig.4.6b that H decreases from its initial value of about 1.45 as a consequence of the turbulent boundary layer developing in favorable pressure gradient. The shape factor continues to decrease in the initial zone of relaminarization, and starts increasing from around the location of $C_{p,min}$, which is also a region of constant C_f. The shape factor continues to increase in the retransition zone, as opposed to an expected decreasing trend, possibly due to the following reasons.

- The increase in H may be reflecting the residual or relaxing effects of relaminarization in the initial region of adverse pressure gradient.
- While the flow near the wall is undergoing retransition (as inferred by the C_f rise), the outer part of the boundary layer may be responding to the adverse pressure gradient without being affected by the onset of retransition.

Further downstream, having reached a peak of about 2.2, H decreases sharply due to retransition. The shape factor increases again, indicating the development of the post-retransition turbulent boundary layer in the adverse pressure gradient. It may be noticed that the identification of retransition from the increase of C_f from its minimum and the decrease of H from its maximum are at distinctly different locations here. This is possibly because the identification of retransition based on C_f reflects near wall effects while that based on H is the overall response of the boundary layer.

4.5 Boundary layer parameters – results for DP1

The streamwise variation of the boundary layer parameters for DP1 are presented in Fig. 4.7 a,b in a manner similar to those for CP1. Results as per the two

definitions for δ, δ^*, θ, R_θ and H have been plotted in the figures and since the two definitions show good agreement (as in CP1), only the curved surface definition will be used in future.

The overall picture of the streamwise variation of these parameters is qualitatively similar to those for CP1 showing features of relaminarization.

4.5.1 THICKNESS RELATED PARAMETERS – DP1

Fig.4.7a shows that the three thickness parameters initially decrease in the favorable pressure gradient region in a manner similar to CP1. Since the fall in K following its maximum value is more gradual and extends over a larger distance (about 40% more) than CP1, all the three thickness parameters for DP1 show a reduction to relatively lower values as compared to CP1. The variation of R_θ also follows the same trend as CP1 but drops down to much lower values.

4.5.2 SKIN FRICTION COEFFICIENT– DP1

Fig.4.7b shows that the variation of C_f follows a trend similar to that in CP1; thus there is an initial increase due to the imposed favorable pressure gradient, a drop indicating relaminarization, an increase further downstream due to retransition and the final reduction due to the effect of the adverse pressure gradient on the newly formed turbulent boundary layer. All these features are also marked in the figure. However, the following differences may be observed. The gradient of C_f during the initial rise and the drop further downstream is lower as compared to CP1; this is consistent with the lower pressure gradient in DP1. In spite of this, $C_{f,min}$ seems to be lower than in CP1, perhaps because of the longer zone of acceleration.

4.5.3 SHAPE FACTOR – DP1

Fig.4.7b shows that the qualitative trend of H in DP1 is similar to that in CP1. The initial reduction of H is less prominent compared with the CP1 results, consistent with the lower favorable pressure gradient in DP1. As in CP1, a large part of the increase in H downstream of the location of $C_{p,min}$, where the adverse pressure gradient is still small. There seems to be a better agreement between the locations of the start and end of retransition as could be judged from C_f and H variations.

4.6 Boundary layer parameters – results for CP2

In flow CP2, the boundary layer profiles were not measured and hence only the C_f results are presented.

4.6.1 Skin friction coefficient– CP2

Fig.4.8 shows the streamwise variation of C_f for CP2; the results are qualitatively similar to that in CP1. The sharp decrease in C_f and very low value of $C_{f,min}$ achieved ($\cong$0.0002) are indications of relaminarization occurring in spite of a very short extent of the acceleration zone ($\cong 7\delta_o$). Unlike in CP1, it is noticed in the figure that C_f continues to drop after the $C_{p,min}$ location.

4.7 Boundary layer parameters – results for flat surface flow FP1

The streamwise variation of the boundary layer parameters for FP1 are presented in a manner similar those of CP1 in Fig.4.9 a,b. Like the two convex surface flows CP1 and DP1, this flow also shows evidence of relaminarization.

4.7.1 Thickness related parameters – FP1

The boundary layer thickness (Fig.4.9a) shows a trend similar to as CP1 and reaches a minimum value (nearly the same as in CP1) consistent with the effect of similar acceleration in both flows. The trends of parameters δ^*, θ and R_θ are also qualitatively similar to those in CP1.

4.7.2 The skin friction coefficient– FP1

Fig.4.9b shows that the variation of C_f for FP1 and is qualitatively similar to that in CP1, but the decrease of C_f in FP1 is not as steep as in CP1. The minimum values of C_f reached at the end of relaminarization are nearly the same in both flows. The more rapid drop of C_f for CP1 compared to FP1 can be clearly attributed to the effect of convex curvature in promoting relaminarization.

4.7.3 The shape factor – FP1

The streamwise variation of H (Fig.4.9b) is qualitatively similar to that in CP1; however, after having decreased initially, H becomes nearly constant after the location of K_{max}. As in CP1, H increases in the region beyond $C_{p,min}$ location. Even though the K variation is matched in FP1 and CP1, the minimum value of H reached in the favorable

pressure gradient is higher and the maximum value reached later is lower in FP1 compared to CP1. These can be attributed to effects of curvature in CP1. As in CP1, the identification of the locations of retransition from C_f and H_{max} values is slightly different probably due to the narrow zones of strong acceleration.

4.8 Boundary layer profiles in wall coordinates

The velocity profiles plotted in wall coordinates are sensitive individually to both pressure gradient and surface curvature as discussed in the literature survey in Chapter 2. Hence, while interpreting the profile data, it is appropriate to keep in mind the individual effects of the pressure gradient and curvature.

4.8.1 FLOW CP1

The measured velocity profiles are plotted in wall coordinates in Fig.4.10a - 4.10d for CP1; separated as per the four regions demarcated in the C_f plot of Fig.4.6b. The friction velocity u^* has been consistently derived from the interpolated values of the measured hot-film skin friction data. The interpolated values in the retransition zone, where a large change takes place in a short distance, is matter of judgement and might contain errors, but it has been found that the errors can only shift the profile in the plot and do not affect the shape of the profile.

The plots in Fig.4.10 contain small vertical lines indicating the edge of the boundary layer and also contain the reference log-line. The inset shows plots of U/U_o and C_f, with symbols of the points in the inset being the same as those used in the profile plots at respective streamwise locations.

In the favorable pressure gradient region (Fig.4.10a), the wake component diminishes and eventually goes below the reference log-line. Such a trend is typical of accelerated turbulent boundary layers (Fernholz & Warnack [1998]). The law of the wall has virtually disappeared at x = 1.085m, which is midway in the favorable pressure gradient zone. The disappearance of log-law is typical of relaminarizing boundary layers (as shown in Fig.2.2 from Warnack & Fernholz [1998]).

In the relaminarization zone (Fig.4.10b), C_f starts dropping (see the inset plot) and so does u^*. This results in the upward shift of the profiles on the u^+ axis with downstream distance. The effect of the weak pressure gradient at the edge of the

boundary layer is clearly seen. The figures show features more related to the acceleration effects than those of convex curvature.

In the retransition zone (Fig.4.10c), the profiles shift downwards on the u^+ scale towards the reference log-line, consistent with the increase in u^*. In the adverse pressure gradient region far downstream, especially at the last station (Fig.4.10d), the profile shows a tendency to redevelop a logarithmic region.

4.8.2 FLOW DP1

The boundary layer velocity profiles in wall coordinates (Fig.4.11) for DP1 are plotted in a manner similar to CP1. The results are qualitatively similar to CP1; however, the outer region that develops after the break-down of the law-of-the-wall is less thick in the y^+ scale, and the inner region extends over higher u^+ coordinates, as compared to CP1.

4.8.3 FLOW FP1

The boundary layer velocity profiles in wall coordinates (Fig.4.12) for FP1 are qualitatively similar to those in CP1. Here also, the outer region seems to be more prominent as in CP1.

4.9 Streamwise turbulence intensity profiles

4.9.1 THE INITIAL BOUNDARY LAYER

Fig.4.13 shows the profiles of the streamwise turbulence intensity u' for the initial zero-pressure-gradient turbulent boundary layer on the flat surface for flows CP1, DP1 and FP1. As may be seen, the present results show features typical of the turbulent boundary layer in zero pressure-gradient and are broadly consistent with the results of Klebanoff [1955].

4.9.2 FLOW CP1

The streamwise variation of the turbulence intensity profile is presented in Fig. 4.14a - 4.14d for CP1. The symbols used for each profile are also shown in the inset plot of U/U_o at respective x locations.

In the acceleration region (Fig.4.14a), the turbulence intensities in the outer 90% of the boundary layer reduce rapidly, with significant reduction at x = 1.085m and

1.125m. This reduction is typical of relaminarization by acceleration (as seen in Fig.2.3, data of Blackwelder & Kovasznay [1972]). Since turbulence intensities also decrease in convex surface boundary layers (as observed in Fig.2.14a, data of So & Mellor [1973]), the observed is a combined effect of the two.

Some reduction in the turbulence intensities in the inner 10% of the boundary layer is also evident. The profiles also seem to show two distinct inner and outer regions: the outer region is almost flat with very low turbulence intensities, while the inner region still has significant turbulence fluctuations. Due to lack of data very close to the wall, the peak values have not been picked up in the measurements.

Fig.4.14b shows the turbulence intensity profiles for the region in-and-around the $C_{p,min}$ location, where it may be observed that the inner region shows an increase in the turbulence intensity and the outer region is hardly affected. The peak is now visible and is progressively moving outwards as the pressure gradient is relieved.

Fig.4.14c shows the turbulence intensity profiles for the adverse pressure-gradient region; these stations are downstream of the location $C_{f,max}$ (in Fig.4.6b), which is the location of the end of retransition. It is noticed here that the peak value decreases with distance, while its location moves out in the boundary layer, and that the changes in profile beyond 0.6δ are negligible. The decreasing trend of the peak value of the turbulence intensities is in contrast with the feature normally expected for a turbulent boundary layer in adverse pressure gradient.

As discussed in Chapter 2, since relaminarization essentially involves two layers, namely the inner laminar and the outer rotational inviscid layers, the entire boundary layer does not quickly respond to the wall layer alone undergoing retransition. These results suggest that even in the presence of the adverse pressure gradient, the nearly de-coupled layers of the relaminarized boundary layer are not behaving like a 'single' turbulent layer for some distance. This behavior might have also been aided by convex curvature which tends to suppress turbulence in the outer boundary layer. At the last station at x = 1.30m (Fig. 4.14d), the plot shows the expected behavior of a typical turbulent boundary layer in adverse pressure-gradient by having increased intensities all across the boundary layer, including a peak value which has moved outwards.

4.9.3 FLOW DP1

The streamwise turbulence intensity profiles for DP1 are presented in Fig.4.15a - 4.15c. The results show many features broadly similar to those of CP1. Fig.4.15a shows a small increase in the outer 90% of the boundary layer at x = 0.95m (which may be an effect of the sudden change in the wall boundary condition from flat to convex curvature). At x = 1.1m the turbulence intensities are reduced throughout the boundary layer and are qualitatively similar to those in CP1. Fig.4.15b shows the turbulence intensity profiles for a region in-and-around the $C_{p,min}$ location. As in CP1, the peak is now progressively growing and moving outwards - a process that continues up to x = 1.32m. Further into the adverse pressure gradient (Fig.4.15c), the turbulent boundary layer is showing the expected behavior (as in the last station in CP1, Fig. 4.14d) by having increased intensities all across the boundary layer, including a peak which has moved outwards.

4.9.4 FLOW FP1

The streamwise turbulence intensity profiles for FP1 (Fig. 4.16a - 4.16c) show that the development of the profiles is qualitatively similar to that in CP1, with large reduction of the turbulence intensities in the outer region during acceleration (Fig.4.16a). The peak value of the intensities in the inner region in the zone in-and-around the $C_{p,min}$ location increases, while there is no change in the outer region (Fig.4.16b). There is a reduction of the peak value and flattening of the inner-region profile in the adverse pressure gradient (Fig.4.16c). Even at the last measured station (Fig.4.16c) the outer layer intensities have not increased much.

4.10 Features of turbulence and shear stress fluctuations

The boundary layer streamwise velocity and wall shear-stress fluctuations can provide useful information on flows undergoing transition to turbulence or relaminarization. In what follows, selected time traces and spectra of hot-wire and hot-film data are presented for CP1, DP1 and FP1. Only hot-film data are presented for CP2, since hot-wire measurements were not made for this flow.

All the hot-wire measurements were made using a single probe; the calibration constants for several tungsten wires used were nearly the same (maximum difference in the constants were < 6%), and all the data were acquired with the same amplifier gain. In view of this, the voltage fluctuations can be considered to represent the

velocity fluctuations to approximately the same scale for all the flows, and hence relative comparisons can be made. Similarly, since a single hot-film gage was used for the entire series of the experiments, the voltage fluctuations from these measurements represent the shear-stress fluctuations to the same scale for all the flows enabling comparisons between data sets.

4.10.1 FLOW CP1

The time trace of the streamwise-velocity fluctuation data in the near-wall region (y < 0.6mm) is shown for selected stations in Fig.4.17; also included in the figure is a plot of the streamwise variation of U/U_o with the hot-wire locations shown.

The fluctuation at the initial station (x=0.885m) is typical of a turbulent boundary layer. As the flow accelerates, a progressive quenching of turbulence is observed, with the intensities reaching a minimum at x=1.125m. Such quenching is typical of relaminarizing boundary layers (Badri Narayanan & Ramjee [1969]). At the $C_{p,min}$ location (x=1.145m), the amplitude starts increasing and continues downstream in the adverse pressure gradient region indicating retransition.

The power spectral density (p.s.d.) distributions of the velocity fluctuation data at selected streamwise stations show (Fig.4.18) that, in the acceleration region, there is an appreciable reduction of the energy levels, especially at lower frequencies. Maximum reduction in energy is seen in the streamwise zone x=1.085 - 1.125m. Further downstream, at the $C_{p,min}$ location of x=1.145m, the energy levels increase significantly in response to the relief in the favorable pressure gradient.

The time-trace and the spectra of the shear-stress fluctuations are shown in Fig.4.19, 4.20 respectively, plotted in the same format as the hot-wire data, these plots show features similar to the observations from the hot-wire data. Here also, a significant quenching is observed in the time trace data (Fig.4.19); the amplitudes reach a minimum at x = 1.085m, remain low up to x=1.148m and increase further downstream indicating retransition. The spectra (Fig.4.20) also show substantial decrease in the energy levels during acceleration. Unlike the hot-wire data, the reduced intensity levels of the skin friction fluctuations continue even up to the location of $C_{p,min}$, suggesting that the wall layer following relaminarization is responding slowly to the relief in the favorable pressure gradient.

4.10.2 FLOW DP1

The time-trace of the velocity fluctuations for DP1 (Fig.4.21), while being broadly similar to those in CP1, shows relatively reduced quenching consistent with the lower pressure gradient in this flow. The spectra (Fig.4.22) show minor differences (consistent with the time trace data) until about the end of acceleration (x = 1.2m), where significant reductions at very low frequencies are observed. These effects are moderate when compared to CP1, consistent with the lower pressure gradients.

In contrast to the velocity data, the shear-stress fluctuations (Fig.4.23) and the associated spectra (Fig.4.24) show considerable quenching during acceleration, especially at lower frequencies, being qualitatively similar to that in CP1.

4.10.3 FLOW CP2

In flow CP2, involving the highest acceleration applied over the shortest distance in the present experiments, we see that the quenching of the shear-stress amplitudes (Fig.4.25) as well as the reduction in the energies at lower frequencies in the spectra (Fig.4.26) are even more spectacular than those observed in CP1; the minimum level reached is about one-tenth of the initial energy. It is interesting that the quenching is so dramatic in spite of the short duration of the favorable pressure gradient, which must be a result of the combined effects of high acceleration and convex surface curvature.

4.10.4 FLOW FP1

The time traces of the velocity fluctuations for FP1 (Fig.4.27) are qualitatively similar to those of CP1. However, the spectra (Fig.4.28) show that the reduction of the turbulence energy is gradual in FP1 as compared to CP1 and the minimum level reached is much higher than in CP1 (being nearly double). The shear-stress fluctuation plots of the time-trace (Fig.4.29) and the spectra (Fig.4.30) are qualitatively similar to those in CP1, suggesting that the wall layers are largely affected by the pressure gradient, which are almost identical in the two flows.

4.11 Discussion

Having presented the experimental results of CP1, CP2 and DP1 developing under the combined action of acceleration and convex surface curvature, and the results of the flat surface flow FP1, it is now appropriate to consolidate the results and assess the effects of surface curvature and pressure gradient history on

relaminarization. Keeping in view the difficulties associated with characterizing a relaminarizing flow, an attempt will be made to analyze the results on the basis of certain important events associated with relaminarization that have actually occurred in these flows. These events include a significant drop in the skin friction coefficient, an increase of H towards laminar values, and a remarkable reduction of the turbulence intensities and shear stress fluctuations.

4.11.1 ASSESSMENT OF CONVEX CURVATURE EFFECTS

In order to understand the convex curvature effects, we will directly compare the experimental results of CP1 and FP1, since both flows have the same initial conditions and acceleration history.

MEAN FLOW PARAMETERS

A comparison plot of C_f for CP1 and FP1 (FIg.4.31) shows that the variation of C_f in the initial turbulent boundary layer in response to acceleration is very similar in both flows. However, the maximum value of C_f attained in the neighborhood of K_{max} and Λ_{max} locations is somewhat higher for CP1. In the relaminarization region, the drop in Cf is more rapid in CP1 as compared to FP1. The rapid fall in C_f for CP1 may therefore be attributed to the effects of convex curvature. Further support to this view will also be discussed in the context of the quasi-laminar solutions for the two flows in Chapter 5.

The shape factor H rises steeply to a value exceeding 2.1 in CP1 (Fig.4.6b), in contrast with a very small rise noticed in FP1 (Fig.4.9b). Even DP1 also showed relatively higher values of H_{max} (>2.0) in spite of having lower favorable pressure gradients as compared to FP1. The above feature suggests that both CP1 and DP1 have attained relatively higher degree of relaminarization influenced primarily by convex curvature.

The minimum values of δ^*, θ and R_θ reached at the end of relaminarization are lower for CP1 as compared to FP1, implying a higher degree of relaminarization, again attributable to curvature effects.

TURBULENCE PARAMETERS

We have already discussed the turbulence intensity profiles for CP1 and FP1 (Fig.4.14 and Fig.4.16 respectively). A quantitative comparison of the streamwise development of the turbulence intensities, normalized with the respective values at the

beginning of acceleration, is now shown in Fig.4.32a - 4.32c for y/δ of 0.1, 0.2 and 0.5 respectively. The streamwise distance x_a is measured from the beginning of acceleration.

As the flow accelerates with streamwise distance, the turbulence intensities in CP1 are not only lower but also decrease at a faster rate than FP1 at all the y/δ plotted. In fact, the turbulence intensity in FP1 shows hardly any reduction in the initial stage at y/δ = 0.5. The differences are as high as about 20% at x_a = 0.225 and y/δ = 0.1. At the end of the favorable pressure gradient, the turbulence intensities at y/δ = 0.1 for CP1 is much lower (about 50%) than the value for FP1. The large reduction in the turbulence intensities observed in CP1 with respect to FP1 is due to the influence of convex curvature in CP1. It is unlikely that the small mismatch in the pressure distribution around the location of $C_{p,min}$ between CP1 and FP1 (Fig.3.19) would affect the conclusions drawn here.

A comparison of the velocity spectra for CP1 and FP1 (Fig.4.18 and Fig.4.28) shows that the reduction of the turbulence energy in the lower frequencies in CP1 is very early and abrupt reaching a much lower value (less than 50%) than that attained in FP1. This may be seen as an effect of convex curvature in CP1.

In summary, the mean and the turbulence features discussed above indicate the strong effect of convex curvature resulting in the higher degree of relaminarization of CP1. The observed effects are consistent with the stabilizing influence of convex curvature on turbulence in zero pressure-gradient flows. Our expectation that the effect of convex curvature in promoting relaminarization while acting in combination with acceleration is well brought out in the above results.

4.11.2 Assessment of pressure history effects

It is very informative to assess if the changes in the boundary layer properties, particularly during the later stages of relaminarization, can be correlated in terms of some gross property of the acceleration parameter K. The integral $I(K)$ defined in Eqn.3.1 is a possible choice. The different properties of the boundary layer like the integral thickness parameters, the shape factor, the skin friction coefficient and the maximum values of the normalized turbulent intensity are shown plotted against $I(K)/I(K)_{max}$ in Figs.4.33 - 4.37 for flows CPI and DPI; it is to be noted that the results downstream of $I(K)_{max}$ in the adverse pressure gradient region are plotted to the right of

$I(K)_{max}$ for clarity. Interestingly, upstream of $I(K)_{max}$, parameters like δ^*, θ and u'/U_e exhibit some degree of collapse, while the H and C_f show significant history effects. Downstream of $I(K)_{max}$, H and u'/U_e show some degree of collapse suggesting the dominant effect of adverse pressure gradient in triggering changes in boundary layer properties through retransition of the relaminarized boundary layer.

For the first time, comparisons of boundary layer parameters assessing possible history effects of acceleration have been attempted here in the context of relaminarizing boundary layer flows. This was made possible by designing the experiments in such a way that the integral measure of acceleration is nearly the same for the two flows, while the acceleration history was different.

The limited exercise undertaken here examining the history effects of pressure gradients have clearly shown that important parameters like H and Cf reveal significant history effects. Unfortunately, there is hardly any experiment in literature on relaminarizing flows where a similar exercise could be under taken, which would have enabled drawing certain general conclusions.

CHAPTER 5
CALCULATIONS OF THE RELAMINARIZED FLOWS

The experimental results discussed earlier have clearly shown the effect of convex curvature in promoting relaminarization. In this chapter an attempt has been made for predicting the four relaminarization flows. It may be noted that different approaches are needed to calculate the complete flow, consisting of calculation regimes as illustrated in Fig.2.9. The relaminarization zone, (d) in the figure, is calculated here using the quasi-laminar equations (QLE) of Narasimha & Sreenivasan [1973]. The turbulent boundary layers present initially (zone a) and after retransition are calculated using the lag-entrainment method of Green (Desai & Kiske [1982]). The zone b+c, referred to as the island of ignorance by Sreenivasan [1982], continues to be a difficult task to model; as also the retransition zone (e). Hence these two regions are not modeled.

The focus of this chapter is the calculation of the relaminarization zone to possibly provide further evidence on curvature effects. Since there are no methods known for the calculation of the relaminarization of accelerated turbulent boundary layers on a curved surface, we have used QLE, without any modeling for curvature effects, in calculating the later stages of relaminarization on the surface. Based on the success of the quasi-laminar equations in various relaminarizing flows on a flat plate having a duration of acceleration exceeding $25\delta_o$, Narasimha & Sreenivasan [1973] had suggested that a critical value of Λ of about 50 for the method to be applicable. In all the four present experiments, the duration of acceleration is shorter (7 to $14\delta_o$); the value of Λ_{max} is just about 50 for DP1 but much higher in the other cases. This exercise will also provide an opportunity to assess the applicability of the quasi-laminar calculation method for the prediction of relaminarizing flows, for the short zones of acceleration encountered in the present experiments.

5.1 Calculation procedure and validation of QLE

The quasi-laminar equations were introduced to in Sec.2.1.3. In the present context, QLE were applied along the curved surface using the velocity determined from the wall pressure distribution as the boundary layer edge condition. A summary of the formulation and the procedure adopted for calculation is presented in Appendix E.

A Fortran program written to implement this calculation method, was successfully validated using data from a large number of relaminarizing boundary layer flows on a flat surface found in the literature, including some flows predicted by Sreenivasan [1974]. Details of these calculations and comparison of results are reported in Mukund [2002]. Appendix E contains sample calculations for flows BK, BR3 and WF4 (see Table 2.1 for code reference). These plots show comparisons of the present calculations with not only the experimental data but also with the calculations of Sreenivasan [1974] wherever available. The agreement of the present calculations with the experimental data as well as with the calculations of Sreenivasan is very good.

5.2 Comparison of the QLE with the present experimental data

5.2.1 PREDICTION OF C_f

In this section, we compare the predictions of C_f using QLE and lag-entrainment method for respective calculation zones with measured values for CP1, CP2, DP1 and FP1 are shown plotted in Fig.5.1 –5.4 respectively.

As may be observed in Fig.5.1 and Fig.5.2, the quasi-laminar predictions for convex surface flows CP1 and CP2 are surprisingly good in the later stages of relaminarization, despite the fact that the methodology does not use any modeling for curvature. The excellent agreement suggests that curvature effects are negligible in the later stages of relaminarization and that CP1 and CP2 have relaminarized very early due to the stabilizing influence of curvature. It is well known (Narasimha & Ojha [1966]) that convex curvature has only second order effect on the laminar (and hence also laminarized) boundary layer. Also, during relaminarization the boundary layer thickness δ decreases by a large extent (by about 50% in CP1) thus reducing the value of the local curvature parameter $k\delta$.

For DP1 (Fig.5.3) on the other hand, the predictions reflect the experimental trend but some disagreement is observed. The reason for the observed departure is

likely to be the fact that the maximum value of Λ for DP1 was barely adequate for QLE to be applicable.

In contrast to the predictions for CP1 and CP2, the predictions for FP1 are unsatisfactory; in particular the predicted fall in C_f in the relaminarization zone is much steeper compared to the experimental data. The inability of QLE to predict FP1 (having Λ_{max} significantly higher than critical) could be attributed to the fact that the extent of the acceleration zone was relatively short ($\cong 12\delta_o$) as compared to a exceeding $25\delta_o$ encountered in other relaminarizing flows on flat plates which have been successfully predicted by QLE (Table 3.2 gives the duration of these flows). This has been the first time that QLE has been tested on a relaminarizing flow on a flat plate with duration as low as $12\delta_o$. The flow WF4 of Warnack & Fernholz [1998] had a duration of acceleration of about $20\delta_o$ and the quasi-laminar predictions for this flow are also unsatisfactory as may be seen in Fig.E3 in the appendix.

In view of the above results, the success of the calculations using QLE for CP1 and CP2 on the convex surface suggests that the approximations made in deriving QLE are better satisfied on convex surface flows. This may possibly be because the outer layer of the curved surface boundary layer responds very quickly to curvature effects leading to an earlier freezing of the Reynolds stress. Further, the islands of ignorance in these curved boundary layer flows are indeed shortened, once again reflecting the promoting effect of convex curvature on relaminarization.

5.2.2 PREDICTION OF R_θ

The calculations of R_θ for the three flows CP1, DP1 and FP1 (shown in Fig.5.1, 5.3 and 5.4 respectively) indicate that the predictions are good up to half way through acceleration, but some departures are observed downstream, being appreciable in CP1 and DP1. Such differences were also observed in the calculations for other flows (such as in flow BK, shown in Fig.E2).

5.3 Turbulent boundary layer predictions

The lag-entrainment method of Green as coded by Desai & Kiske [1982] was used to calculate the turbulent boundary layers present before acceleration as well as after retransition. The experimental value of R_θ present at relevant locations was used as the initial condition for both cases. These two calculations were made for flows CP1,

CP2, DP1 and FP1 and are shown plotted for the C_f data in Fig.5.1-Fig.5.4 respectively.

In the initial constant pressure region, the figures show that the calculated C_f for the respective flows is nearly constant and match with the experimental values. As the flow accelerates, the calculated values of C_f increase as would be expected in a favorable pressure gradient, while the experimental values continue to be constant for some distance further downstream before increasing.

The turbulent boundary calculations in the post retransition zone show good agreement in the beginning for all the flows, but some departure is noticed in the convex surface flows, reflecting the effect of curvature in adverse pressure gradient.

5.4 Location of retransition

The relaminarized boundary layer is in a disturbed state due to the presence of fluctuations convected from the turbulent boundary layer ahead of acceleration. Thus, when the pressure gradient is relieved, the boundary layer undergoes quick retransition, generally close to the location of $C_{p,min}$. However, the present experiments show that retransition is postponed into the mild adverse pressure gradient region present beyond the $C_{p,min}$ location. This has also happened in flows A1, A2 and B1 of Brandt [1993]. An attempt has been made here to explain the delay in retransition using the inner laminar-layer solution of QLE.

In the present analysis, the value of the momentum thickness Reynolds number

$$R_{\theta,i} = \frac{\theta_i u_s}{\nu} \qquad \ldots 5.1$$

(where θ_i refers to the momentum thickness of the inner layer and u_s = u_s (x) is the velocity on the streamline which separates the inner and outer layers) is calculated using the inner laminar-layer solutions of the quasi-laminar calculations at the $C_{p,min}$ location for several relaminarization experiments; these are tabulated in Table 5.1. The table also lists the location of $C_{f,min}$ (from which the location of the onset of retransition can be inferred) with respect to the location of $C_{p,min}$.

It is evident from the table that in cases where retransition has occurred close to the $C_{p,min}$ location, the value of $R_{\theta,i}$ is greater than a critical value of about 220-240, whereas in cases where retransition occurs beyond the $C_{p,min}$ location $R_{\theta,i}$ is less than

the critical value. This range of R_θ is not inconsistent with what is observed for natural transition; which may be assessed using the semi-empirical equations of either Hall & Gibbings [1972] or Abu Ghannam & Shaw [1980], relating R_θ at the start of natural transition with the freestream turbulence level. Considering the turbulence level just outside inner layer to be about 2.5%, these relations predict R_θ to be around 250.

This analysis of $R_{\theta,i}$ suggests that a critical value of about 220-240 could be used as an empirical guide to assess if retransition is postponed beyond $C_{p,min}$. Since there is no reason to believe in the validity of the quasi-laminar equations beyond the $C_{p,min}$ location, the critical value of $R_{\theta,i}$ cannot be used to determine the location of retransition in cases where it is postponed beyond the $C_{p,min}$ location.

CHAPTER 6
CONCLUSIONS

With a view to understand relaminarization near the leading edge of a swept-wing at high-lift as well as to provide a data base for modeling the flow, experiments on relaminarization under the combined action of acceleration and streamwise convex curvature have been conducted at low speeds. These building block experiments in 2D flow differ from earlier work on relaminarizing flows in the following major aspects; (i) inclusion of streamwise convex curvature, (ii) significantly reduced extent of acceleration, being about 10-14δ_o for the different flows investigated here, as against 25-30δ_o observed in flows reported earlier, and (iii) a region of adverse pressure gradient at the end of acceleration (like what is encountered on a swept wing at high-lift) affecting the retransition process. The experimental geometry and test parameters have been carefully chosen to provide conditions very similar to those that occur on swept wings at realistic Reynolds numbers.

Three relaminarizing boundary layer flows on the convex wall, having different acceleration histories but the same integral of the acceleration parameter *K*, have been documented. In order to explicitly bring out the likely effects of convex curvature from the experimental results, measurements were also made on a relaminarizing flow on a flat plat having a pressure distribution very similar to one of the convex surface flows documented. The measurements made consisted of surface pressure distribution along the model centerline, streamwise mean-velocity and turbulent intensity profiles in the boundary layer using a hot-wire probe, and mean and fluctuating components of wall shear stress at several streamwise stations using surface mounted hot-films.

The experimental results showed strong features of relaminarization in all the four flows (including the flow on the flat plate). The degree of relaminarization, as judged by the maximum attained value of the shape factor, was appreciably higher for the convex surface flows compared to the flat surface flow in virtually the same pressure gradient, indicating the stabilizing influence of convex curvature in promoting relaminarization.

Explicit comparisons of certain boundary layer properties on the convex surface and flat surface flows (both having similar pressure gradients and initial flow conditions) showed the following features in the convex surface flow experiments : a more rapid fall in skin friction coefficient during relaminarization, higher maximum value of the shape factor, lower value of the momentum-thickness Reynolds number, larger reduction of the relative turbulence intensity, and finally greater and more rapid reduction of the turbulence energy at lower frequencies in the near-wall region. Based on these results, it is concluded that convex surface curvature has strongly aided acceleration in relaminarizing the boundary layer in a very effective manner.

The predictions of skin friction using the quasi-laminar equations (without modeling for curvature effects) for the two higher acceleration flows on the convex surface were surprisingly good. This suggests that curvature effects are negligible in the latter stages of relaminarization and that the two flows have relaminarized very early due to the stabilizing influence of curvature. Further evidence supporting the above conclusion comes from the fact that the prediction for the flat surface flow was less satisfactory even though the maximum value of the pressure gradient parameter for this flow was considerably above critical, presumably due to the short extent of acceleration.

In view of the above results, the success of the calculations using quasi-laminar equations on the convex surface suggests that the approximations made in deriving the equations are better satisfied on convex surface flows. This may be possibly because the outer layer of the curved surface boundary layer responds very quickly to curvature effects leading to an earlier freezing of the Reynolds stress. Further, the islands of ignorance in these curved boundary layer flows are indeed shortened, once again reflecting the aiding effect of convex curvature on relaminarization.

The flows reported here are the first set of experiments at low speed providing strong evidence that flow can indeed relaminarize in relatively short zones of acceleration ($<14\delta_o$). These observations are not very surprising since the occurrence of relaminarization has in fact been reported in supersonic expansion corners by Sternberg [1954] and by Narasimha & Viswanath [1975], where the zone of acceleration could be even smaller (typically $2\text{-}3\delta_o$) than those encountered here.

In summary, the new experimental results obtained here for examining the effects of convex surface curvature on relaminarization, and the detailed comparisons of the

data with predictions based on QLE, indicate that convex curvature can have surprisingly strong effects in promoting or aiding the relaminarization process of an accelerated turbulent boundary layer. This fact clearly would have to be taken into account in assessing the effects of possible relaminarization on swept wings in the aerodynamic design of flight vehicles.

Suggestions for future work

The present experiments were at comparatively high Reynolds number based on the momentum thickness. Experiments conducted at much higher Reynolds numbers on both flat and convex surfaces will be more realistic in simulating flight conditions.

Convex curvature effects on relaminarization could not be quantified from the present experiments. Though it is difficult to quantify the effects, experiments on surfaces having different curvature parameters and acceleration levels will help in better understanding of the effects of curvature.

The main motivation for the present 2D experiments was an initial exploration in understanding 3D relaminarization on swept wings in flight. Thus, the logical continuation is a wind tunnel study of relaminarization on swept wings having 3D flows. Such experiments could be at high Reynolds numbers and for a variety of curvature parameters. The present work will help in both designing the experiments, simplifying the measurements and understanding the results.

We have seen in Sec.2.1.3 that there exist a few computational methods to model relaminarization but these methods do not include curvature effects. Also, the differential models that exist lack the rational approach of the quasi-laminar equations. Notable contributions can be done in this field by developing differential methods of solution, while using the approach adopted in the quasi-laminar equations.

APPENDIX A

ESTIMATES OF CURVATURE PARAMETER ON SWEPT WINGS

Source	Geometry	M_∞	$(k\theta_{11})_{lam}$	$(k\theta_{11})_{tur}$	$(k\delta)_{lam}$	$(k\delta)_{tur}$
Arnal & Juillen [1990]	RA16SC1 Airfoil with flap	0.14	0.0015	0.0045	0.015	0.045
Van Dam et al [1993]	Boeing 737-100					
	α=16.4°; δ_f=15°	0.20	0.0015	0.0045	0.015	0.045
	α= 7.7°; δ_f=40°	0.20	0.0015	0.0045	0.015	0.045
	α=13.4°; δ_f=40°	0.17	0.0018	0.0054	0.018	0.054

ASSUMPTIONS MADE

$\theta_{11,lam}$ obtained from $\overline{R} \cong 245$ (Arnal & Juillen [1990])

$\theta_{11,turb} \cong 3\ \theta_{11,lam}$ (guided by the results from Table 2.1, Brandt [1993])

$\delta_{lam} \cong 10\ (\theta_{11,lam})$

$\delta_{turb} \cong 10\ (\theta_{11,turb})$

SYMBOLS USED

M_∞ = Freestream Mach number

k^{-1} = Radius of curvature

θ_{11} = Momentum thickness of the attachment line boundary layer

lam = Value of the assumed laminar boundary layer

turb = Value of the assumed turbulent boundary layer

$\overline{R}$ = Characteristic Reynolds number on the attachment line

α = Airfoil / wing incidence angle

δ_f = Flap deflection angle

APPENDIX B

GEOMETRIC DETAILS OF THE PRESSURE-GENERATOR AIRFOILS USED FOR THE FOUR EXPEIMENTS

1. DETAILS OF CP PRESSURE GENERATOR USED FOR CP1 AND CP2 EXPERIMENTS

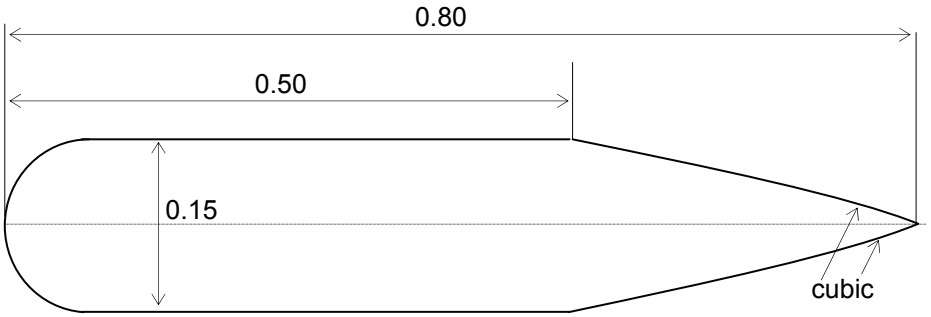

2. THE COORDINATES OF THE DP PRESSURE GENERATOR USED FOR DP1 EXPERIMENTS

Upper Surface		Lower Surface	
x, m	y, m	x, m	y, m
0.9200	0.1000	0.9200	0.1000
0.9228	0.1129	0.9242	0.0874
0.9328	0.1231	0.9351	0.0783
0.9534	0.1271	0.9589	0.0699
0.9735	0.1250	0.9794	0.0612
0.9956	0.1226	1.0019	0.0516
1.0279	0.1192	1.0347	0.0377
1.0712	0.1146	1.0787	0.0189
1.1215	0.1093	1.1299	-0.0028
1.1718	0.1040	1.1811	-0.0246
1.2222	0.0986	1.2320	-0.0419
1.2725	0.0933	1.2826	-0.0520
1.3229	0.0880	1.3332	-0.0620
1.3732	0.0827	1.3837	-0.0709
1.4236	0.0773	1.4342	-0.0790
1.4739	0.0720	1.4843	-0.0796
1.5242	0.0667	1.5339	-0.0711
1.5746	0.0614	1.5832	-0.0551
1.6249	0.0560	1.6323	-0.0368
1.6753	0.0507	1.6814	-0.0185
1.7256	0.0454	1.7305	-0.0001
1.7759	0.0401	1.7797	0.0182
1.8223	0.0352	1.8249	0.0351

3. DETAILS OF FP PRESSURE GENERATOR USED FOR FP1 EXPERIMENTS

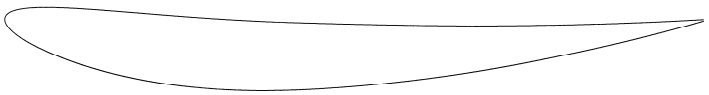

Airfoil : NACA 5410
Chord : 0.5m

4. LOCATION DETAILS OF THE PRESSURE GENERATORS IN RESPECTIVE EXPERIMENTS

Flow name	**CP1**	**DP1**	**FP1**	**CP2**
Pressure generator name	CP	DP	FP	CP
horizontal distance of leading edge x, m	1.000	0.920	1.160	1.000
vertical distance of leading edge y, m	0.095	0.095	0.075	0.055
vertical distance of trailing edge y, m	0.080	0.035	0.060	0.160

APPENDIX C

UNCERTAINTIES DUE TO VERTICAL TRAVERSING OF HOT-WIRE

Boundary layer mean velocity profiles were measured on the convex surface using hot-wires by traversing the probe vertically (normal to the tunnel axis); the distance normal to the convex surface was obtained by considering of the local surface slope. Since the two flows under investigation have large streamwise pressure gradients, an assessment has been made of the likely errors in the measured mean velocity.

By traversing the probe vertically instead of normal to the convex surface, one is measuring the velocity $U_{vertical}$ at distance $x-\Delta x$ instead of the intended velocity U_{normal} at x. This is illustrated in Fig.C1-C2. Compared to U_{normal}, $U_{vertical}$ is lower in the favourable pressure gradient region and higher in the adverse pressure gradient region. U_{normal} at x is evaluated by interpolation of the $U_{vertical}$ data at $x-\Delta x$ for various profiles measured.

Fig.C3 shows a plot of the ratio $U_{vertical}/U_{normal}$ at the boundary layer edge at the measured distance x for the two flows CP1 and DP1. The ratio varies between 0.985 to 1.01 for CP1 and is even smaller for DP1, consistent with the respective pressure gradient levels. Notwithstanding the small differences, an assessment of the errors in the boundary layer integral thickness parameters has been made at various x stations for CP1. The results given in Table C shows that the errors are less than about 0.4%.

Table C. Estimated errors in the integral thickness parameters due to traversing vertically - Flow CP1

x, m	δ^*, mm	θ, mm	H	Remarks
1.085	0.910	0.764	1.191	Uncorrected
	0.912	0.763	1.194	Corrected
1.185	0.976	0.507	1.925	Uncorrected
	0.977	0.506	1.930	Corrected

APPENDIX D
CALIBRATION OF HOT-FILMS

As mentioned in Sec.3.4.3, the hot-film gage was glued on top of a cylindrical plug and flush mounted in holes for usage and calibration.

Hot-film calibration was done in the zero pressure-gradient turbulent boundary layer on the upstream flat plate for the expected range of the shear stress. The locations are indicated in Table 3.6 and 3.7 for the convex and flat surface experiments respectively. The reference shear stresses were obtained from velocity profiles measured at different free-stream velocities using a pitot tube. Fig.3.9 shows some of these profiles in the wall-law coordinates.

The equation used for calibration for hot-films is of the form

$$\frac{E^2}{R\Delta T} = \frac{E_o^2}{R\Delta T} + A(\tau_w)^{1/3}$$

where A = Calibration constant to be determined

E = Mean voltage output of CTA in flow condition (volts)

E_o = Mean voltage output of CTA in no-flow condition (volts)

R = Operating resistance of the gauge (Ω)

ΔT = Difference between the gauge and the tunnel fluid temperature (°C)

τ_w = Wall shear stress (kgf/cm^2)

Temperature in the wind tunnel was continuously monitored using a thermocouple probe; ΔT was deduced from the gage temperature calculated using a plot provided by the gage manufacturer.

Experience has shown that the measurement uncertainty can be reduced by taking the E_o term to the LHS of the equation and find the least-square linear fit for the plot of

$$\left(\frac{E^2}{R\Delta T} - \frac{E_o^2}{R\Delta T}\right) \quad vs \quad \left(\tau_w{}^{1/3}\right)$$

The calibration consisted of acquiring several sets of data at different times of the day and for 3-4 days and obtaining a consolidated calibration line. The calibration constants thus obtained were stable for a long time. A typical calibration plot is shown in Fig.3.10.

APPENDIX E

THE QUASI-LAMINAR EQUATIONS

The details of the quasi-laminar equations as formulated by Narasimha & Sreenivasan [1973] and Sreenivasan [1974] is given below.

The development of an incompressible two-dimensional turbulent boundary-layer flow is governed by the equations

$$\frac{\partial u}{\partial x}+\frac{\partial v}{\partial y}=0 \qquad \ldots\ldots\ldots \text{(E1)}$$

$$u\frac{\partial u}{\partial x}+v\frac{\partial u}{\partial y}=U\frac{dU}{dx}+\nu\frac{\partial^2 u}{\partial y^2}+\frac{\partial \tau}{\partial y} \qquad \ldots\ldots\ldots \text{(E2)}$$

Consider a situation in which a sharp favorable pressure gradient is applied beginning at a point x_i on a turbulent boundary layer developing under constant pressure up to that point.

Consider a limiting analysis for large values of Λ. In the outer region of the boundary layer the viscous stress and the Reynolds stress are negligible compared to the acceleration; a suitable outer limit of Eqn.E2, with $\bar{y}=y/\delta$ fixed (bars denoting outer variables, so that $\bar{u}=u,\ \bar{v}=v,\ \bar{x}=x$), would therefore be

$$\bar{u}\frac{\partial \bar{u}}{\partial \bar{x}}+v\frac{\partial \bar{u}}{\partial \bar{y}}=U\frac{dU}{dx} \qquad \ldots\ldots\ldots \text{(E3)}$$

representing plane inviscid rotational flow being convected downstream along streamlines without loss or diffusion. Towards the wall ($\bar{y}\to 0$), there will be a non-zero slip velocity u_s given by

$$u_s^2(x)=\left[U^2(x)-U^2(x_i)\right]+u_s^2(x_i) \qquad \ldots\ldots\ldots \text{(E4)}$$

found from the Bernoulli's equation along the zero streamline in the outer flow. The derivation of this equation is given in Sreenivasan [1974].

The inner layer has the slip velocity u_s at its other edge and satisfies the no-slip boundary condition at the wall. It is described by the limit $\Lambda^{-1} \to 0$ with $\hat{y} = y/\hat{\delta}$ fixed, where $\hat{\delta}$, the inner layer thickness, is $O(\Lambda^{-1/2}\bar{\delta})$: the corresponding limit of Eqn.E2, with the caret (cap on top of the variable) denoting the inner variables with (again $\hat{u} = u, \hat{v} = v, \hat{x} = x$), is the laminar boundary layer equation

$$\hat{u}\frac{\partial \hat{u}}{\partial \hat{x}} + \hat{v}\frac{\partial \hat{u}}{\partial \hat{y}} = U\frac{dU}{dx} + \nu\frac{\partial^2 \hat{u}}{\partial \hat{y}^2} \qquad \text{. . . . . (E5)}$$

is obtained for the quasi-laminar region ignoring the Reynolds stress from Eqn.E2.

The two equations (E3 & E5) are matched as per the method of Van Dyke [1964]. A pictorial representation of the formulation is shown in Fig.2.7.

THE PRESENT METHOD OF SOLUTION

The solution procedure is outlined by Sreenivasan [1974]. The highlights of the simplifications made and the specific procedure adopted, all within the purview of the procedure described by Sreenivasan [1974], are presented below.

1. The initial location x_o for starting the calculations should be specified, strictly speaking, in the quasi-laminar region. However, it is reasonable to assume that the region between the start of the pressure gradient and the quasi-laminar region is so small as to make no significant changes in the mean-velocity profiles. So x_o can be specified at the starting of acceleration or slightly downstream. In the present calculations, x_o is specified at a convenient point slightly downstream of start of acceleration.

2. The slip velocity $u_s(x)$ is calculated from Eqn.E4. The value of $u_s(x_o)$ is a small non-zero number so chosen as to match the initial value of the calculated R_θ.

3. The outer layer velocity profile is obtained in the form of the power law as

$$\frac{\bar{u}}{U} = u_s + (1 - u_s)\bar{y}^{n(x)} \qquad \text{. . . . . .(E6)}$$

The initial value of the power $n(x_o)$ is determined from turbulent boundary layer calculations. A value of 1/7 was found universally valid for the range of Reynolds number present in the current context. To obtain n downstream, a marching technique detailed by Sreenivasan [1974] is used.

4. The inner layer may be solved using any convenient laminar boundary layer calculation method. For some of the flows (like BR3*), KRS found that he could fit the Falkner-Skan similarity profile. A program written to solve the inner boundary layer equations using the Falkner-Skan similarity profile showed that only some flows (like BR3) gave good predictions. Looking at a more generalized variety of data (including some recent ones) it was found that the integral calculation method of Thwaites [1949] was more suitable.

   The Thwaites' method in its original form has certain drawbacks (Dey and Narasimha [1990]); it cannot handle high pressure-gradients (such as those encountered in relaminarizing boundary layers). The length dimension scaled with δ is difficult to measure accurately. Instead, an extension of the method by Dey & Narasimha [1990], which accounts for larger pressure gradients and scaled with the momentum thickness, was used for the inner layer calculations.

5. The momentum thickness for the full boundary layer is calculated by adding the momentum defect of the inner and outer layers as

$$U^2\theta = U^2\overline{\theta} + u_s^2\hat{\theta} \qquad \ldots\ldots\ldots \text{(E7)}$$

6. The skin friction coefficient for the boundary layer is calculated by normalizing the inner-layer wall shear-stress by the dynamic pressure at the edge of the boundary layer.

THE SOLUTION

A Fortran program was developed to implement this calculation procedure and was validated using ten different relaminarizing boundary layer flows from literature. Fig.E1 – Fig.E3 show sample calculations for flows BK, BR3 and WF4 respectively.

* See Table 2.1 for code reference

REFERENCES

Abu-Ghannam, B.J. & Shaw, R., [1980]	Natural transition of boundary layers – the effect of turbulence, pressure gradient and flow history, *J.Mech.Engg. Sci.*, V22, P213.
Ahmed, S.R., [1973]	Calculation of the inviscid flow field around 3D lifting wings fuselages and wing-fuselage combinations using panel method, WG, *Rep.No. DLR-FB 73_102,* DFVLR, Institut fur Aerodynamik, BraunSchweig, Germany
Alving, A.E., Smits, A.J. & Watmuff, J.H., [1990]	Turbulent boundary relaxation from convex curvature, *J.Fluid Mech*., V211, P529.
Arnal, D. & Juillen, J.C., [1990]	Leading edge contamination and relaminarization on a swept wing at incidence, *Proc: Numerical and Physical Aspects of Aerodynamic Flows IV, Ed: T.Cebeci, Springer-Verlag*, P391.
Back, L.H. & Seban, R.A., [1967]	Flow and heat transfer in a turbulent boundary layer with large acceleration parameter. *Proc. Heat Transfer and Fluid Mech. Institute*, Stanford University Press, V20, P410.
Badri Narayanan, M.A., [1968]	An experimental study of reverse transition in two-dimensional channel flow, *J.Fluid Mech*., V31, P609.
Badri Narayanan, M.A. & Ramjee, V., [1969]	On the criteria for reverse transition in a two-dimensional boundary layer, *J.Fluid Mech*., V35, P225.
Badri Narayanan, M.A., Rajagopalan, S. & Narasimha, R., [1974]	Some experimental investigations on the fine structure of turbulence. *Rep.No.74FM 15.,* Dept. Aero. Engg., Ind.Institute. of Sci., Bangalore
Badri Narayanan, M.A., Rajagopalan, S. & Narasimha, R., [1977]	Experiments on the fine structure of turbulence, *J.Fluid Mech*., V80, P237
Batchelor, G.K. & Proudman, I., [1954]	The effect of rapid distortion of a fluid in turbulent motion, *Quart.J.Mech.Appl.Math.,*V7, N83.
Blackwelder, R.F. & Kovasznay, L.S.G., [1972]	Large-scale motion of a turbulent boundary layer during relaminarization. *J.Fluid Mech*., V53, P61.

Bourassa, C., Thomas, F.O., & Nelson, R.C., [2000]	Experimental investigation of turbulent boundary layer relaminarization with application to high-lift systems: preliminary results, *AIAA 2000-4017.*
Bradshaw, P., [1969]	The analogy between streamline curvature and buoyancy in turbulent shear flow, *J. Fluid Mech*., V36, P177.
Bradshaw, P., [1971]	An introduction to turbulence and its measurement, *Pergamon Press.*
Bradshaw, P., [1973]	Effects of streamline curvature on turbulent flow, *AGARDograph*, No.169.
Brandt, R., [1993]	Relaminarized boundary layers subjected to adverse pressure gradients. PhD thesis, CUED/A-Aero/TR-21, Univ. Cambridge.
Chen, K.K. & Libby, P.A., [1968]	Boundary layers with small departures from Falkner-Skan profiles, *J. Fluid Mech*., V33, P273
Crouch, J [1996]	Private communications, Boeing Commercial Airplane Group, USA
Dey, J. & Narasimha, R. [1990]	An extension of Thwaites method for calculation of incompressible laminar boundary layers, *J.Indian Institute of Science,* V1,P11.
Desai, S.S. & Kiske, S., [1982]	A computer program to calculate turbulent boundary layer and wakes in compressible flow with arbitrary pressure gradient based on Greens Lag-entrainment method, *Bericht No.89/1982,* Ruhr University, Bochum.
Ellis, L.B. & Joubert, P.N., [1974]	Turbulent shear flow in a curved duct, *J.Fluid Mech*., V62, P65.
Escudier, M.P., Abdel-Hameed, A., Johnson, M.W. & Sutcliffe, C.J., [1998]	Laminarization and re-transition of a turbulent boundary layer subjected to favourable pressure gradient, *Experiments in Fluids,* V25, P491.
Eskinazi, S. & Yeh, H., [1956]	An investigation of fully developed turbulent flow in a curved channel, *J. Aero. Sci*., V23, P23.
Fernholz, H.H. & Warnack, D., [1998]	The effects of a favourable pressure gradient and of the Reynolds number on an incompressible axisymmetric turbulent boundary layer. Part 1. The turbulent boundary layer, *J.Fluid Mech*., V.359, P329.
Gibson, M.M., Verriopoulos, C.A. & Vlachos, N., [1984]	Turbulent boundary layer on a mildly curved convex surface, 1:mean flow and turbulence measurements, *Expt. Fluids*, V2, P17.

Gillis, J.C. & Johnston, J.P., [1983]	Turbulent boundary-layer flow and structure on a convex wall and its redevelopment on a flat wall, *J. Fluid Mech*., V135, P123.
Hall, D.J. & Gibbings, J.C., [1972]	Influence of stream turbulence and pressure gradient on boundary-layer transition, *J.Mech.Engg.Sci.*, V14, P134.
Hunt, I.A. & Joubert, P.M., [1979]	Effects of small streamline curvature on turbulent duct flow, *J. Fluid Mech*., V91, P633.
Ichimiya, M., Nakamura, I. & Yamashita, S., [1998]	Properties of relaminarizing turbulent boundary layer under a favorable pressure gradient, *Experimental. Thermal & Fluid Sc.* P37.
Klebanoff, P.S., [1955]	Characteristics of turbulence in a boundary layer with zero pressure gradient, *NACA Rep. 1247*.
Kline, S.J. & McClintock, F.A., [1953]	Describing uncertainties in single-sample experiments, *Mech. Engg.*, V1, P3.
Kreskovsky, J.P., Shamroth, S.J. & McDonald, H., [1974]	Parametric Study of Relaminarization of Turbulent Boundary Layers on Nozzle Walls, *NASA Contractor Report*, CR-2370.
Krishnan, V., Mukund, R. & Subashchander, N., [2000]	Calibration studies of NAL 1.5m low speed wind tunnel, *PD EA 0013, NAL, Bangalore.*
Laufer, J., [1962]	Decay of non-isotropic turbulent field. *In Miszellaneen de angewandte Mechanik, Festschrift Walter Tollmien, Akademie-Verlag,* Berlin.
Launder, B.E., [1963]	The turbulent boundary layer in a strongly negative pressure gradient, *Rep.No.71. Gas Turbine Lab., Massachusetts Institute of Technology, Cambridge.*
Launder, B.E., [1964]	Laminarization of the turbulent boundary layer in a severe acceleration. *J.App.Mech.*,V.31, P707.
Launder, B.E. & Loizou, P. A., [1992]	Laminarization of three-dimensional accelerating boundary layers in a curved rectangular-sectioned duct, *Int. J. Heat and fluid flow,* V.13, No.2, P124.
Launder, B.E., & Stinchcombe. H.S., [1967]	Non-normal similar turbulent boundary layers, *Imp.Coll. Note TWF/TN21. Dept.Mech.Engg.*
Liepmann, H.W., & Skinner, G.T., [1954]	Shearing stress measurements by use of a heated element, *NACA Tech.Note 3268.*
Meroney, R.N. & Bradshaw, P. [1975]	Turbulent boundary-layer growth over a longitudinally curved surface, *AIAA Journal*, V13, No.11, P1448.

Moretti, P.M. & Kays, W.M. [1965]	Heat transfer in turbulent boundary layer with varying free stream velocity and varying surface temperature – an experimental study. *Int. J. Heat & Mass Transfer*, V8, P1187.
Moser, R.D. & Moin, P., [1987]	The effects of curvature in wall bounded turbulent flows, *J.Fluid Mech*., V175, P479.
Muck, K.C., Hoffman, P.H. & Bradshaw, P., [1985]	The effect of convex surface curvature on turbulent boundary layers, *J.Fluid Mech*., V161, P347.
Mukund, R., [2002]	Calculation of relaminarizing using quasi-laminar equations, *PD EA 0202*, National Aerospace Laboratories, Bangalore, India
Narasimha, R., [1977]	The three archetypes of relaminarization, *Proc. Sixth Canadian Congress of Appl. Mech.*, P503
Narasimha, R. & Ojha, S.K., [1967]	Effect of longitudinal surface curvature on boundary layers, *J. Fluid Mech*., V29, P187
Narasimha, R. & Sreenivasan, K.R., [1973]	Relaminarization in highly accelerated turbulent boundary layers, *J.Fluid Mech*., V61, P417.
Narasimha, R., & Sreenivasan, K.R., [1979]	Relaminarization of fluid flows, *Adv.Appl.Mech*., V19, P221.
Narasimha, R. & Viswanath, P.R., [1975]	Reverse transition at an expansion corner in supersonic flows. *AIAA.J.* V13, P693
Patel, V.C., [1965]	Calibration of the Preston tube and limitations on its use in pressure gradients. *J.Fluid Mech*., V23, P85.
Patel, V.C., [1969]	The effects of curvature on the turbulent boundary layer*, ARC, R&M 3599.*
Patel, V.C. & Head, M.R. [1968]	Reversion of turbulent to laminar flow. *J.Fluid Mech*., V.34, P371.
Patel, V.C., & Sotiropoulos, F., [1997]	Longitudinal curvature effects in turbulent boundary layers, *Progress in aerospace sciences*, V33, P1.
Prabhu, A., Narasimha, R., & Rao, B.N.S., [1983]	Structure and mean-flow similarity in curved turbulent boundary layers, *IUTAM symposium on structure of complex turbulent shear flow,* Springer, New York
Prabhu, A., & Sundarasiva Rao, B.N., [1981]	Turbulent boundary layers in a longitudinally curved stream, *Report 81 FM 10*, Dept. Aero. Engg., Indian Inst. of Science, Bangalore.
Ramaprian, B.R., & Shivaprasad, B.G., [1977]	Mean flow measurements in turbulent boundary layers along mildly curved surfaces, *AIAA Journal*, V15, N2, P189.

Ramaprian, B.R., & Shivaprasad, B.G., [1978]	The structure of turbulent boundary layers along mildly curved surfaces, *J. Fluid Mech*., V85, part2, P273.
Ramjee, V., [1968]	Reverse transition in a two-dimensional boundary layer flow., Ph.D. Thesis., Dept.Aero.Eng., Ind.Institute.Sci., Bangalore.
Rosenhead, L., [1963]	*Laminar Boundary Layers*, Clarendon Press, Oxford
Schraub, F.A. & Kline, S.J., [1965]	A study of the structure of the turbulent boundary layer with and without longitudinal pressure gradients. ReportMD-12, Thermo-sciences Division, Stanford Univ.
Schwarz, A.C. & Plesniak, M.W. [1996]	Convex turbulent boundary layers with zero and favorable pressure gradients, *J.Fluid Engg.*, V118, P787.
Smits, A.J., Young, S.T.B. & Bradshaw, P. [1979].	The effect of short regions of high surface curvature on turbulent boundary layers, *J.Fluid Mech*., V94, P209.
So, R.M.C. & Mellor, G.L., [1972]	An experimental investigation of turbulent boundary layers along convex surfaces, *NASA CR 1940.*
So, R.M.C. & Mellor, G.L., [1973]	Experiment on convex curvature effects in turbulent boundary layers, *J. Fluid Mech*., V60, P43.
Sreenivasan, K.R., [1972]	Notes on the experimental data on reverting boundary layers, *Rep.No.72 FM2. Dept. Aero.Engg., Ind.Inst.Sci. Bangalore*
Sreenivasan, K.R., [1974]	Mechanism of reversion in highly accelerated turbulent boundary layers. PhD thesis, Dept. Aero. Engg. Ind.Institute.Sci. Bangalore.
Sreenivasan, K.R., [1982]	Review Article : Laminarescent, Relaminarizing and Retransitional Flows. *Acta Mechanica*, V.44, P1.
Sreenivasan, K.R., & Narasimha, R., [1978]	Rapid distortion of axisymmetric turbulence, . *J.Fluid Mech*., V.84, P497.
Sternberg, J., [1954]	The transition from a turbulent to a laminar boundary layer. *Rep. No. 906*, Army Ballistic.Res.Lab, Aberdeen.
Subaschandar, N., [1996]	Private communications, National Aerospace Laboratories, Bangalore
Thompson, B.G.J., [1973]	The prediction of boundary-layer behaviour and profile drag of infinite yawed wings, *RAE Tech Rep*. No, 73091.
Thwaites, B., [1949]	Approximate calculation of the laminar boundary layer, *Aero. Quarterly*, No.1., p245.
Van Dam, C.P., Viggen, P.M.H.W., Yip, L.P. & Potter, R.C., [1993]	Leading-edge transition and relaminarization phenomena on a subsonic high lift-system, *AIAA* Paper 93, P3140.

Van Dyke M., [1962]	Higher approximations of boundary-layer theory, Part 1 – General analysis, *J.Fluid Mech*., V14, P161
Van Dyke M., [1964]	*Perturbation methods in fluid mechanics*, Academic press, New York.
Viala, S. & Aupoix, B., [1995]	Prediction of Boundary Layer Relaminarization using Low Reynolds Number Turbulence Models, *33rd Aerospace Sciences Meeting and Exhibit, Reno, NV*, AIAA 95-0862.
Warnack, D. & Fernholz, H.H., [1998]	The effects of a favorable pressure gradient and of the Reynolds number on an incompressible axisymmetric turbulent boundary layer. Part 2. The boundary layer with relaminarization. *J.Fluid Mech*., V.359, P357.
Wattendorf, F.L., [1935]	A study of the effect of curvature on fully developed turbulent flow, *Proc. Roy. Soc.,* V148A, P565.
Wilcken, H., [1930]	Turbulente Grenzschichten an gewölbten Flächen, Ing. Archiv. V1, P357.
Wilson, D.G., & Pope, J.A., [1954]	Convection heat transfer in gas turbine blades, *Proc., Inst.Mech. Eng.,* London V168, P861.
Yip, L.P., Viggen, P.M.H.W., Hardin, J.D. & Van Dam, C.P., [1993]	In-flight pressure distributions and skin friction measurements on a subsonic transport high-lift wing section. *AGARD,* CP-515.

Table 2.1 Experiments of relaminarization due to high acceleration						
Reference	**Code**	**Initial Velocity, m/s**	**Initial R_θ**	**K_{max} x 10^6**	**x_a/δ_o**	**Remarks**
Launder [1964]			320 1000			
Moretti & Kays [1965]		≅19 ≅18	1410 2820	3.51 3.39		
Schraub & Kline [1965]			590			
Back & Seban [1967]		36.3 15.9	1200 400	2.2 5.0		
Badri Narayanan & Ramjee [1969], Ramjee [1968]	BR1 BR2 BR3 BR4 BR5 BR6	14.33 8.53 9.14 11.40 6.68 4.54	1650 310 410 2050 1240 780	3.6 8.0 8.0 2.85 5.2 7.0	27 49 33 23 23 24	
Blackwelder & Kovasznay [1972]	BK	3.0	2500	4.7	27	
Sreenivasan [1972]	S1 S2 S3		675 940 1250			
Badri Narayanan et al [1974, 1977]			1850			
Brandt [1993]	A1 A2 A3 A4 B1 B2	8 12 16 20 8 12	373 559 730 839 280 482	10.5 7.1 5.5 4.9 4.3 3.3	66 57 57 56	 Intermittent RL Intermittent RL
Warnack & Fernholz [1998]	WF2 WF4	7.77 7.79	862 2564	4.0 3.88	27 20	Axisymmetric flow
Escudier et al [1998]		4	1700	4.4	23	
Ichimiya et al [1998]		6	799	6	32	
Bourassa et al [2000]		4 5	1545 ~1810	4.10 3.29		

Table 2.2 Criteria proposed for relaminarization by high acceleration			
Reference	Flow studied	Method for identification of relaminarization	Criteria proposed for relaminarization
Launder [1963,1964]	2D nozzle flow	---	$K \geq 2\text{x}10^{-6}$ for about 20δ
Moretti & Kays [1965]	2D nozzle flow	Failure of a Stanton number prediction procedure	$K \geq 3.5\text{x}10^{-6}$
Schraub & Kline [1965]	2D boundary layer in a water channel	Cessation of bursting in wall region	$K.c_f^{-1/2}$; $K \geq 3.5\text{x}10^{-6}$
Patel [1965]	Accelerated wall layer in pipe flow	Breakdown of log-law in wall layer	$-\Delta_p = -\nu p'/U^{*3} = K(2/c_f)^{3/2} \geq 0.025$
Launder & Stichcombe [1967]	Sink – flow boundary layer	Departure from normal boundary layer characteristics	$K.c_f^{-3/2}$
Back & Seban [1967]	Highly accelerated boundary layer	Reduction of the heat transfer and skin friction below that given by a standard prediction procedure	$K \geq 3\text{x}10^{-6}$
Patel & Head [1968]	Accelerated wall layer in pipe flow	Departure of wall-layer flow from a modified wall law	$-\Delta_\tau = -\nu\tau'/U^{*3} \geq 0.009$
Bradshaw [1969]	Highly accelerated boundary layer	Overlapping of energy containing and dissipating eddy scales	$\tau^2/\nu\varepsilon \leq 12$
Badri Narayanan & Ramjee [1969]	Highly accelerated boundary layer	Decrease in (u'/U)	$Re_\theta \leq 300$
Narasimha & Sreenivasan [1973]	Highly accelerated boundary layer	Flow described by Quasi-laminar limit	$\Lambda = -\delta/\tau_o \; dp/dx \geq 50$
Brandt [1993]	Highly accelerated boundary layer	---	$K^* = \nu/U_o^2 \; dU/dx > 8.1\text{x}10^{-6}$

Table 2.3 Experiments on channels with convex surface curvature

Reference	R_θ	Aspect Ratio	kh *
Wattendorf, [1935]	50,000	18.0	0.053
Eskinazi & Yeh, [1956]	69,000	15.5	0.055
Ellis & Joubert, [1974]		13.2	0.083 0.017
Hunt & Joubert, [1979]	60,000	13.2	0.05
Moser & Moin, [1987]	2,990	∞, (DNS)	0.0127
* 2h = height of channel			

Table 2.4 Turbulent boundary layer experiments on convex surfaces

Reference	R_θ	Aspect Ratio	δ_o/R_w
Gibson et al [1984]	3300	3.0	0.008
Meroney & Bradshaw, [1975]	5400	6.0	0.01
Muck et al., [1985]	4850	6.0	0.01
Ramaprian & Shivaprasad,[1977,1978]	4600	2.5	0.013
Prabhu & Sundarasiva Rao, [1981]	1471	2.0	0.038
Bandyopadhyay & Ahmed [1993]	---	2.49	0.0385
Gillis & Johnston, [1983]	4700	6.7	0.05
Patel, [1969]	4000	5.0	0.071
So & Mellor, [1973]	2900	8.0	0.075
Alving et al [1990]	6000	8.13	0.08
Prabhu & Sundarasiva Rao, [1981]	3703	2.0	0.086
Gillis & Johnston, [1983]	4700	6.7	0.1
Prabhu & Sundarasiva Rao, [1981]	5969	2.0	0.124
Smits et al., [1979]	6000	6.0	0.17
Wilcken, [1930]	2600	6.5	0.25

Table 3.1. Features of pressure-generator airfoils selected					
Profile name	**Thickness ratio, %**	**Chord, m**	**Characteristics**	**Name of flow documented**	**Profile**
CP	19	0.8	Designed for convex wall experiments, provides large values of K_{max}	CP1, CP2	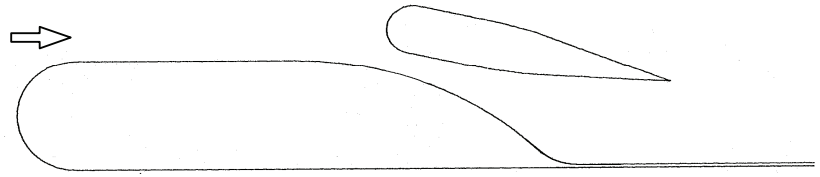
DP	22	0.9	Designed for convex wall experiments, provides moderate values of K_{max}	DP1	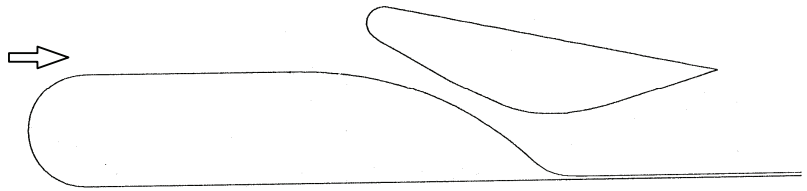
FP	10	0.5	designed for the flat plate experiments to produce pressure gradients similar to CP1 (convex surface)	FP1	

Table 3.2 Centerline surface pressure-port locations on convex-aft model - x, m							
0.512	0.632	0.752	0.865	0.985	1.105	1.225	1.345
0.532	0.652	0.772	0.885	1.005	1.125	1.245	1.365
0.552	0.672	0.792	0.905	1.025	1.145	1.265	1.385
0.572	0.692	0.812	0.925	1.045	1.165	1.285	1.405
0.592	0.712	0.832	0.945	1.065	1.185	1.305	1.425
0.612	0.732	0.845	0.965	1.085	1.205	1.325	1.445

Table 3.3 Spanwise surface pressure-port locations on convex-aft model				
x, m	**Spanwise location (distance from centerline), m**			
1.025	-0.15	-0.1	0.1	0.15
1.085	-0.15	-0.1	0.1	0.15
1.165	-0.15	-0.1	0.1	0.15
1.245	-0.15	-0.1	0.1	0.15

Table 3.4 Centerline surface pressure-port locations on flat-plate model - x, m							
0.50	0.64	0.78	0.92	1.06	1.20	1.34	1.48
0.52	0.66	0.80	0.94	1.08	1.22	1.36	1.50
0.54	0.68	0.82	0.96	1.10	1.24	1.38	1.52
0.56	0.70	0.84	0.98	1.12	1.26	1.40	1.54
0.58	0.72	0.86	1.00	1.14	1.28	1.42	
0.60	0.74	0.88	1.02	1.16	1.30	1.44	
0.62	0.76	0.90	1.04	1.18	1.32	1.46	

Table 3.5 Spanwise surface pressure-port locations on flat-plate model				
x, m	**Spanwise location (distance from centerline), m**			
0.9	-0.15	-0.1	0.1	0.15
1.1	-0.15	-0.1	0.1	0.15
1.2	-0.15	-0.1	0.1	0.15

Table 3.6 Surface hot-film locations on convex-aft model - x, m						
0.760*	1.025	1.105	1.168	1.232	1.297	1.386
0.934	1.066	1.127	1.189	1.253	1.319	
0.984	1.085	1.148	1.210	1.275	1.341	

* hot-film gauge calibration location

Table 3.7 Surface hot-film locations on flat-plate model - x, m						
0.76*	0.96	1.06	1.16	1.26	1.36	1.46
0.79	0.98	1.08	1.18	1.28	1.38	1.48
0.84	1.00	1.10	1.20	1.30	1.40	1.50
0.89	1.02	1.12	1.22	1.32	1.42	1.52
0.94	1.04	1.14	1.24	1.34	1.44	

* hot-film gauge calibration location

Table 3.8 Features of the Initial boundary layer						
Flow	**Surface**	U_∞, m/s	U_o, m/s	δ_o, mm	$k\delta_o$	$R_{\theta o}$
CP1	Convex	9.6	11.3	26.5	0.0275	1710
DP1	Convex	9.6	11.3	26.5	0.0275	1710
CP2	Convex	13.0	not measured		$\cong$ 0.0275	$\cong$ 2000
FP1	Flat	12.5	11.72	24.1	---	1670

Table 3.9 The acceleration and related parameters in the experiments							
Flow	**Surface**	$C_{p,min}$	L_a/δ_o	K_{max} x10^6	$I(K)$ x10^6	K^*_{max} x10^6	Λ_{max}
Flat plate critical values	Flat	------	-----	$\cong$3.5	------	$\cong$8.1	$\cong$50
CP1	Convex	-4.74	10	6.2	30.1	13.4	158
DP1	Convex	-4.15	14	3.8	29.2	6.4	58
CP2	Convex	-6.07	7	9.0	29.1	30.0	325
FP1	Flat	-3.35	12	6.2	34.0	16.4	159

Table 5.1 Retransition location in relaminarizing flows			
Reference	**Flow**	**Location of $C_{f,min}$ in reference to $C_{p,min}$**	**$(R_\theta)_{QL\text{-}inner}$ at $C_{p,min}$ location**
Badri Narayanan & Ramjee	BR2	At	340
Blackwelder & Kovasznay [1972]	BK	Before	600
Brandt [1993]	A1	After	168
	A2	After	217
	A3	At	243
	A4	At	270
	B1	After	164
Warnack & Fernholz	WF2	At	300
	WF4	At	270
Present	CP1	After	154
	DP1	After	200
	FP1	After	170
Minimum value when retransition is occurring at $C_{p,min}$ location			243
Maximum value when retransition is occurring after $C_{p,min}$ location			217

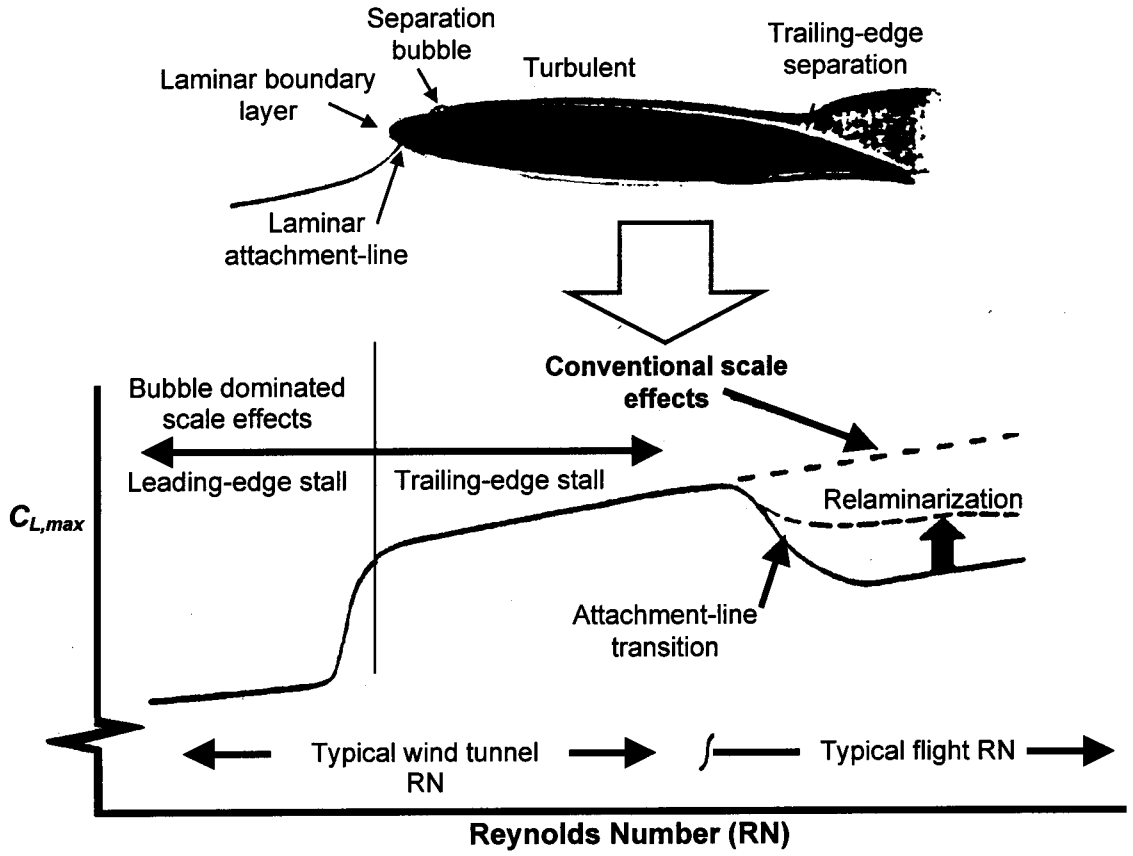

Fig.1 Effect of attachment-line transition and relaminarization on maximum lift ($C_{L,max}$) for a singe-element lifting surface. From Van Dam et al [1993]

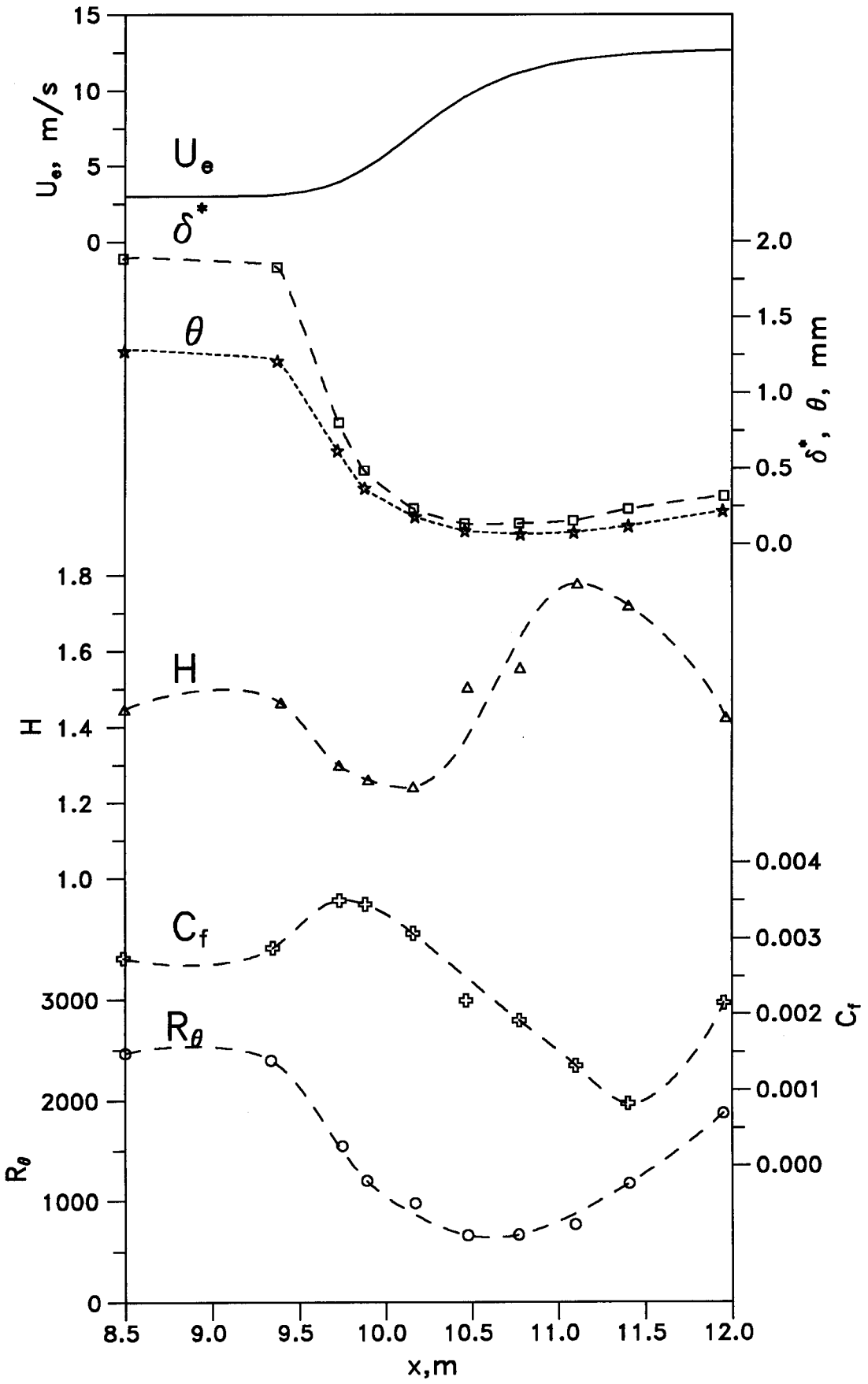

Fig.2.1 The streamwise variation of boundary layer parameters during relaminarization – Flow of Blackwelder & Kovasznay [1972]

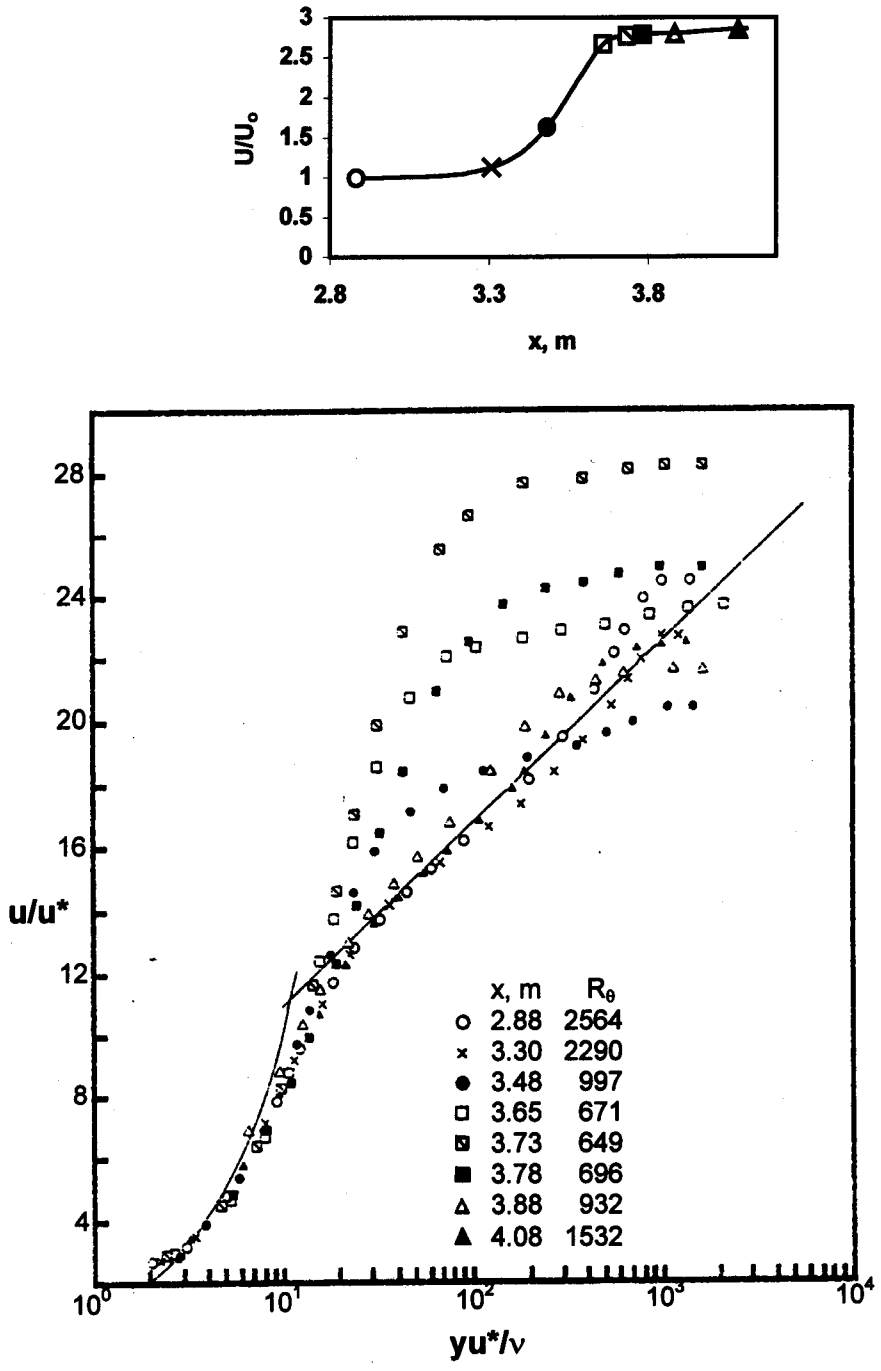

Fig.2.2 Boundary layer profiles of the mean velocity in inner-law scaling during relaminarization, flow -Case 4 of Warnack & Fernholz [1998]. Top figure shows the symbols in the velocity plot at respective streamwise locations

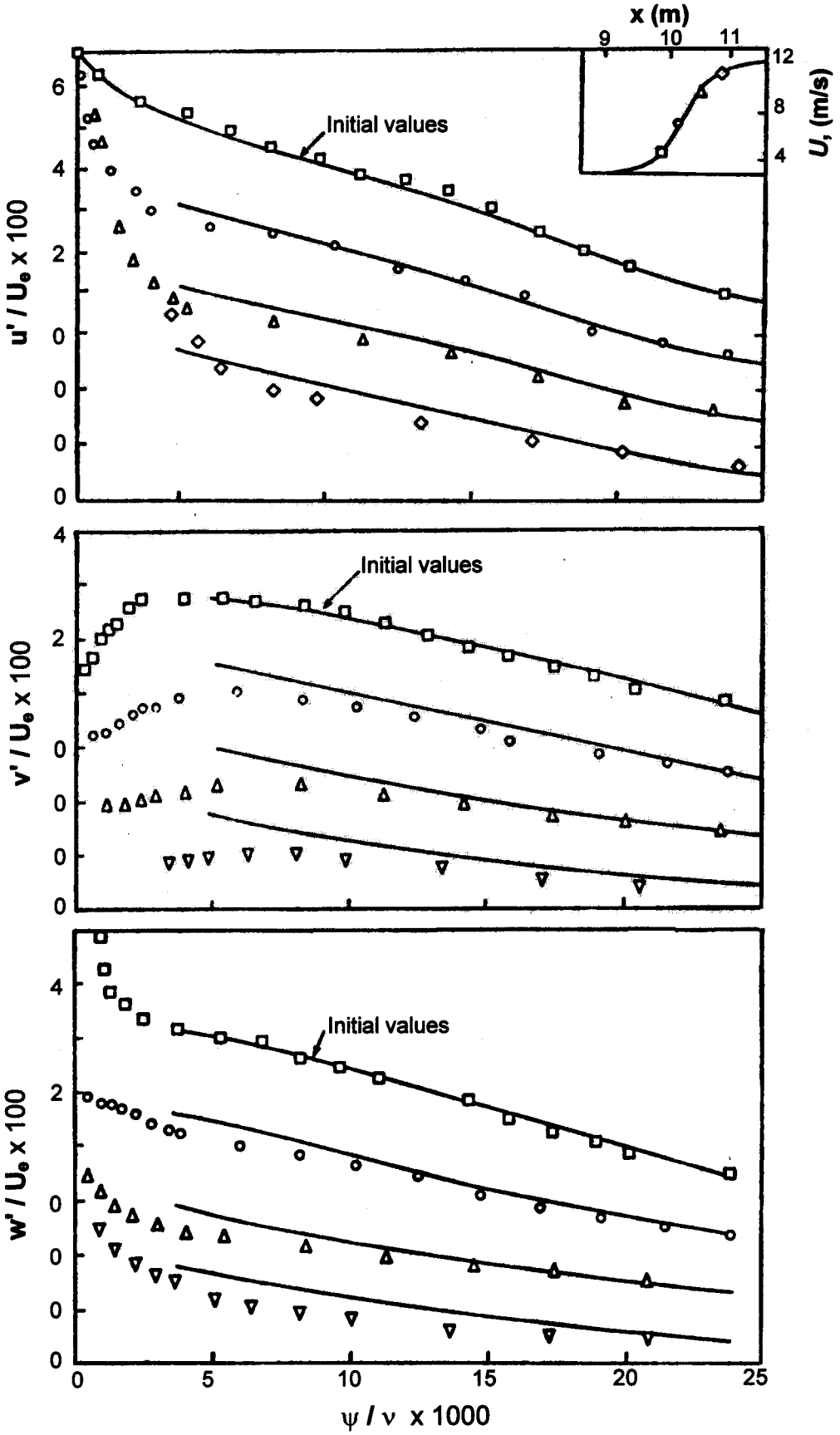

Fig. 2.3 Comparison of measured turbulence intensity distributions across normalized streamlines in the outer layer, data from Blackwelder & Kovasznay [1972], with that predicted using rapid distortion theory of Sreenivasan [1974]

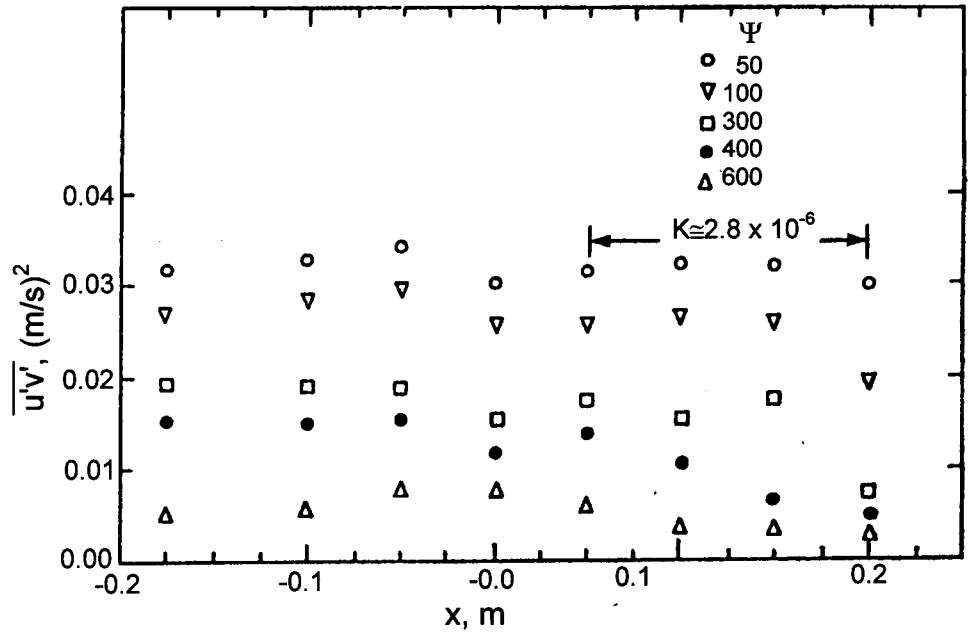

Fig.2.4 The 'freezing' of Reynolds shear stress along outer streamlines (Ψ) during relaminarization, flow of Badri Narayanan et al [1974], data from Sreenivasan [1982]

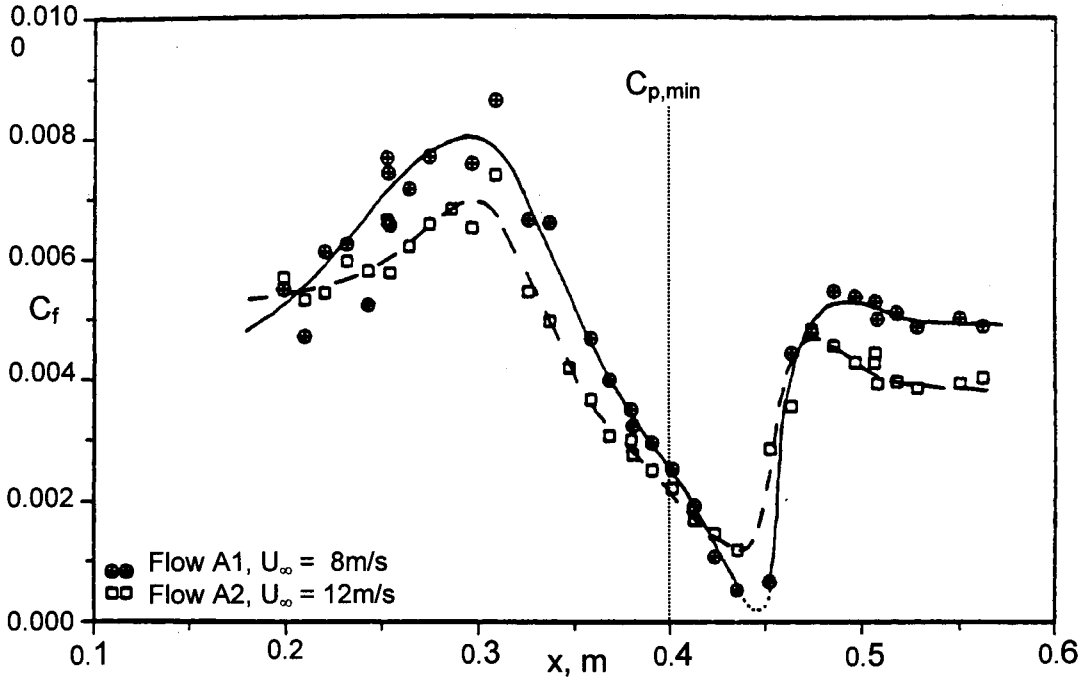

Fig.2.5 The streamwise variations of C_f in the experiments of Brandt [1993]. Lines drawn for clarity. The interpolated dotted line for flow A1 represents the region inside the laminar separation bubble. Note that C_f continues to drop beyond $C_{p,min}$ location.

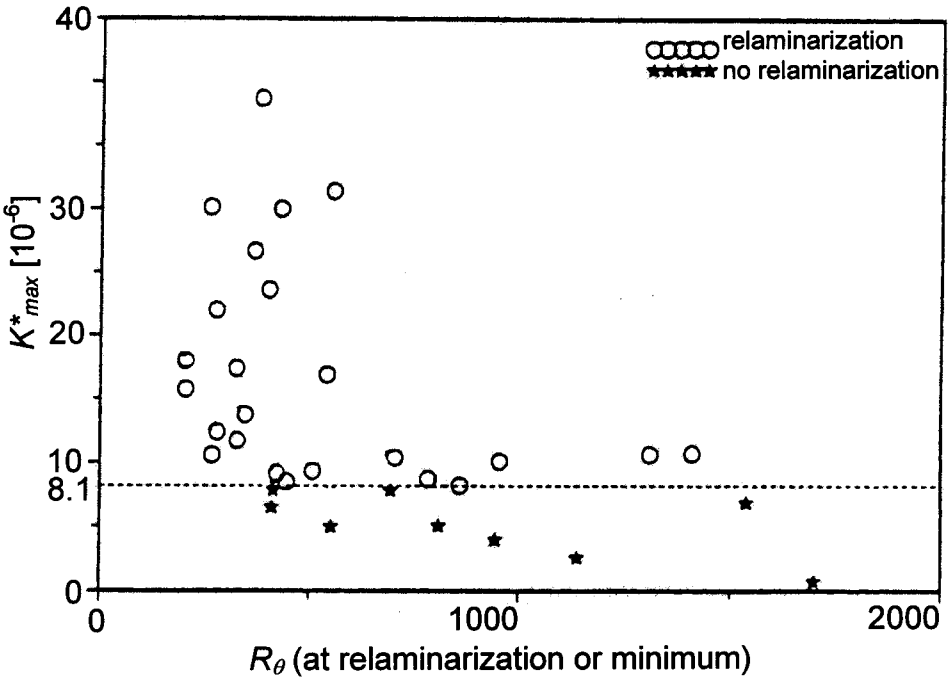

Fig.2.6 The acceleration parameter K^* of Brandt [1993] plotted for various experiments from literature (see Brandt [1993] for details). All relaminarizing data are above the critical value of 8.1×10^{-6} and all non-relaminarizing data are below.

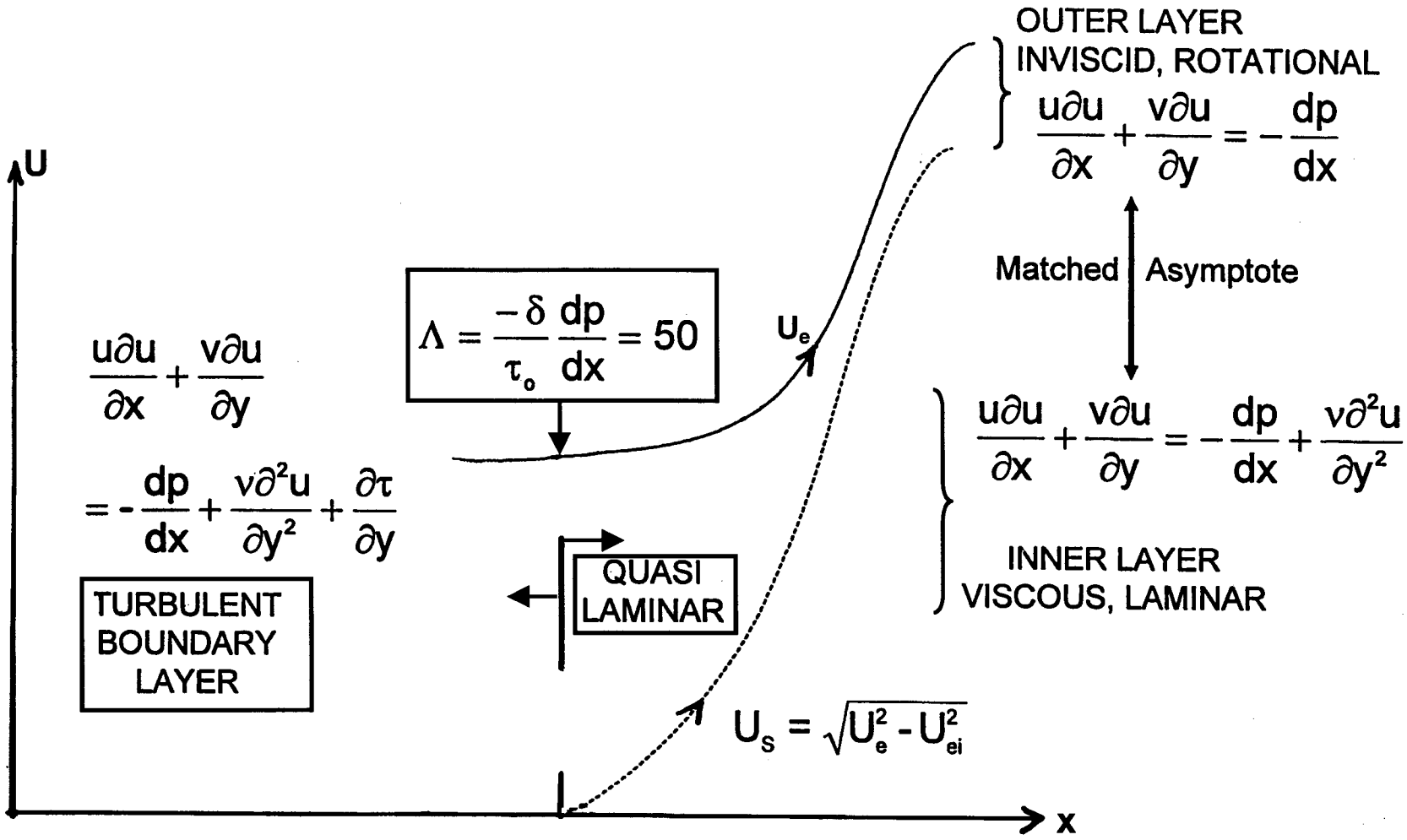

Fig.2.7 Highlights of the Quasi-laminar equations of Narasimha and Sreenivasan [1973]

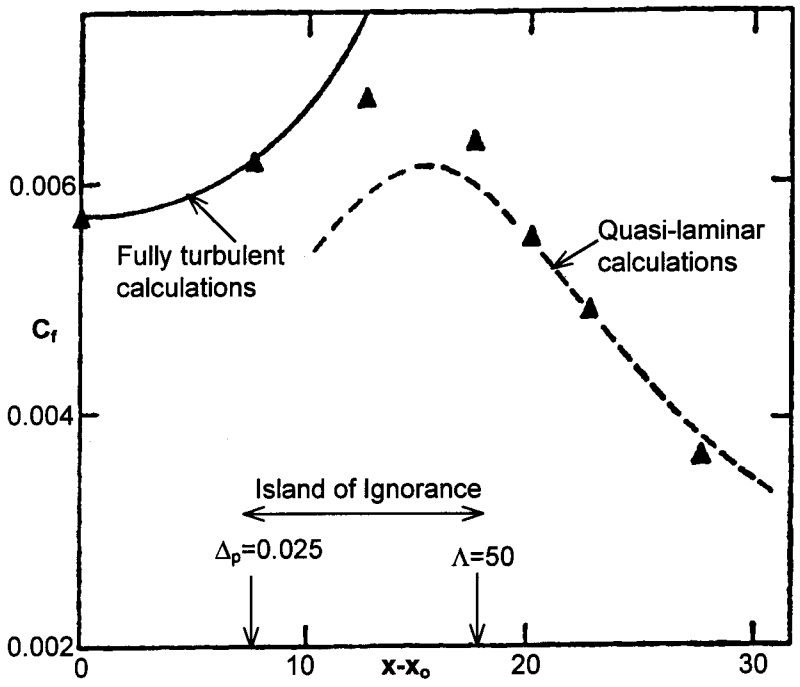

Fig.2.8 Schematic showing the matching of C_f from quasi-laminar equations during the latter stages of the relaminarization process (From Sreenivasan [1982])

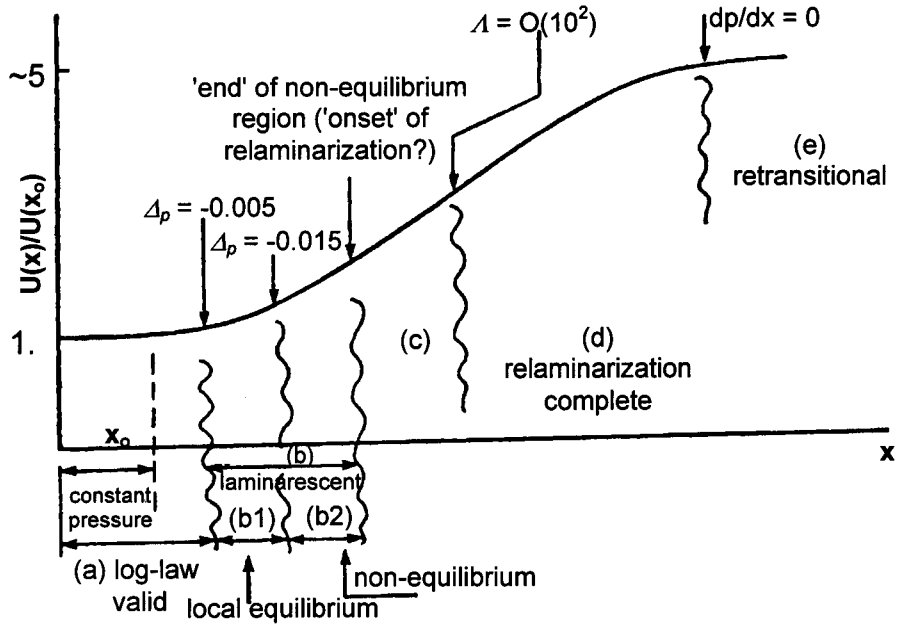

Fig.2.9 Schematic showing a broad classification of the flow field during relaminarization (from Sreenivasan [1982])

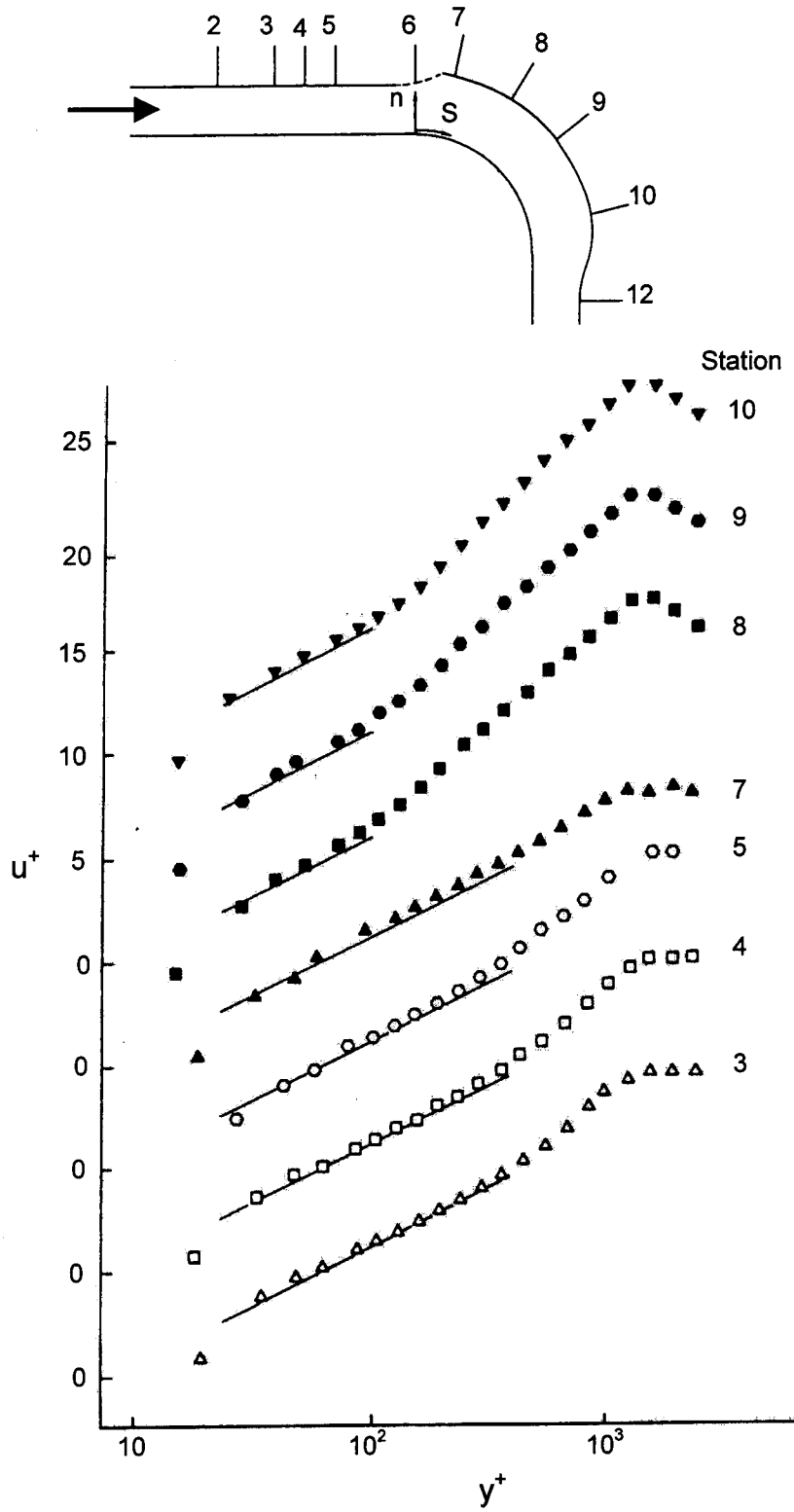

Fig. 2.10 Streamwise variation of the velocity profile plotted in wall variables
Figure at top gives the measurement stations
-- convex surface experiments of Gillis & Johnston [1983]

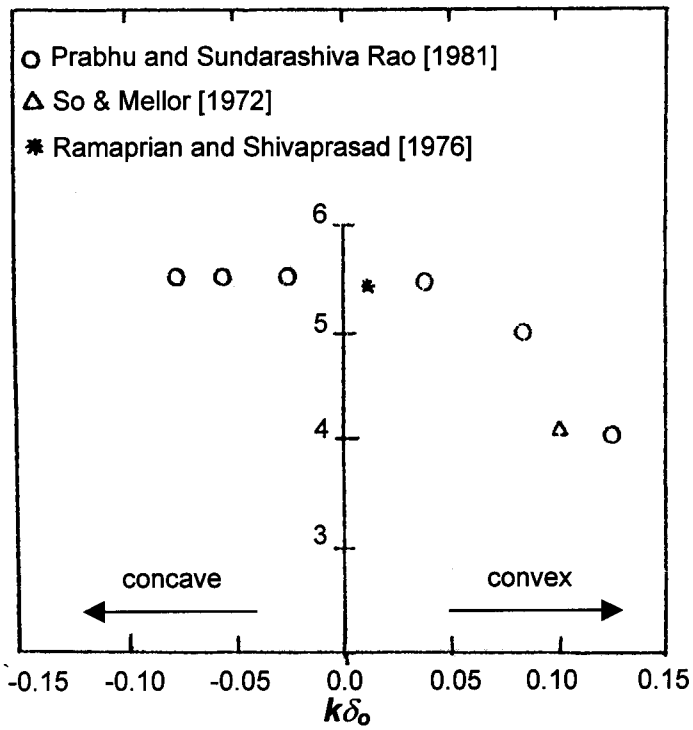

Fig.2.11 Variation of the intercept B of the wall law with $k\delta_o$ from Prabhu et al [1983]

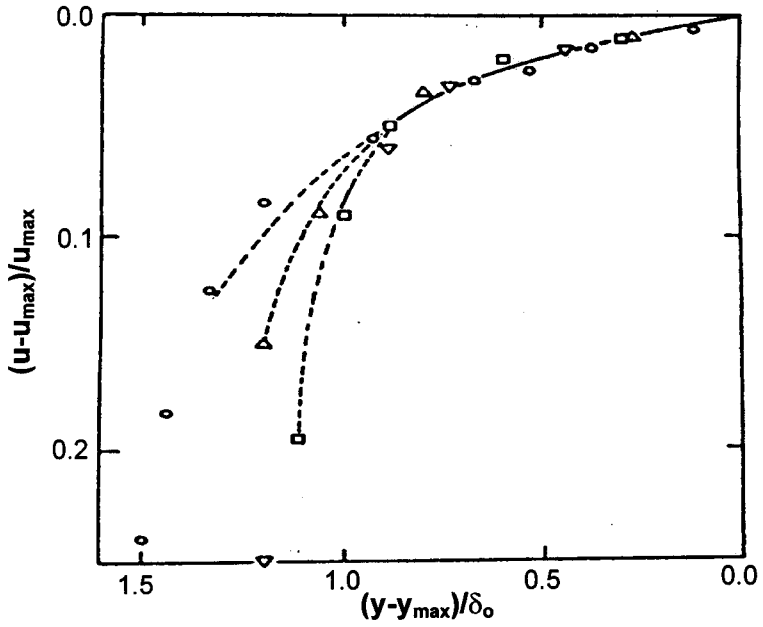

Fig. 2.12 Outer region mean flow similarity in convex surface boundary layers. The variables are centred at the location (y_{max}) of the mean velocity profile. Different symbols correspond to profiles at different streamwise distances on the convex surface boundary layer, from Prabhu et al [1983]

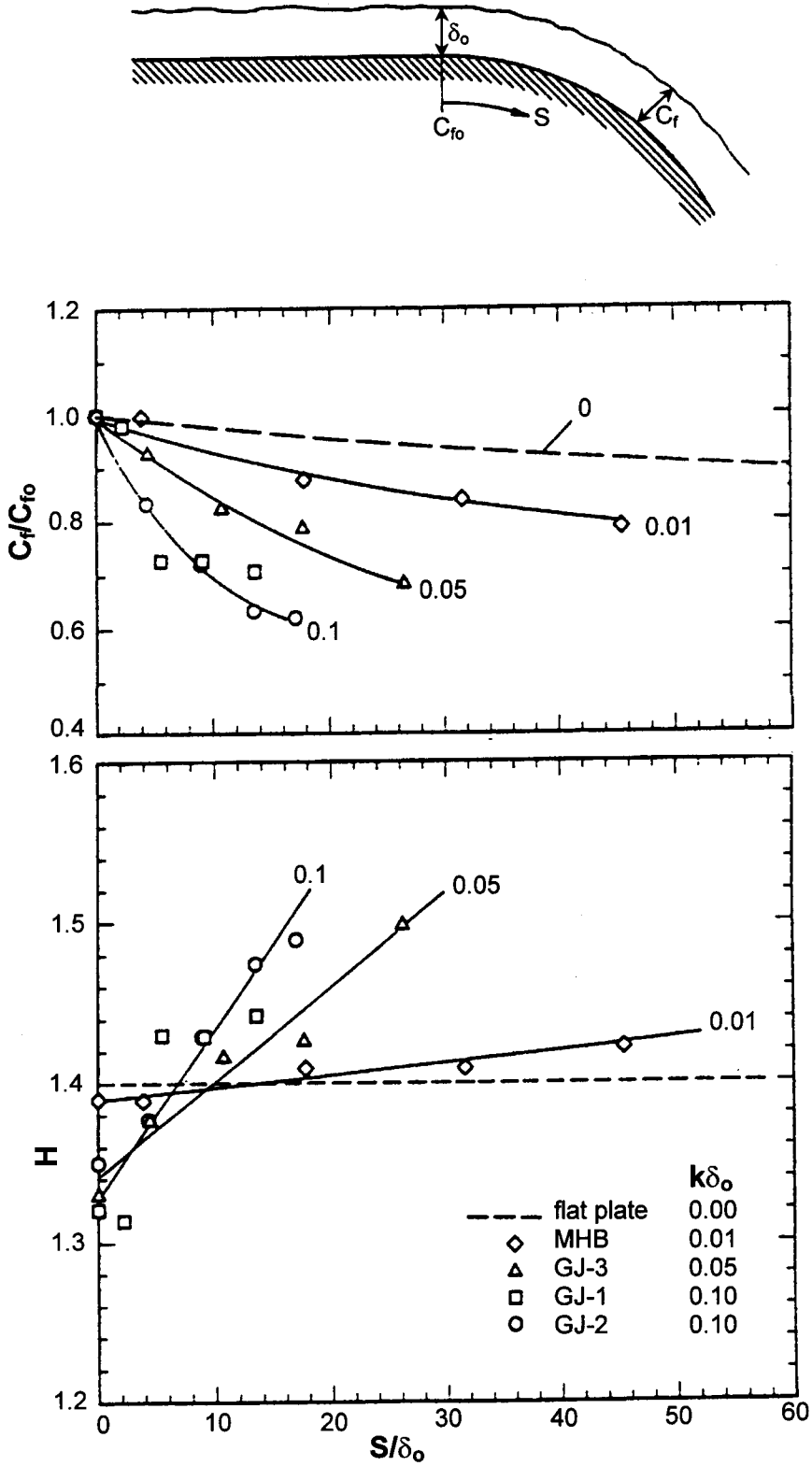

Fig.2.13 Streamwise variation of C_f and H on a convex surface for various $k\delta_o$ from Patel & Sotiropoulous [1997]. Experiments of Muck at al [1985] – MHB and Gillis & Johnston [1983] – GJ

Top sketch shows the geometry of the curved test section and nomenclature

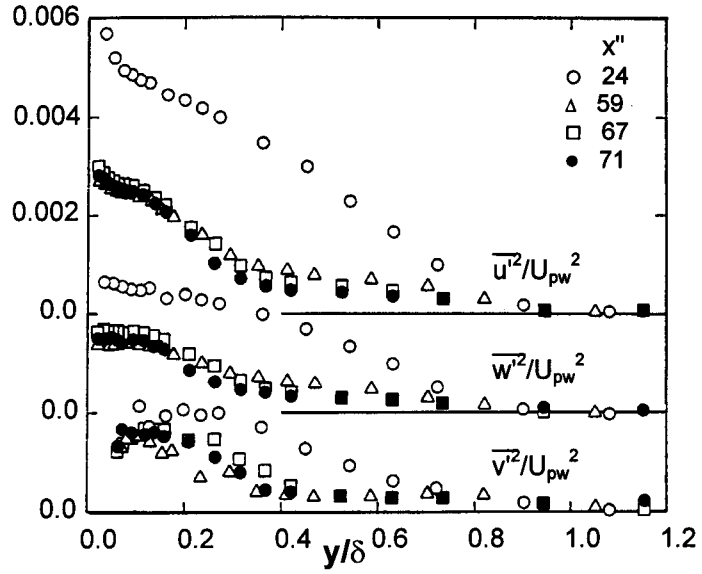

a) Distribution of turbulence intensities in the boundary layer

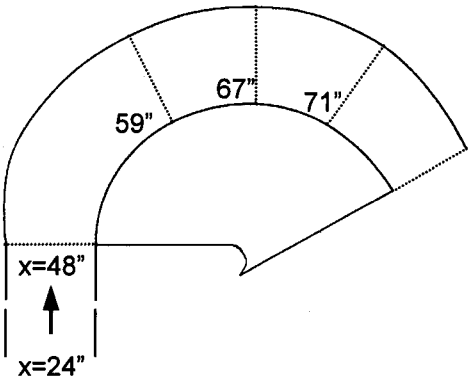

d) Sketch of the convex surface showing relevant distances

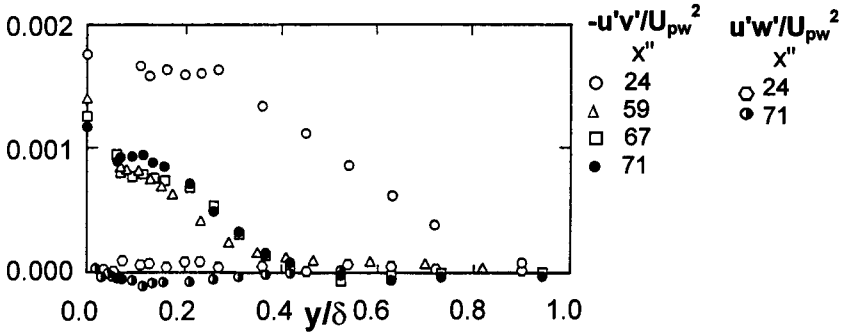

b). Distribution of shear stress in the boundary layer

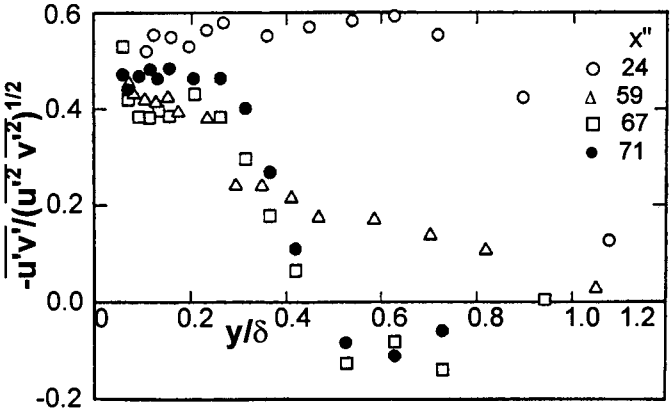

c). Distribution of shear correlation coefficient in the boundary layer

Fig 2.14 Distribution of various turbulence parameters in the convex-surface boundary layer. Experiments of So & Mellor [1973]

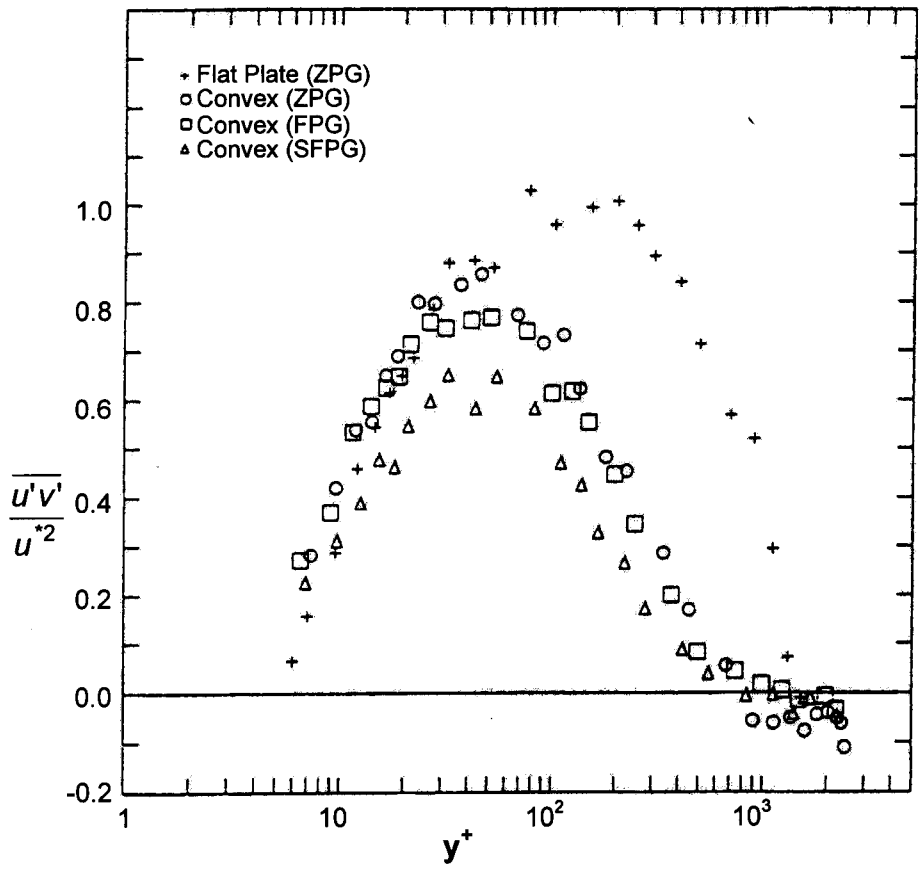

Fig. 2.15 Reynolds shear stress profiles of a turbulent boundary layer on flat and convex walls, with different streamwise pressure gradients - Experiments of Schwarz & Plesniak [1996]

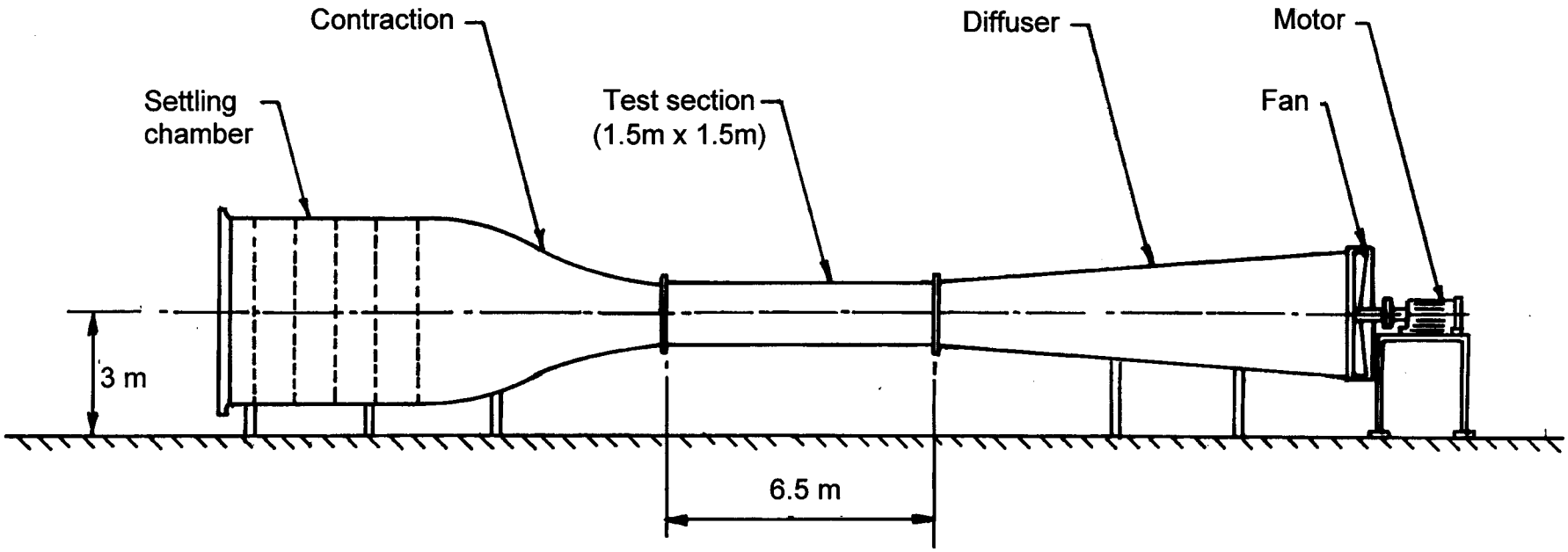

Fig.3.1 Schematic of 1.5m x 1.5m Low Speed Wind Tunnel

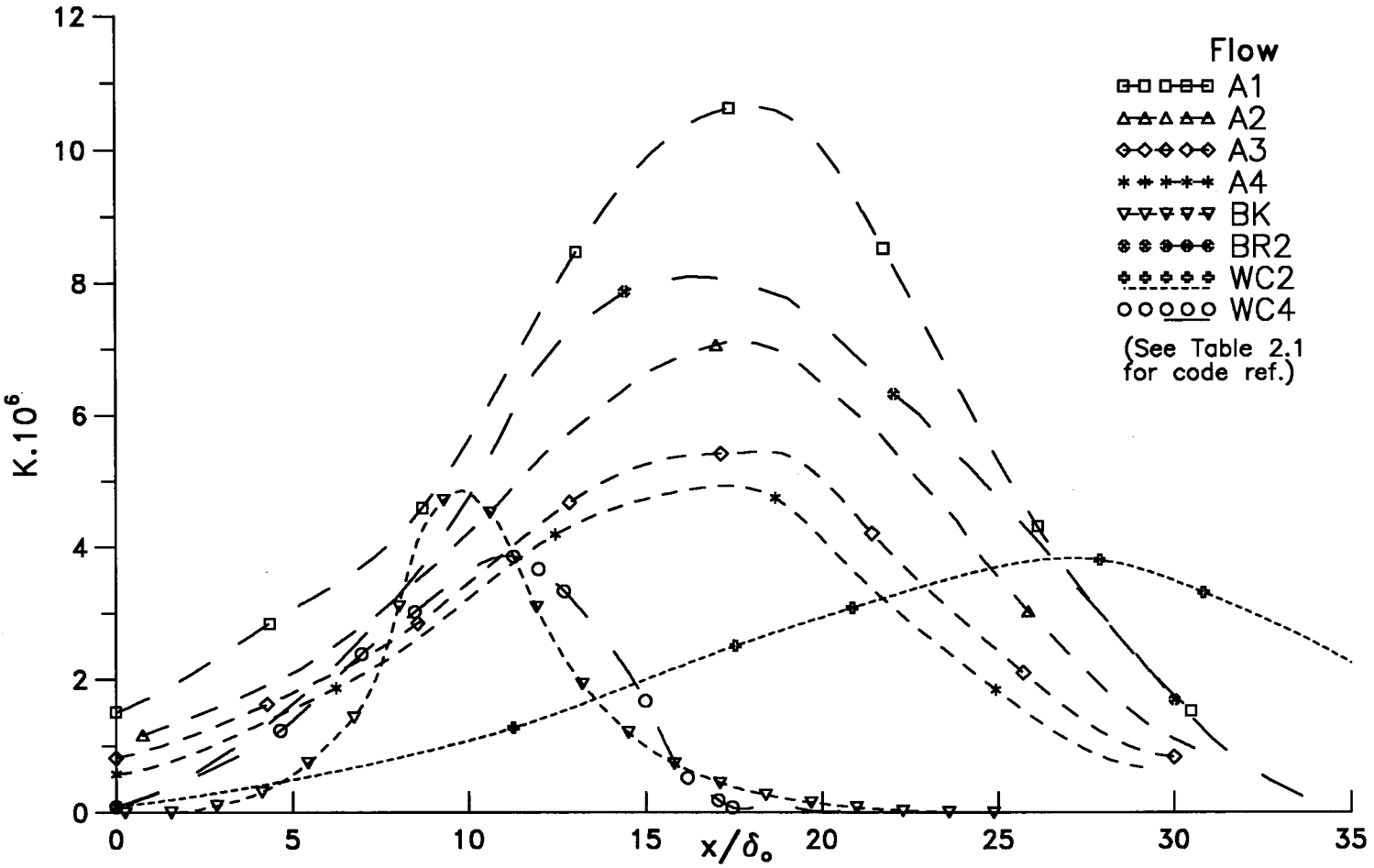

Fig.3.2 The streamwise variation of K for various experiments from literature, also showing the normalised extent of acceleration

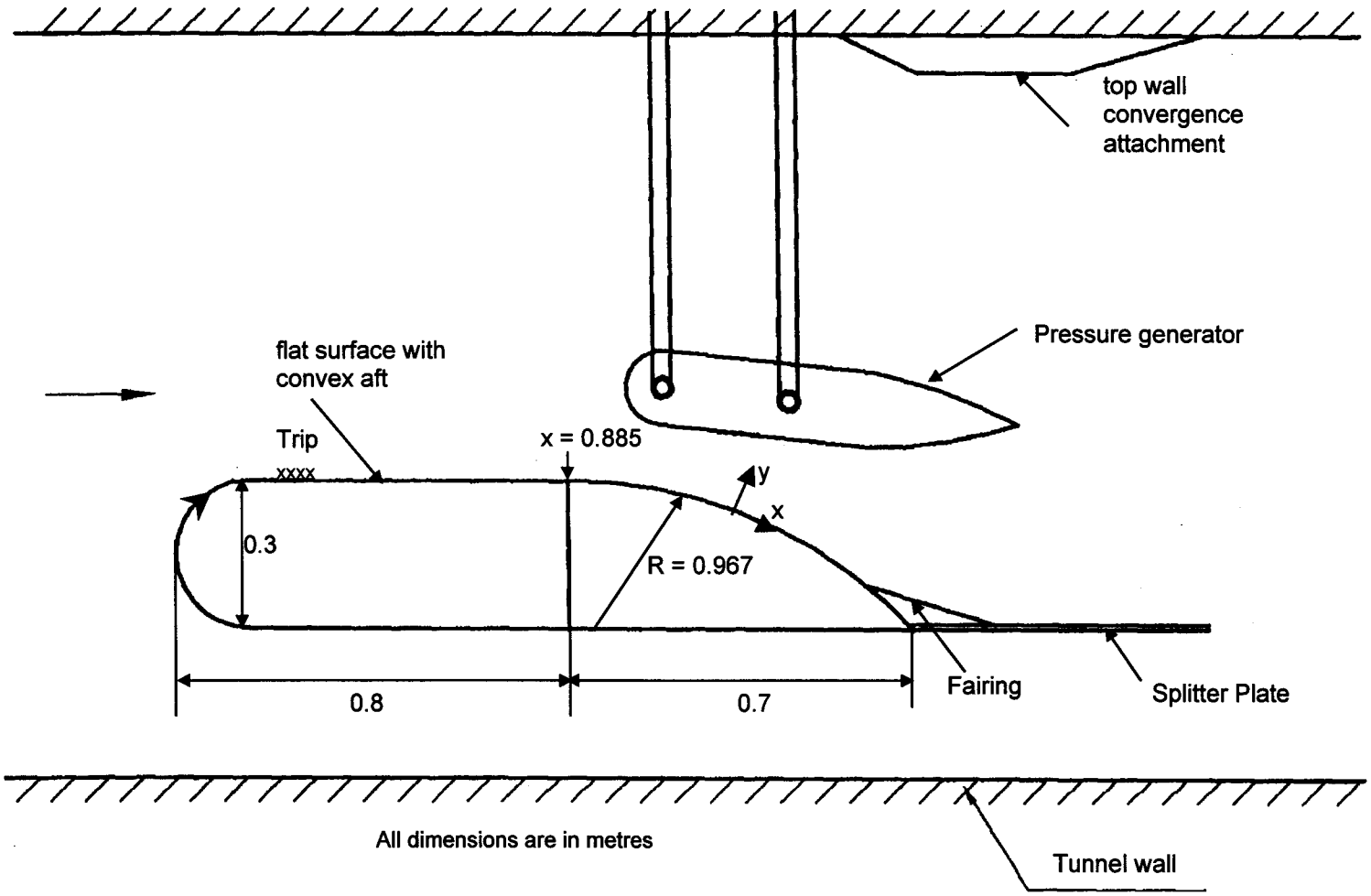

Fig. 3.3 Sketch of the model layout in 1.5m wind tunnel
-- convex surface experiments

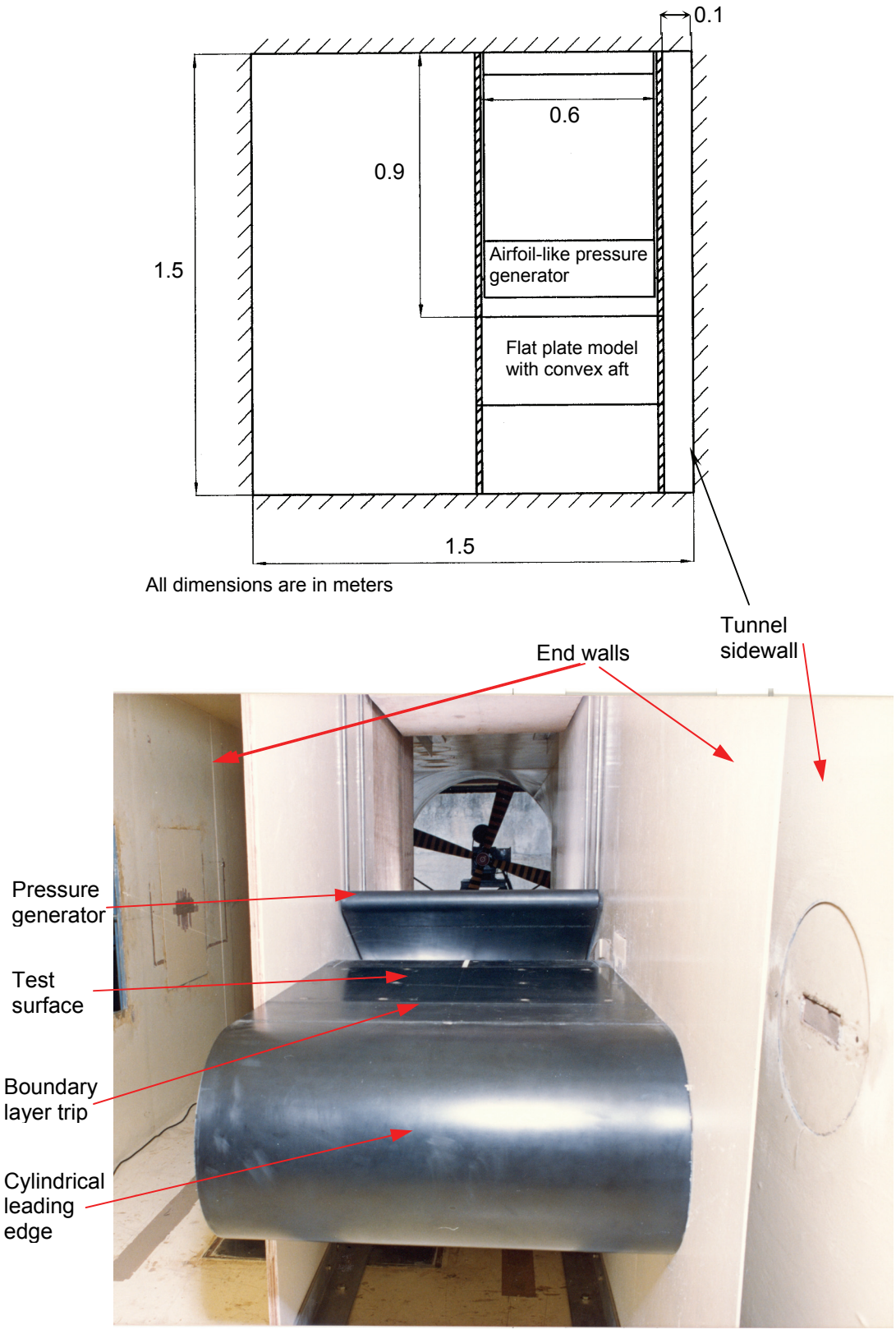

Fig.3.4 A sketch of the front view of the model setup and its photograph -- convex surface experiments

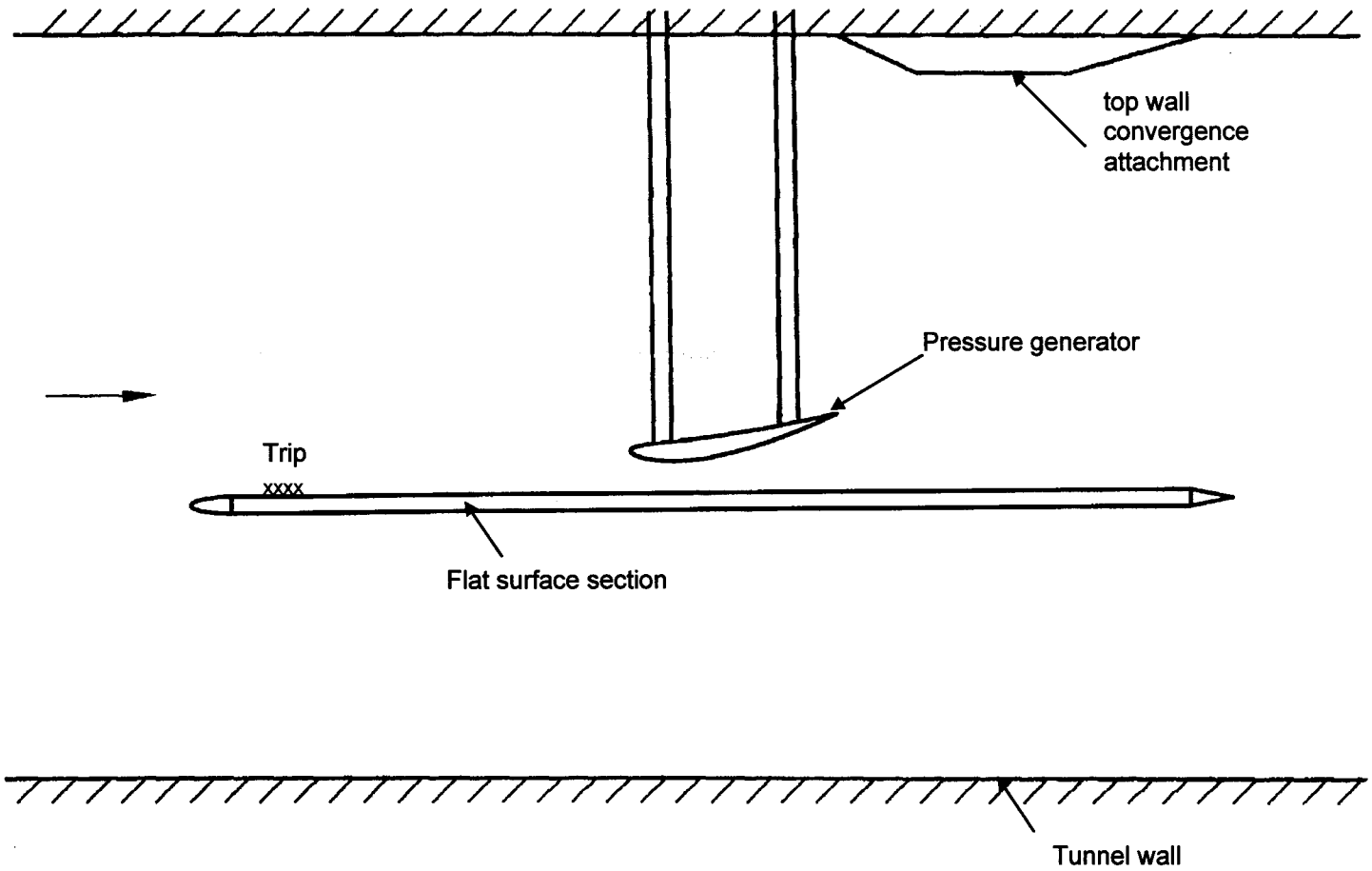

Fig. 3.5 Sketch of the model layout in 1.5m wind tunnel
-- flat surface experiments

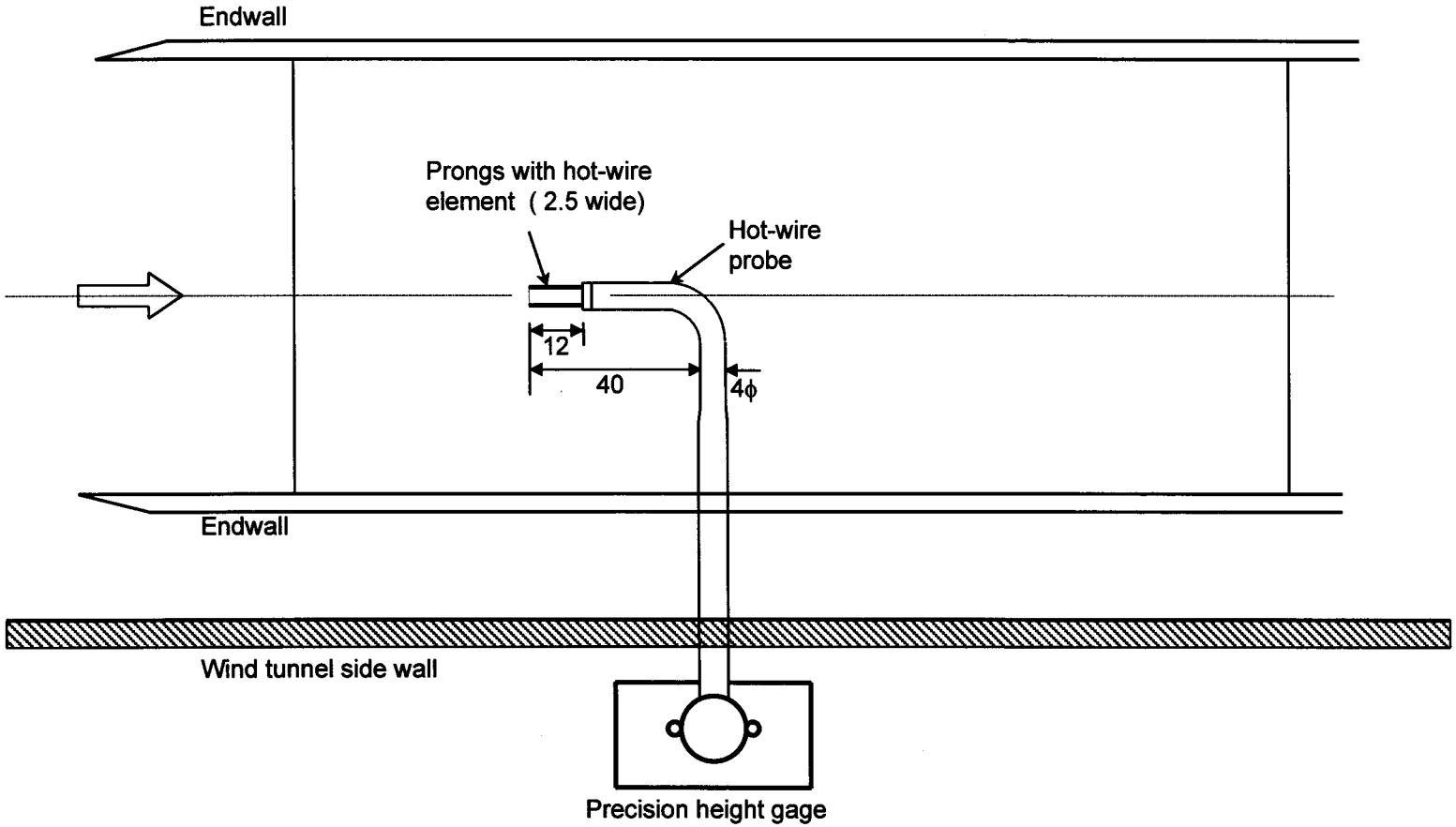

Fig. 3.6 Schematic of the top view of the model section showing the special hot-wire probe in location (all dimensions in mm, figure not to scale)

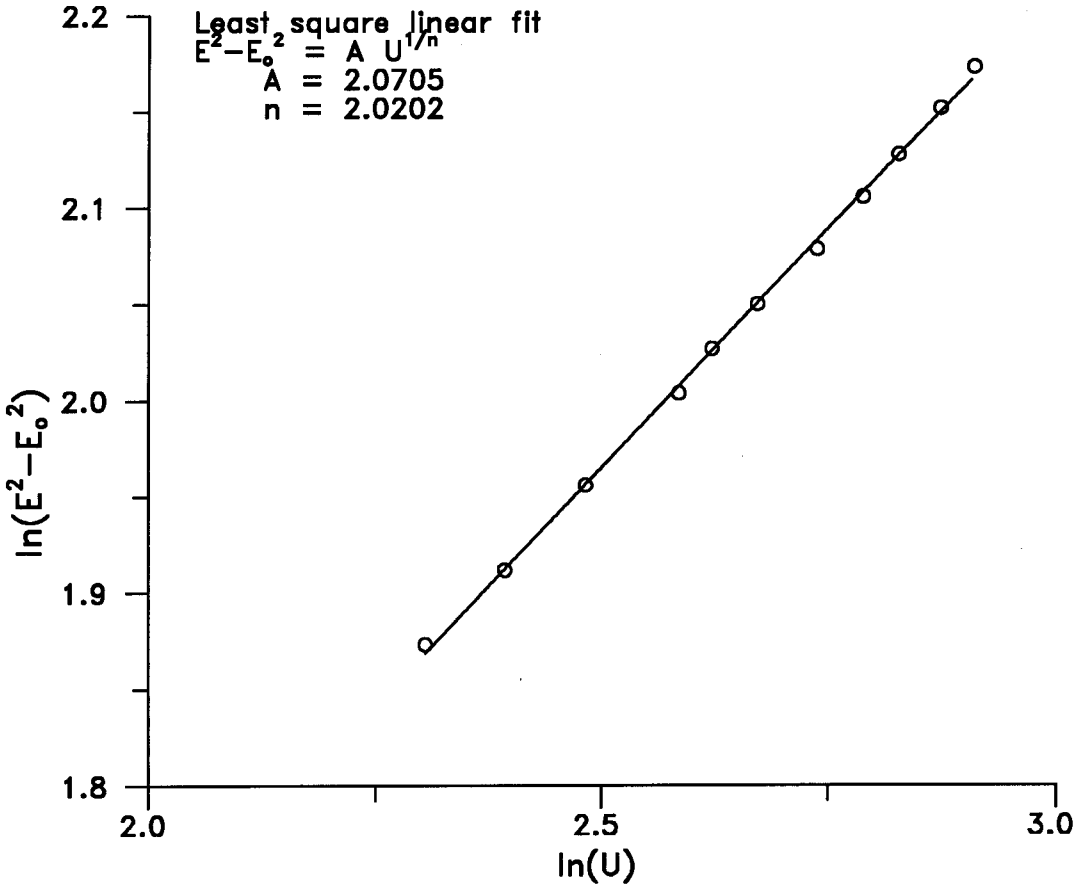

Fig 3.7 A typical calibration plot of the hot-wire probe

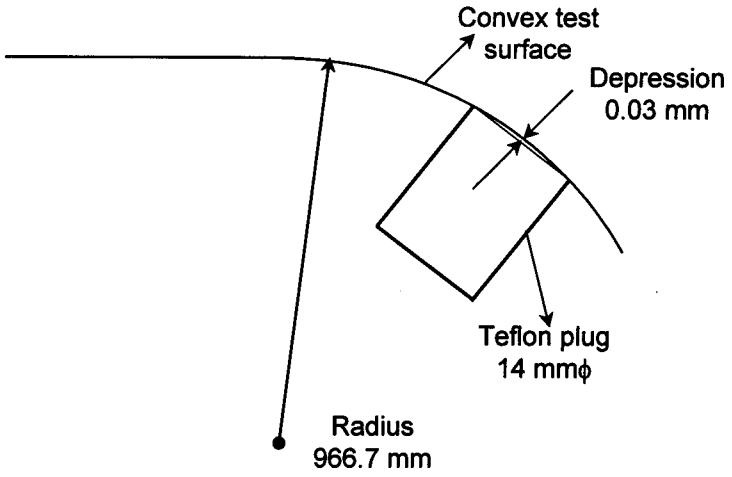

Fig.3.8 Sketch of the convex test surface with an exaggerated view of the Teflon plug for mounting the hot-film gage, illustrating that the dimensions of the depression caused by the flat top of the plug is negligible.

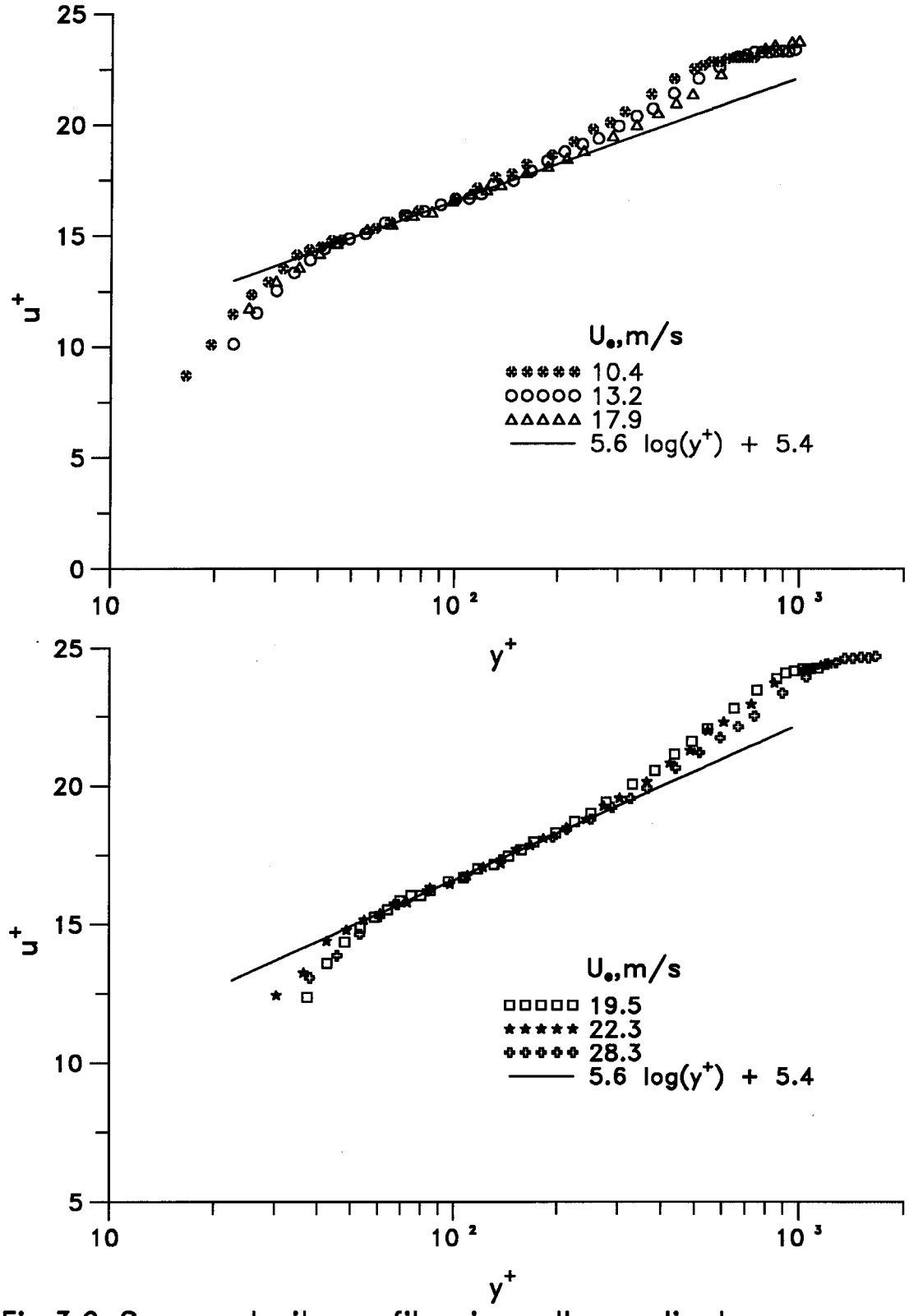

Fig.3.9 Some velocity profiles in wall coordinates used for hot-film calibration

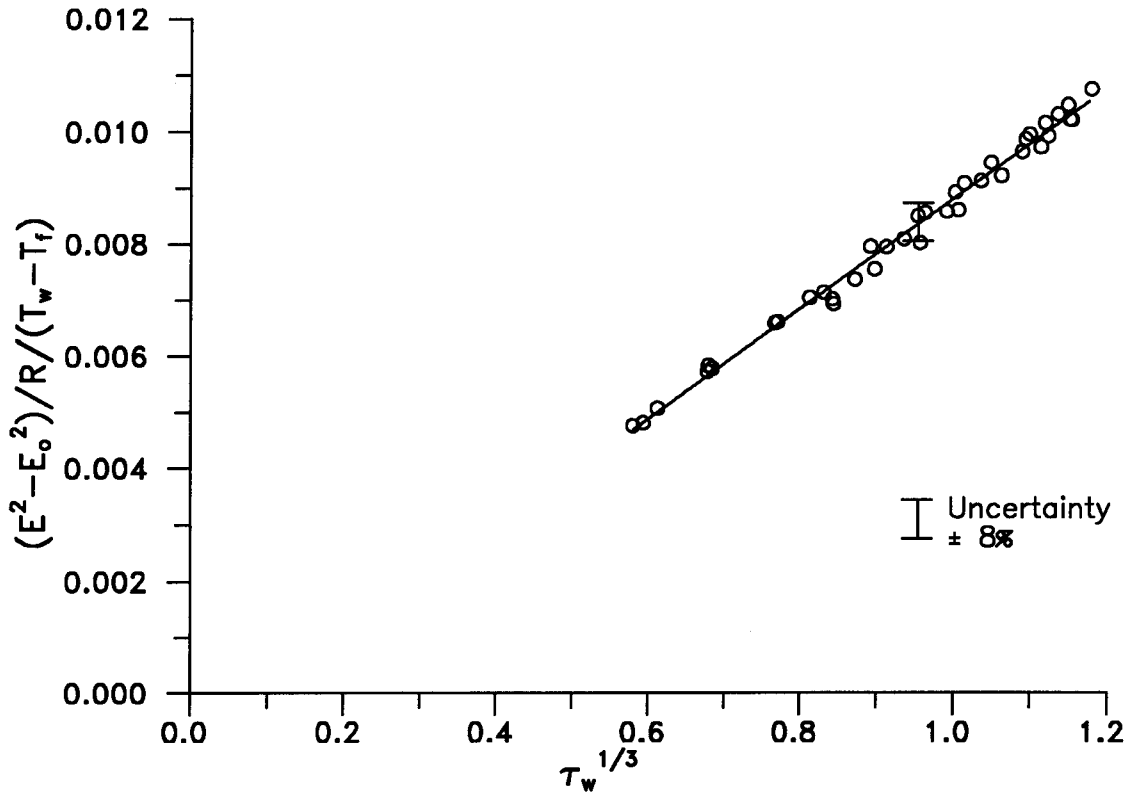

Fig.3.10 A typical calibration plot of the hot-film gage Contains several data sets

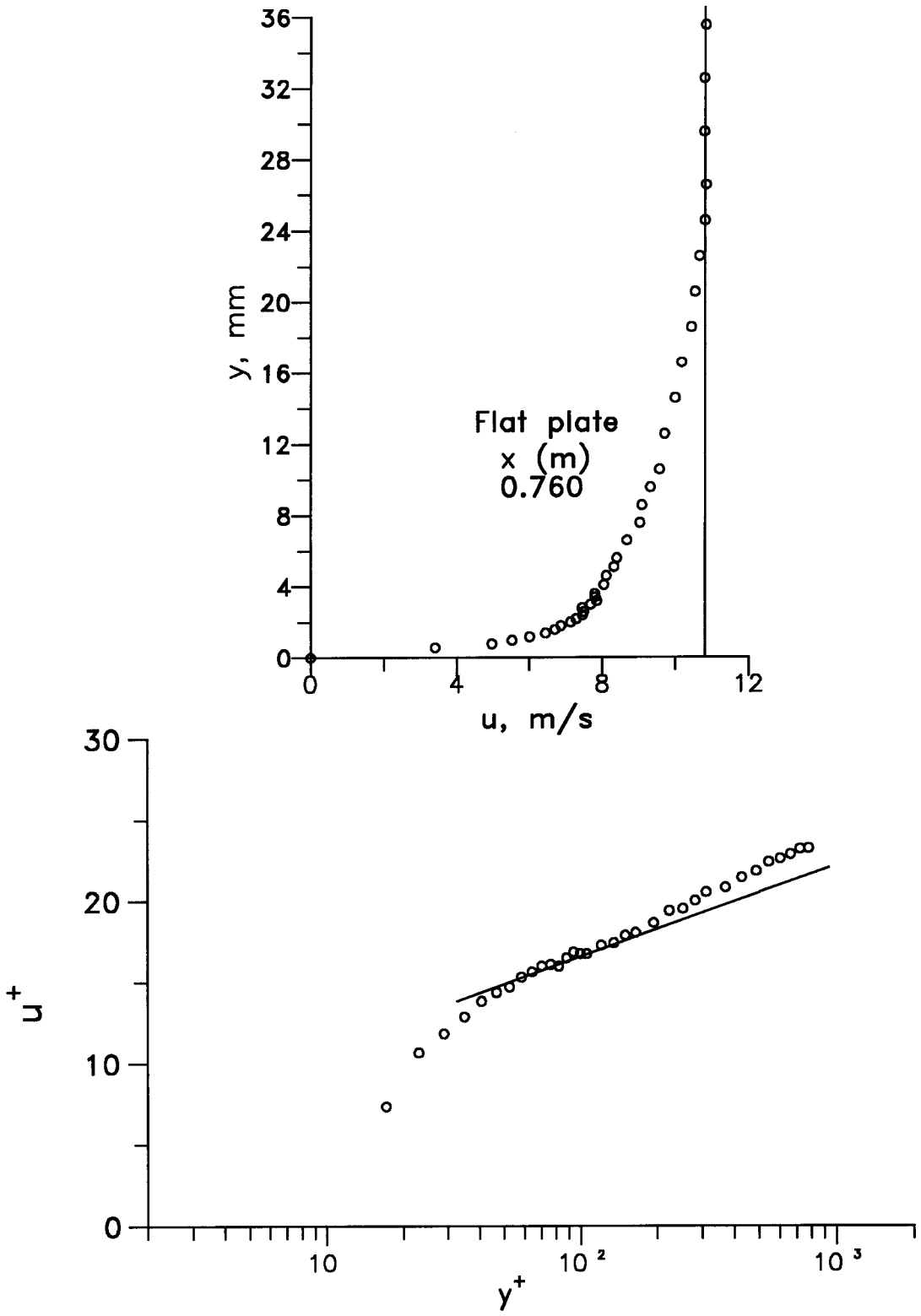

Fig.3.11 The boundary layer profile of the initial zero pressure-gradient region in linear & wall coordinates – Flow CP1 and DP1

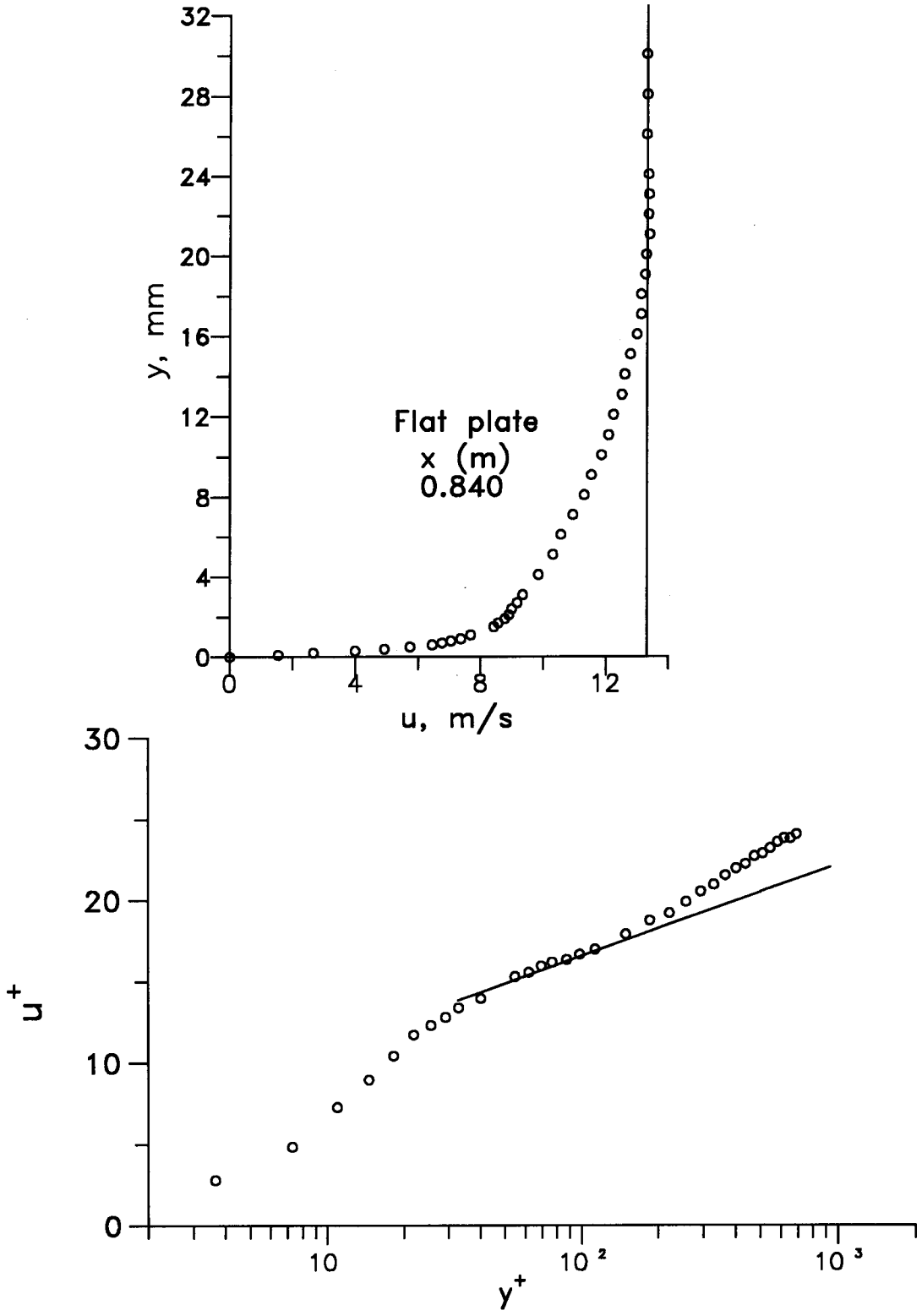

Fig.3.12 The boundary layer profile of the initial zero pressure-gradient region in linear & wall coordinates – Flow FP1

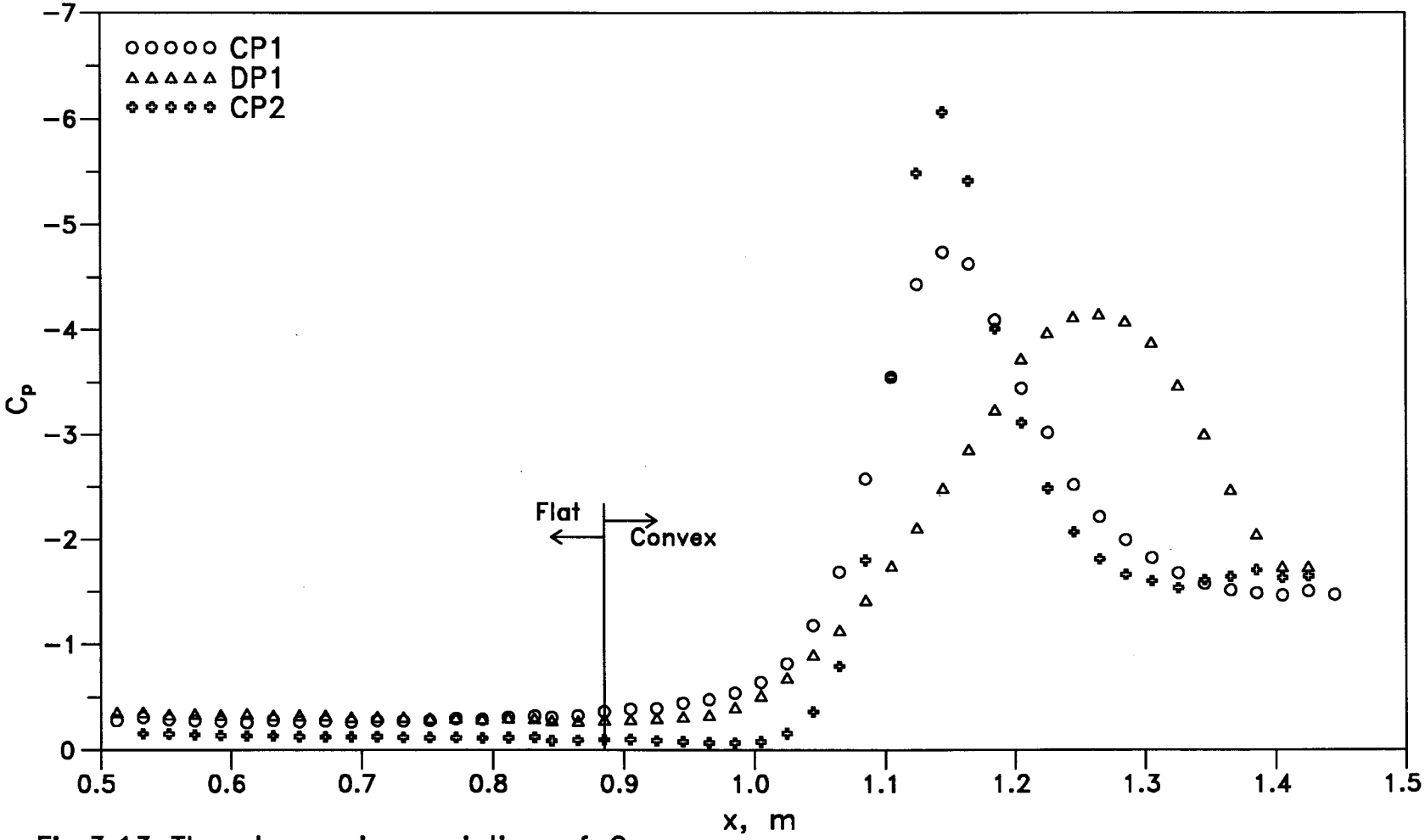

Fig.3.13 The streamwise variation of C_p in the three convex surface flows

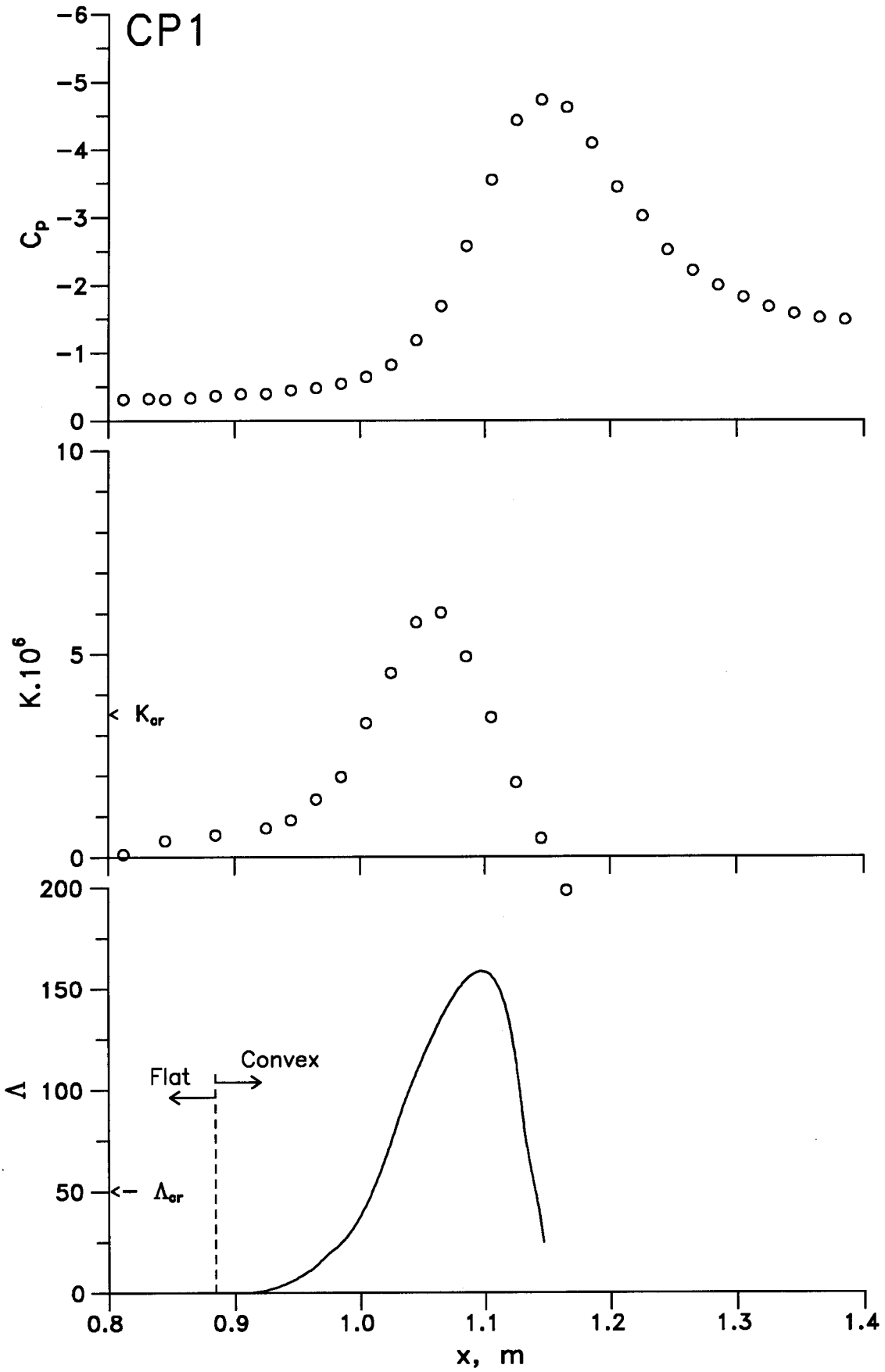

Fig.3.14 Streamwise variation of the acceleration and pressure gradient parameters -- flow CP1

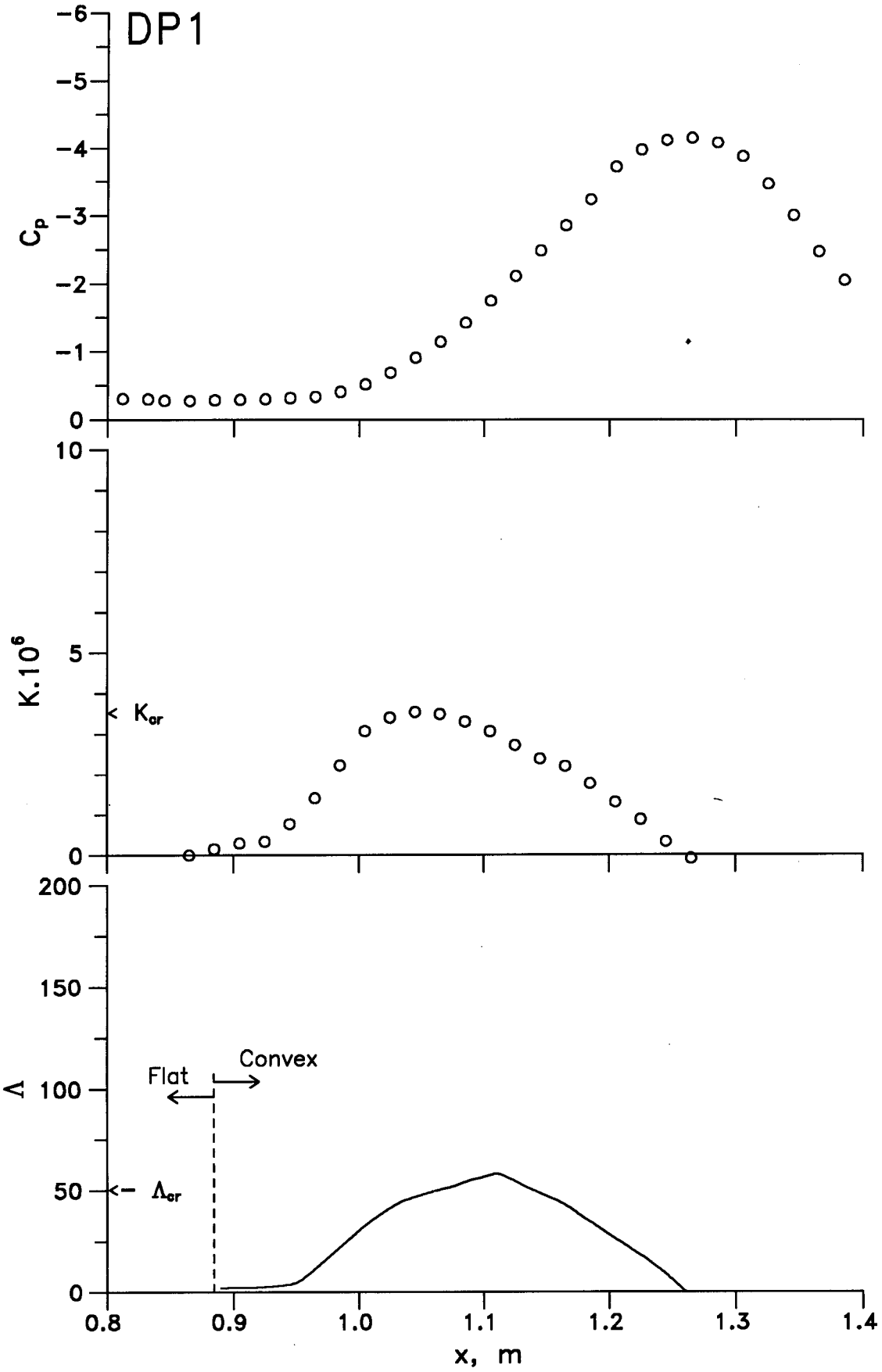

Fig.3.15 Streamwise variation of the acceleration and pressure gradient parameters -- flow DP1

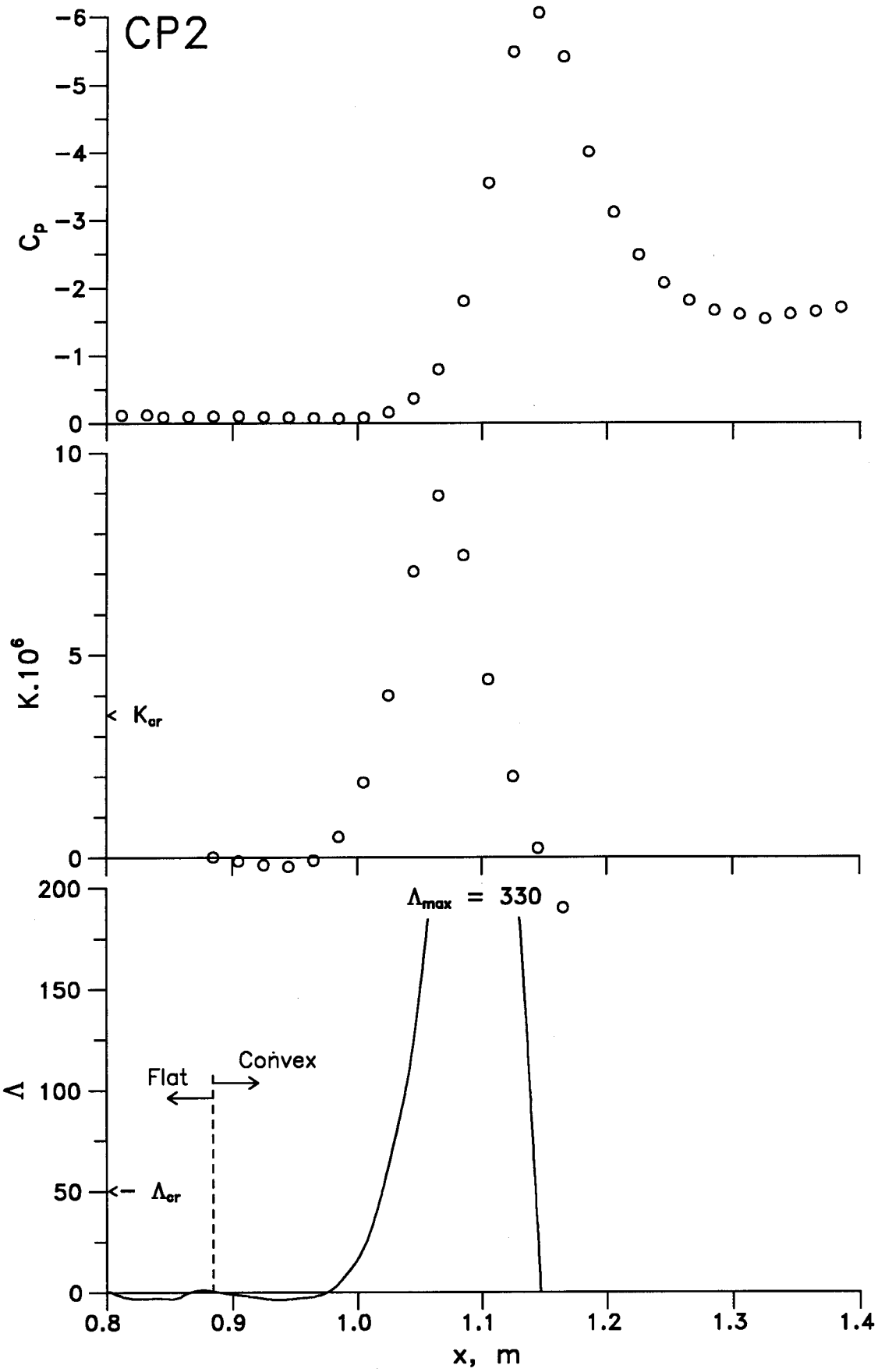

Fig.3.16 Streamwise variation of the acceleration and pressure gradient parameters -- flow CP2

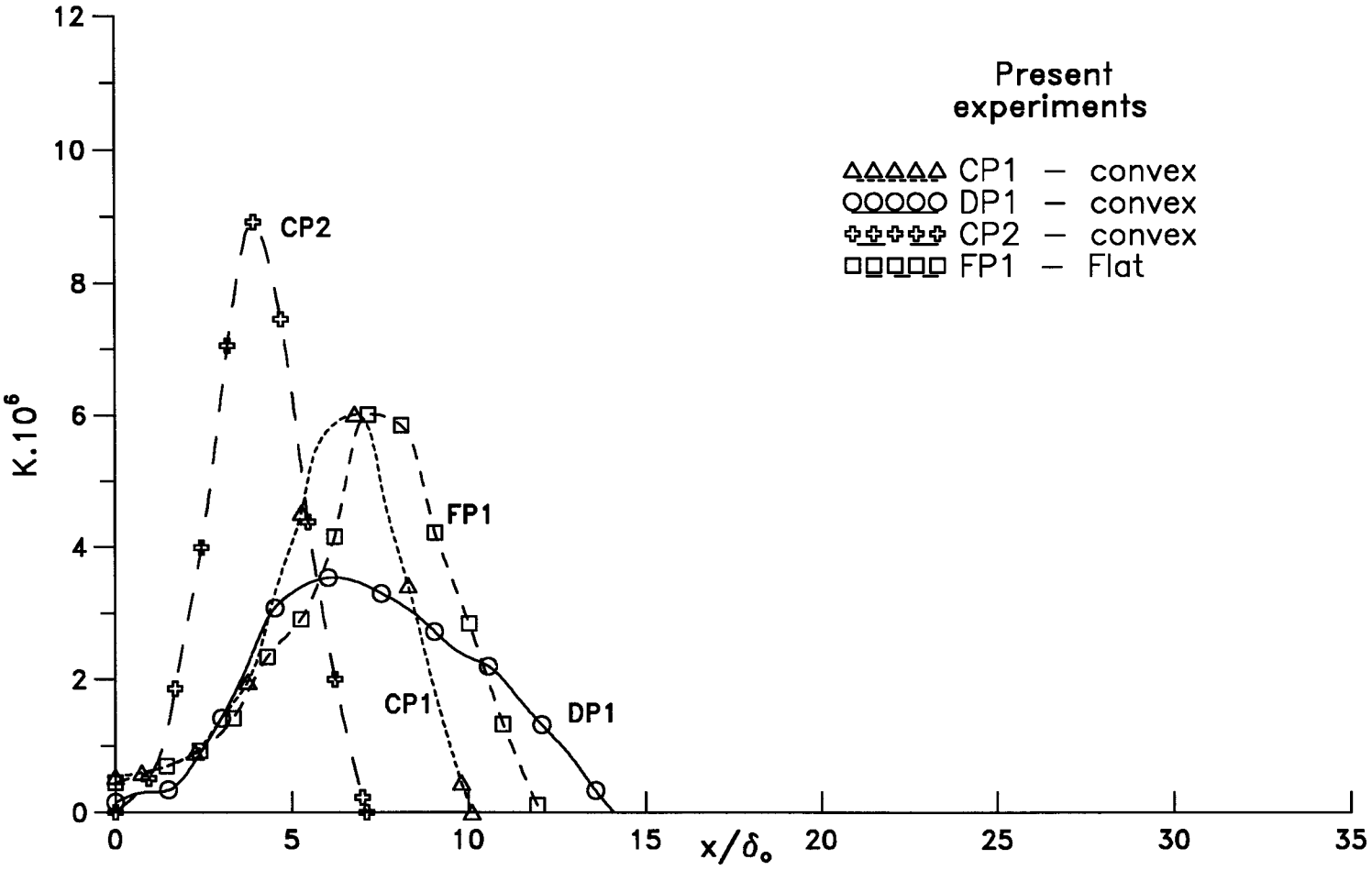

Fig.3.17 The streamwise variation of K for the present experiments, also showing the normalised extent of acceleration

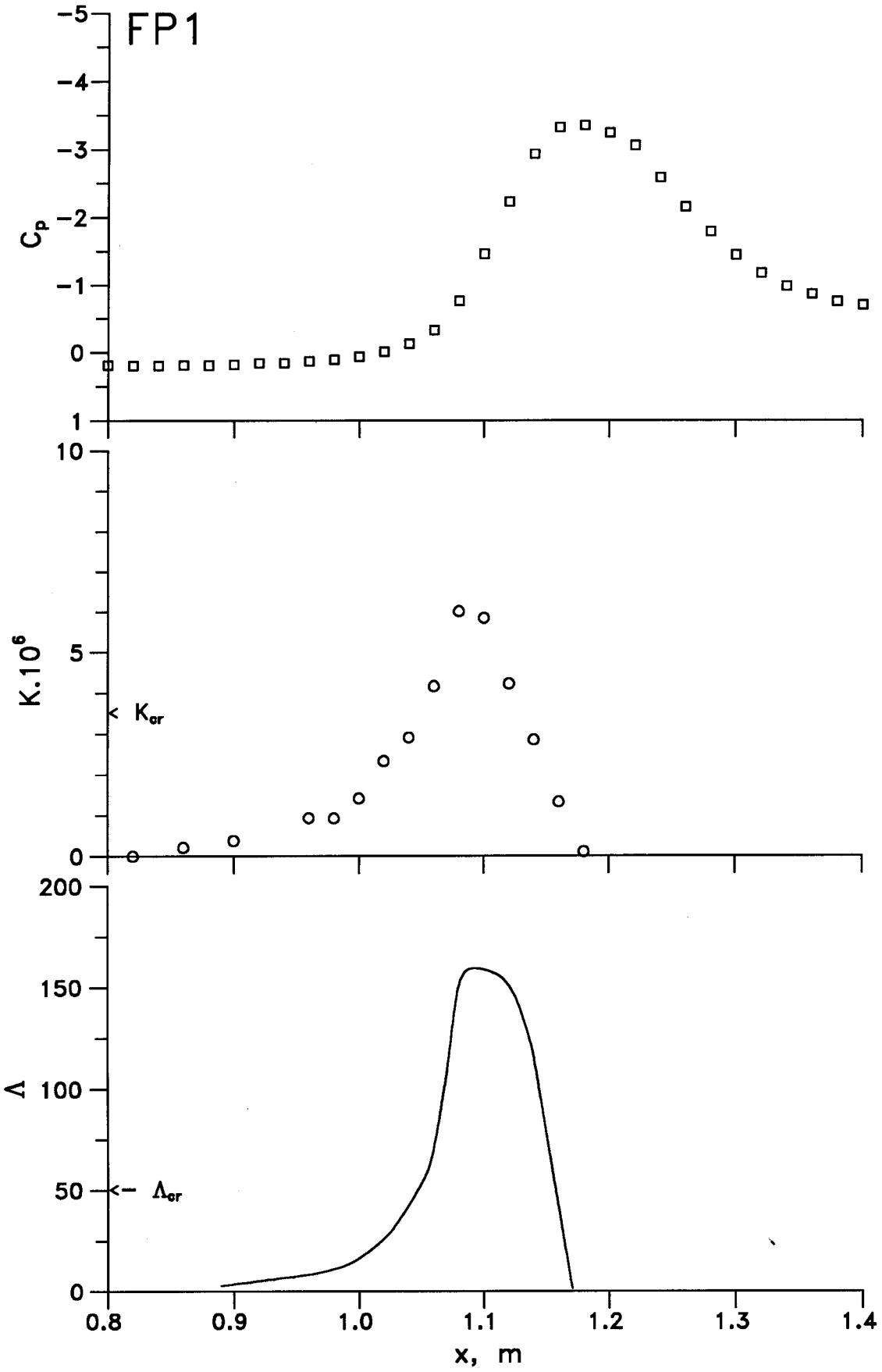

Fig.3.18 Streamwise variation of the acceleration and pressure gradient parameters -- flow FP1

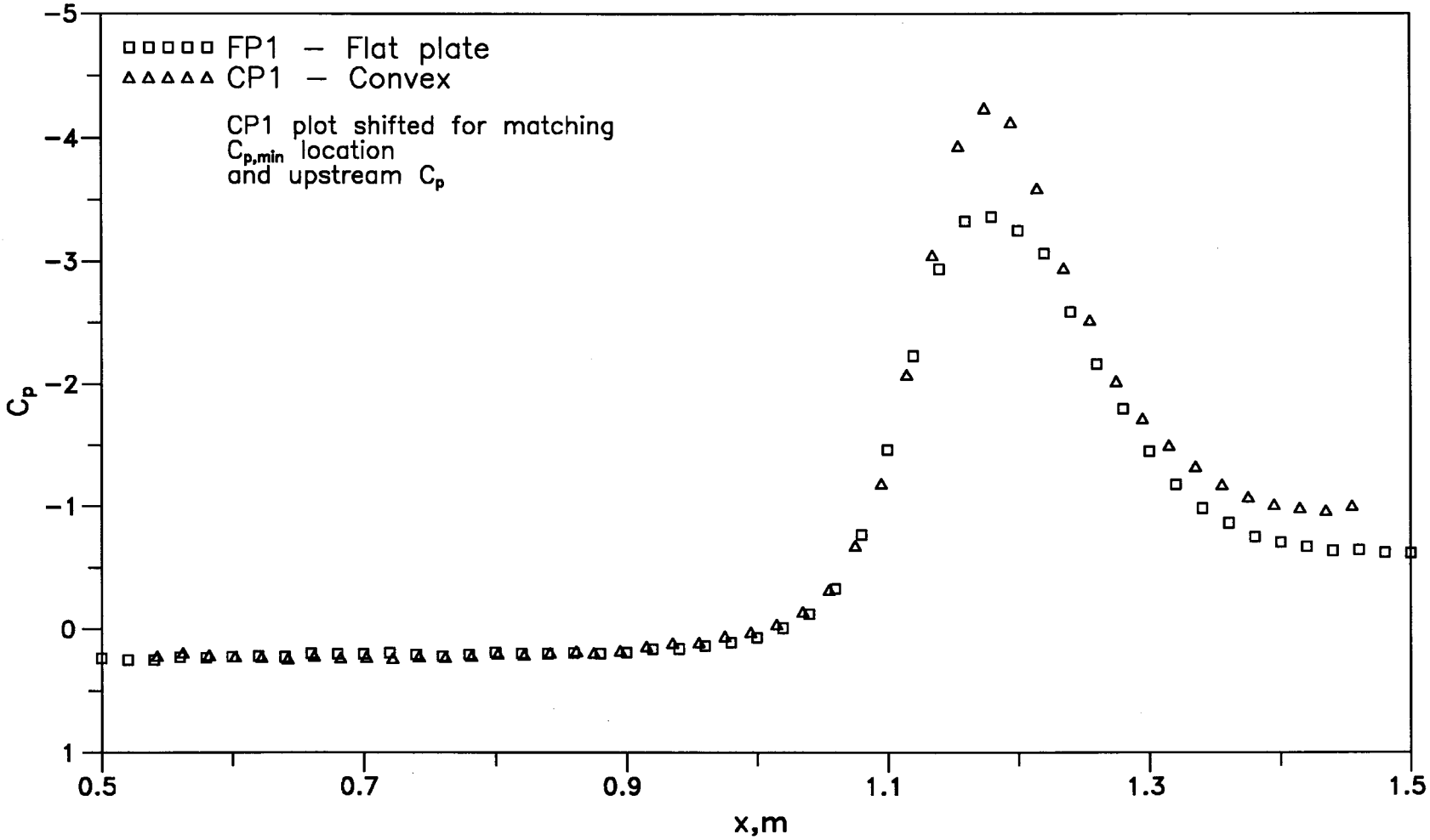

Fig.3.19 Streamwise variation of C_p for FP1, compared with CP1

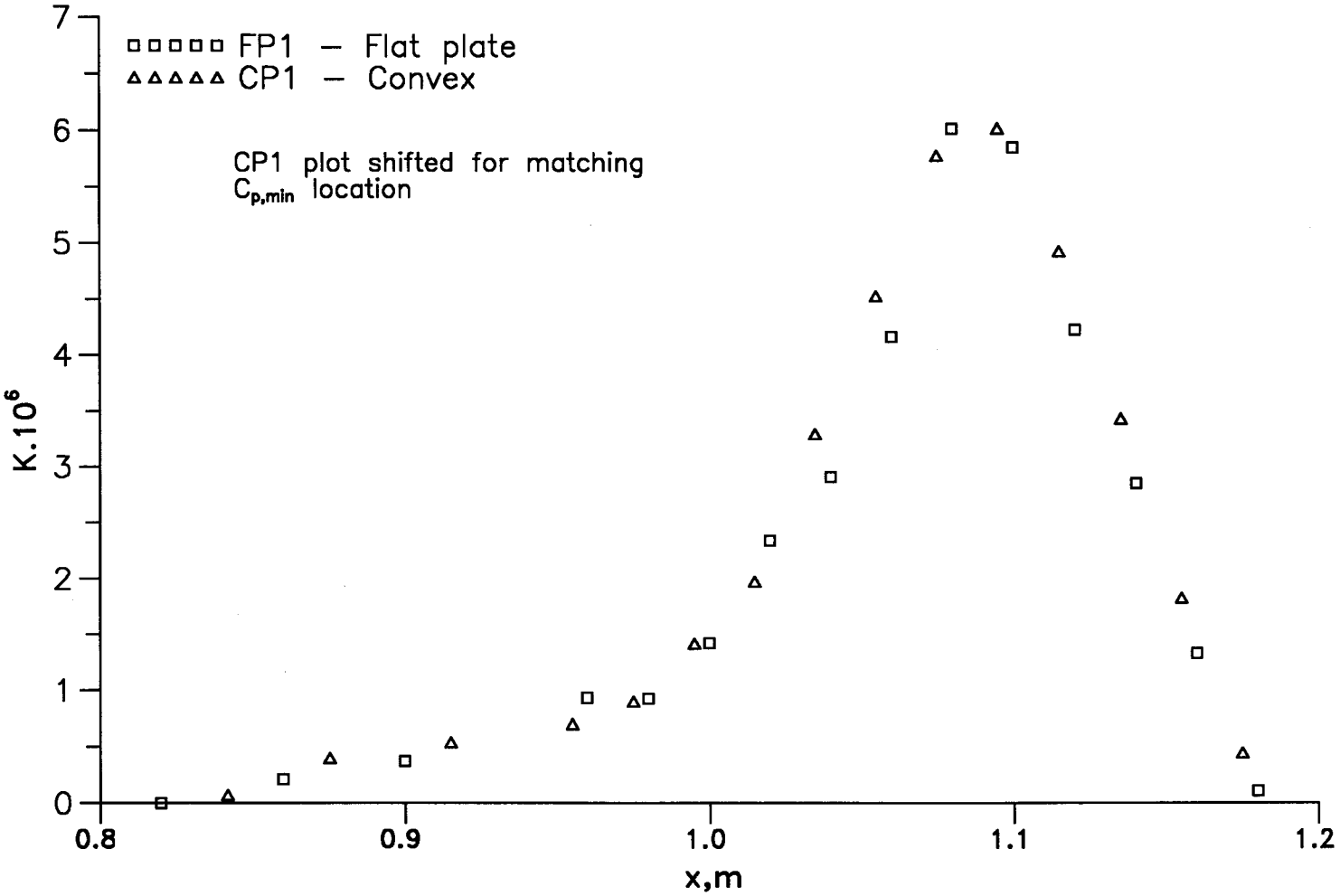

Fig.3.20 Comparison of the streamwise variation of K for FP1 and CP1

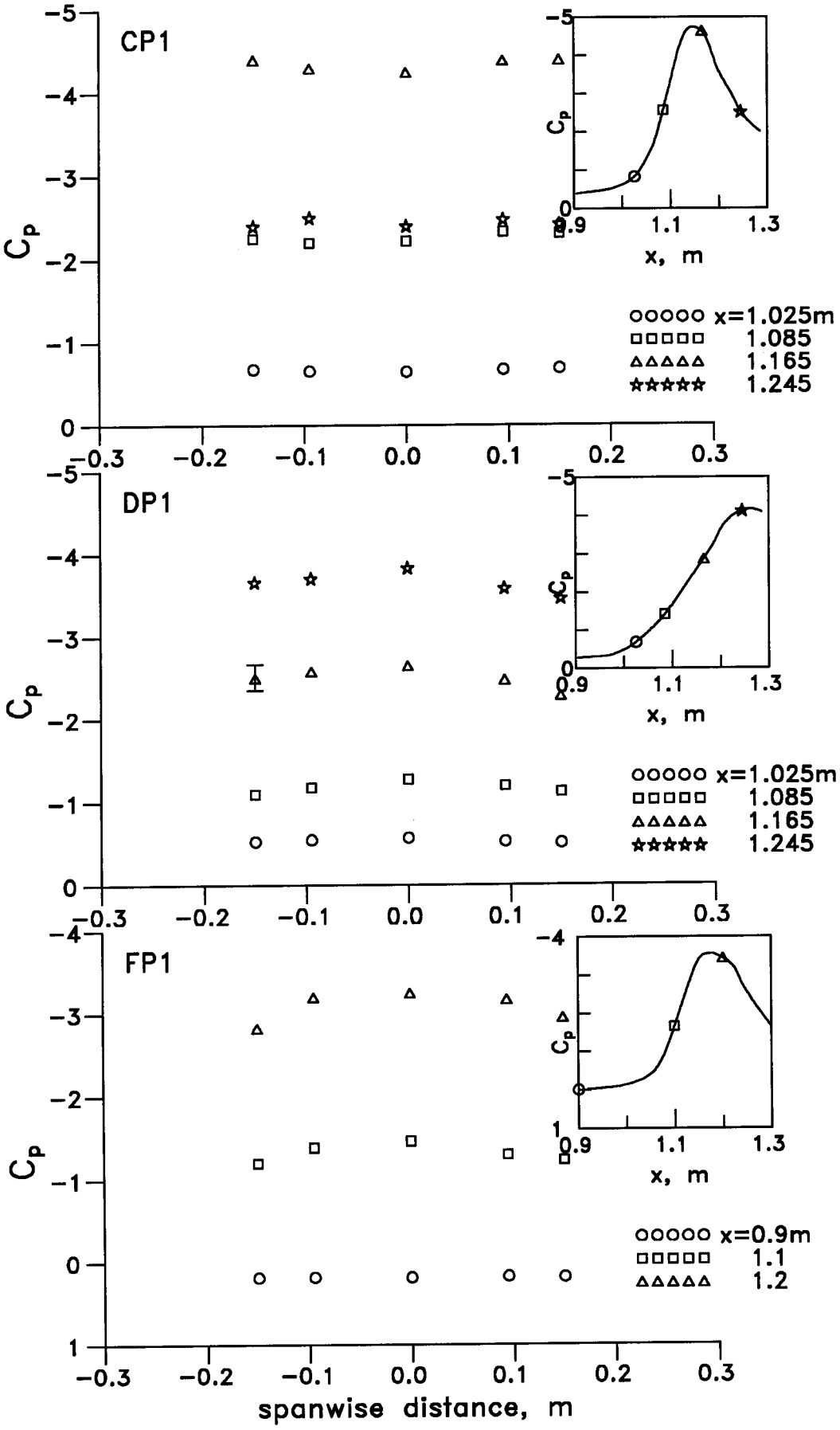

Fig.3.21 Spanwise static pressure distribution in CP1,DP1 & FP1. The symbol in the inset plots show centreline C_p distribution at relevant locations

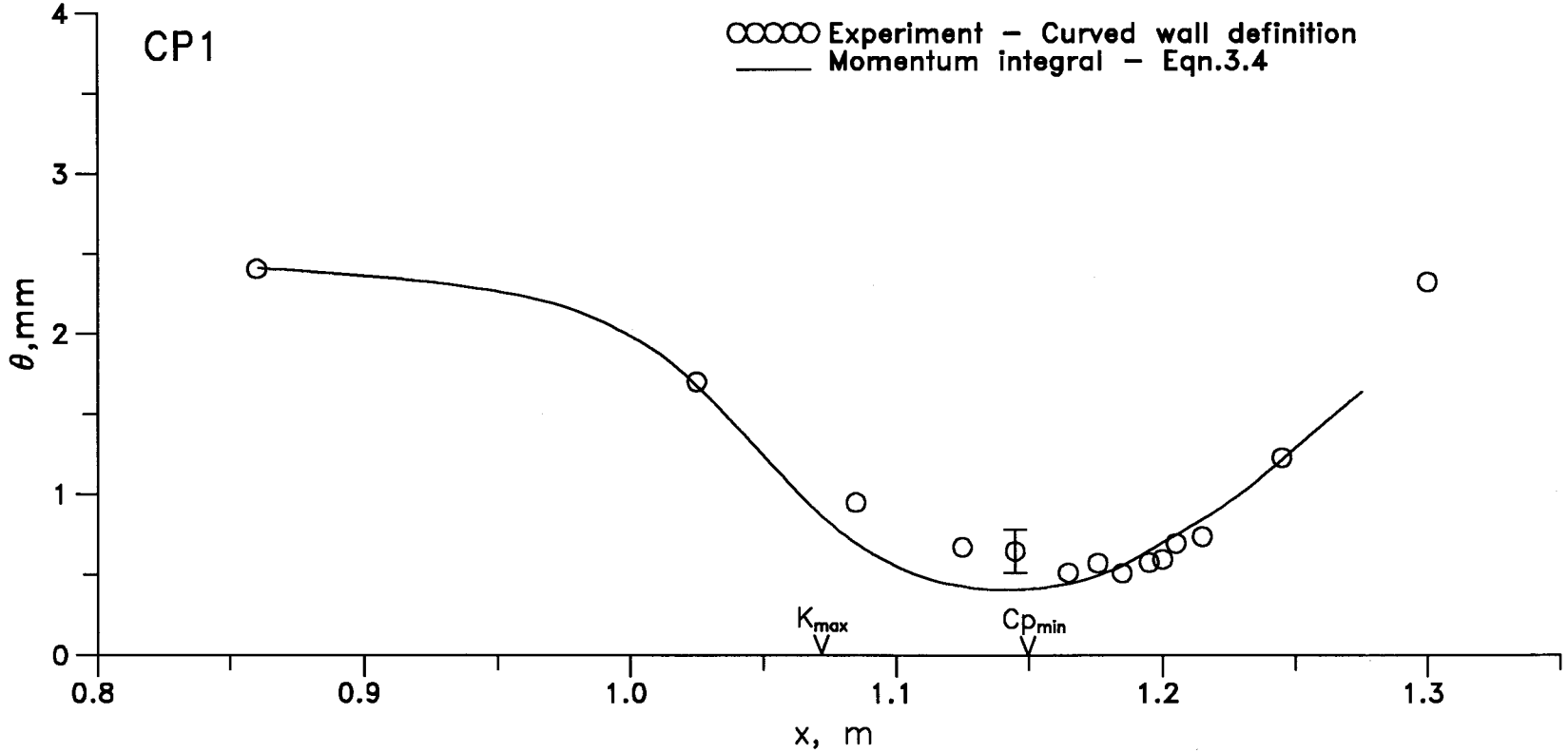

Fig.3.22 Comparison of the momentum thickness calculated using the momentum integral equation with experiments – flow CP1

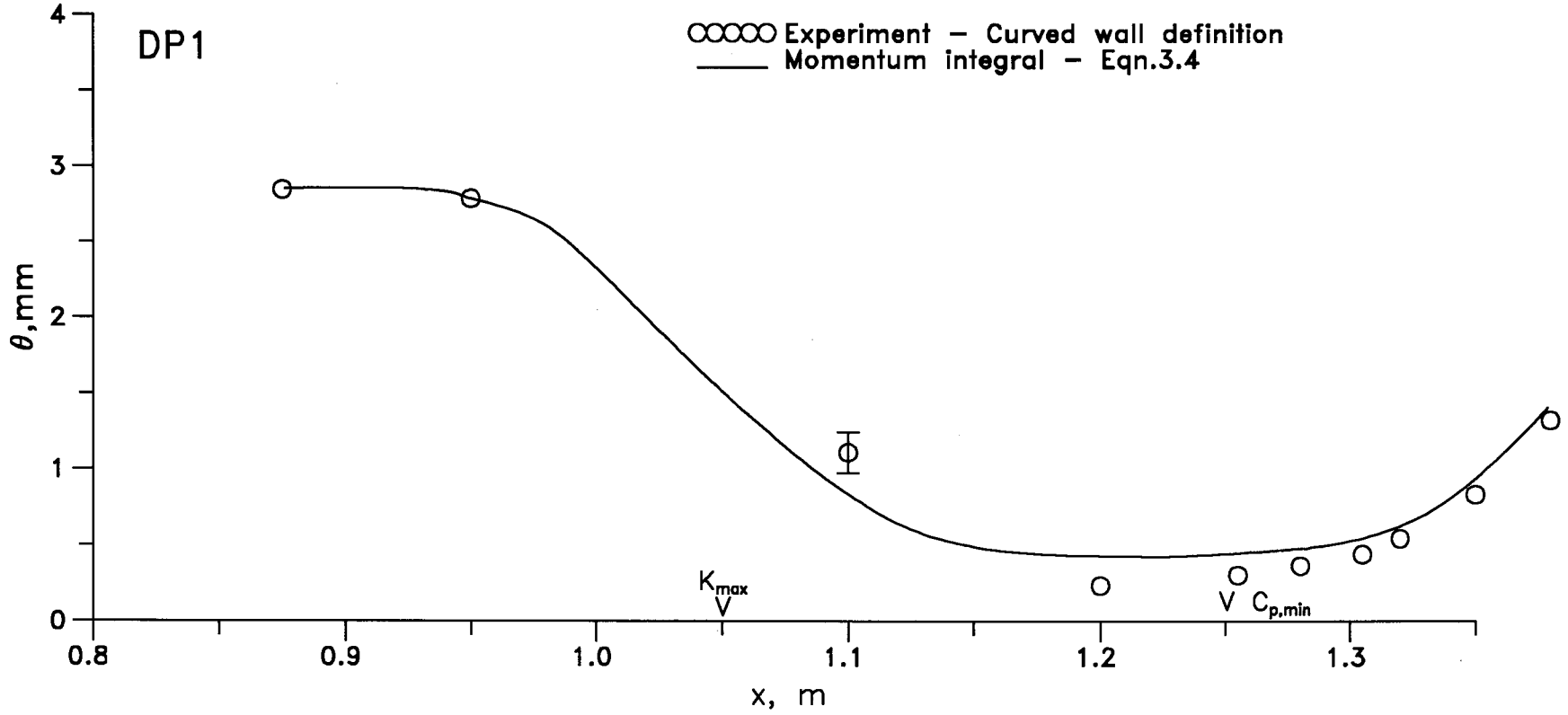

Fig.3.23 Comparison of the momentum thickness calculated using the momentum integral equation with experiments – flow DP1

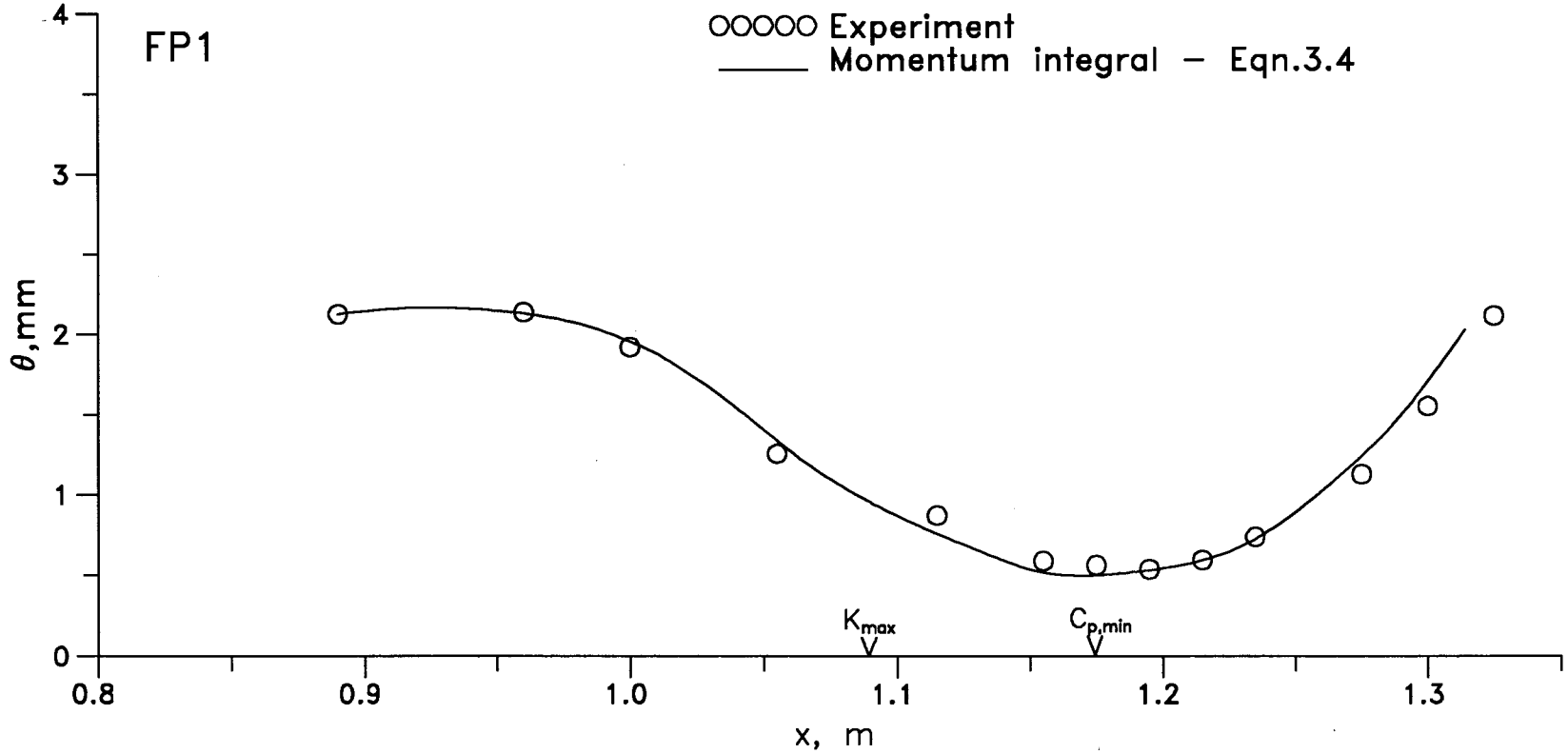

Fig.3.24 Comparison of the momentum thickness calculated from the momentum integral equation with experiments – Flow FP1

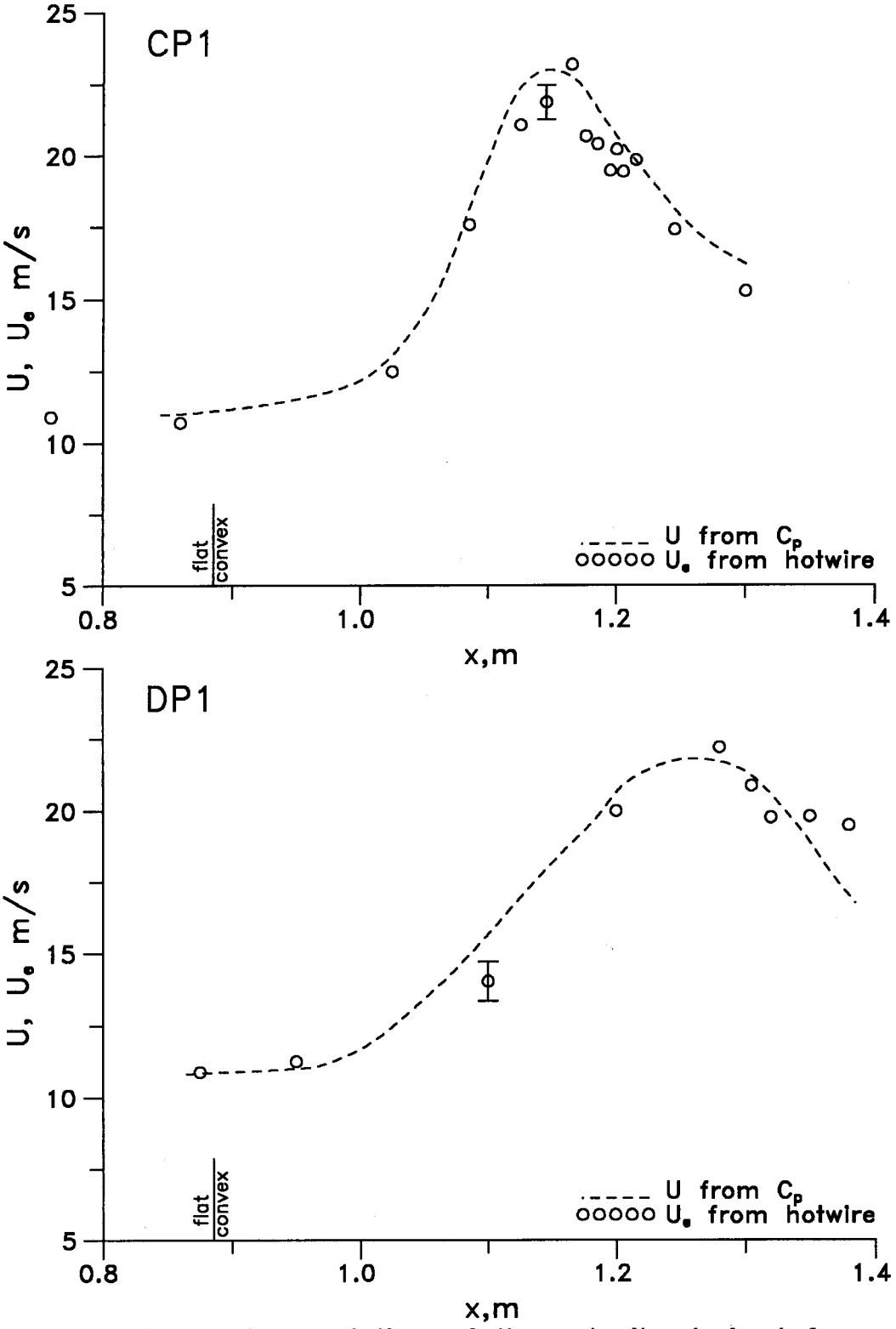

Fig.4.1 The streamwise variation of the velocity derived from surface pressure distribution and the hot-wire edge velocity

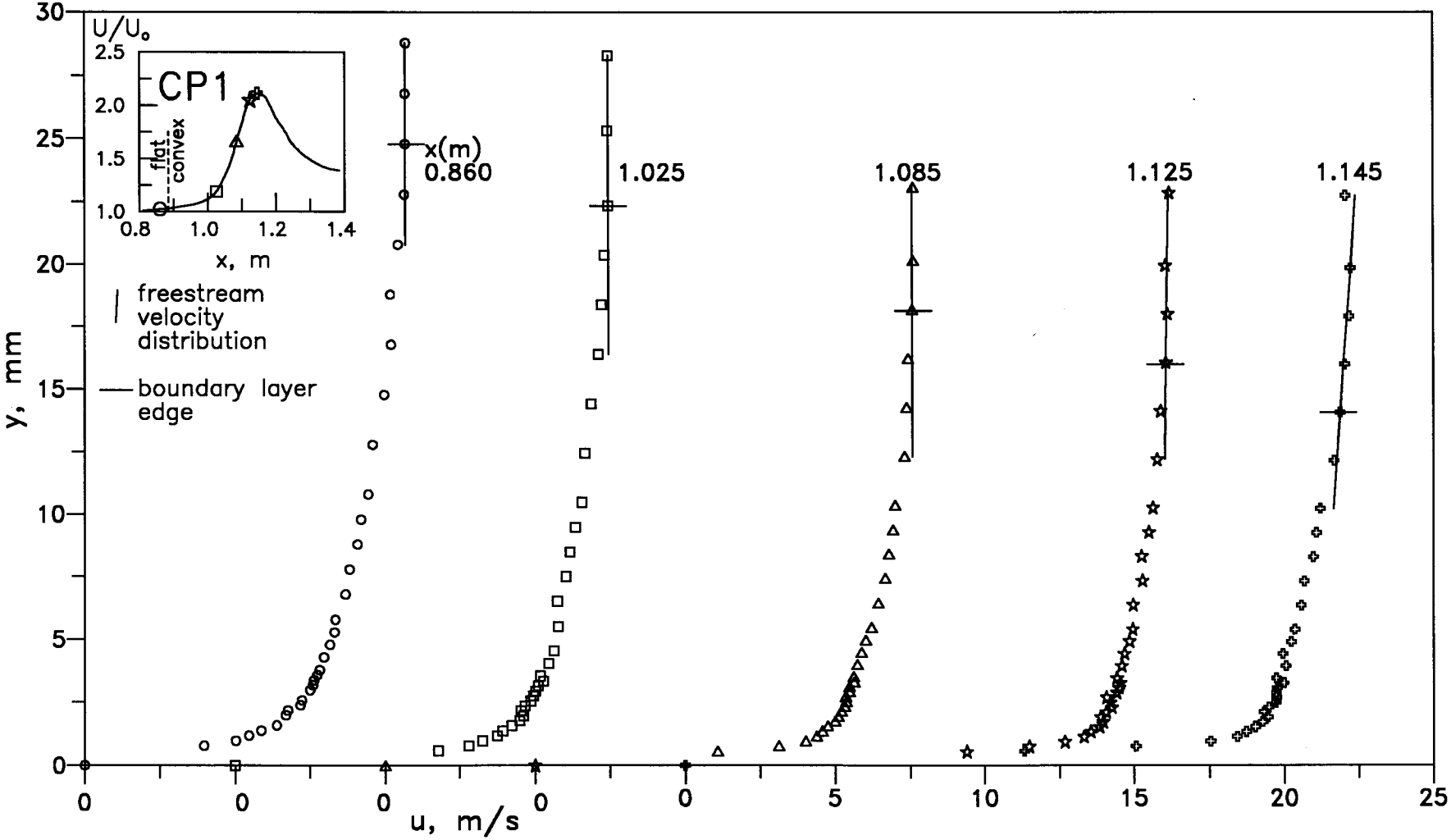

Fig.4.2a Boundary layer mean velocity profiles : Flow CP1
Dimensional form, x axis shifted

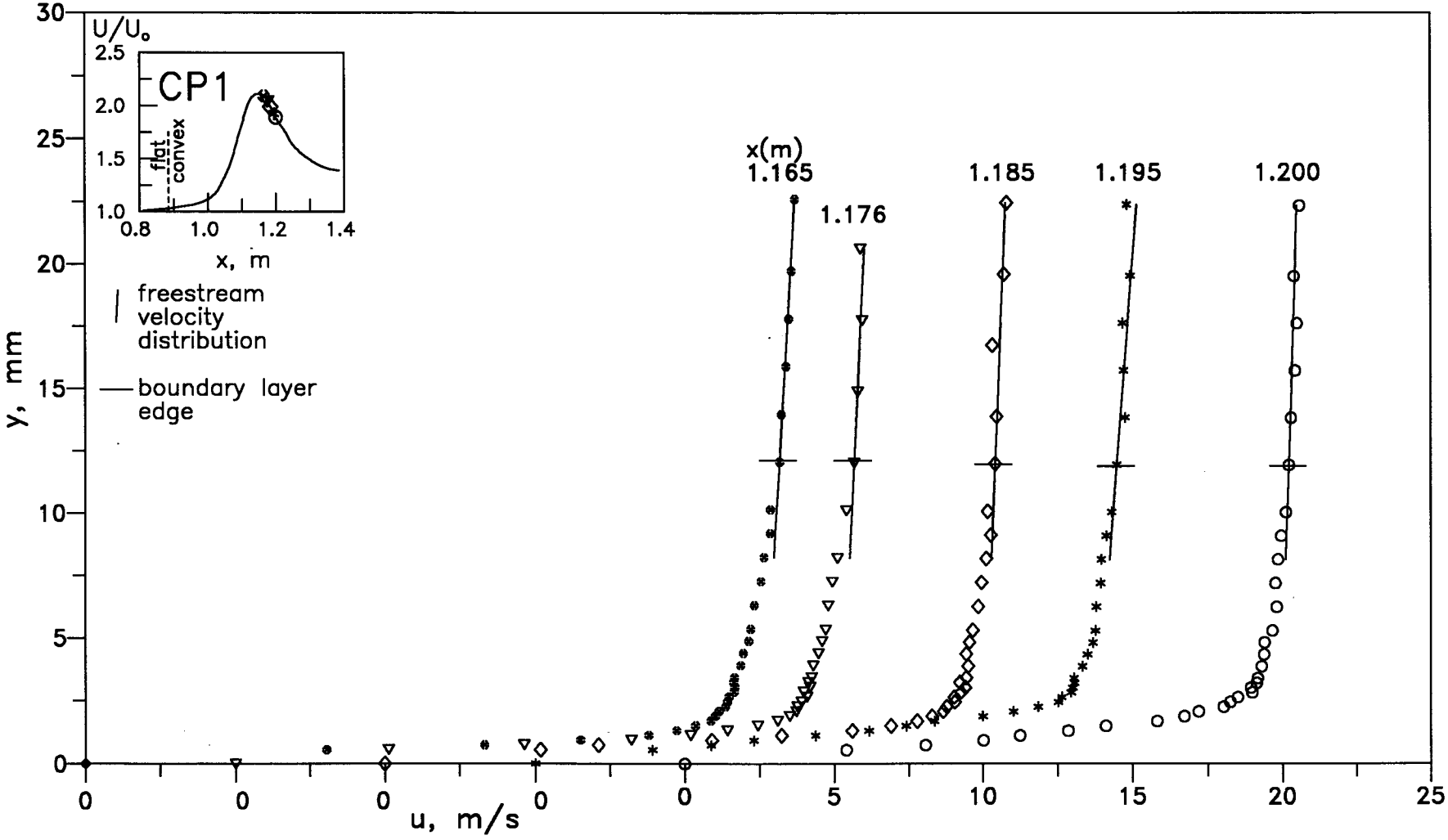

Fig.4.2b Boundary layer mean velocity profiles : Flow CP1
Dimensional form, x axis shifted

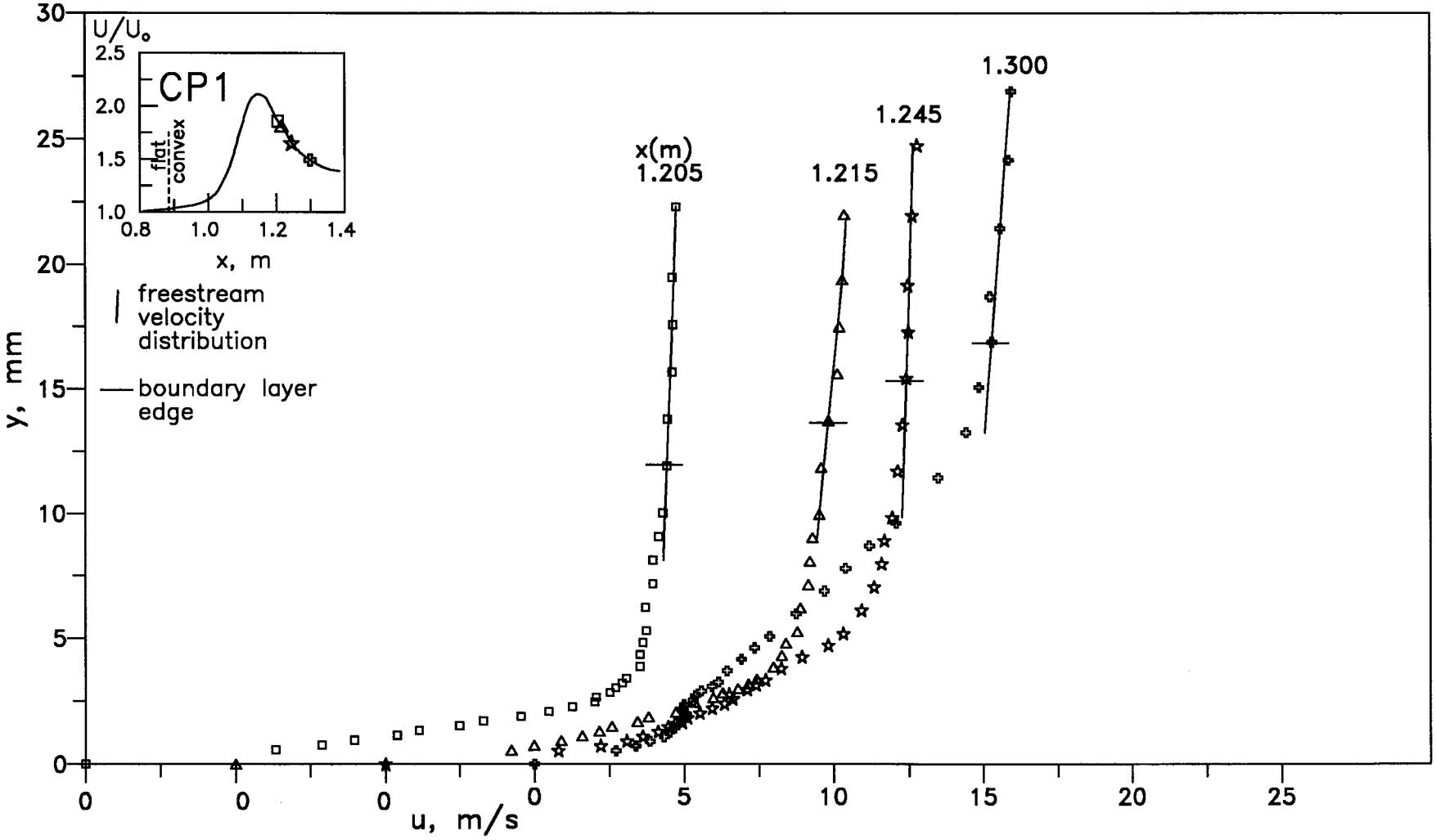

Fig.4.2c Boundary layer mean velocity profiles : Flow CP1
Dimensional form, x axis shifted

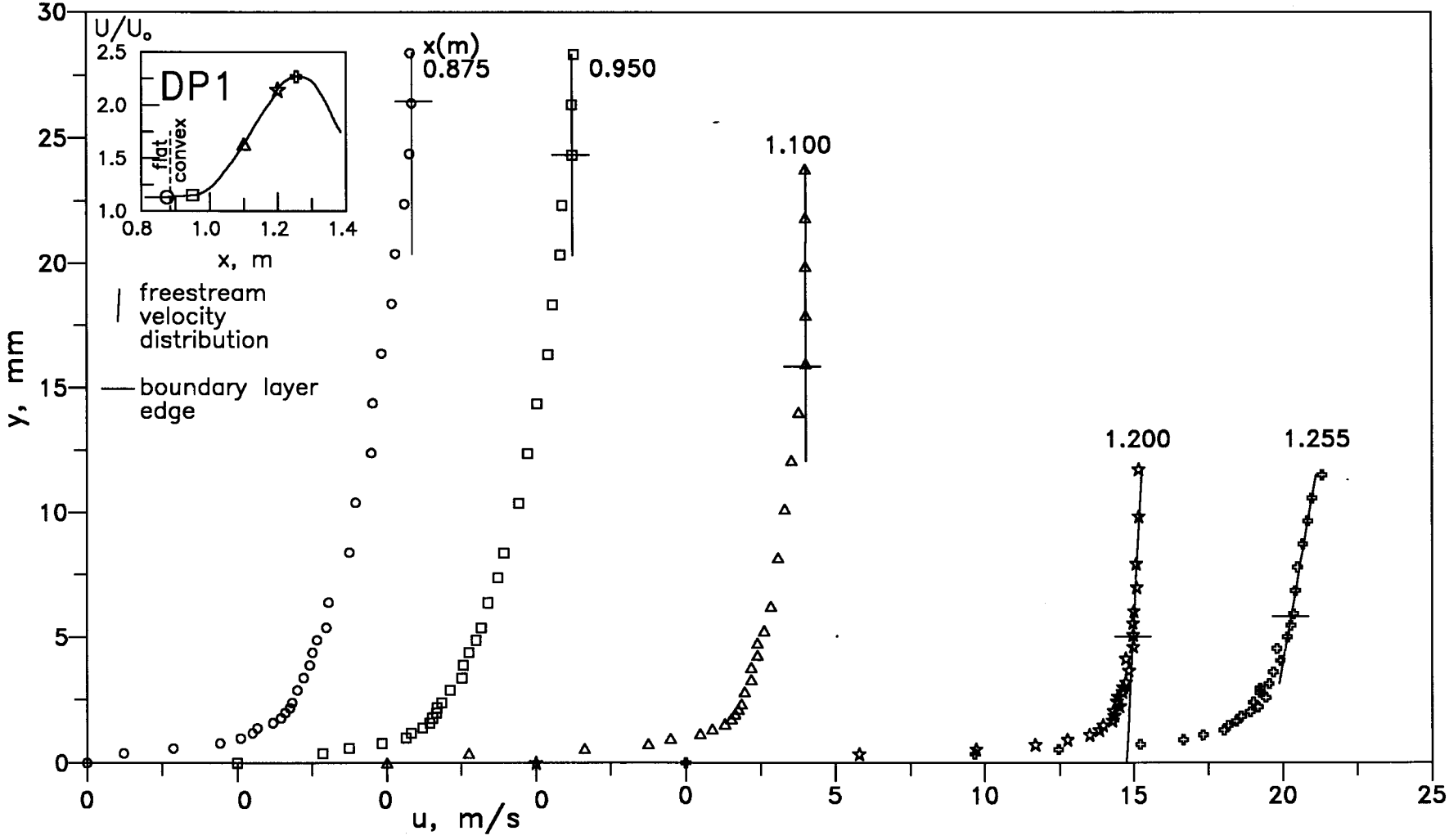

Fig.4.3a Boundary layer mean velocity profiles : Flow DP1
Dimensional form, x axis shifted

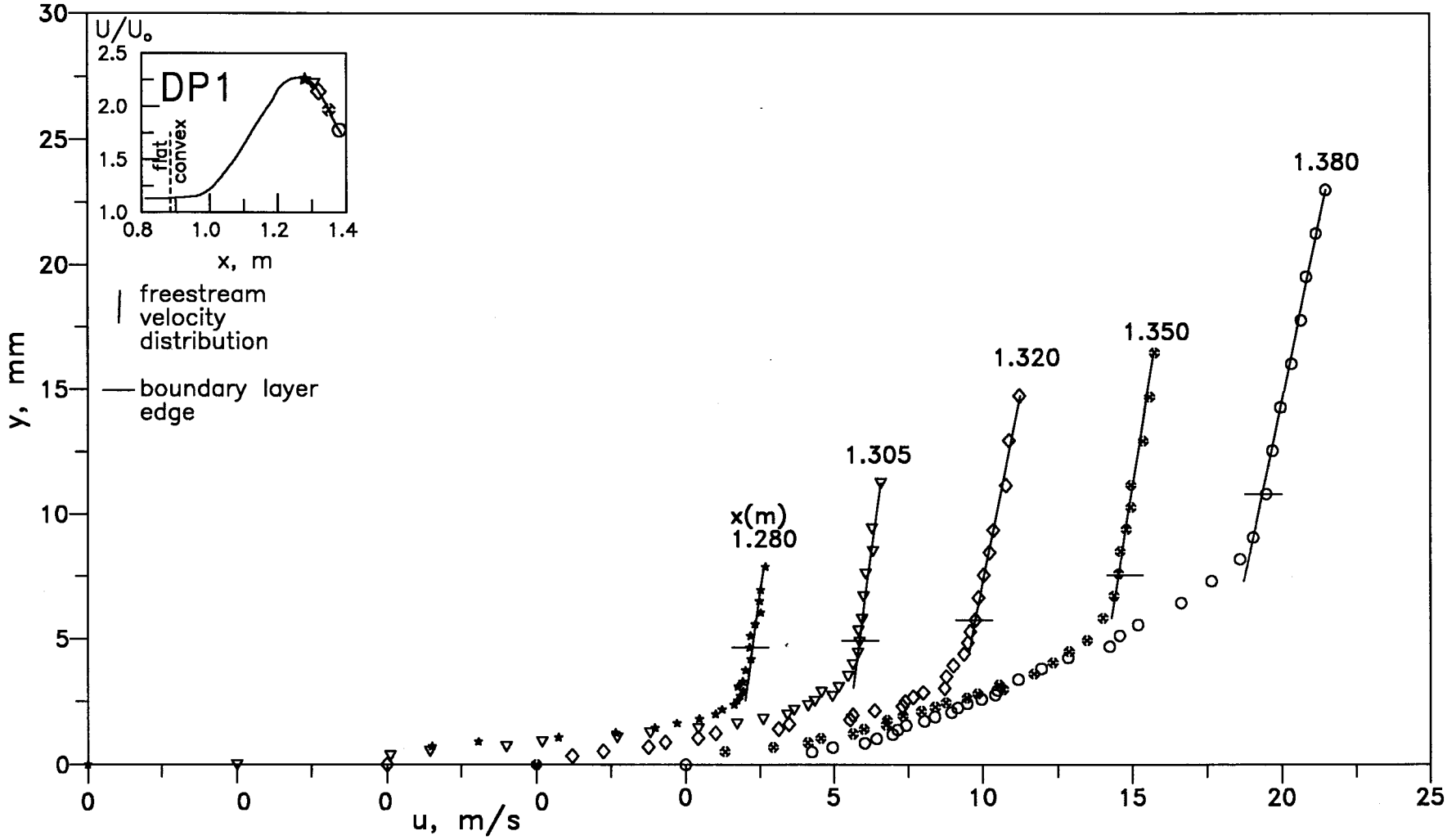

Fig.4.3b Boundary layer mean velocity profiles : Flow DP1
Dimensional form, x axis shifted

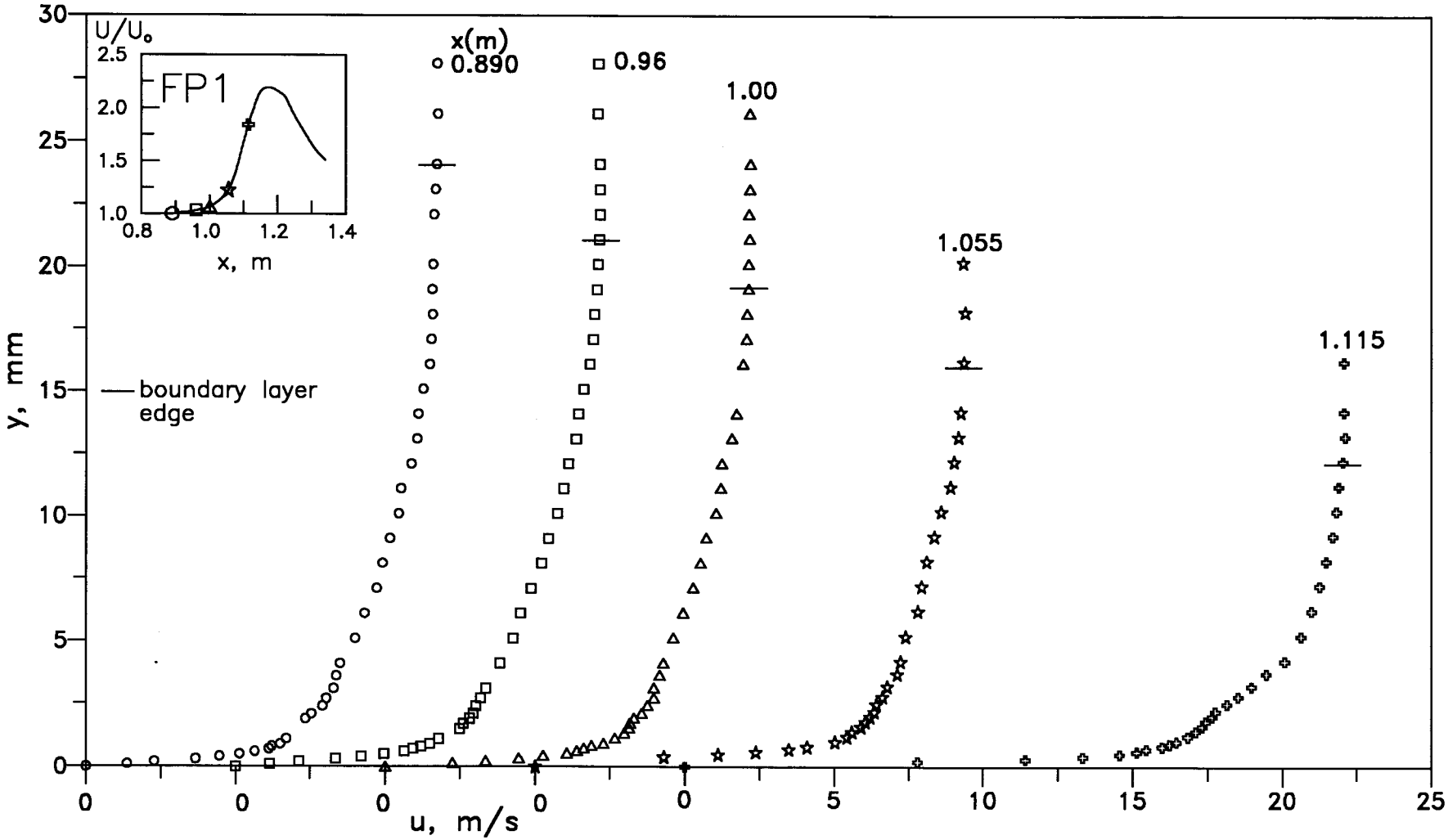

Fig.4.4a Boundary layer mean velocity profiles : Flow FP1
Dimensional form, x axis shifted

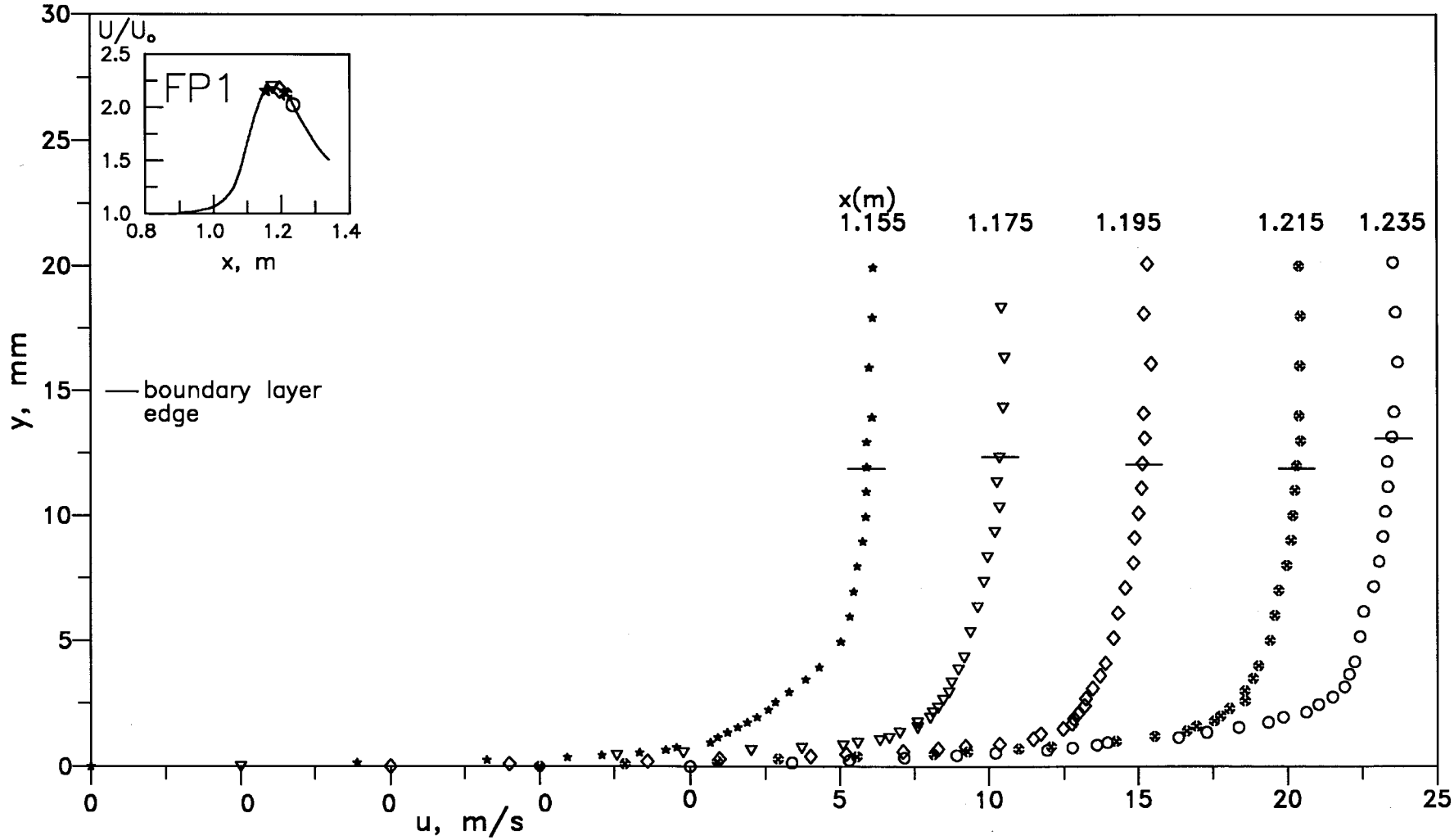

Fig.4.4b Boundary layer mean velocity profiles : Flow FP1
Dimensional form, x axis shifted

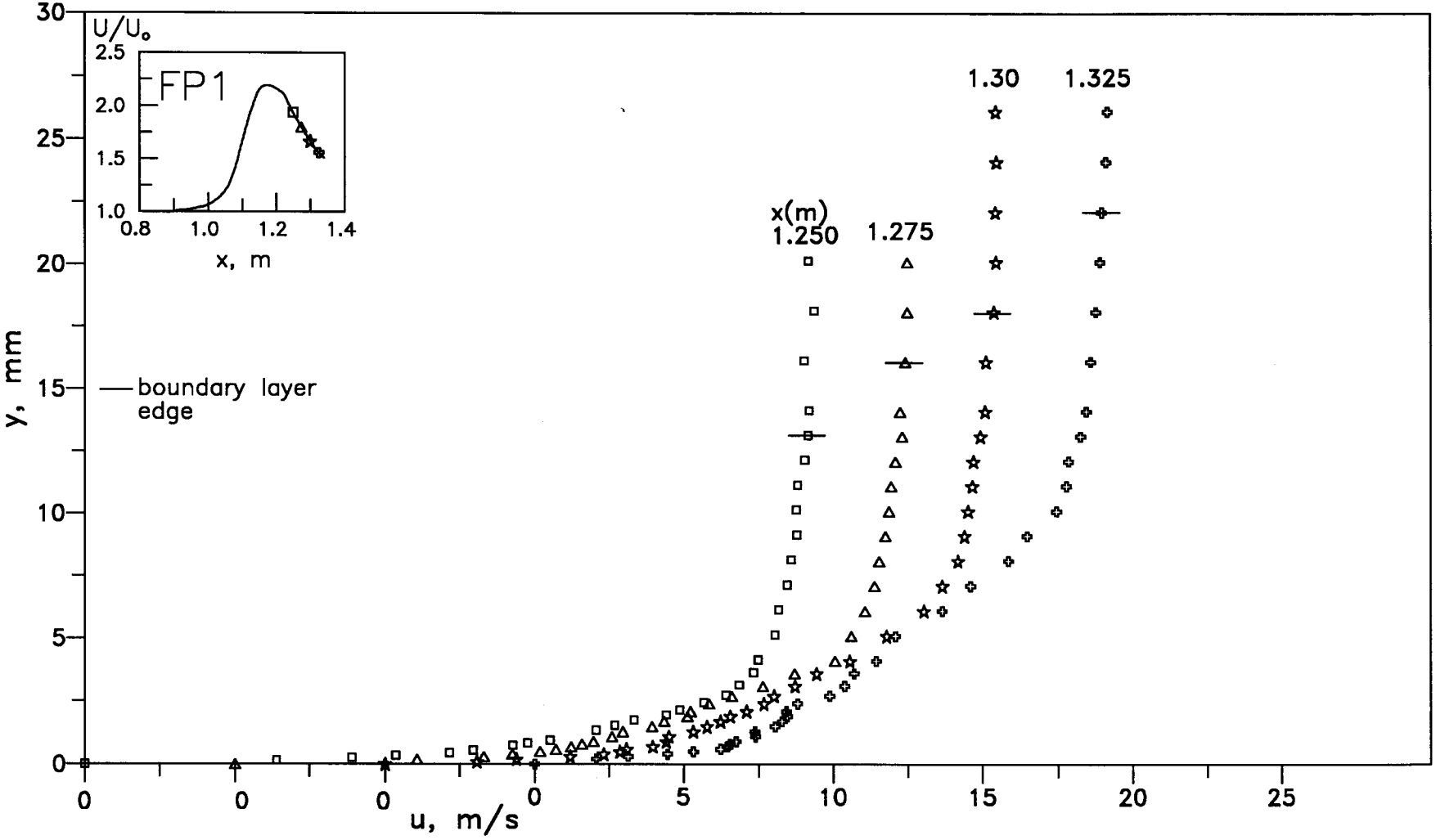

Fig.4.4c Boundary layer mean velocity profiles : Flow FP1
Dimensional form, x axis shifted

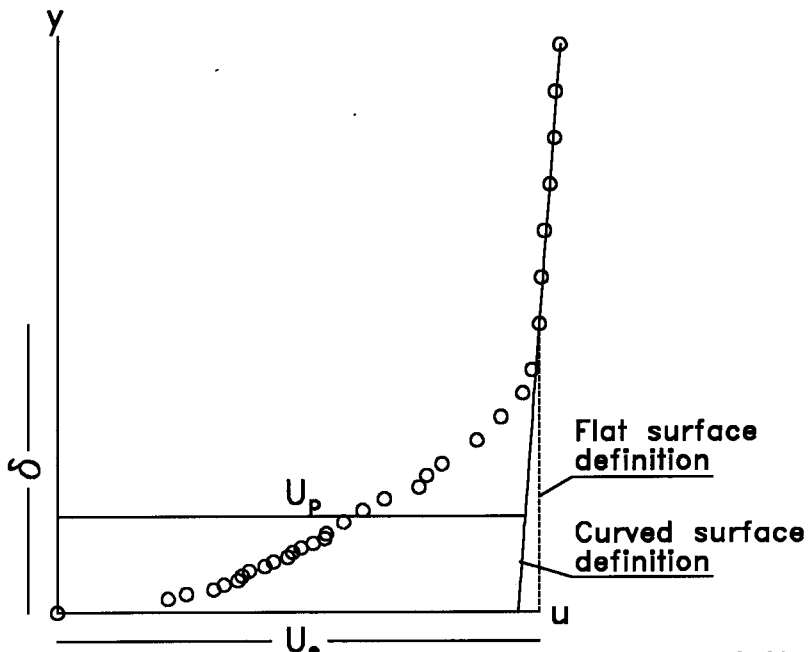

Fig.4.5 Schematic illustrating the two definitions of U_p for calculating δ^* and θ (Eqn.4.1 & 4.2) in the convex surface experiments

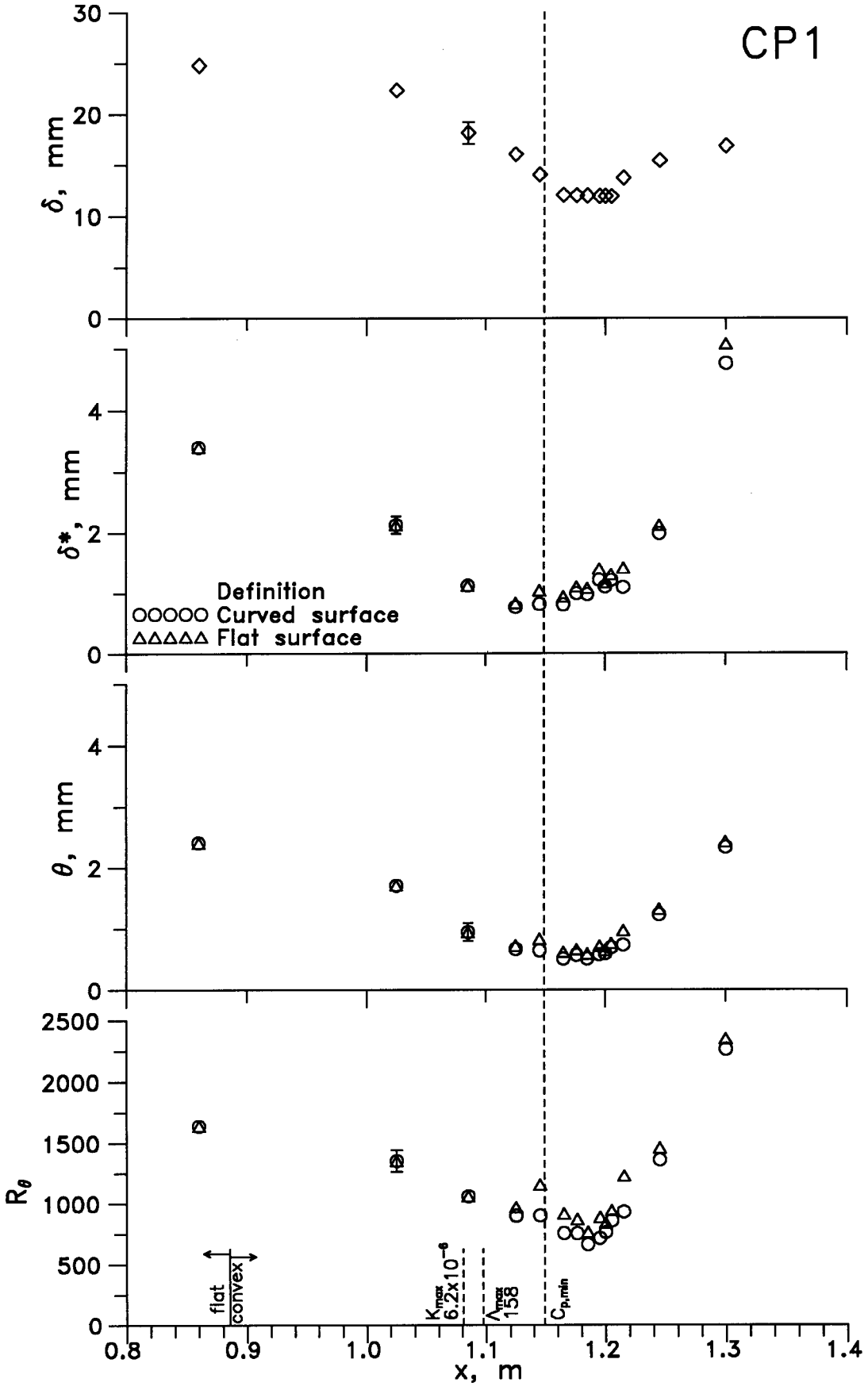

Fig.4.6a The streamwise variation of the boundary layer thickness parameters and momentum thickness Reynolds number : CP1

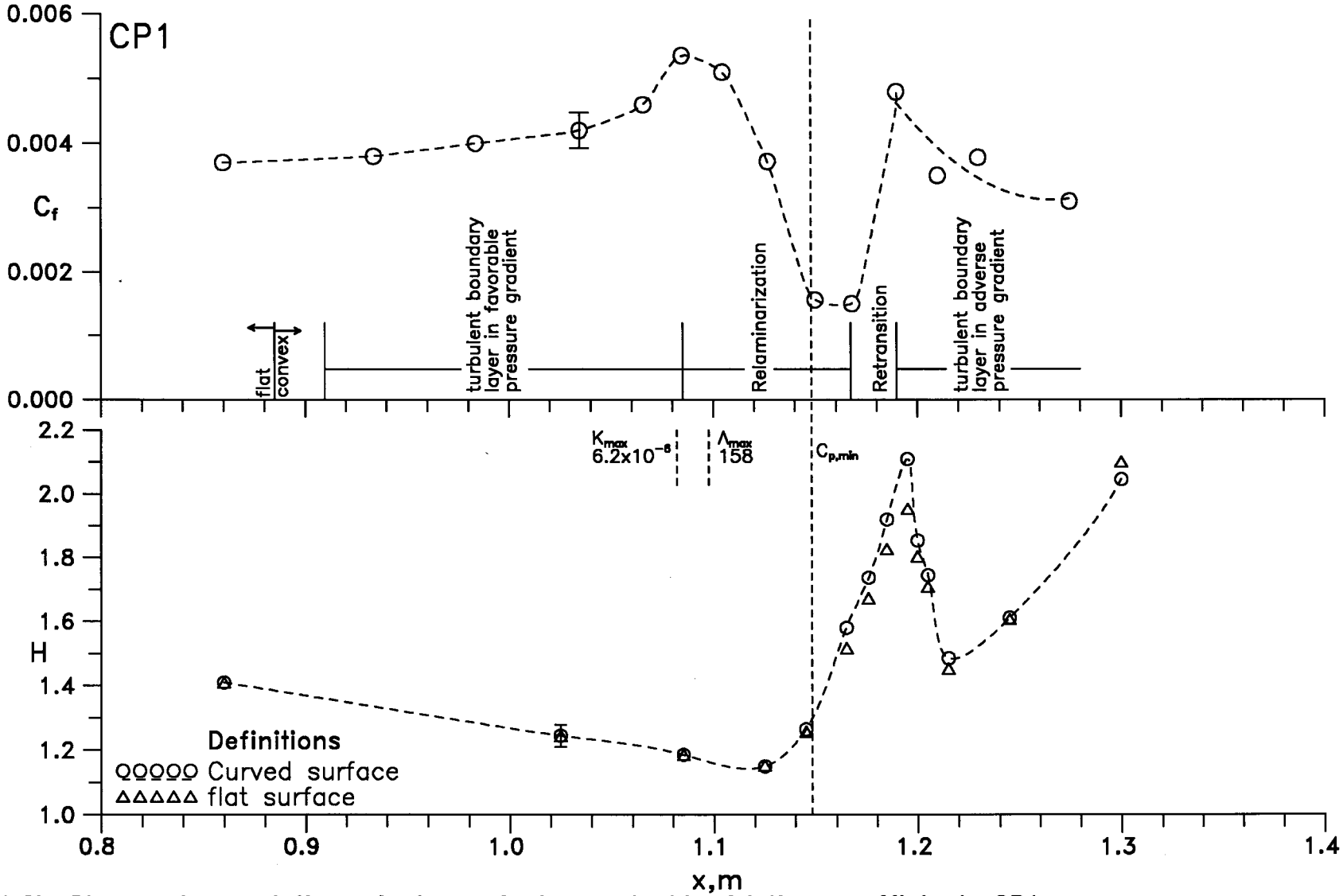

Fig.4.6b Streamwise variation of shape factor and skin friction coefficient: CP1
Lines drawn for clarity

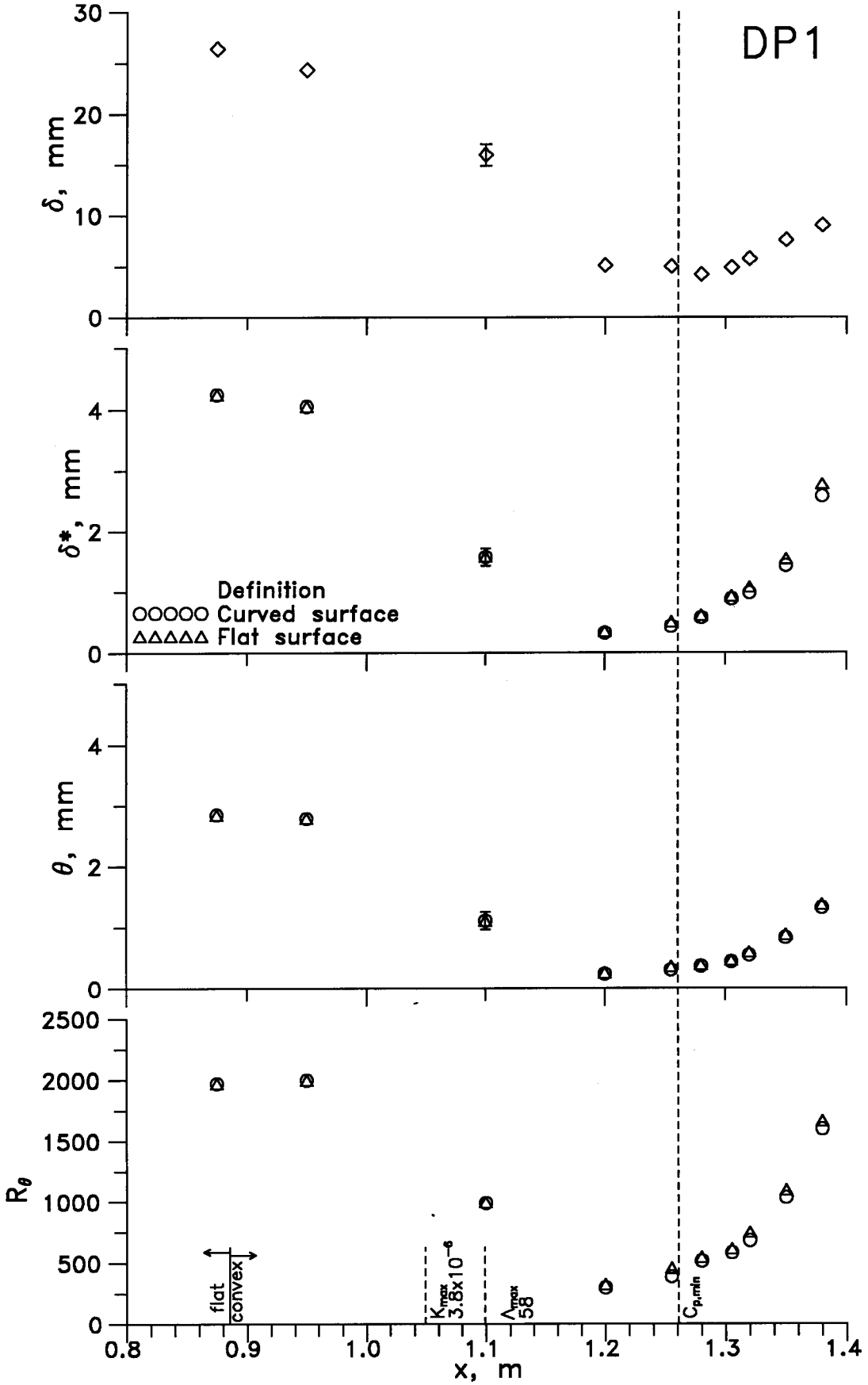

Fig.4.7a The streamwise variation of the boundary layer thickness parameters and momentum thickness Reynolds number : DP1

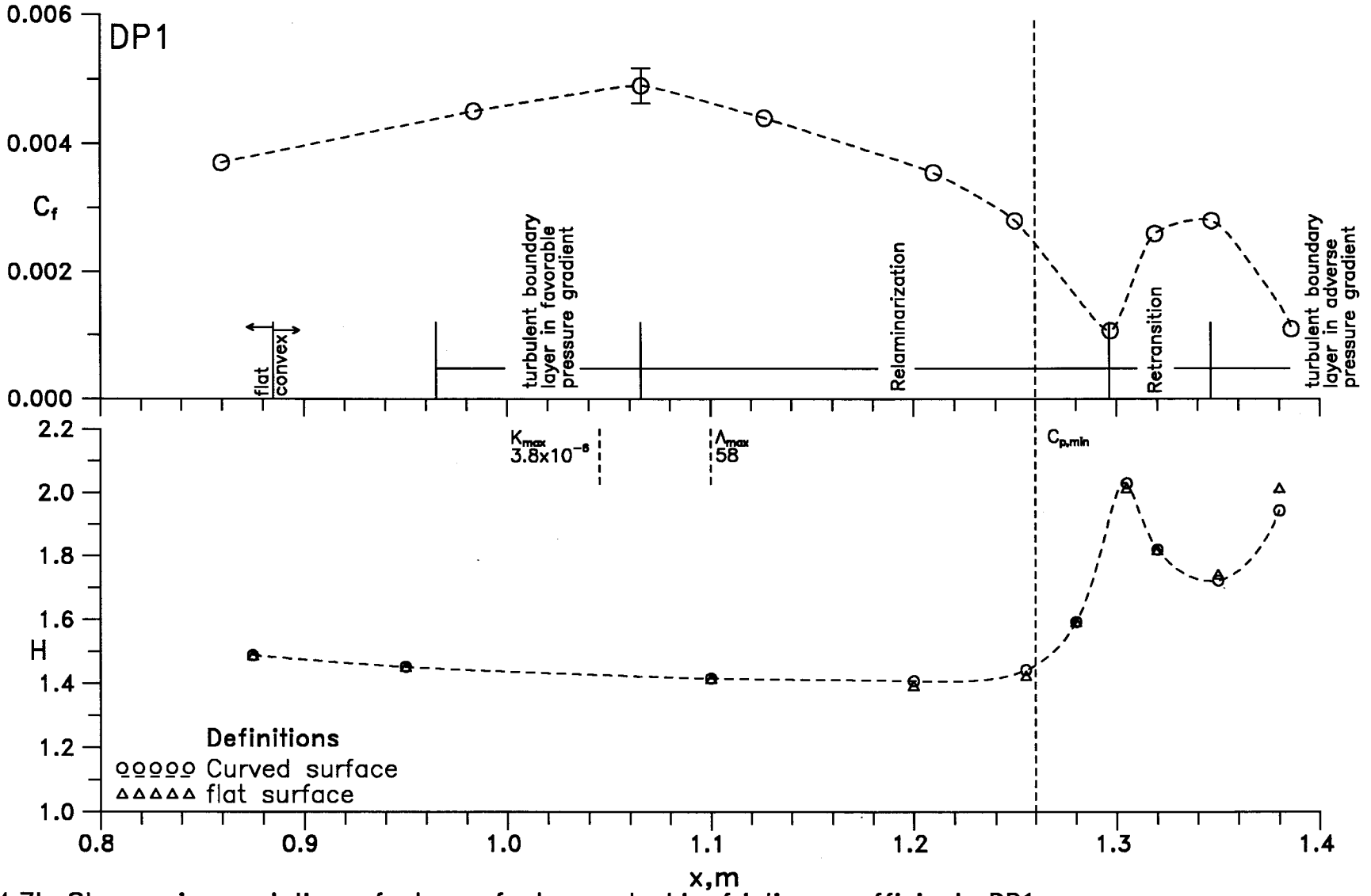

Fig.4.7b Streamwise variation of shape factor and skin friction coefficient: DP1
Lines drawn for clarity

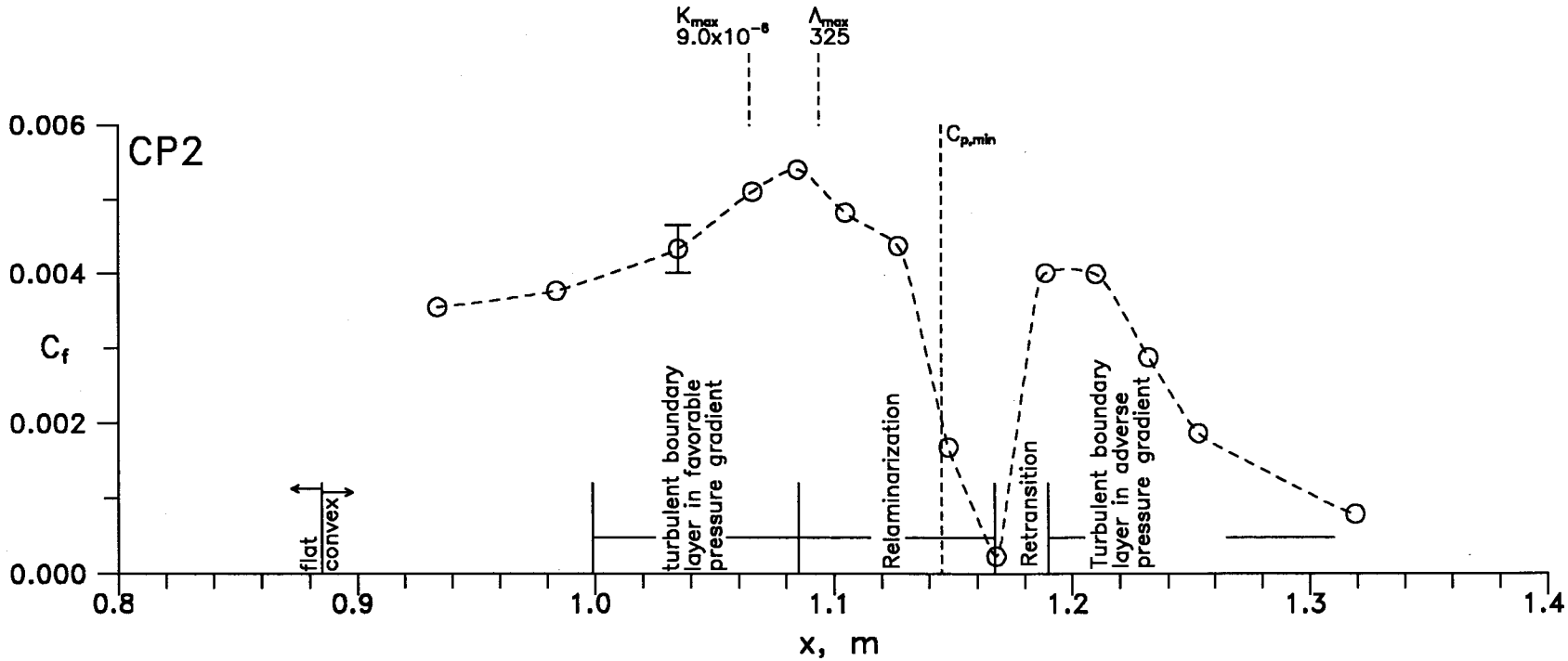

Fig.4.8 The streamwise variation of skin friction coefficent : CP2
Lines drawn for clarity

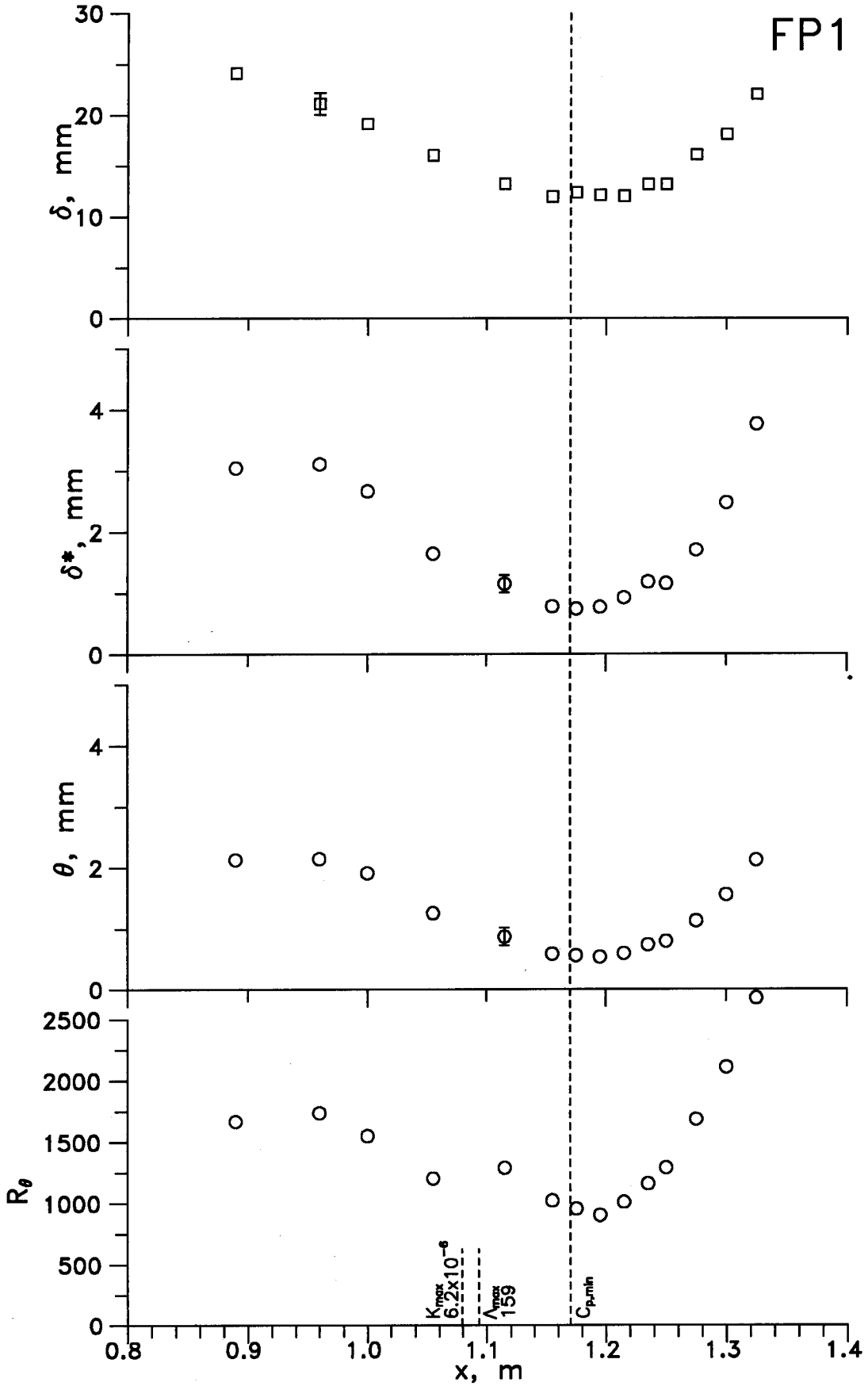

Fig.4.9a The streamwise variation of the boundary layer thickness parameters and momentum thickness Reynolds number : FP1

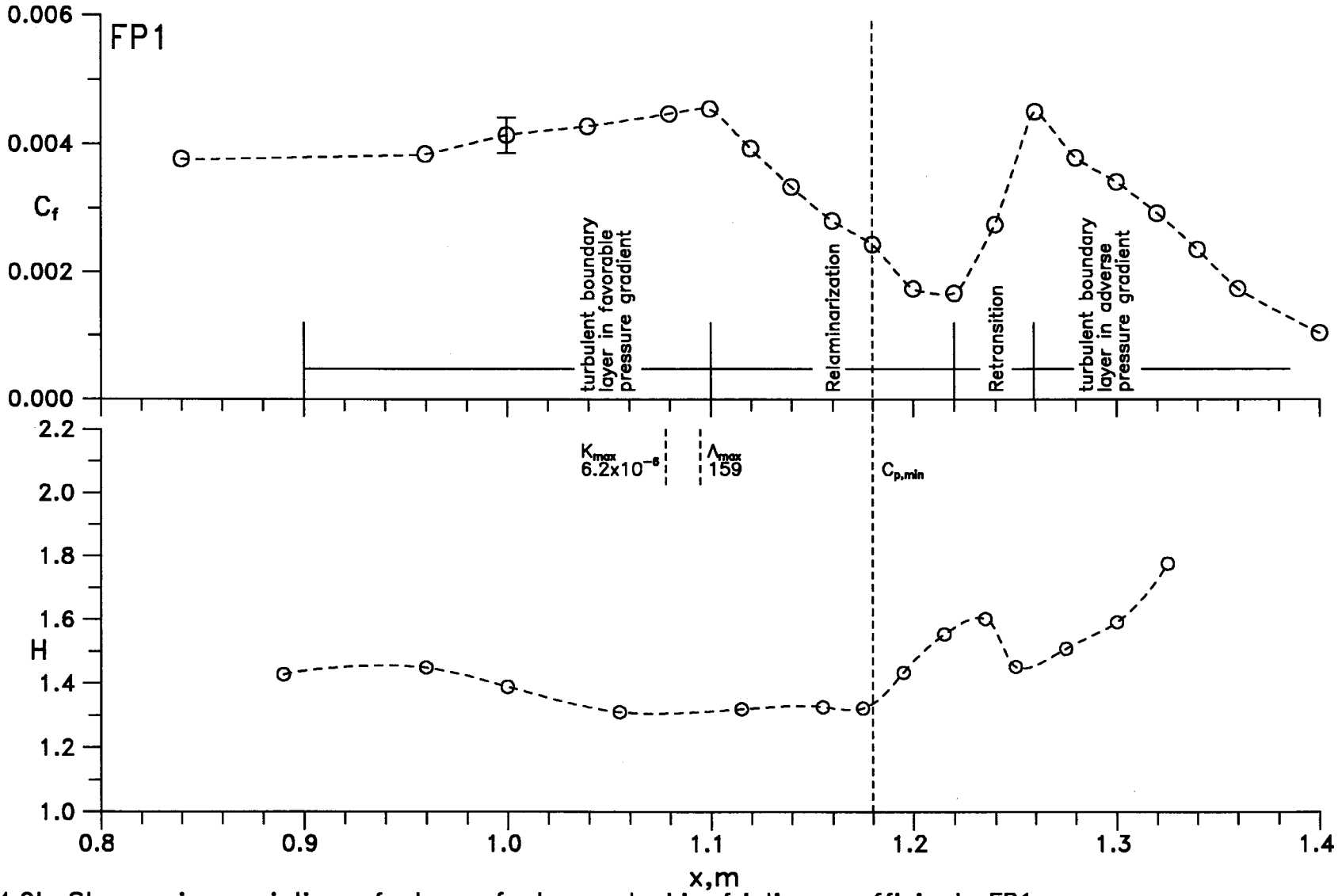

Fig.4.9b Streamwise variation of shape factor and skin friction coefficient: FP1
Lines drawn for clarity

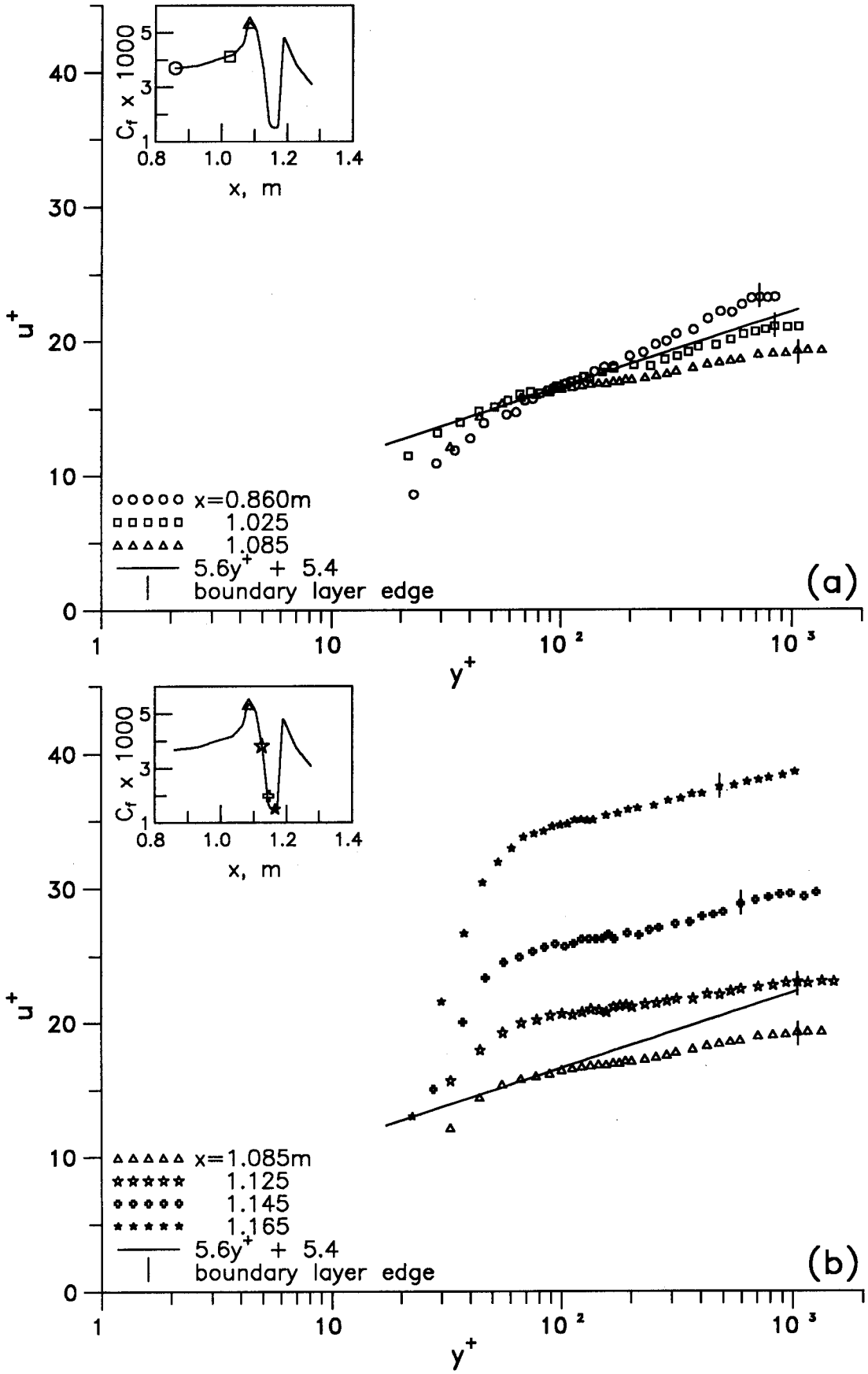

Fig.4.10 Boundary layer mean velocity profiles in wall coordinates : CP1 continued – – –

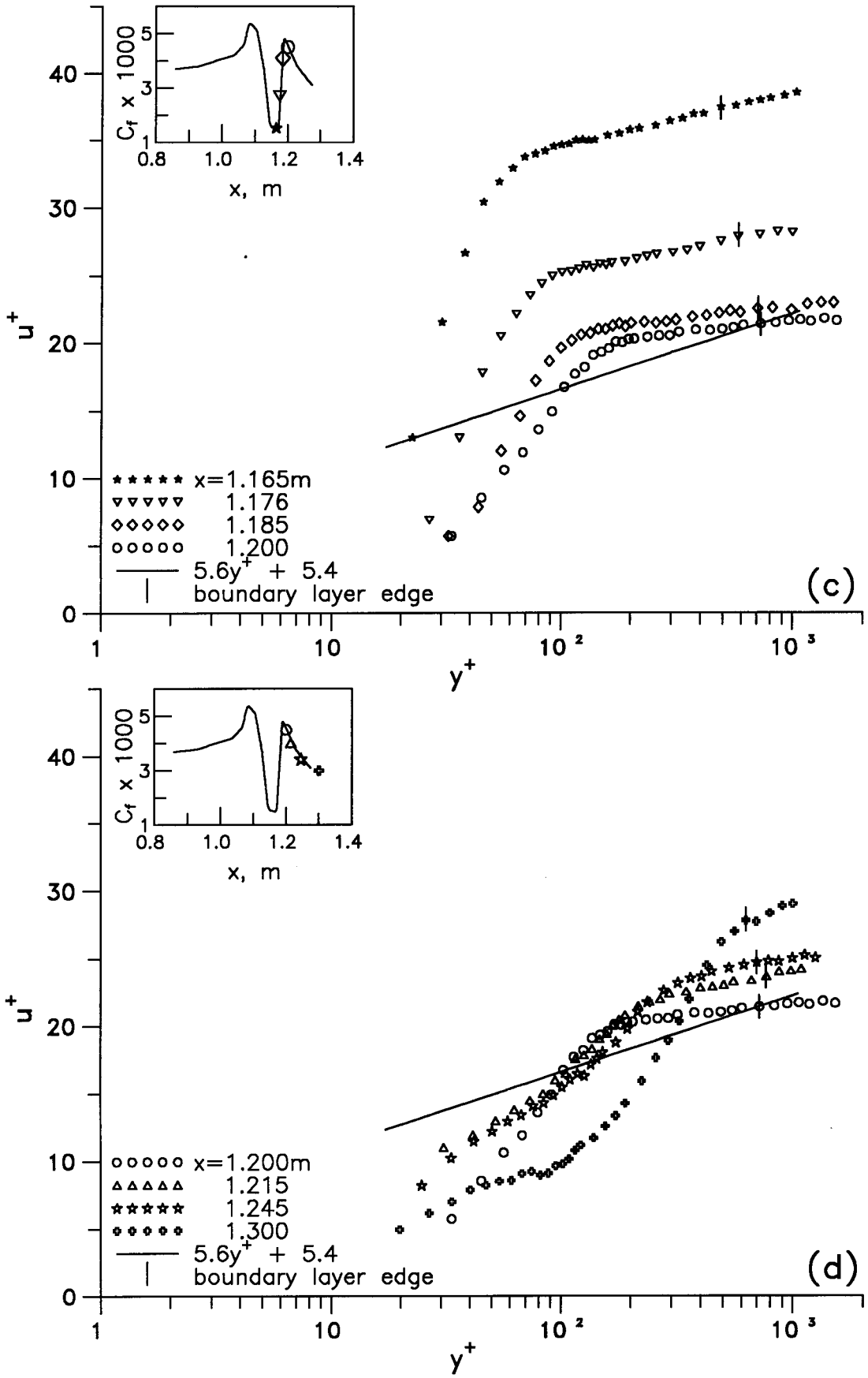

Fig.4.10 Boundary layer mean velocity profiles in wall coordinates : CP1 — — — concluded

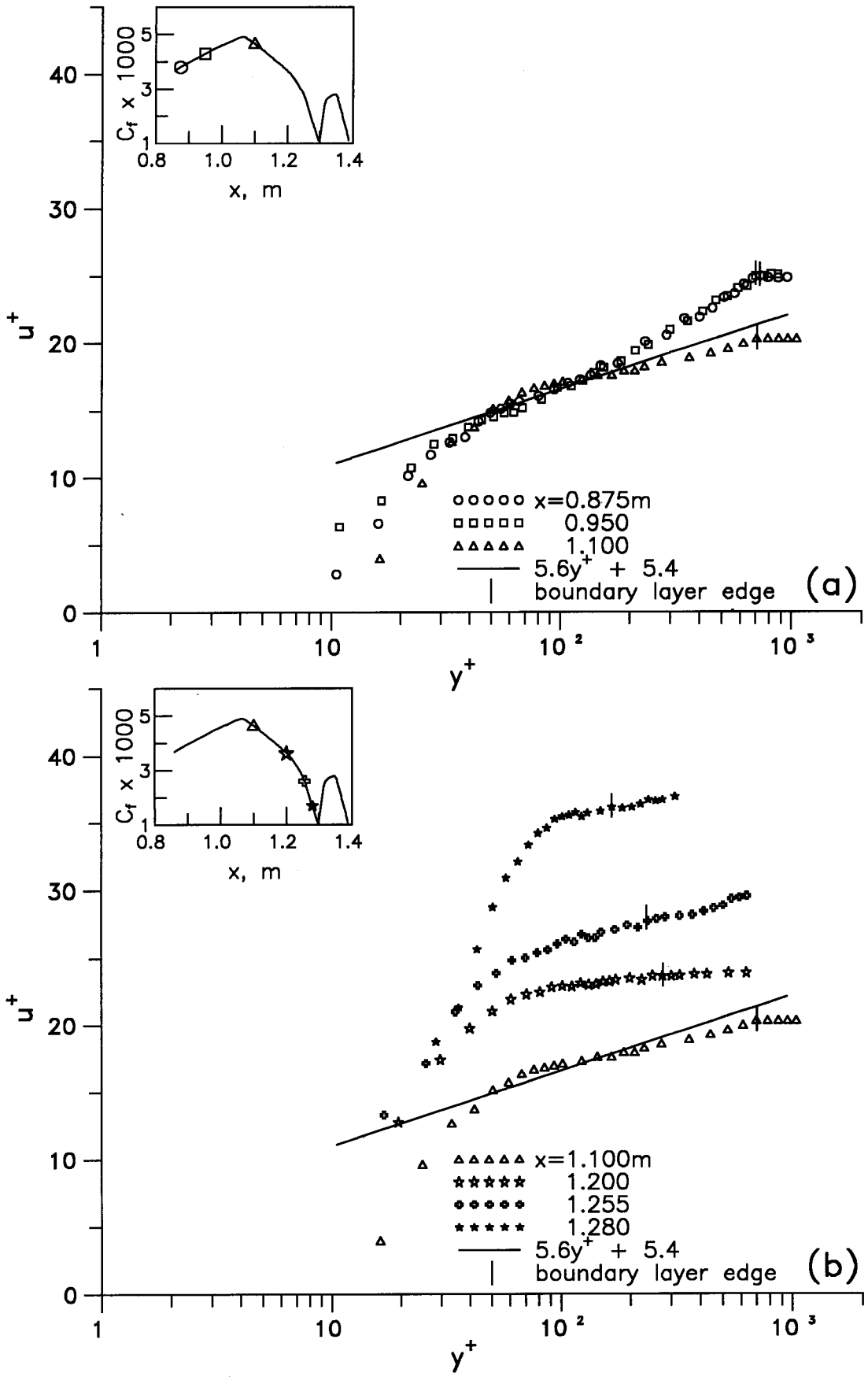

Fig.4.11 Boundary layer mean velocity profiles in wall coordinates : DP1 continued – – –

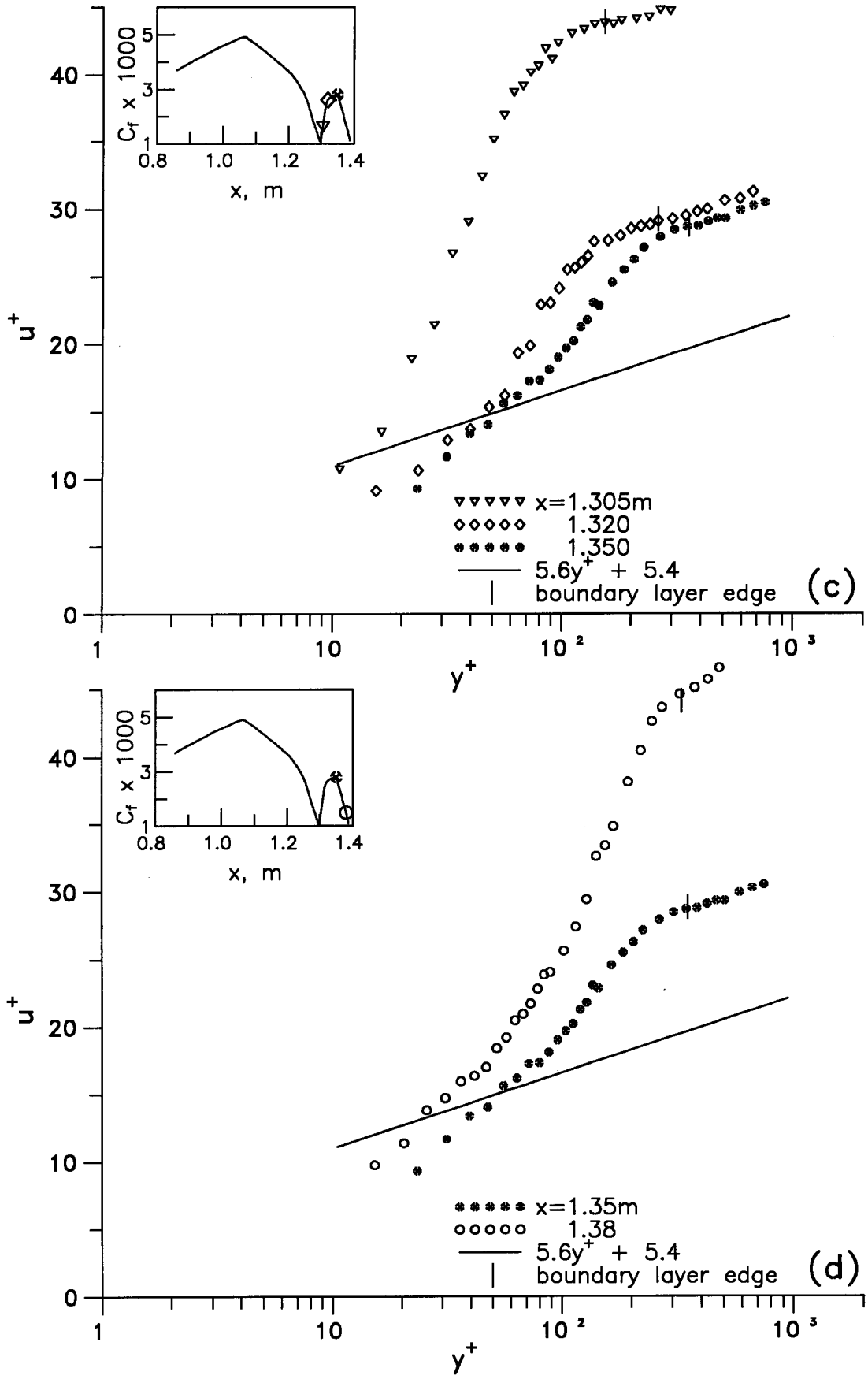

Fig.4.11 Boundary layer mean velocity profiles in wall coordinates : DP1 — — — concluded

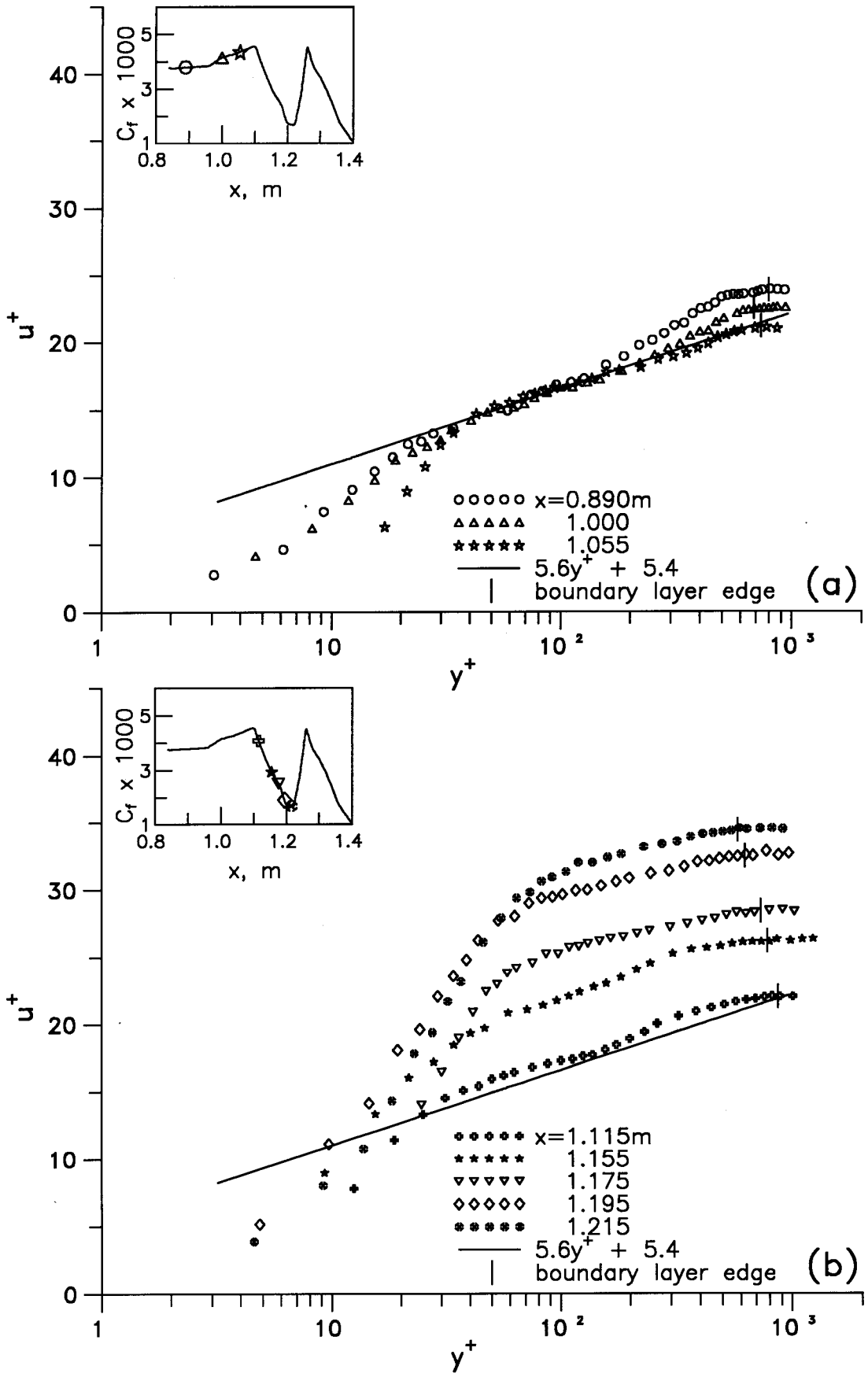

Fig.4.12 Boundary layer mean velocity profiles in wall coordinates : FP1 continued – – –

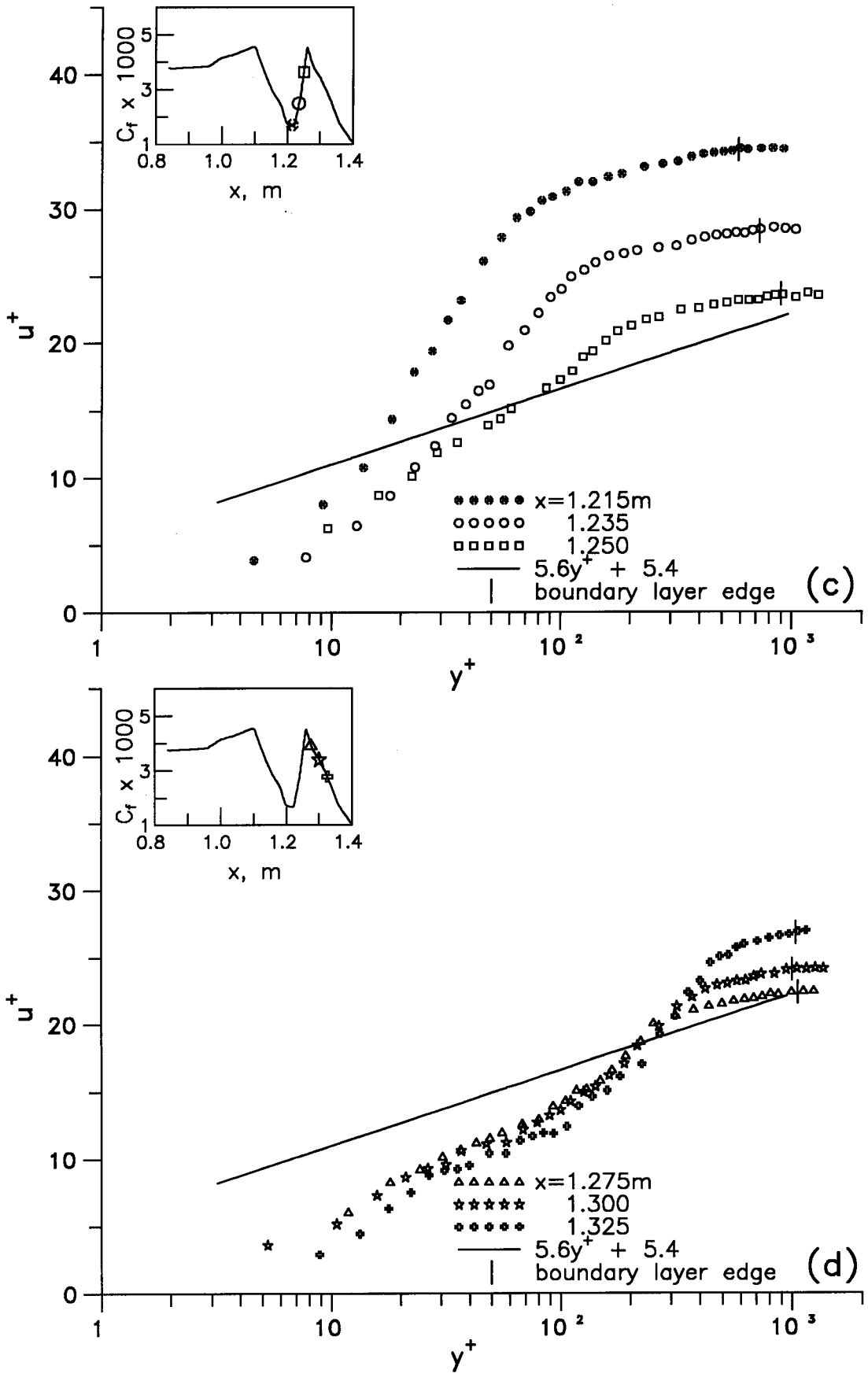

Fig.4.12 Boundary layer mean velocity profiles in wall coordinates : FP1 — — — concluded

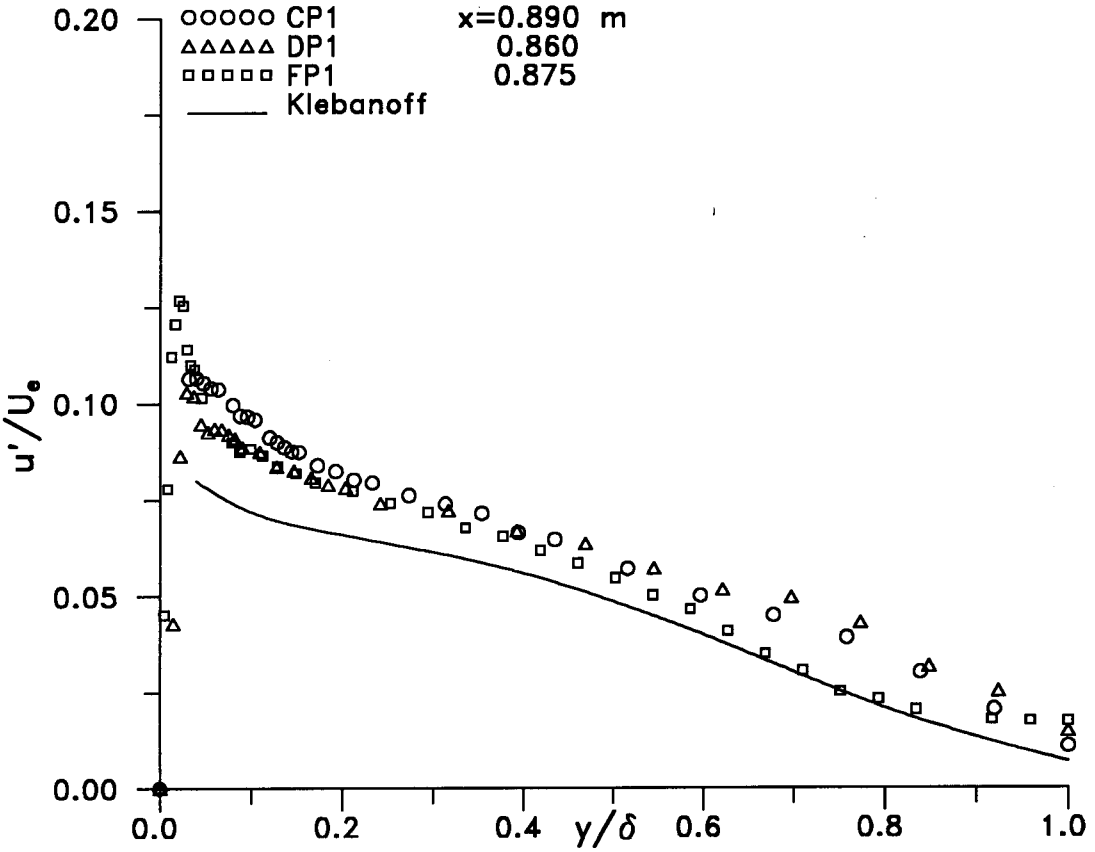

Fig.4.13 Streamwise turbulence intensity profiles before acceleration : flows : CP1, DP1 and FP1

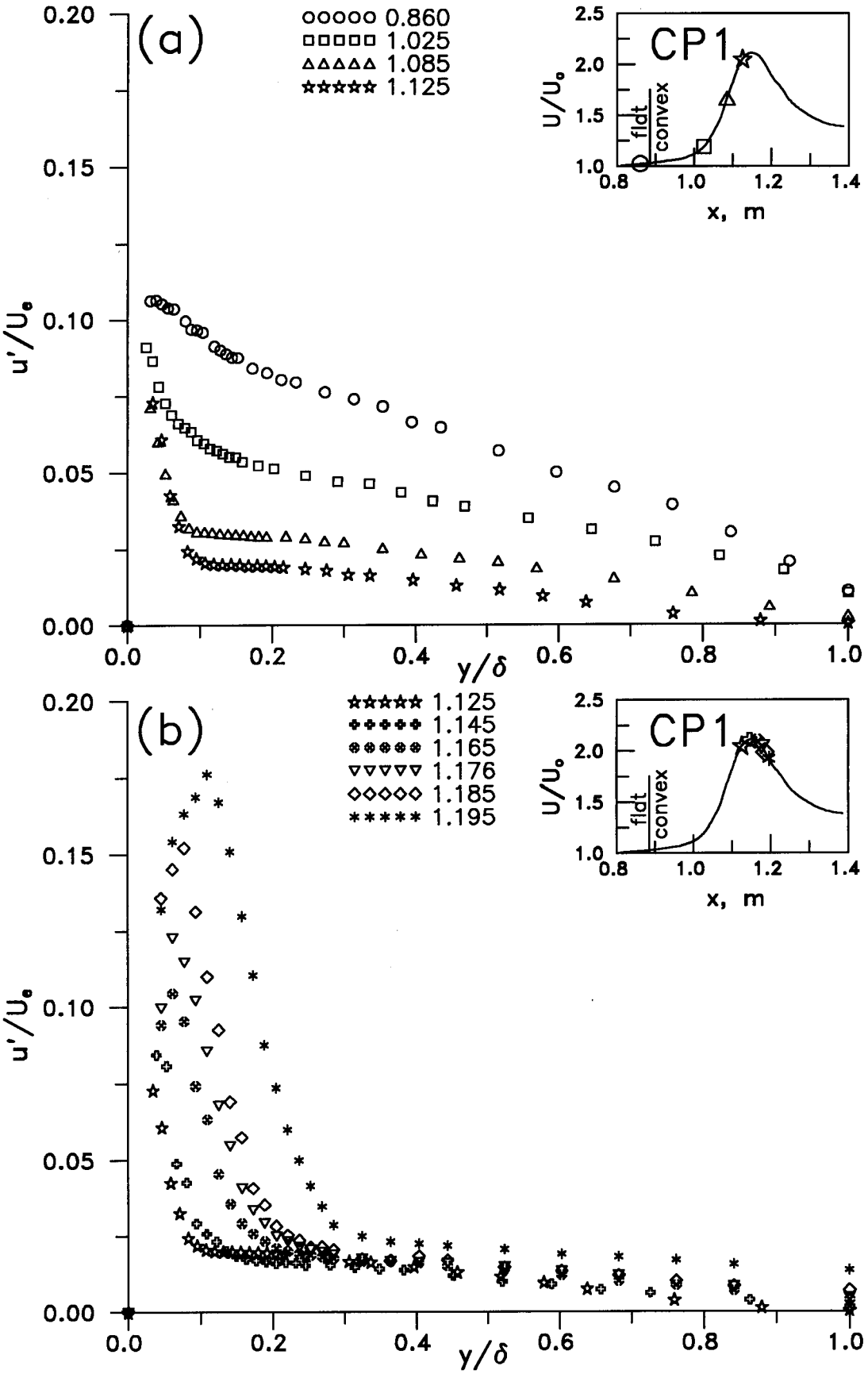

Fig.4.14 Streamwise turbulence intensity profiles : CP1 continued – – –

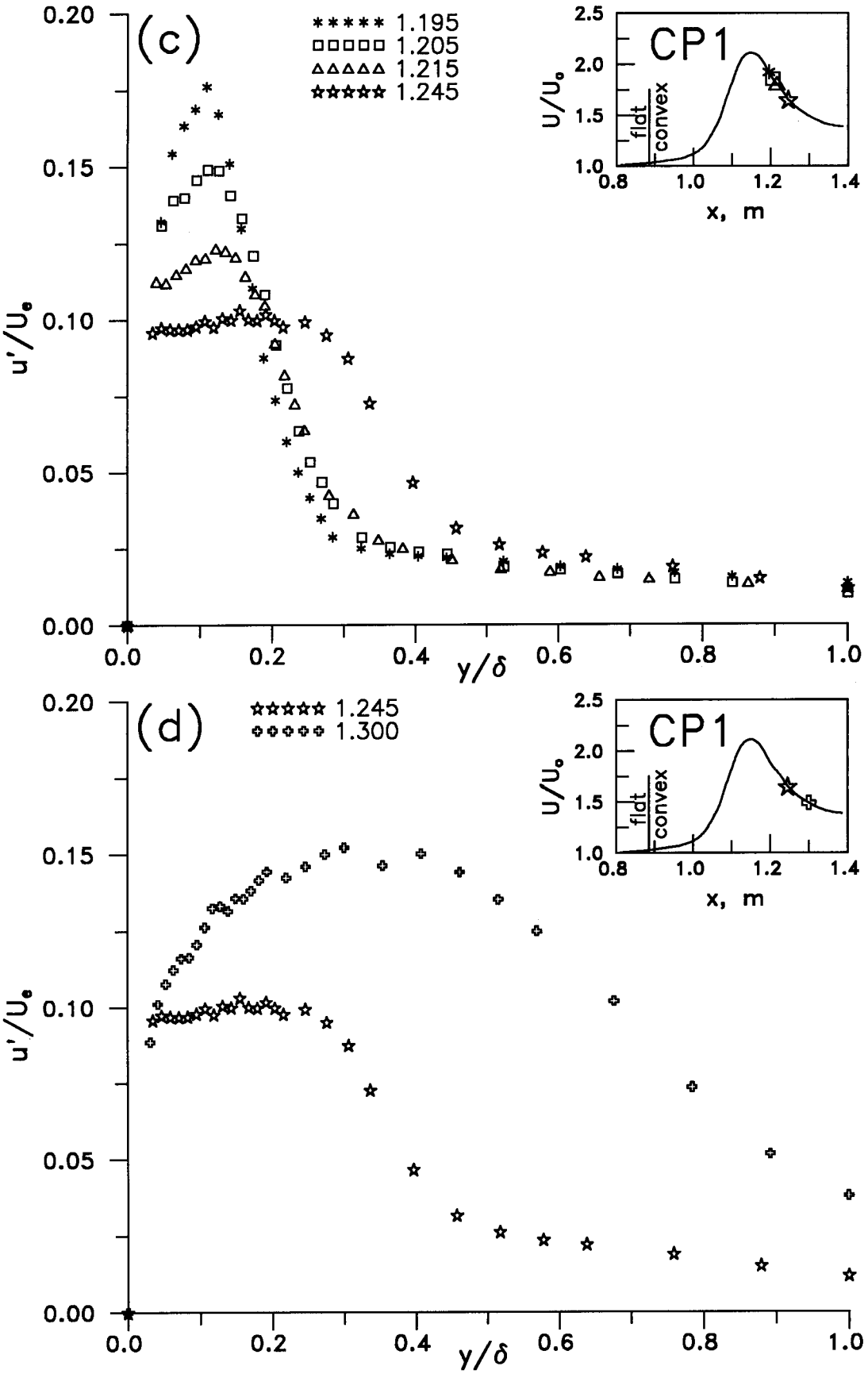

Fig.4.14 Streamwise turbulence intensity profiles : CP1
— — — concluded

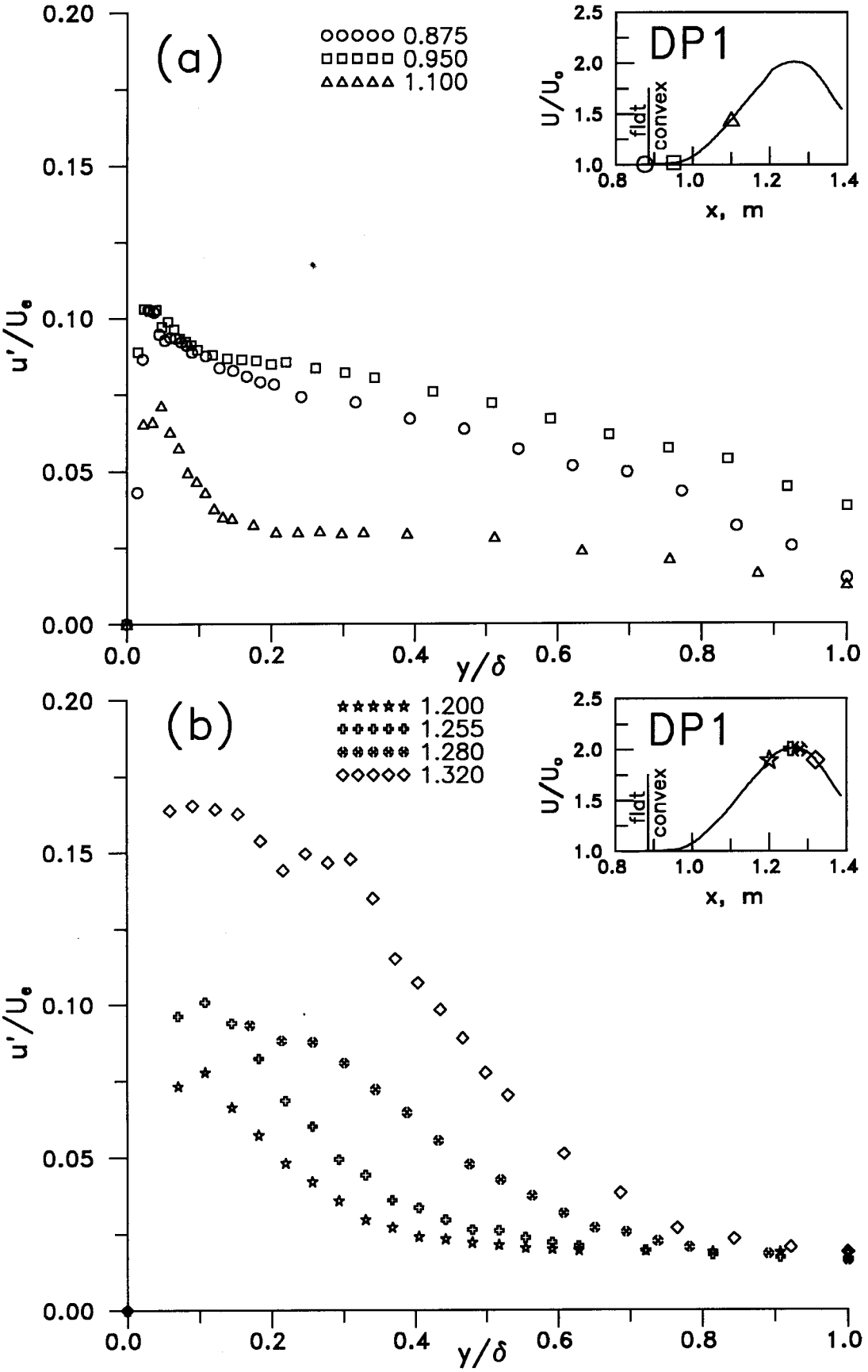

Fig.4.15 Streamwise turbulent intensity profiles : DP1
continued – – –

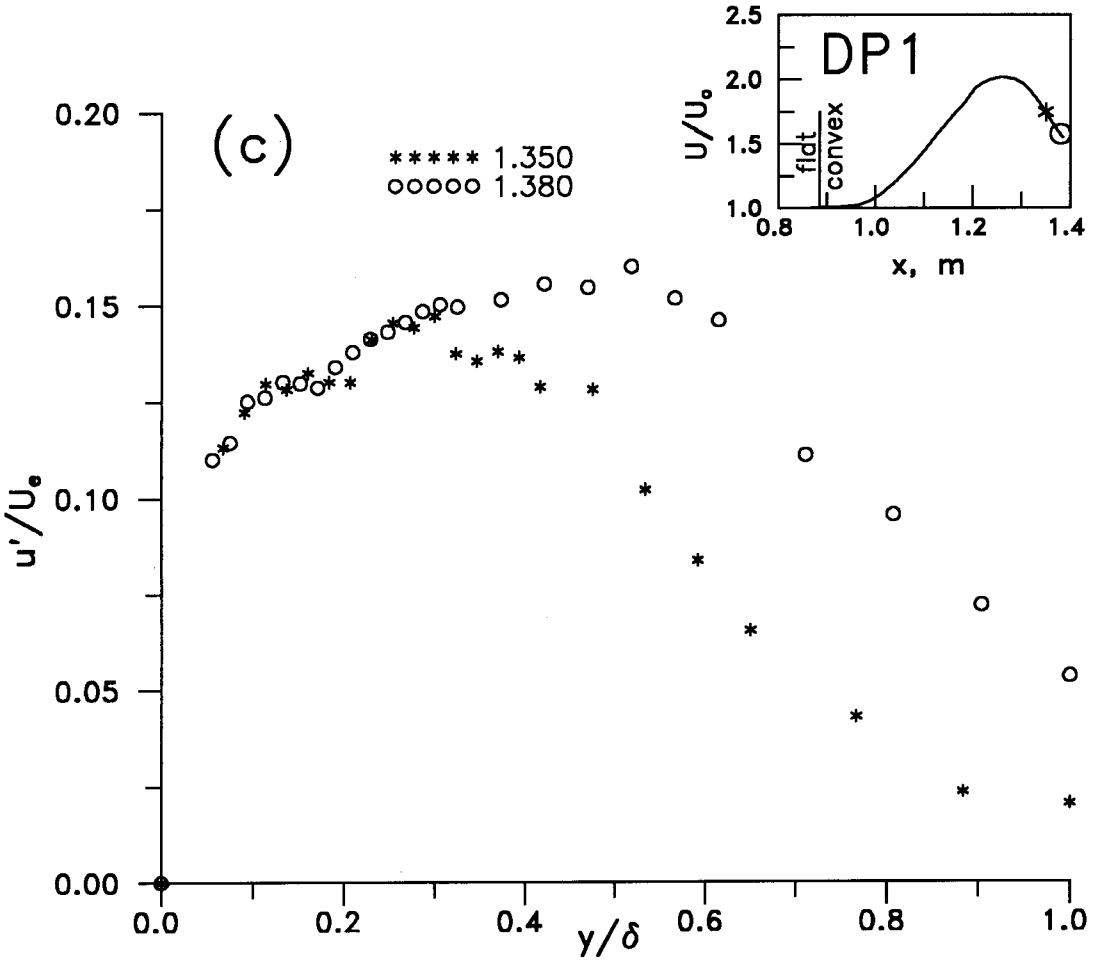

Fig.4.15 Streamwise turbulent intensity profiles : DP1
– – – concluded

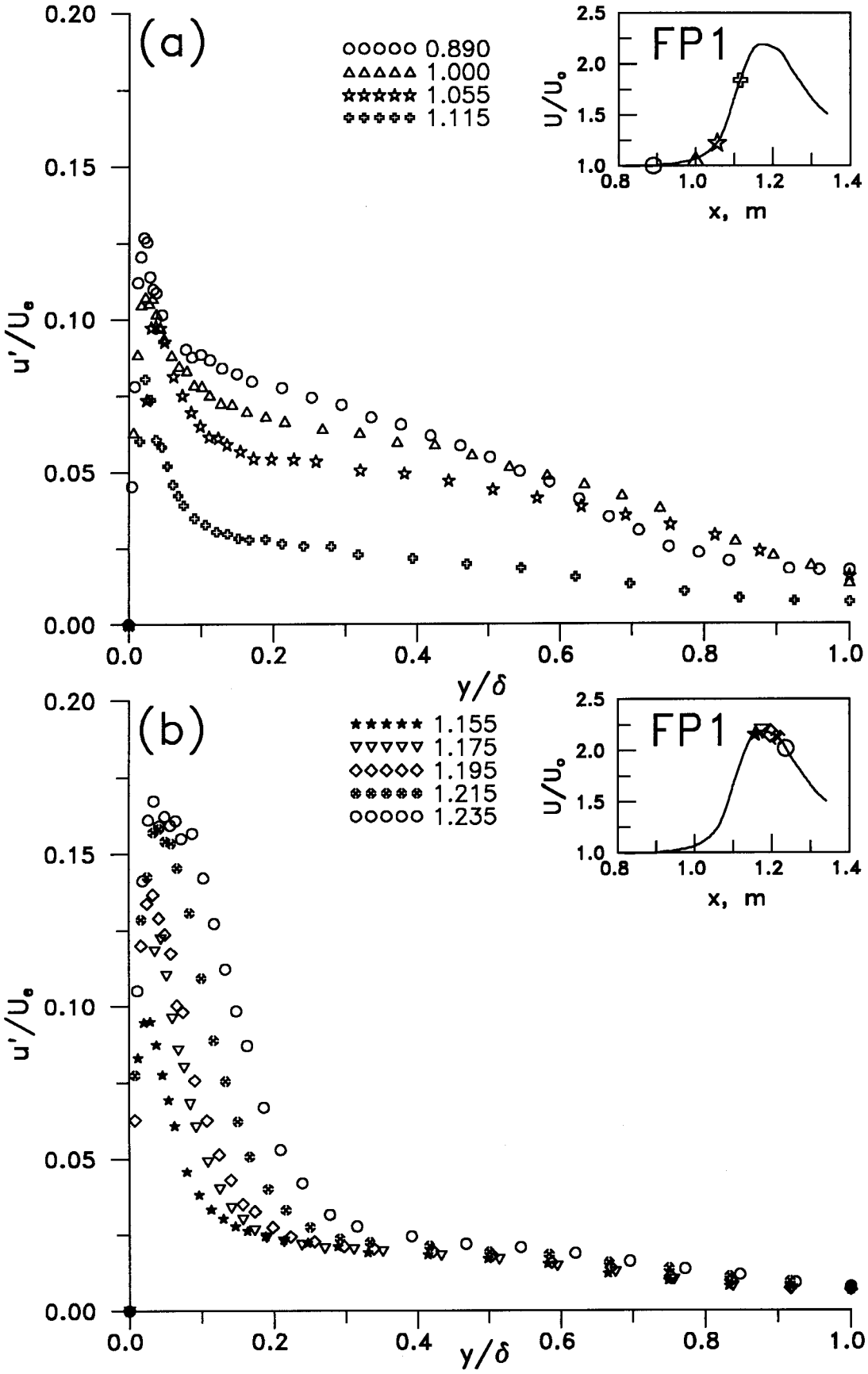

Fig.4.16 Streamwise turbulence intentity profiles : FP1
continued – – –

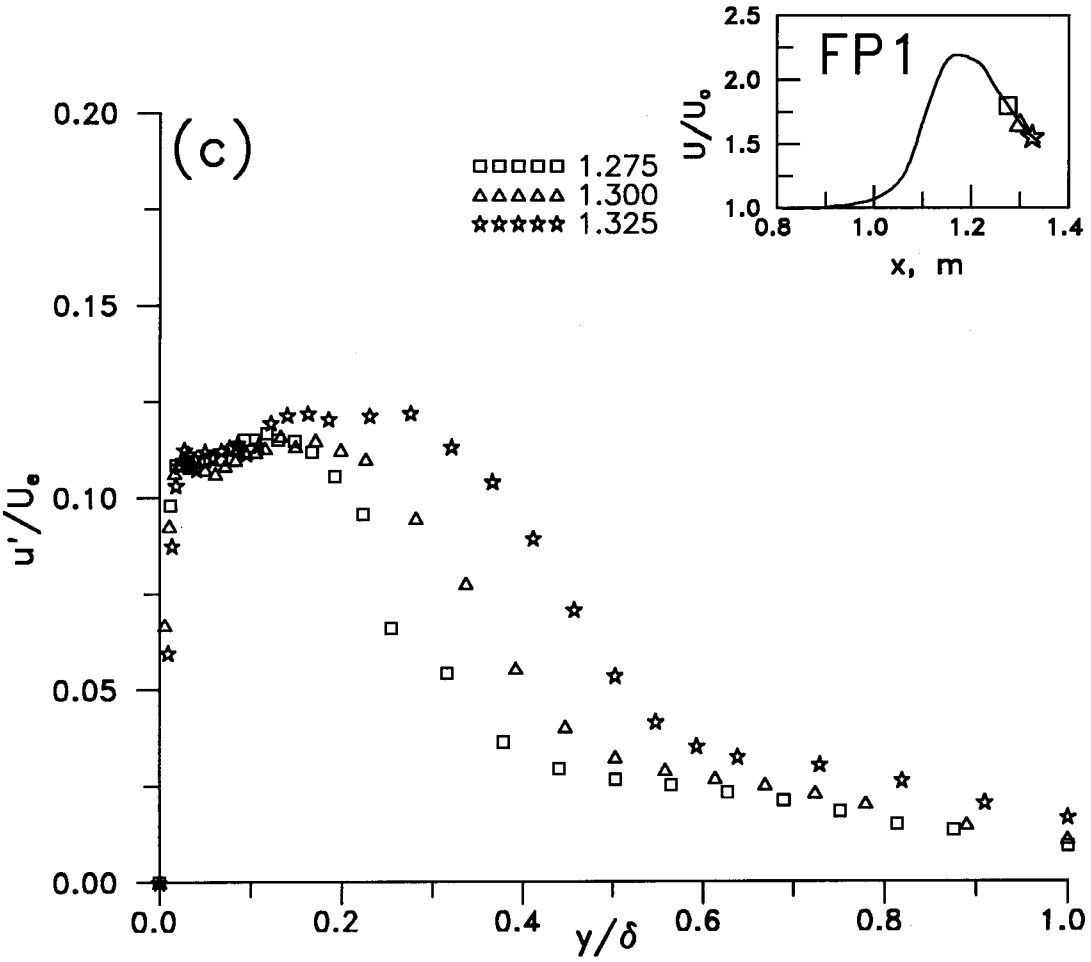

Fig.4.16 Streamwise turbulence intensity profiles : FP1
— — — concluded

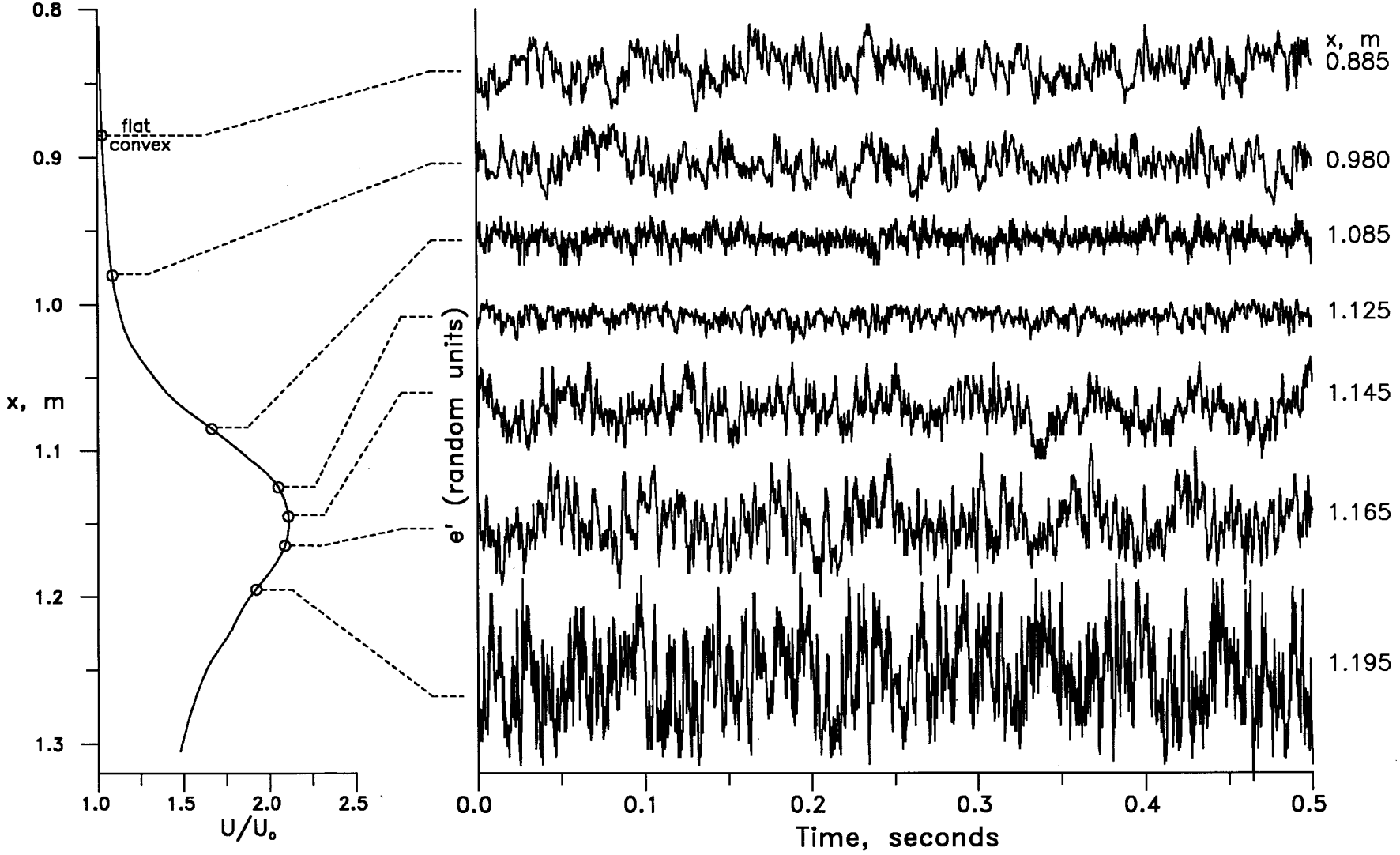

Fig.4.17 Time trace of velocity fluctuations : Flow CP1

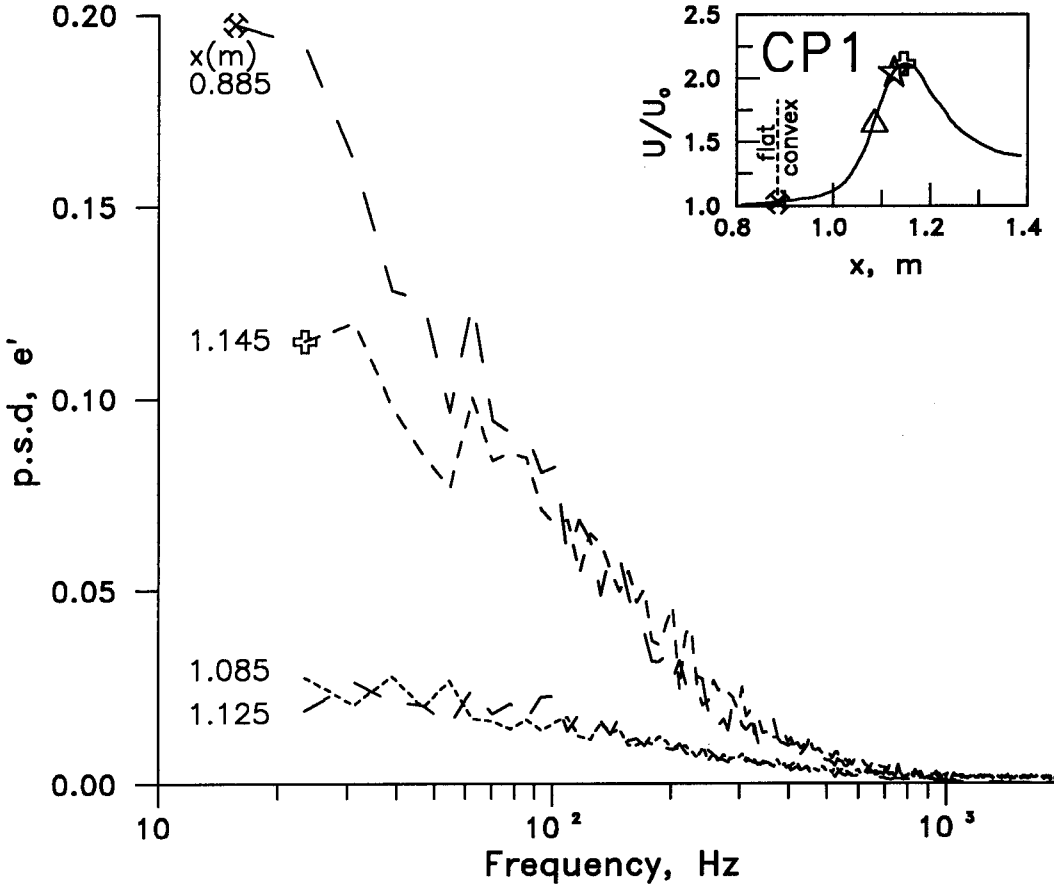

Fig.4.18 Power spectral density of velocity fluctuations : CP1

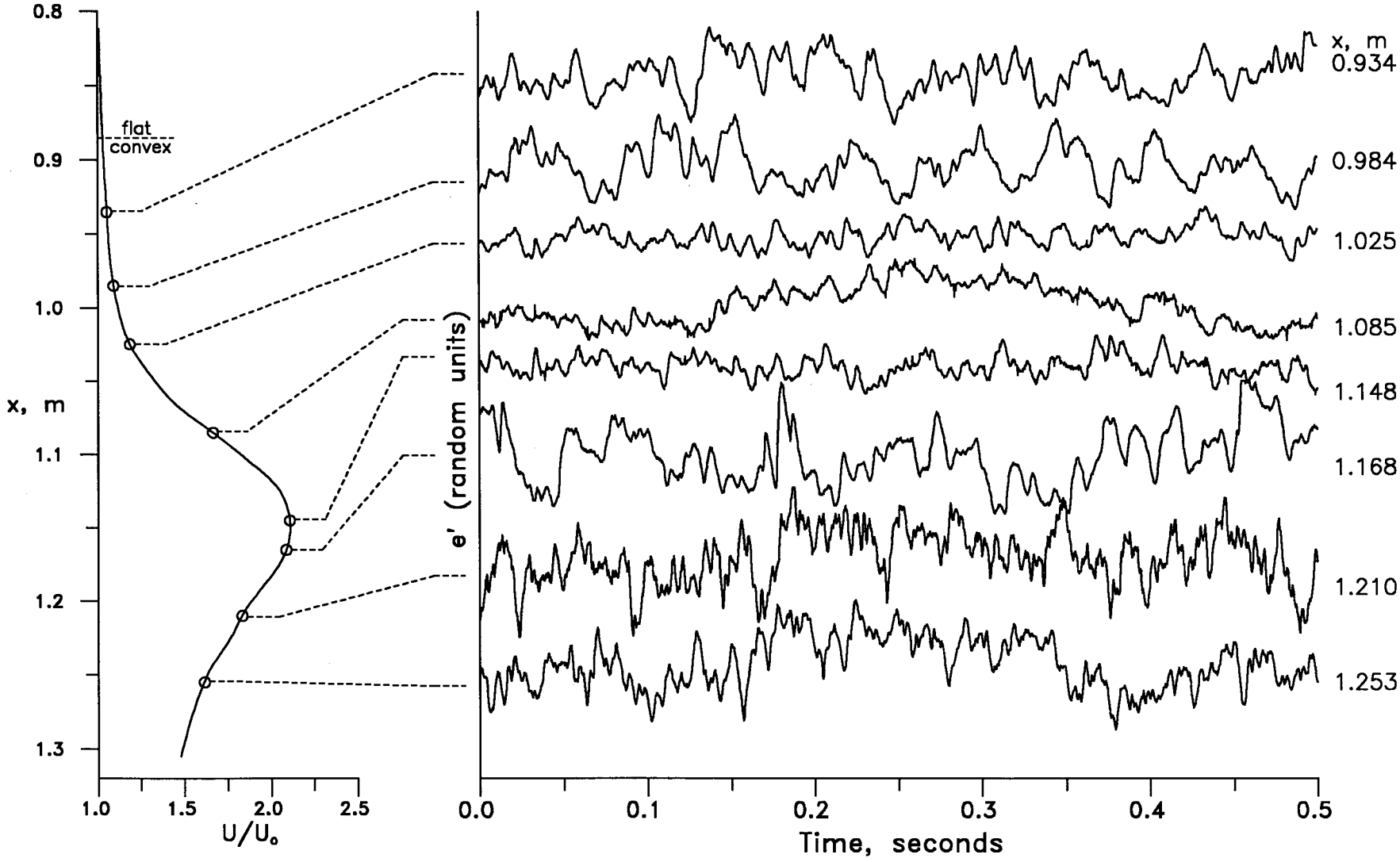

Fig.4.19 Time trace of shear stress fluctuations : Flow CP1

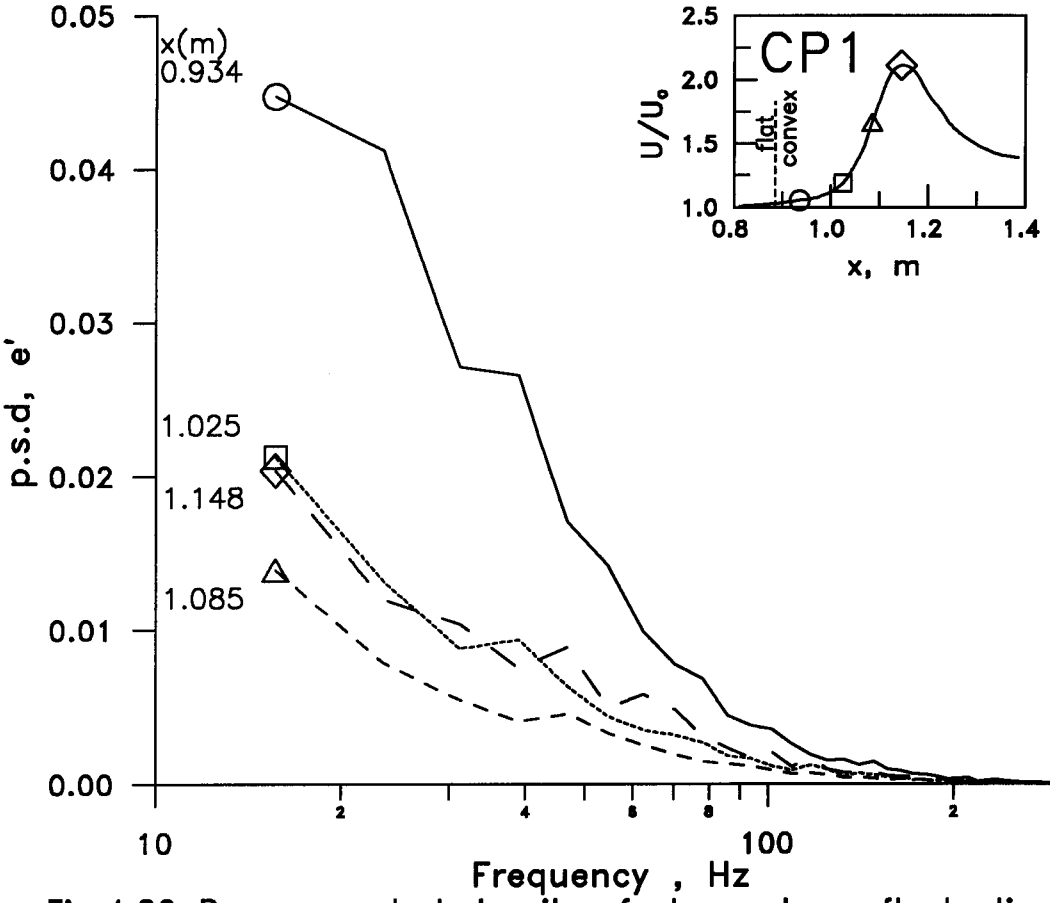

Fig.4.20 Power spectral density of shear stress fluctuations : CP1

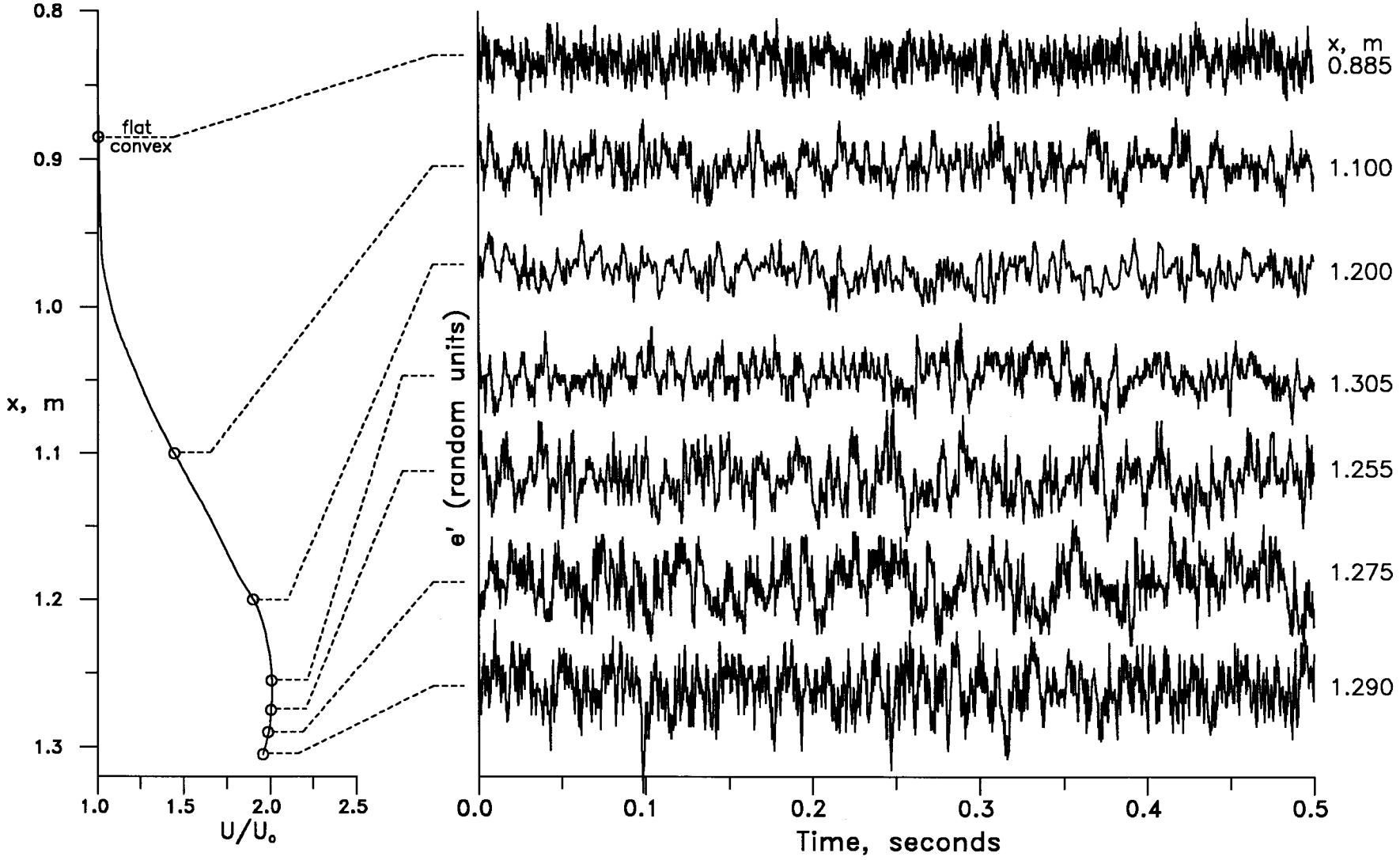

Fig.4.21 Time trace of velocity fluctuations : Flow DP1

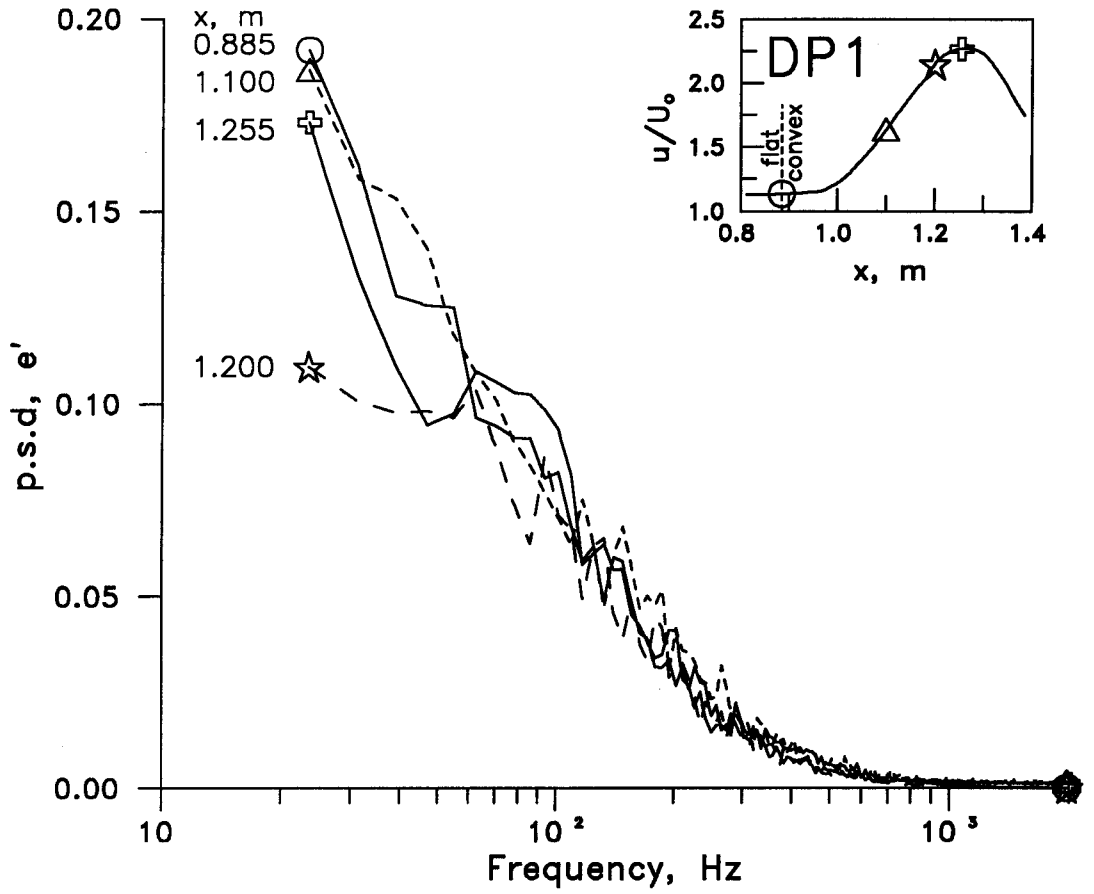

Fig.4.22 Power spectral density of velocity fluctuations : DP1

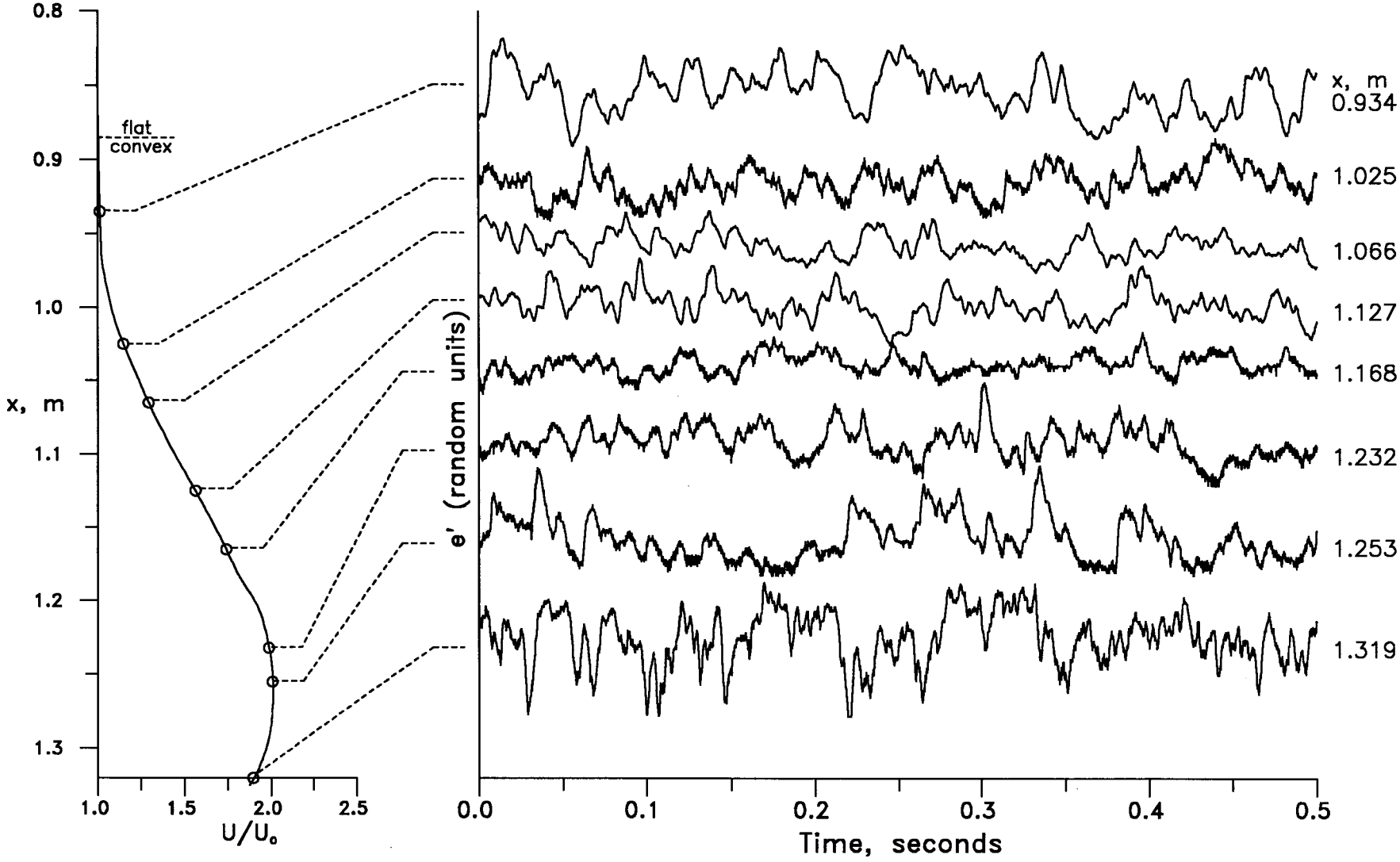

Fig.4.23 Time trace of shear-stress fluctuations : Flow DP1

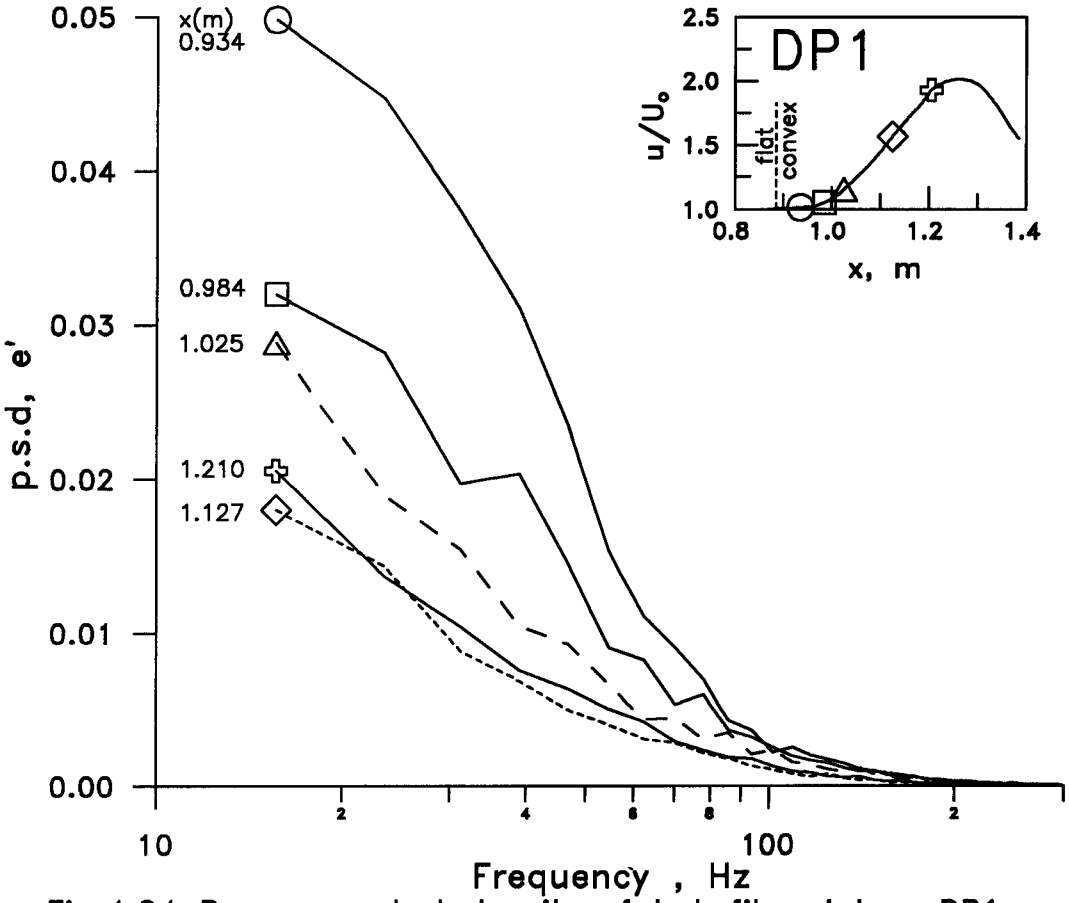

Fig.4.24 Power spectral density of hot-film data : DP1

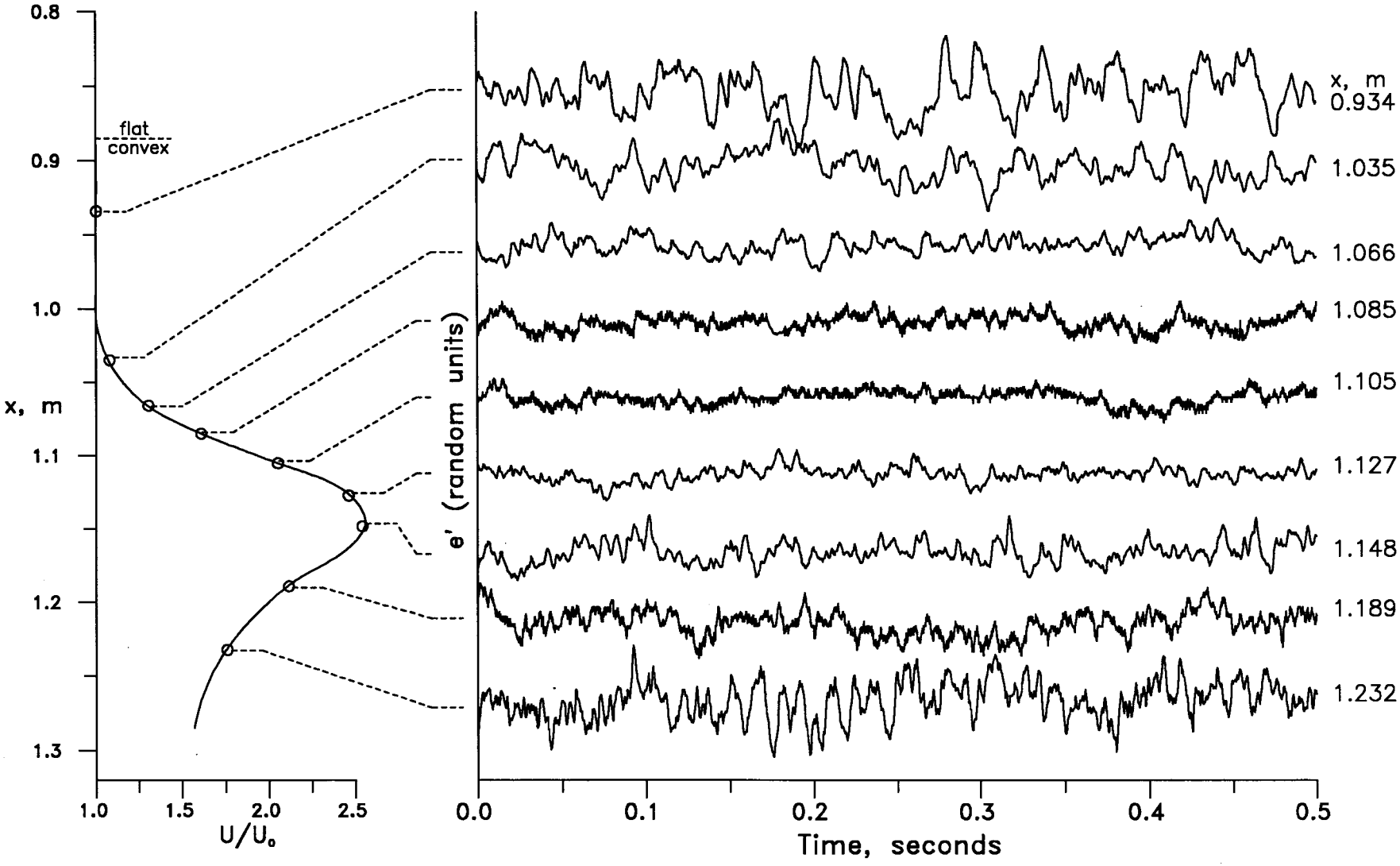

Fig.4.25 Time trace of shear stress fluctuations: Flow CP2

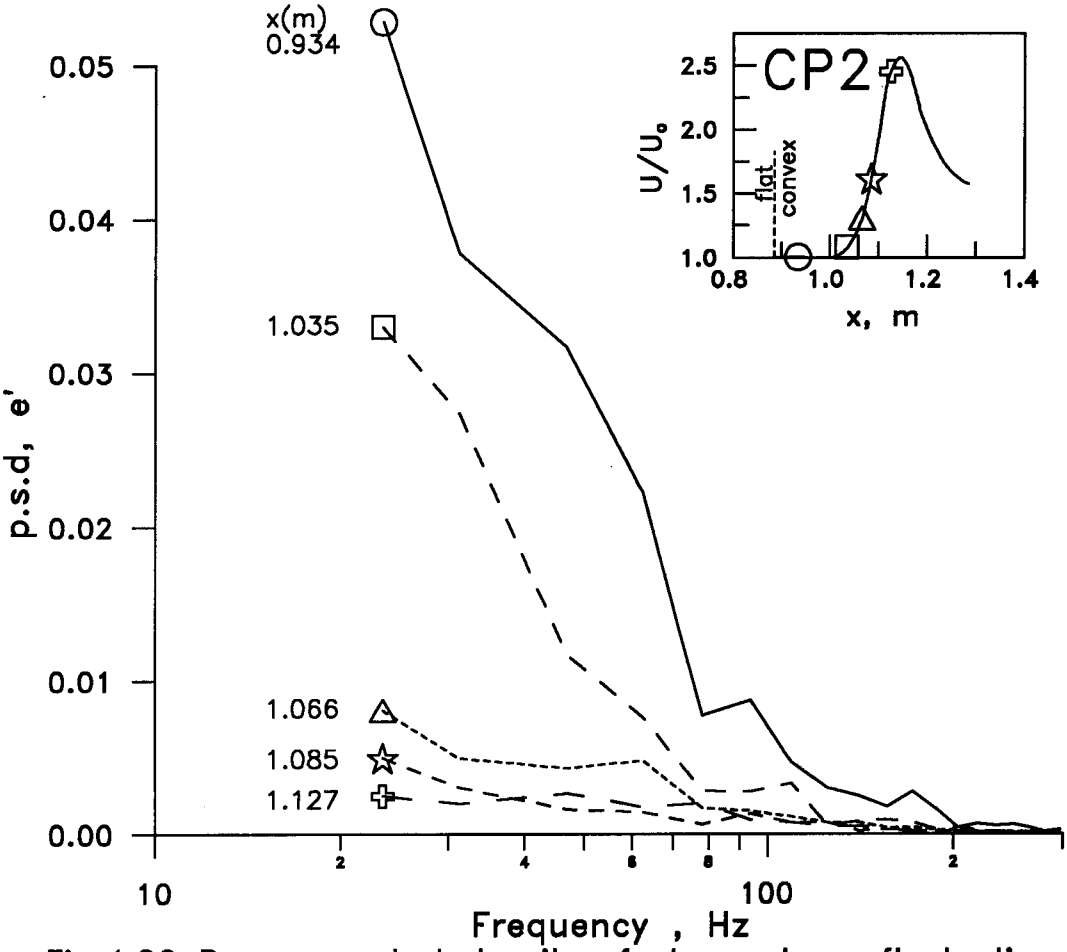

Fig.4.26 Power spectral density of shear stress fluctuations : CP2

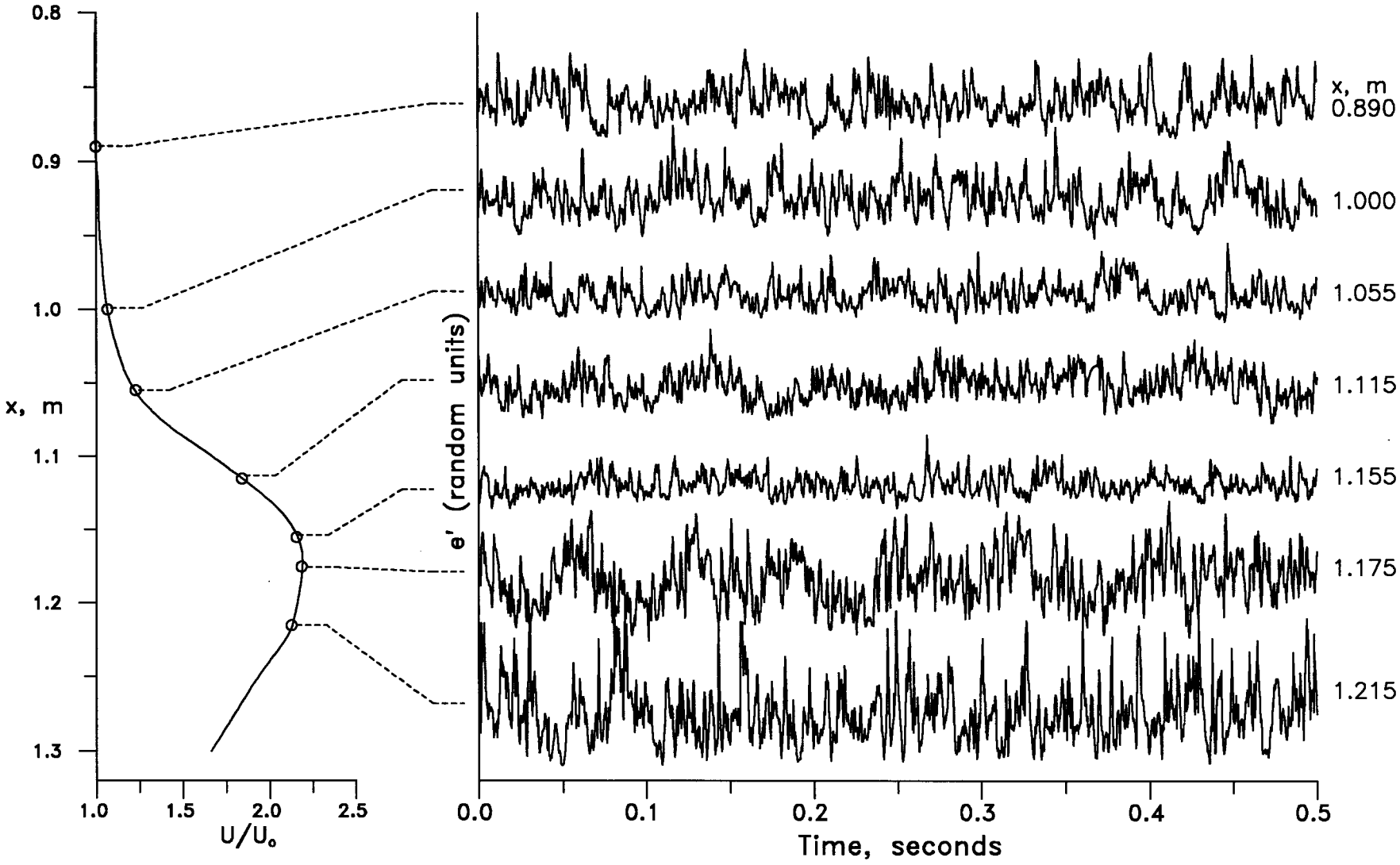

Fig.4.27 Time trace of velocity fluctuations : Flow FP1

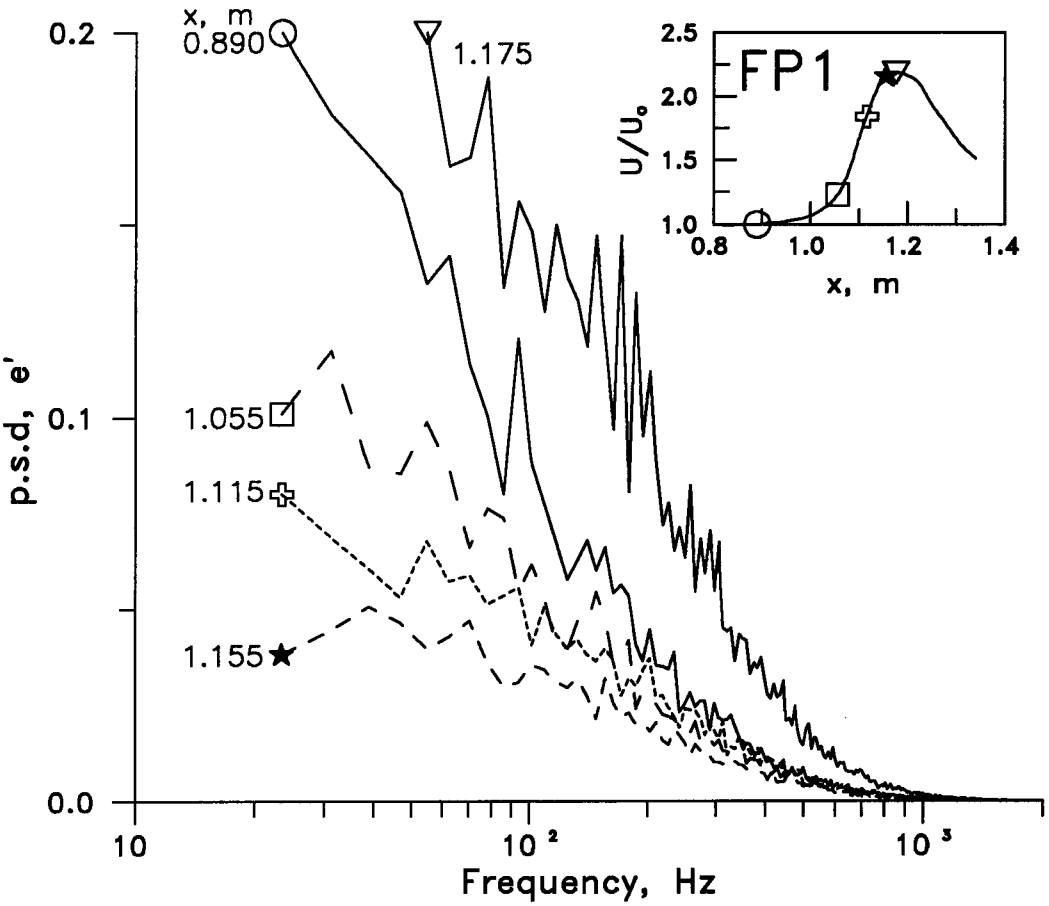

Fig.4.28 Power spectral density of velocity fluctuations : FP1

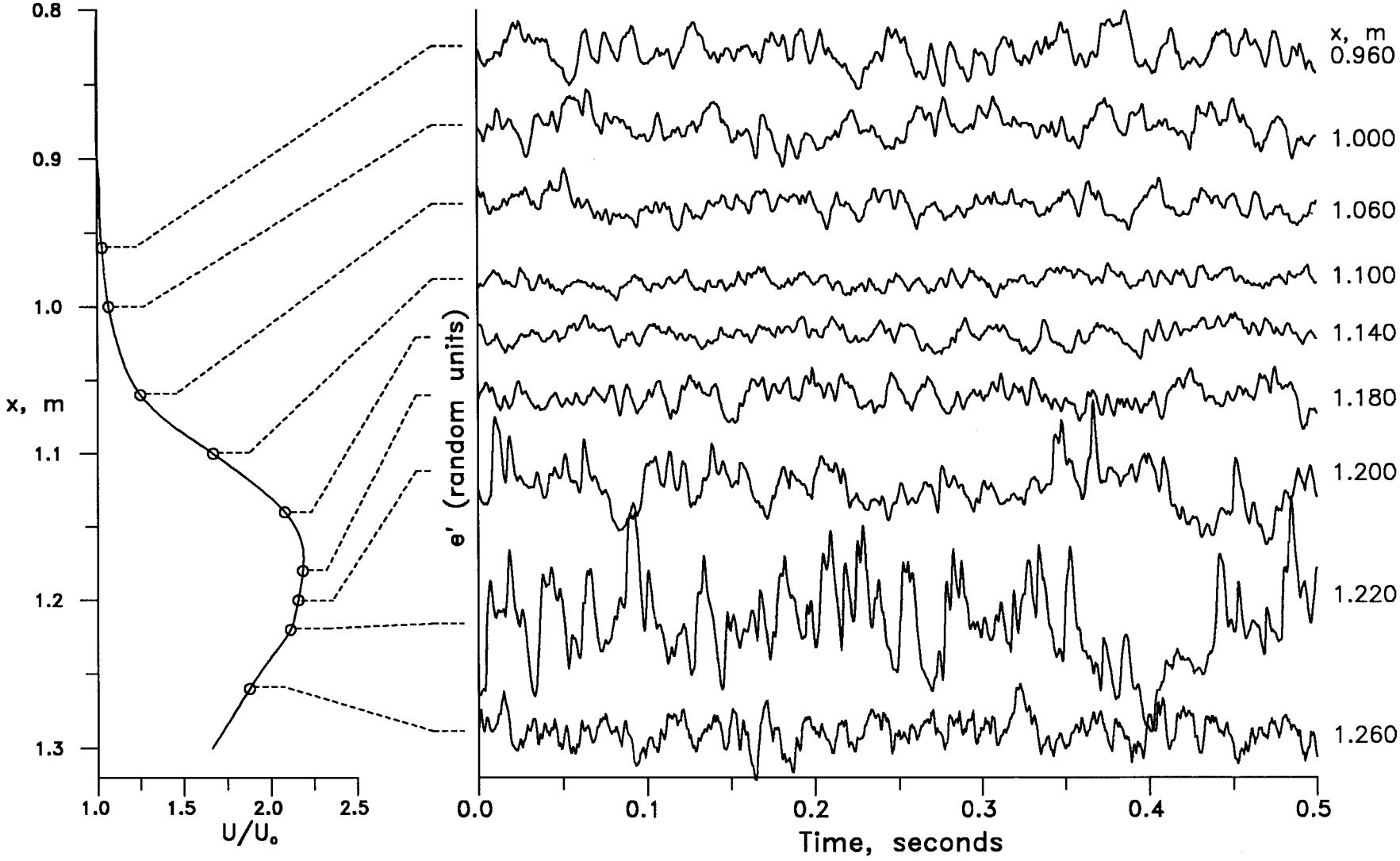

Fig.4.29 Time trace of shear stress fluctuations : Flow FP1

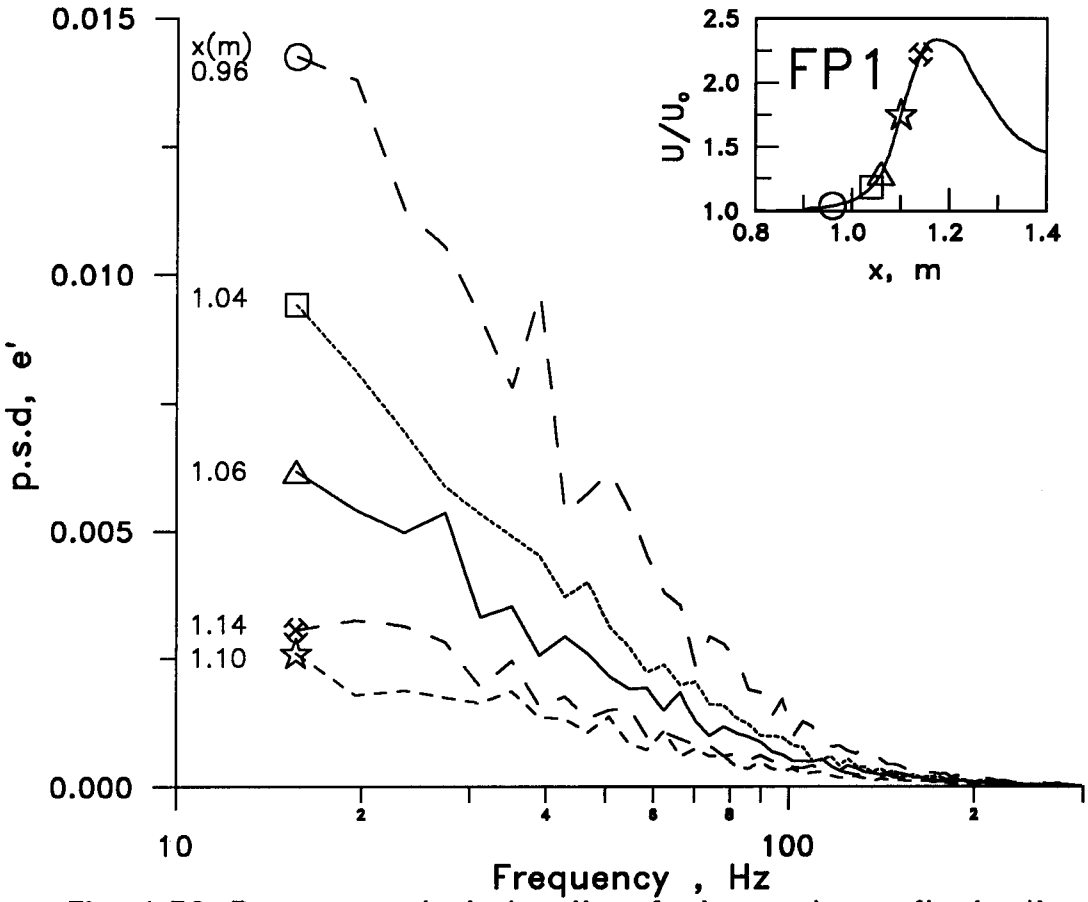

Fig 4.30 Power spectral density of shear stress fluctuations : FP1

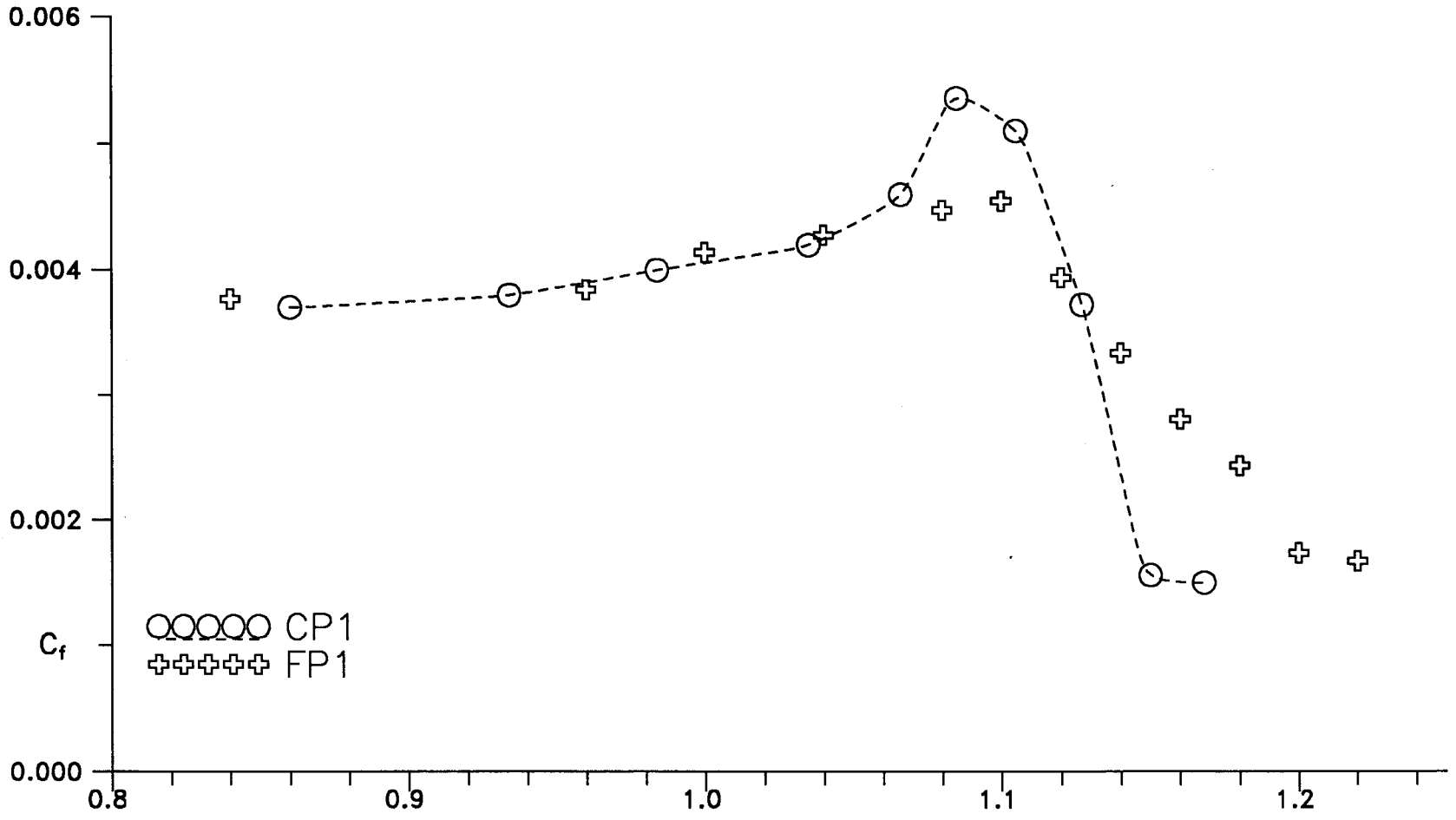

Fig.4.31 Comparison of C_f for CP1 and FP1

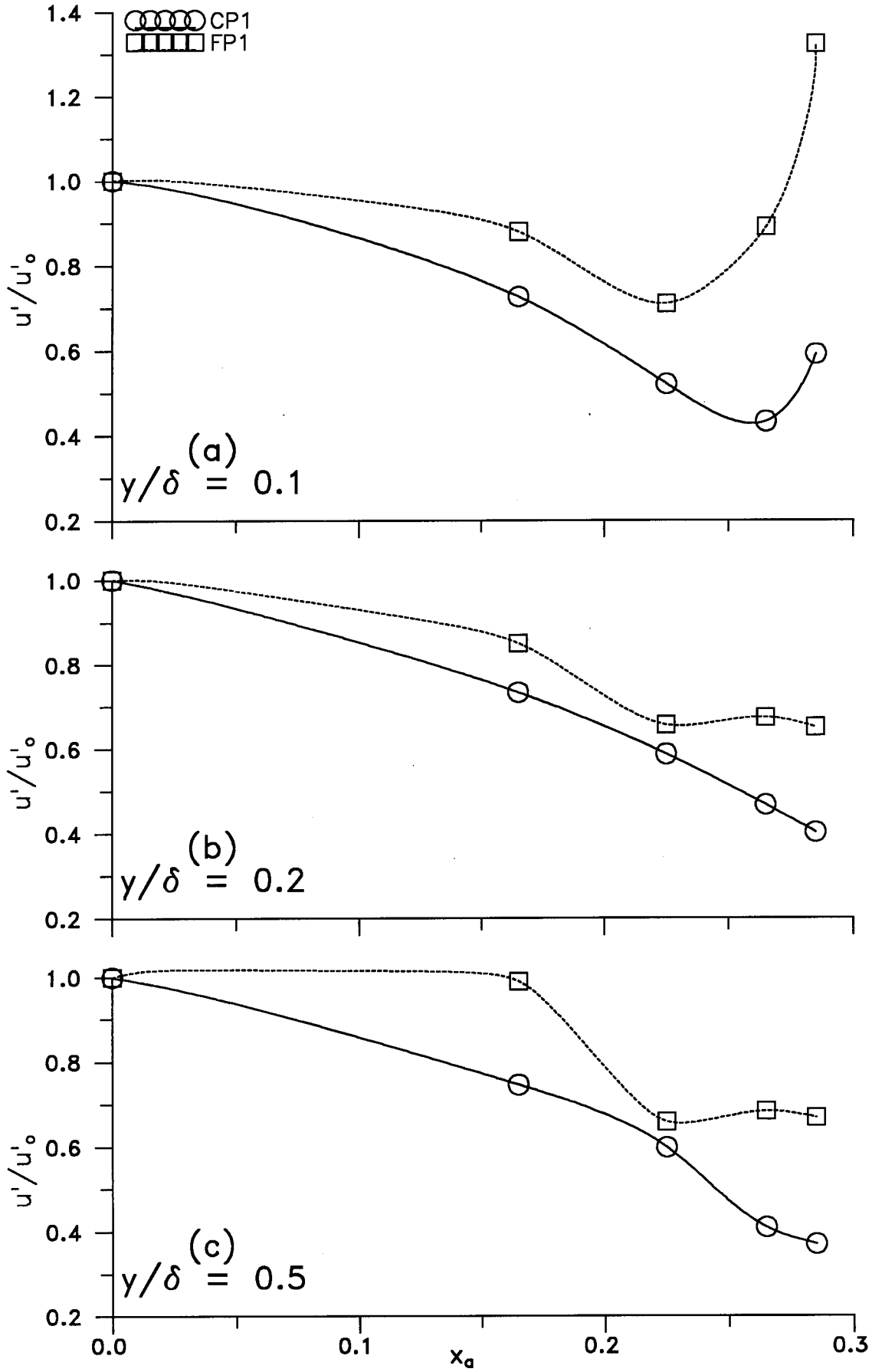

Fig.4.32 Reduction of turbulence with streamwise distance on convex surface flow CP1, compared with flat surface flow FP1

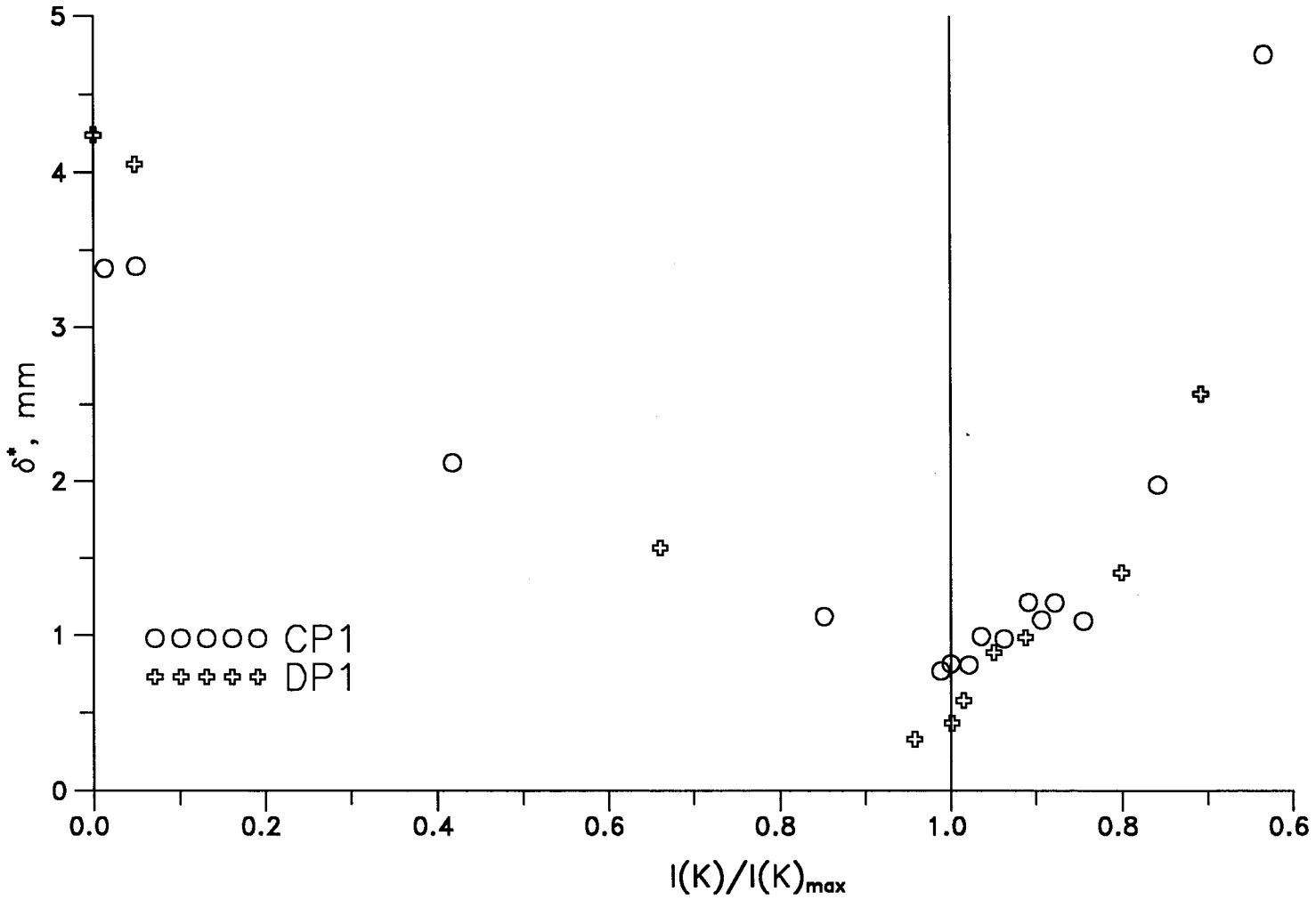

Fig.4.33 Comparison of the variation of displacement thickness with I(K) Flow CP1 and DP1

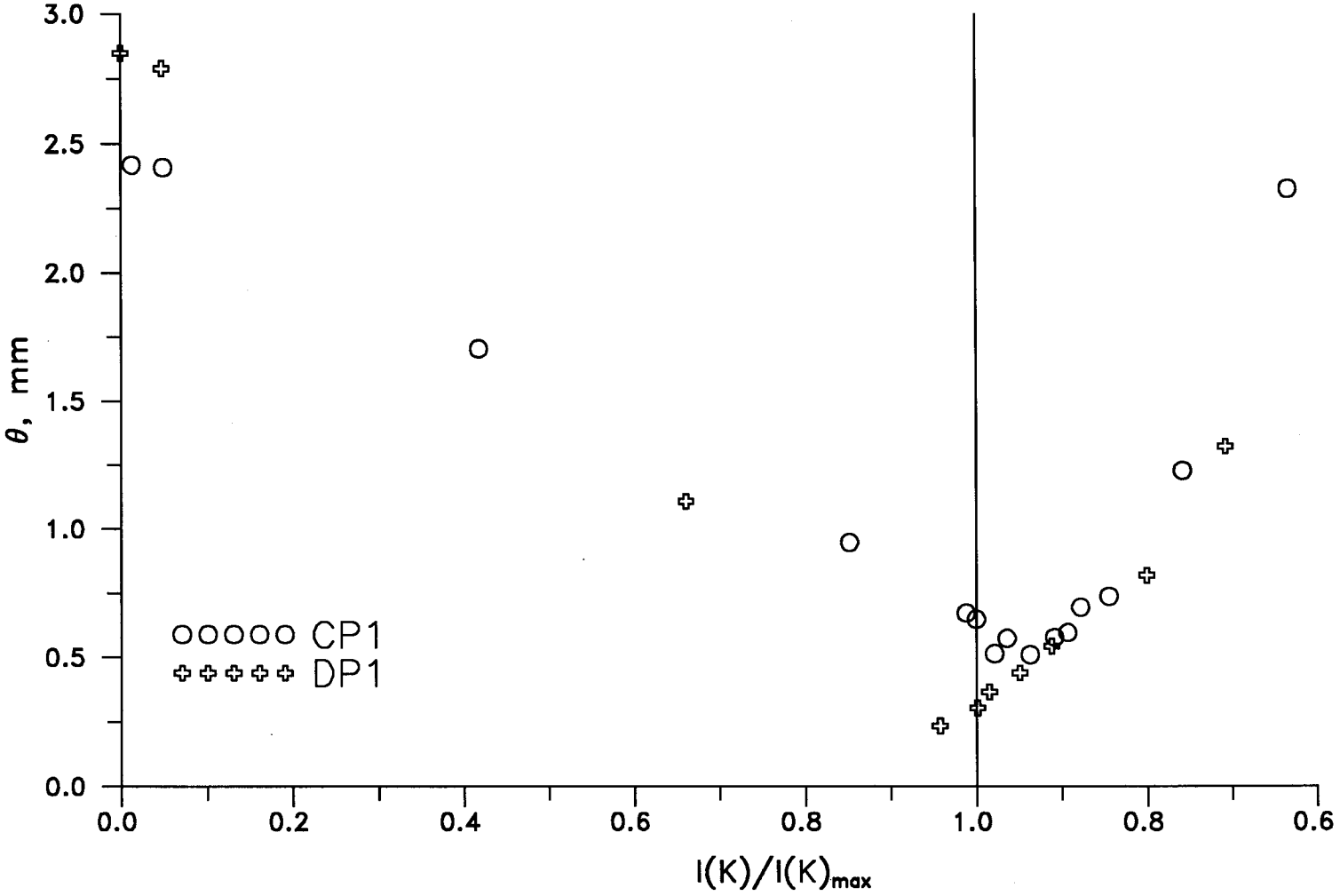

Fig.4.34 Comparison of the variation of the momentum thickness with I(K) Flow CP1 and DP1

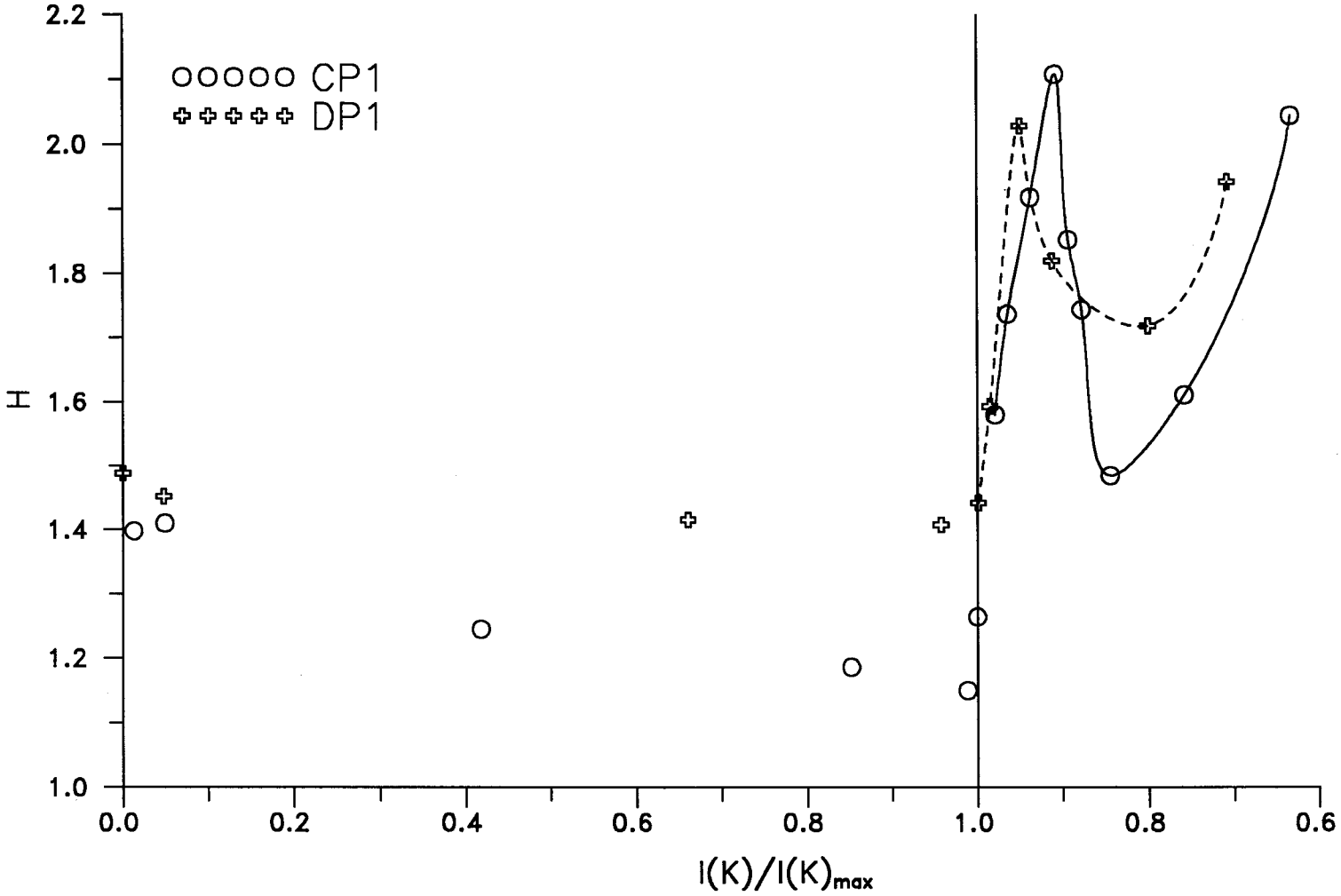

Fig.4.35 Comparison of the variation of shape factor with I(K) Flow CP1 and DP1

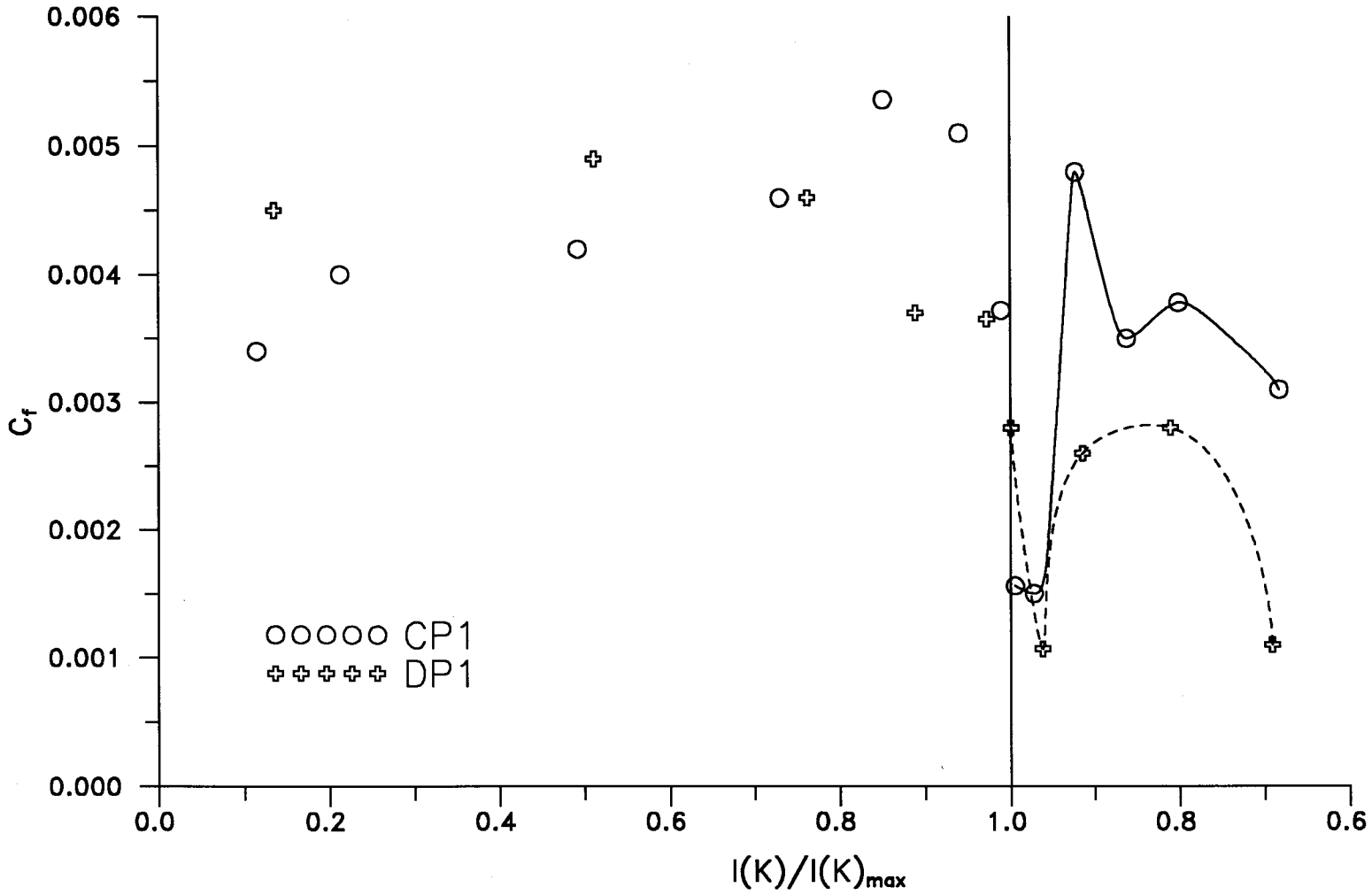

Fig.4.36 Comparison of the skin friction coefficient with I(K) Flow CP1 and DP1

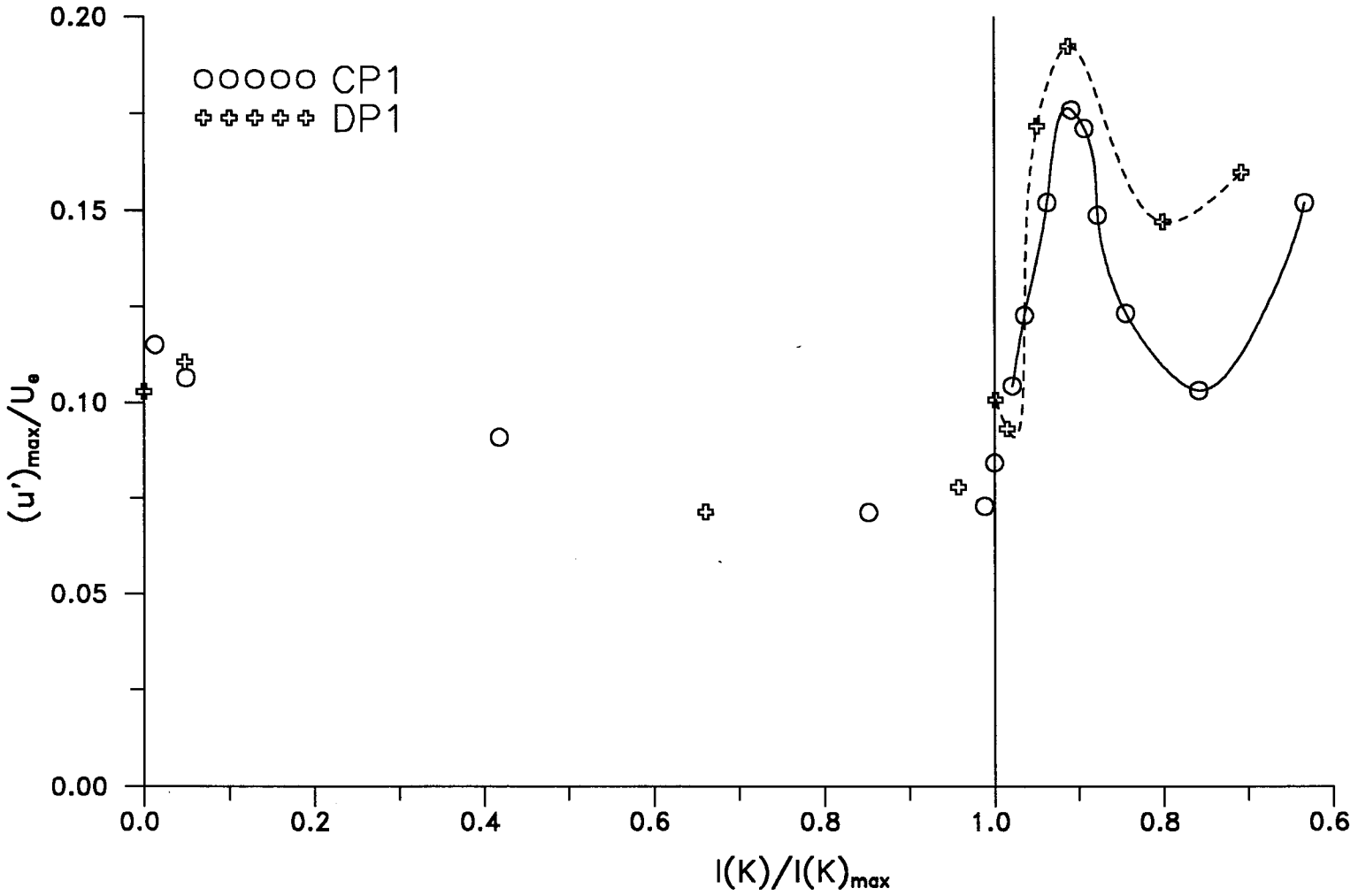

Fig.4.37 Comparison of the variation of observed maximum of turbulence intensity with I(K) : flow CP1 and DP1

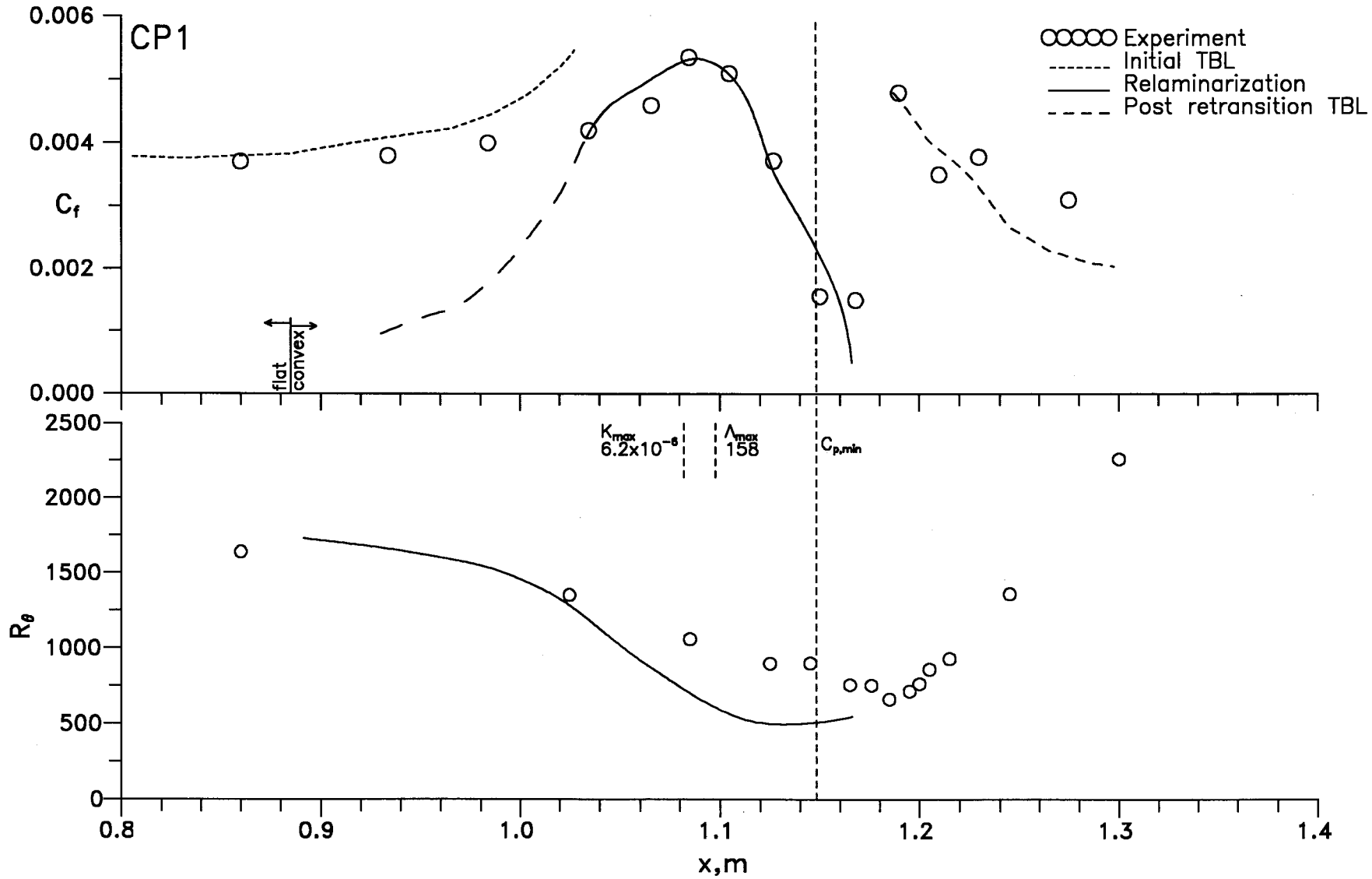

Fig.5.1 Comparison of experimental data with calculations : CP1
Relaminarization : Quasi-laminar equations
Turbulent boundary layer (TBL) : Lag entrainment method

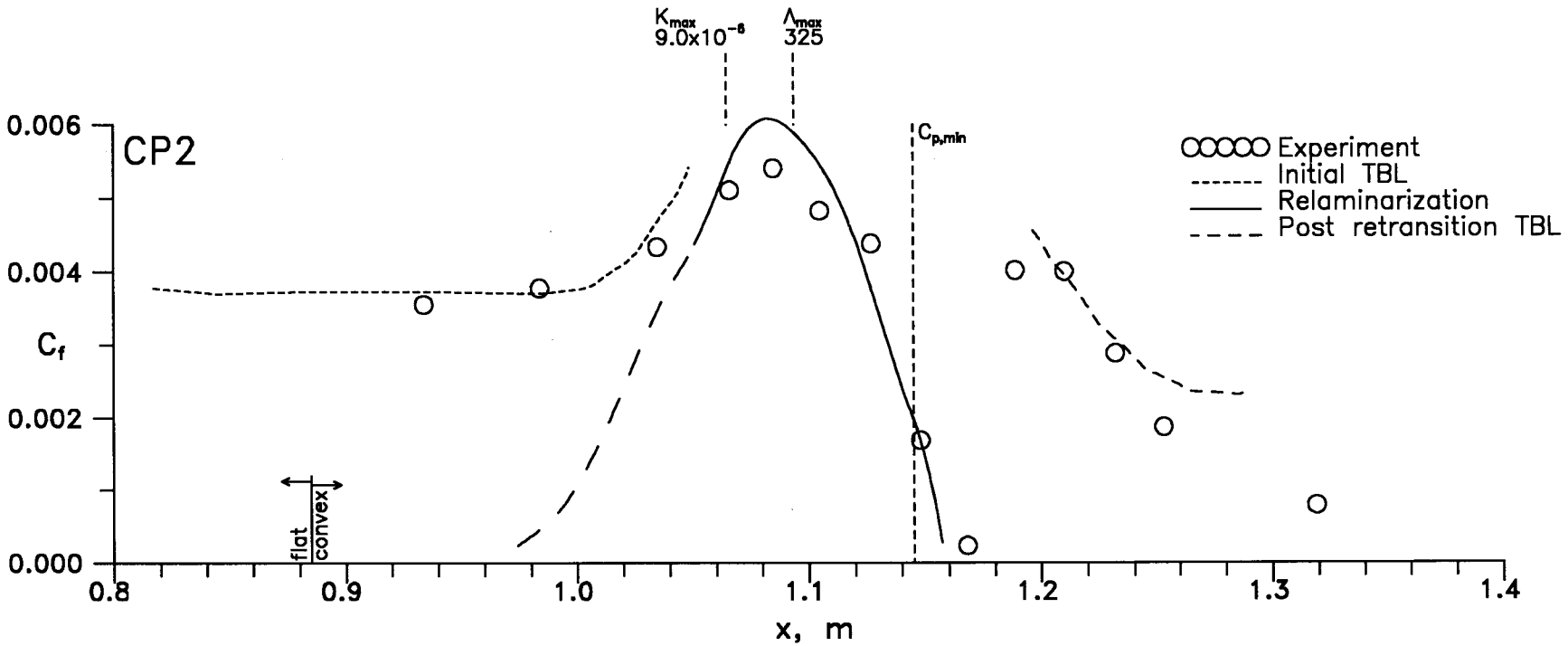

Fig.5.2 Comparison of experimental data with calculations : CP2
Relaminarization : Quasi-laminar equations
Turbulent boundary layer (TBL) : Lag entrainment method

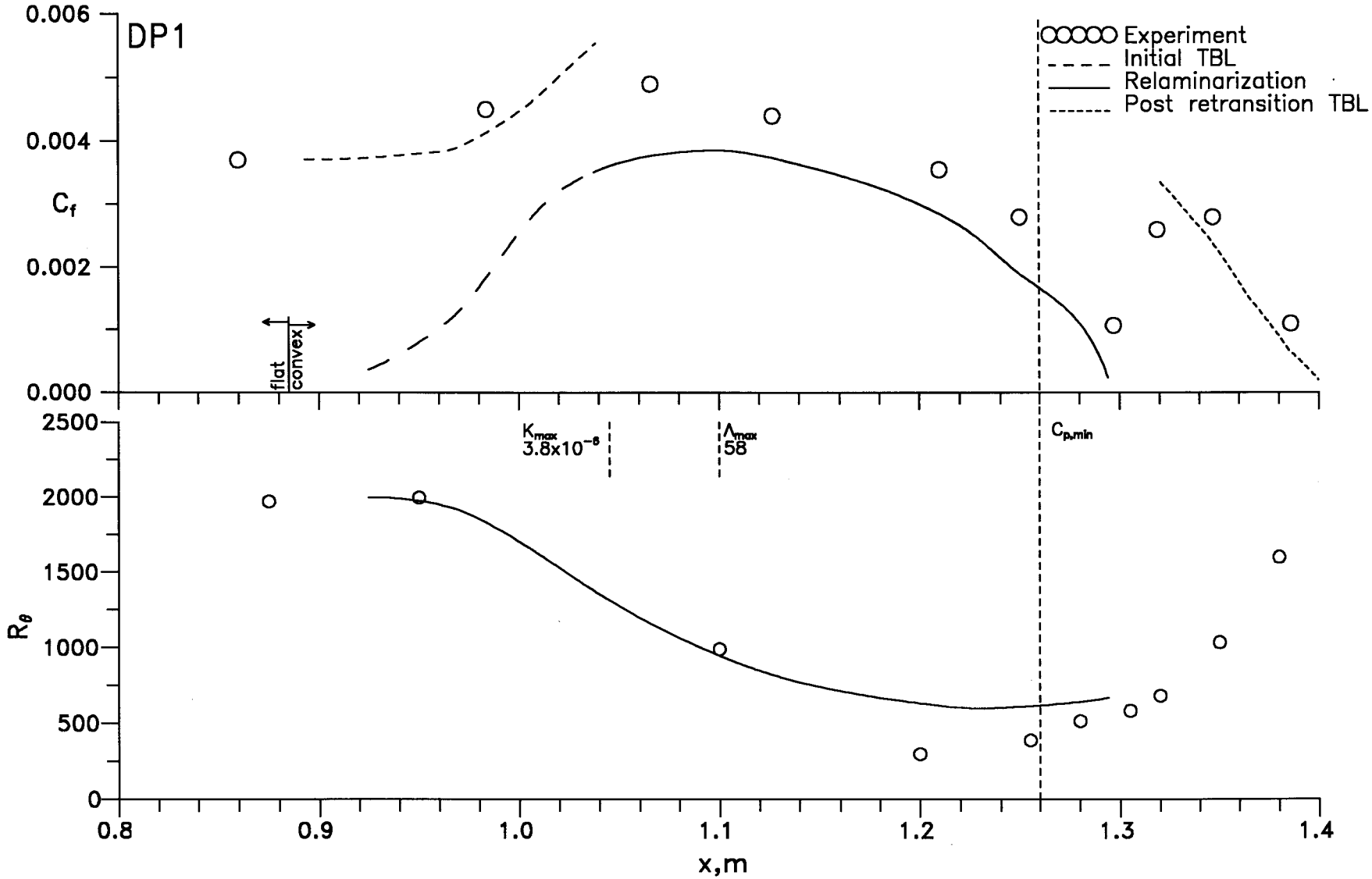

Fig.5.3 Comparison of experimental data with calculations : DP1
Relaminarization : Quasi-laminar equations
Turbulent boundary layer (TBL) : Lag entrainment method

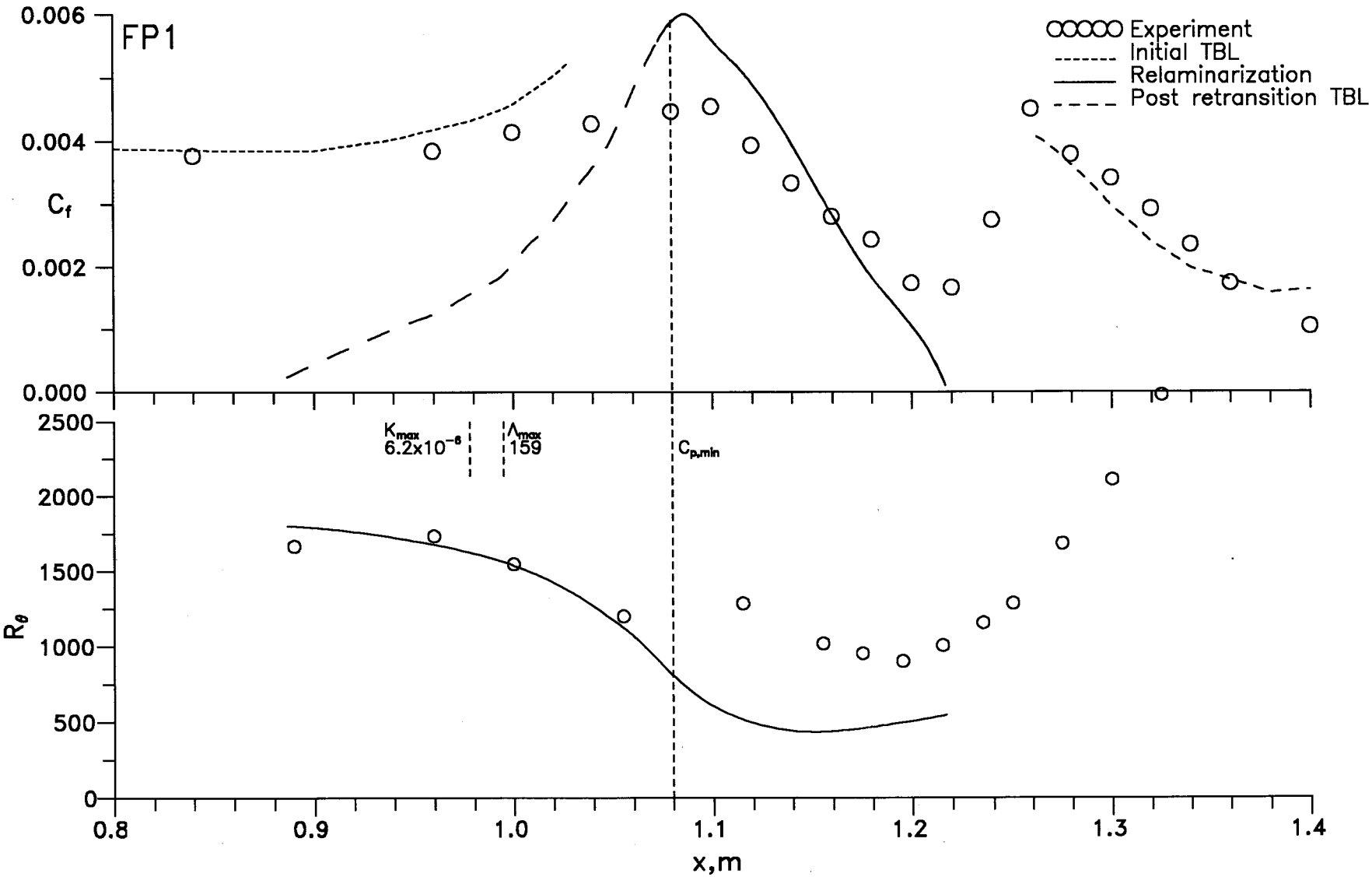

Fig.5.4 Comparison of experimental data with calculations : FP1
Relaminarization : Quasi-laminar equations
Turbulent boundary layer (TBL) : Lag entrainment method

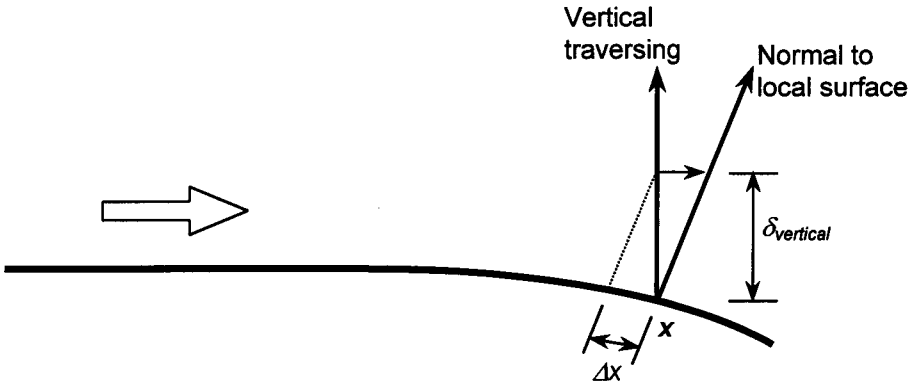

Fig.C1 Sketch illustrating the difference between traversing the hot-wire probe vertically and normal to the local surface. Notice that the probe, being at streamwise distance x moves to distance of x-Δx, when traversed vertically by a distance $\delta_{vertical}$

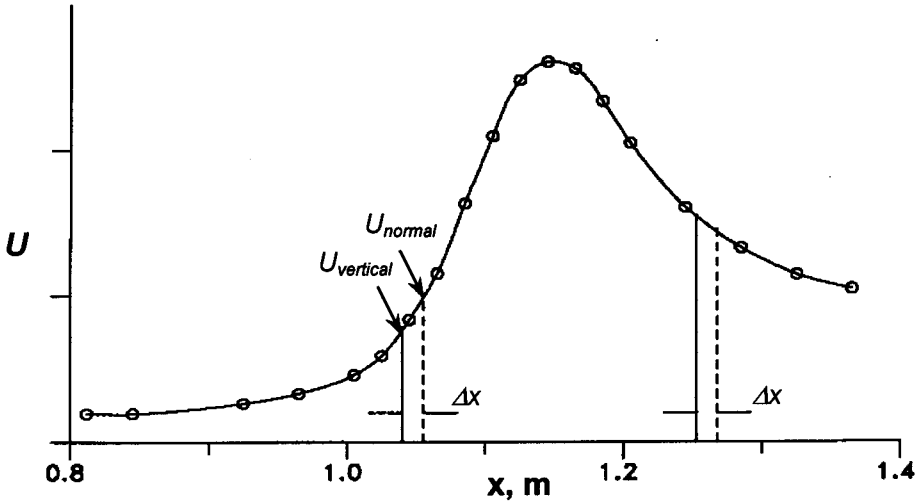

Fig.C2 Sketch illustrating that the velocity $U_{vertical}$ measured at x-Δx is lesser than U_{normal} in the acceleration region and higher in the deceleration region

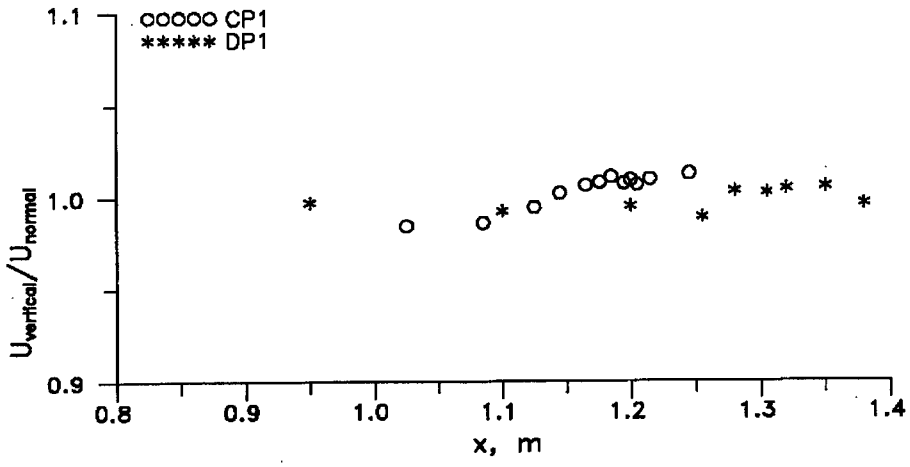

Fig.C3 The streamwise variation of the ratio of $U_{vertical}$ and U_{normal} for the two flows CP1 and DP1

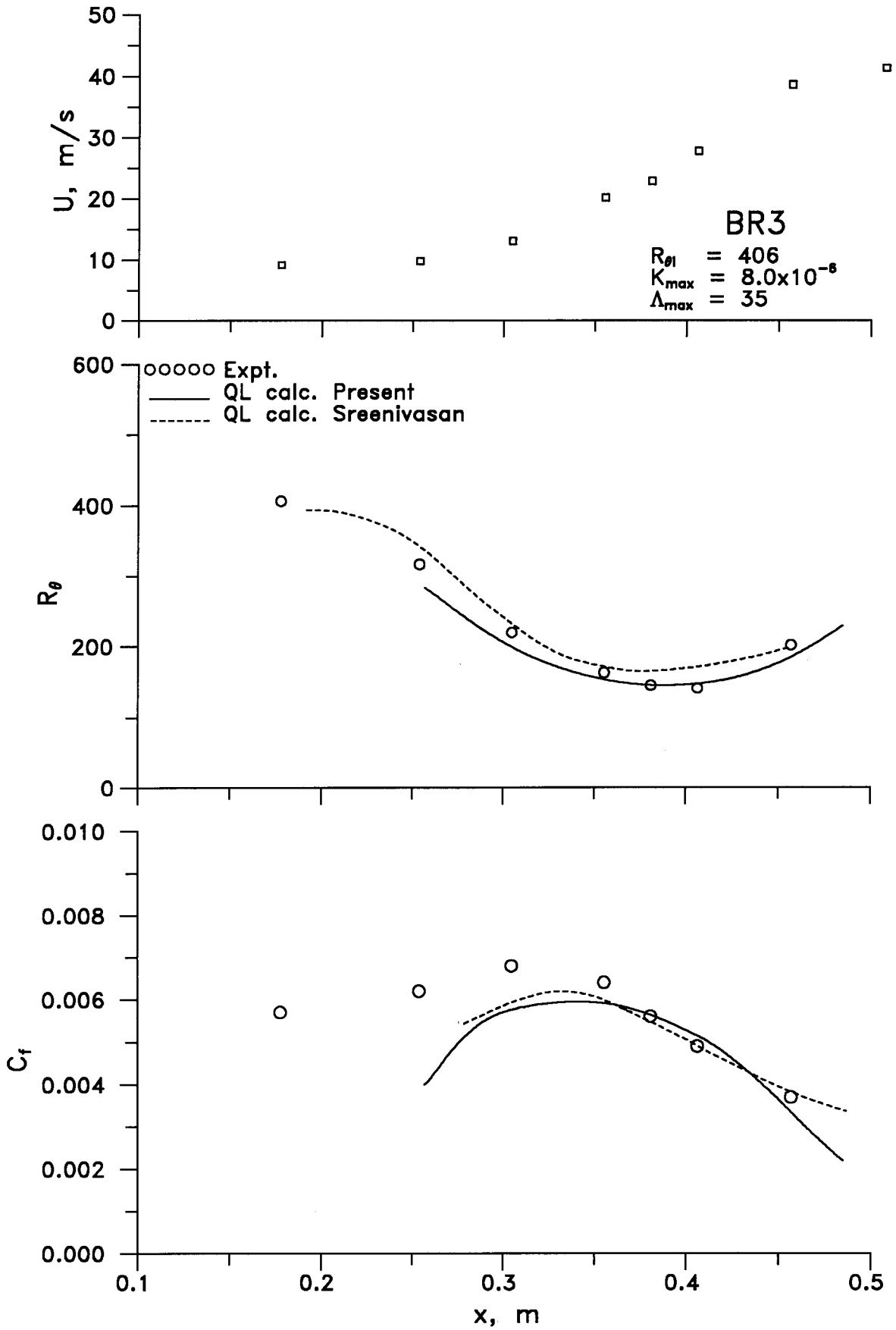

Fig.E1 Comparison of quasi-laminar calculations with experiments of Badrinarayanan & Ramjee

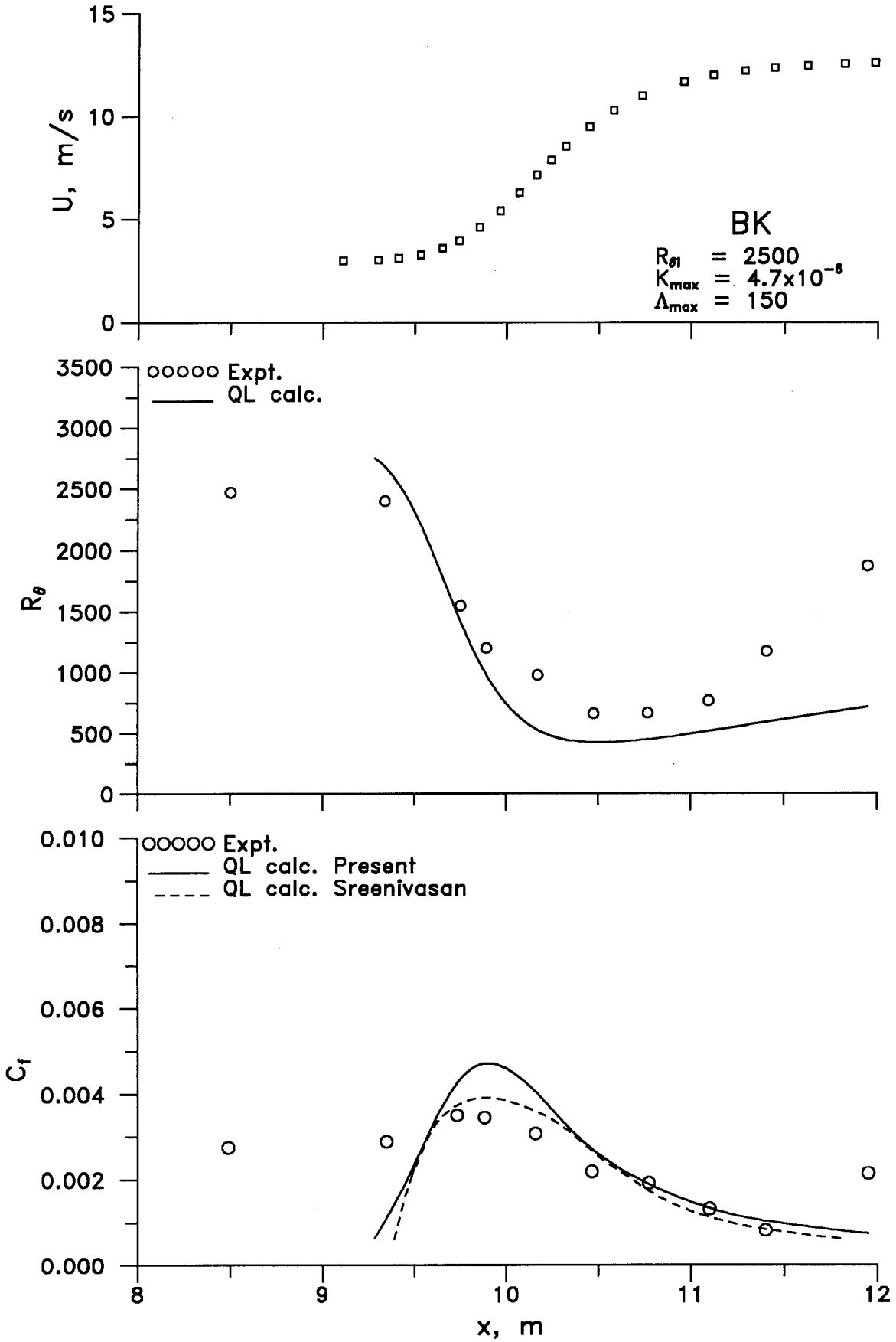

Fig.E2 Comparison of quasi-laminar calculations with experiments of Blackwelder & Kovasznay

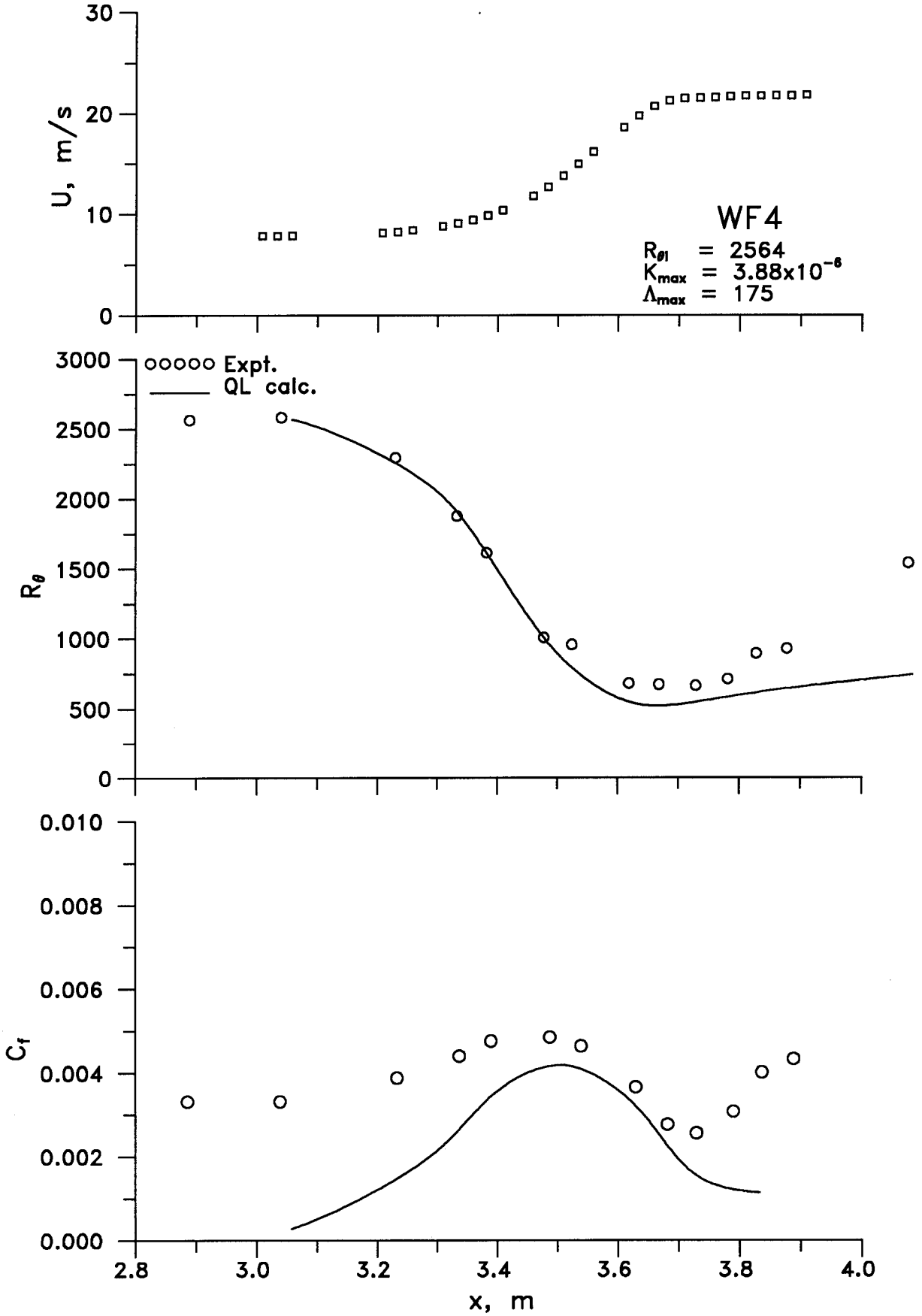

Fig.E3 Comparison of quasi-laminar calculations with experiments of Warnack & Fernholz